RAMAN SPECTROSCOPIC STUDIES OF PHASE EQUILIBRIA IN BINARY MONOVALENT METAL NITRATES

KANGCHENG XU


CENTRE FOR NFLD. STUDIES
MEMORIAL UNIVERSITY
OF NEWFOUNDLAND

RAMAN SPECTROSCOPIC STUDIES OF PHASE EQUILIBRIA IN BINARY MONOVALENT METAL NITRATES

By

KANGCHENG XU

A thesis submitted to the

School of Graduate Studies

in partial fulfilment of the

requirements for the degree of

Doctor of Philosophy

Department of Chemistry
Memorial University of Newfoundland

May, 1997

St. John's, Newfoundland

Abstract

Raman spectroscopy has been developed as a complementary tool to X-ray and thermal methods for phase equilibrium studies of new materials. Raman measurements for mixtures as a function of mole fraction can give the composition for congruently and incongruently melting compounds. Stable and metastable compounds may be identified by comparison to the characteristic spectra obtained from the rapidly quenched or slowly cooled samples from the melts. The presence of longitudinal optic (LO) modes in the Raman spectrum provides a method to identify non-linear crystals. Temperature induced phase transitions can be followed by the measurement of the Raman spectra as a function of temperature. Kinetic information may be obtained for phase transitions with slow conversion.

For the first time Raman spectroscopy has been applied to systematically investigate the structural phase transitions in binary nitrate systems. The binary nitrate systems studied in the present work are KNO_3-$RbNO_3$, $NaNO_3$-KNO_3 , $LiNO_3$-MNO_3 (M = K, Rb, Cs), and $AgNO_3$-MNO_3 (M = K, Rb, Cs).

Raman studies of the KNO_3-$RbNO_3$ system indicated that rubidium ion may substitute for potassium ion up to 67 mol% in the KNO_3 II crystal and up to 80 mol% in the KNO_3 III crystal. The substitutional crystals retained the transitions of phase I to III to II of KNO_3 on cooling and the metastable property of KNO_3 III at room temperature. Chemical substitution of this type was used for a lattice dynamical analysis of potassium nitrate to assign the bands in the external vibrational region. The results supported the assignment of the 52 cm^{-1} band in KNO_3 II to a mode primarily due to translatory motion of cations against anions. A

transition of the KNO_3 III structure to the $RbNO_3$ IV structure was observed for crystals containing 80 and 90 mol% $RbNO_3$. The R3m microscopic structure in the KNO_3 III solid solutions seemed to become disordered when Rb^+ was more than 50 mol% in the substitutional crystal. These structural details offer a possible explanation for the abnormal solid solubility in the KNO_3-$RbNO_3$ system.

Raman spectra were measured for mixed crystals of $NaNO_3$-KNO_3 quenched from different temperatures. Temperature dependent Raman spectra were measured to actually follow the phase transitions. The Raman studies indicated that there existed limited solid solutions $Na_{1-x}K_xNO_3$ (NaII) and (KIII) as well as the $R\bar{3}m$ solid solution and there existed structural phase transitions of the $R\bar{3}m$ solid solution to these limited solid solutions in addition to exsolution of the components from the $R\bar{3}m$ solid solution. It was suggested that two vertical lines be added to the published phase diagram, one to indicate the solid solution $Na_{0.95}K_{0.05}NO_3$ (NaII) and the other to indicate the solid solution $Na_{0.15}K_{0.85}NO_3$ (KIII). Three slightly different structures were found for the $R\bar{3}m$ solid solution below the solidus: in the $NaNO_3$ terminal phase the solid solution behaved like $NaNO_3$ I, in the KNO_3 terminal phase the solid solution behaved like KNO_3 I, in the intermediate concentration phase the solid solution was in a new disordered state. The new disordered state was quenchable and the Raman studies suggested that it was caused by phase separation of the $NaNO_3$ I and KNO_3 I structures on a microscopic or submicroscopic scale. The existence of the three slightly different structures suggested that $NaNO_3$-KNO_3 was a limited solid solution system rather than a continuous solid solution system.

Raman studies of the $LiNO_3$-KNO_3 system revealed a new compound $KLi(NO_3)_2$ which

could exist in a narrow temperature range just below the solidus and in the vicinity of equimolar point. The existence of the new compound suggested that $LiNO_3$-KNO_3 is a simple syntectic system with a congruently melting compound instead of a eutectic system.

The fact that the congruently melting compounds $KLi(NO_3)_2$, $RbLi(NO_3)_2$ and $CsLi(NO_3)_2$ had very similar Raman spectra in both external and internal vibrational regions suggested that they have the same structure. A detailed analysis of the Raman spectra revealed that in the crystals the lithium ion was tetrahedrally coordinated by the nitrate ions to form polymeric complexes in which part of the nitrate ions acted as unidentate ligands and the other part acted as bidentate ligands. The heavier alkali metal ions acted as counterions.

Raman studies of the compounds $KAg(NO_3)_2$ and $RbAg(NO_3)_2$ were consistent with the published crystal structure. There existed polymeric complexes of silver and nitrate ions and the nitrate ions acted as both unidentate and bidentate ligands. Potassium or rubidium ions acted as counterions. Raman studies suggested that the Li-NO_3 complexes in $KLi(NO_3)_2$, $RbLi(NO_3)_2$ and $CsLi(NO_3)_2$ were similar to the Ag-NO_3 complexes in $KAg(NO_3)_2$ and $RbAg(NO_3)_2$. However, the nature of the bond in the lithium complexes was predominately ionic while the nature of the bond in the silver complexes was considerably covalent.

Judged by the notable differences in Raman spectra, the coordination geometry of Ag-NO_3 changed dramatically in $CsAg(NO_3)_2$. The weak Rayleigh wing and a well separated band at 224 cm^{-1} suggested that the polymeric complexes in $KAg(NO_3)_2$ may have broken down to form simple and discrete entity in $CsAg(NO_3)_2$.

Acknowledgements

I am very grateful to Dr. Murray H. Brooker for his excellent knowledge of Raman spectroscopy, fruitful guidance, and timely encouragement.

I am grateful to Dr. P.A. Poirier and Dr. P. Tremaine for their advice.

I would like to thank Gary Hancock, Bernie Rice, Dr. J. Wang and Dr. N. Wen in our group for their help in my study and work.

Financial support in the form of a Memorial graduate fellowship is greatly acknowledged.

Dedication

To my wife and daughter for their love and support.

Table of Contents

List of Tables

List of Figures

List of Abbreviations and Symbols[1] Used

1. b.c.c. – body centred cubic.
2. D – disordered state.
3. DSC – differential scanning calorimeter.
4. DTA – differential thermal analysis.
5. IR – infrared.
6. K – the KNO_3 structure.
7. KI – the KNO_3 I structure.
8. KII – the KNO_3 II structure.
9. KIII – the KNO_3 III structure.
10. LO – longitudinal optical.
11. NaI – the $NaNO_3$ I structure.
12. NaII – the $NaNO_3$ II structure.
13. R – Raman.
14. Rb – the $RbNO_3$ structure.
15. RbIV – the $RbNO_3$ IV structure.
16. RSS – residual solid solution.
17. SS – solid solution.
18. TO – transverse optical.

---

[1] Most of the symbols used are explained in the text when they are introduced.

19. TOF – time of flight.

20. XRD – X-ray diffraction.

21. c – speed of light in vacuum (2.998×10^{8} m s^{-1}).

22. e – elementary charge (1.602×10^{-19} C).

23. h – Planck constant (6.626×10^{-36} J s).

24. ΔH_{tr} – the enthalpy of phase transition of the guest crystal to the structure of the host crystal in the solid solution with non-isostructural components.

25. k – Boltzmann constant (1.381×10^{-23} J K^{-1}).

26. T – the temperature.

27. x – the mole fraction of the second component (BNO_3) in $A_{1-x}B_xNO_3$.

28. $x(M^-)$ – the mole fraction of MNO_3.

29. μ – the reduced mass.

CHAPTER 1

INTRODUCTION

Binary nitrate systems are of great interest both in theoretical studies and in practical applications. Nitrate melts were among the first molten salts studied systematically because of the relatively low melting points and large temperature ranges over which the melts are stable. Accurate solidus and liquidus lines have been measured for binary nitrate systems to evaluate theoretical mixing models [1]. The nitrate glasses have glass transition temperatures near room temperature – a feature that has facilitated the study of the structure of glassy solids [2]. In practice the low melting nitrate mixtures are extensively used as solvents in electrochemical studies [3a] and in molten salt preparations [3b]. Molten mixtures of sodium and potassium nitrates have potential applications as energy storage systems [4] and ferroelectric potassium nitrate is regarded as a promising material for random access memory devices [5].

1.1 General Considerations

Solids formed from binary metal nitrate mixtures can exist in a number of states from pure crystalline solids to glasses. The binary solids may be prepared from the molten mixture or from solution, usually aqueous. Alkali metal nitrate glasses have also been formed by condensation from the gas phase on to very cold substrates [6]. Crystalline solids may be a

simple mechanical mixture $ANO_3 \cdot BNO_3$; a substitutional solid solution, $A_{1-x}B_xNO_3$; or a true homogeneous crystal, $AB(NO_3)_2$.

- Mechanical mixtures $ANO_3 \cdot BNO_3$ are defined as intimate associations of the two components in a state of subdivision large enough so that the percent of atoms within the interphase boundary is negligibly small. The properties of the solids will be the sum of the individual components.
- Substitutional solid solutions $A_{1-x}B_xNO_3$ occur when ions of a second type substitute randomly on the lattice sites of ions of the first type on an atomic scale. The crystal structure of the host crystal remains. The properties of the substitutional solid will be similar to those of the pure host crystal but modified by the presence of the guest ions. The crystal structure is denoted in a bracket, for example $K_{1-x}Rb_xNO_3$ (KII) which means: solid solution of KNO_3 and $RbNO_3$ with the KNO_3 II structure.
- Homogeneous crystals $AB(NO_3)_2$ are highly ordered new compounds. All the ions occupy discrete lattice sites. Complexes form in the new compound. The complexes are characterized by strong attractive forces between the constituent ions and follow a strict stoichiometric ratio of small integers. The homogeneous crystal has characteristic properties different from either of the constituent solids.
- Glasses are characterized by the absence of long range order. The ions are in a disordered state similar to the liquid from which the glass was formed. Glasses formed from a liquid with complex ions will retain the short range order of the complex [7a]. Glasses formed from a melt with random distribution of anions and cations will normally have a totally random structure [7b].

The actual state of a solid binary nitrate is dependent on the charge, the radius and the electronic configuration of the cations. A knowledge of the phase diagrams, the heats of mixing and the structures of the melts or the solutions of the binary systems are often helpful in determining the structural features of the solids. Thermodynamic parameters may be used to predict the stable phase under the conditions of consideration. A negative free energy of mixing for the solid solutions $Na_{1-x}K_xNO_3$ at the solidus temperature would indicate a stable solid solution at that temperature. Since the actual enthalpy is positive, the solid solutions would have a tendency toward clustering to each constituent species (exsolution) [8].

Raman and infrared spectroscopy is a convenient technique for investigation of binary nitrate solids because the nitrate ion may serve as a sensitive probe for the nature of the anionic sites. The nitrate ion is perturbed differently by the cations in each of the four solid states. As a result of the perturbation, the vibrational bands of the free nitrate ion are shifted, the degeneracy of the E' modes may be lifted and the bands of the non-degenerate modes may show asymmetric or even multi-peak features. The present study primarily employed Raman spectroscopy rather than IR because the Raman bands tend to be more narrow and Raman studies of the external vibrational region (20 to 300 cm^{-1}) are more easily measured. Furthermore the samples could be prepared and measured in glass tubes under controlled atmospheric conditions.

In mechanical mixtures the nitrate ion of each component salt generates its characteristic spectrum and the spectra are essentially the same as an admixture of the spectra of the pure components. The relative intensity of the set of bands for each component is proportional to the mole fraction of the component while the position of each band remains practically

unchanged when the composition of the binary system changes.

In substitutional crystals, the nitrate ion experiences an average perturbation by both cations. Usually the Raman spectrum has the same pattern as the host crystal and the bands shift gradually with the variation of the ratio of the components [9]. If smaller ions are replaced by larger ones, the frequencies in the external vibrational region will shift to lower wavenumbers due to the expansion of the lattice. The bands in the internal vibrational region will also shift slightly.

In homogeneous crystals, discrete nitrato complexes may exist in which the nitrate ion experiences predominantly the force field of the complex forming cation. The spectra of the solids are practically those of the complexes. If a series of compounds with the same nitrato complex has the same crystal structure, their vibrational spectra will have the same pattern in the internal vibrational region of the nitrate ion [10]. A change of the pattern may then indicate a change in the crystal structure due to the different factor group [11]. When the new compound forms eutectics with the pure components and one of the components is present in excess, the spectrum will be a combination of the compound and the pure component, i.e., a mechanical mixture. If the new compound forms solid solutions with the pure components, complicated spectra will result.

Nitrate glasses have vibrational spectra similar to the melts from which they were formed [7a,7b]. Due to the absence of long range order the vibrational selection rules are relaxed and the spectrum reflects the density of states. Bands are broad because of the wide range of environments frozen into the glass. The symmetric stretching band has a full width at the half height similar to that of the melt (about 20 cm^{-1}) and for some cases it appears asymmetric

or has a doublet profile. The normally Raman forbidden out-of-plane band may appear in the Raman spectra. The bands due to degenerate E' modes may split into two. The most notable features are the diffuse profile in the low wavenumber range and the insensitivity of all bands to the changes of the temperature and small changes in composition.

In the present work the following systems were investigated:

1. The continuous series of solid solutions of KNO_3-$RbNO_3$ for quenched and annealed samples.
2. The continuous series of solid solutions of $NaNO_3$-KNO_3 for samples quenched from 358, 393 and 493 K and annealed samples
3. The temperature dependence of the continuous solid solutions of $NaNO_3$-KNO_3.
4. Systems of $LiNO_3$-MNO_3 (M = K, Rb, Cs) for a reinvestigation of the phase diagram of $LiNO_3$-KNO_3 and for an evaluation of the structure of the congruently melting compounds $KLi(NO_3)_2$, $RbLi(NO_3)_2$ and $CsLi(NO_3)_2$.
5. Systems of $AgNO_3$-MNO_3 (M = K, Rb, Cs) for an evaluation of the structures of the compounds $KAg(NO_3)_2$, $RbAg(NO_3)_2$ and $CsAg(NO_3)_2$.

1.2 Crystal Structures of the Pertinent Nitrates

The crystal structures of all the single nitrates in this study have been well defined by most of the major techniques for structure determination. Table 1.1 summarizes the stable structures of alkali metal nitrates and silver nitrate up to melting point and at atmospheric pressure. At room temperature the crystal structure of $LiNO_3$ has the space group $R\bar{3}c$, Z =

2 which persists at all the temperatures up to the melting point and to pressures up to 40 kb [12]. The crystal consists of alternating layers of lithium ions and nitrate ions. The nitrate ions are located on a plane perpendicular to the C_3 axis. The orientation of the adjacent nitrate ions along the C_3 axis differs by 60^0.

The room temperature phase of sodium nitrate ($NaNO_3$ II) adopts the same structure ($R\bar{3}c$) [13] as $LiNO_3$. At elevated temperatures, disorder in the nitrate ions progresses until above 548 K, when the orientation of the nitrate ions becomes completely disordered. The structure of the high temperature phase $NaNO_3$ I has the space group $R\bar{3}m$ (D_{3d}^5) [14].

The low temperature phase of potassium nitrate (KNO_3 II) is orthorhombic and has the space group Pmcn (D_{2h}^{16}), $Z = 4$ [15]. Between each pair of K planes there are two planes of staggered nitrate ions parallel to (100). The orientation of the adjacent nitrate ion planes along the 2_1 axis differs by 60^0. At about 401 K the orthorhombic KNO_3 II transforms to rhombohedral KNO_3 I which has the same structure as $NaNO_3$ I ($R\bar{3}m$) [16]. On cooling from above 453 K, KNO_3 I does not change directly to phase II, but transforms first to another rhombohedral phase (KNO_3 III) at about 397 K and then reverts to phase II at about 373 K [17]. Phase III is a nonlinear crystal with space group R3m. The primitive rhombohedral unit cell contains one formula unit. The nitrate ions lie in planes perpendicular to the C_3 axis and orient in the same direction. The potassium ions are not located in the centre between the nitrate planes but have different distances to the nitrate ions. The centrosymmetry of the structure is lost and the crystal becomes polar. KNO_3 III is ferroelectric.

The room temperature phases of $RbNO_3$ IV [18] and $CsNO_3$ II [19] have a trigonal structure. The space group is $P3_1$ (C_3^2), $Z = 9$. There are symmetry unrelated three sets of

nitrate sites in the primitive unit cell [20]. At high temperature (above 434 K for $CsNO_3$ I, 437– 492 K for $RbNO_3$ III) the crystal structures are of the CsCl type [21]. The space group is Pm3m (O_h^1), Z = 8. $RbNO_3$ has two more polymorphs above 492 K [22]. $RbNO_3$ II is stable between 492 and 564 K. The $RbNO_3$ II crystal has a b.c.c. lattice and the nitrate groups are orientationally disordered. An earlier report [23] suggested a rhombohedral unit cell for $RbNO_3$ II with the space group $R\bar{3}m$. $RbNO_3$ I exists above 564 K with a cubic structure, space group Fm3m [22].

It should be noted that all the high temperature phases of alkali metal nitrates, with the exception of KNO_3 III, involve some degree of orientational disorder of nitrate groups. KNO_3 III has other interesting properties. If it is dried and kept in vacuum, KNO_3 III can be quenched to room temperature or lower and preserved indefinitely in a metastable state. The volume of the solid increases, instead of decreasing, when potassium nitrate goes from phase III to phase II.

$AgNO_3$ has a unique structure in the MNO_3 series. The space group for the room temperature phase of silver nitrate ($AgNO_3$ II) is Pbca (D_{2h}^{14}), Z = 8 [24]. It is predominantly ionic. However, the silver ions have a tendency to bond to the oxygen atoms, which results in a little distortion in the structure. At temperatures above 433 K, a new phase ($AgNO_3$ I) appears which has the same disordered structure as $NaNO_3$ I ($R\bar{3}m$) [25].

The only available crystallographic data for the binary nitrate compounds in the present work are those of $KAg(NO_3)_2$ and $RbAg(NO_3)_2$. They are isomorphic. The space group is $P2_1/a$ (C_{2h}^5), Z = 4 [26]. There are two crystallographically distinct sites for the nitrate ions. In the crystals the silver ions are tetrahedrally coordinated to four oxygen atoms from four

nitrate ions. Half of the nitrate ions bridge two silver ions by a single atom. The other half of the nitrate ions bridge two silver ions through two different oxygen atoms. The silver ions and the nitrate ions form infinite chains $[Ag_2(NO_3)_4]_n^{2n-}$ (Fig. 1.1). The potassium or rubidium ions link the infinite chains and have little effect on the coordination environment of the nitrate ions.

1.3 Structures of the Nitrates in Liquid State

The structure of the molten nitrates has been studied by neutron diffraction, X-ray diffraction (XRD) and vibrational spectroscopies. Time of flight (TOF) pulsed neutron diffraction studies [27] showed that the nitrate ions experience a different cationic environment in molten $LiNO_3$ and $AgNO_3$ from that in molten $NaNO_3$, KNO_3, $RbNO_3$ and $CsNO_3$. The stronger interionic interactions in the former caused the nitrate ion to assume the shape of an isosceles triangle while the nitrate ion formed an equilateral triangle in the later. The radial distribution function from the X-ray diffraction data [28] also indicated different structures between the two groups of molten salts.

The unique cationic environment of the nitrate ions in molten $LiNO_3$ and $AgNO_3$ has been further verified by Raman and infrared spectroscopies [29-32]. A notable splitting of the antisymmetric bending (E′ mode) of the free nitrate ion was observed in the Raman spectra for these two molten nitrates, whereas the band shape of this mode in the other molten nitrates was symmetric within the accuracy of the experiment.

The coordination of the silver ion in $AgNO_3$ has been studied in detail by X-ray

diffraction [33] and TOF neutron diffraction [34]. About four nitrate ions were found to be tetrahedrally bonded to a silver ion. The shortest distance between silver ions and the nitrate oxygen atoms was observed at 245 pm, which is within the reported shortest Ag-O distance in the $AgNO_3$ I crystal [35]. A model for the Ag-NO_3 orientation in molten $AgNO_3$ was given which was similar to that in the $AgNO_3$ I crystal.

A neutron diffraction study [34] showed that the lithium ion in molten $LiNO_3$ had a similar coordination environment to that in molten $AgNO_3$. The lithium ion was reported [36] to be tetrahedrally surrounded by four nearest nitrate ions, one oxygen atom from each nitrate ion faced toward the lithium ion. The coordination number four in the melt is different from the number of the nearest neighbouring oxygen atoms around the lithium ion in the $LiNO_3$ crystal which is six. The estimated distance of Li-O (210 pm) is shorter than that in the crystal [37]. It was noted [34] that the local structures around the lithium and nitrate ions in the melt of 1:1 $LiNO_3$-$RbNO_3$ were almost the same as those in pure $LiNO_3$ melt.

The situation is more complicated in aqueous solutions because of solvation. Raman studies of the interactions in aqueous alkali nitrate solutions showed [38] that in concentrated solutions of $LiNO_3$ and $NaNO_3$, contact ion pairs were present. The concentrated aqueous $LiNO_3$ solution was interpreted on a quasilattice model [39] because the Raman bands attributed to the nitrate ions in the coordination sphere of the lithium ions and the bands for the solvated nitrate ions coexisted over a range of concentrations. A theoretical model [40] in which the coordination geometry around the lithium ion is tetrahedral has been used to define the structural characteristics of the $LiNO_3$ melt and aqueous solutions.

X-ray diffraction studies [41,42] on the complex formation of silver (I) in concentrated

aqueous nitrate solutions indicated that the silver ion was tetrahedrally coordinated by four oxygen atoms from either water or nitrate ions. The nitrate ion was bonded to each silver ion as a unidentate ligand. The change from melt to aqueous solution involved the replacement of nitrate ions by water but the coordination state of the silver ion persisted.

In short, lithium, silver and perhaps sodium ions have the same tetrahedral coordination environment in melts and aqueous solutions. The other nitrates have different structures with a less well-defined coordination number of about six.

1.4 Phase Diagrams and Other Thermodynamic Properties

Over the years the phase diagrams of all the binary nitrate systems studied in this program have been investigated and reinvestigated by thermal methods. The general features of the binary systems can be regarded as "established", although in several cases there exist significant differences between the reports. The $LiNO_3$-MNO_3 (M = Na, K, Rb, Cs) series manifested a regular change in the type of phase diagram [43]. As the radius of the other alkali metal increased, there is an increasing tendency for the lithium ion to form four coordinated complexes. The $LiNO_3$-$NaNO_3$ and $LiNO_3$-KNO_3 systems appeared to have simple eutectic behaviour, although one report [43] suggested continuous solid solutions in $LiNO_3$-$NaNO_3$.

A congruently melting compound $RbLi(NO_3)_2$ was reported [43] to solidify from the $LiNO_3$-$RbNO_3$ melt at about 463 K. The compound should form eutectics or solid solutions with $LiNO_3$ and $RbNO_3$. Early studies of the $LiNO_3$-$CsNO_3$ system indicated a eutectic system or continuous series of solid solutions. Bol'shakov and co-workers reinvestigated [43]

the system and reported a congruently melting compound $CsLi(NO_3)_2$ at 467 K. The compound formed eutectics with $CsNO_3$ (41 mol% $LiNO_3$, 443 K) and $LiNO_3$ (54 mol% $LiNO_3$, 433 K). Other investigators [44,45] have confirmed the phase diagram of Bol'shakov *et al.*

The $AgNO_3$-MNO_3 series have a similar trend for complex formation in the phase diagrams. A differential thermal analysis (DTA) study of $AgNO_3$-$NaNO_3$ [46] indicated continuous solid solutions in equilibrium with the liquid phase.

The phase diagram of $AgNO_3$-KNO_3 was reported to be more complicated [47,48]. It was noted that in the early studies there were discrepancies in the compositions and temperatures of the characteristic points and in the stabilities of the chemical compounds, and further studies of this system were undertaken. However, even the two most recent investigations did not give consistent results. A DTA study [47] produced a phase diagram with a congruently melting compound $KAg(NO_3)_2$ at 408 K and the compound formed eutectics with KNO_3 and $AgNO_3$. A differential scanning calorimetry (DSC) study [48] indicated only a eutectic point at 391 K and 58 mol% $AgNO_3$. An intermediate (incongruently melting) compound $AgNO_3 \cdot KNO_3$ was suggested to account for the additional discontinuity on the DSC curve. It seems possible that the DSC study did not produce an equilibrium phase diagram.

A congruently melting compound $RbAg(NO_3)_2$ was reported [49] at 407 K in the phase diagram of $AgNO_3$-$RbNO_3$. The compound formed eutectic mixtures with the constituents. In addition, there is an incongruently melting compound $Rb_2Ag(NO_3)_3$ at 399 K and another compound $Rb_3Ag(NO_3)_4$ may exist at lower temperature. No solid solutions were observed.

Two compounds were reported [50] in the phase diagram of $AgNO_3$-$CsNO_3$: a

congruently melting compound $CsAg_3(NO_3)_4$ at 445 K and an incongruently melting compound $CsAg(NO_3)_2$ at 448 K although another report [51] suggested that both compounds melted congruently. Eutectics were found between the pure components and the compounds. No solid solutions were detected.

The enthalpies of mixing have been measured for binary alkali nitrate melts and all have negative values [52]. The magnitude of the molar mixing enthalpy (ΔH^M) increases in a regular fashion with increasing difference between the ionic radius of the cations in the binary system (Tables 1.2 and 1.3). An approximate equation [52] was given to represent the relationship between the observed heats of mixing and the difference in the size of the cations:

$$\Delta H^M = -x(1-x)U\delta^2 \quad kJ/mol \qquad (1.1)$$

Here x is the mole fraction, U is the lattice energy of the mixture, and δ is defined as $(d_1 - d_2)/(d_1 + d_2)$ where d_1 and d_2 are the interionic distances characteristic of the pure compounds.

It was noted [53] that, except for the negative sign, this expression was the same as that for mixing enthalpy of a solid solution from two ionic salts with cations of the same charge and a common anion:

$$\Delta H^M = x(1-x)U\delta^2 \qquad (1.2)$$

The enthalpies of mixing in the silver nitrate-alkali metal nitrate binary melts change similarly with the increasing size of the alkali metal ions [54], from positive values of ΔH^M for lithium and sodium to negative values for potassium and rubidium (Table 1.4). The above

equation for pure ionic melts was modified to represent the observed behaviour of the silver containing nitrate systems:

$$\Delta H^{M} = -x(1-x)[0.586\delta^2 - 0.100(\delta - 0.01)] \quad kJ/mol \qquad (1.3)$$

The linear term in δ takes into account departures from ionicity in $AgNO_3$.

Although the enthalpy of mixing in the melt alone cannot determine the stability of a solid solution, some trend may be expected [8]. There is some doubt about the existence of a solid solution in the $LiNO_3$-$NaNO_3$ system, while it is generally accepted that $AgNO_3$-$NaNO_3$ forms solid solutions.

In the series $LiNO_3$-MNO_3 and $AgNO_3$-MNO_3 (M = Na, K, Rb, Cs), solid solution formation was reported for the $AgNO_3$-$NaNO_3$ system, a eutectic mixture was found for the $LiNO_3$-KNO_3 system, while solid solution or eutectic reactions appeared possible for the $LiNO_3$-$NaNO_3$ system. All the other binary nitrates form compounds and no solid solutions were detected between the compounds and pure components.

1.5 Vibrational Spectroscopic Studies of the Solid Nitrates

Much work has been done to correlate the vibrational spectroscopic features of the nitrates with their crystal structures. The peak position, bandshape, number and intensity of the bands in the internal vibrational region of the nitrate ion are important parameters for structural evaluation. The unperturbed nitrate ion is a triangular planar species of D_{3h} symmetry. Group theory predicts four fundamentals. The symmetry, convenient symbol,

activity and approximate position of the four bands are as follows: the A′ mode (ν_1) is Raman active at about 1050 cm^{-1}; the A″ mode(ν_2) is IR active at about 830 cm^{-1}; the two E′ modes (ν_3 and ν_4) are both Raman and IR active at about 1380 and 720 cm^{-1} respectively.

The symmetric stretching vibration ν_1 is very sensitive to the environment of the nitrate ion. In ionic crystals the nitrate ion experiences an average polarization by the cation field. The stronger the field, the higher the frequency of ν_1. For rhombohedral alkali metal nitrates $LiNO_3$, $NaNO_3$ II and KNO_3 I, the vibrational energy decreases with the increasing size of the cation [55]: Li^+ (1070 cm^{-1}) > Na^+ (1068 cm^{-1}) > K^+ (1055 cm^{-1}). Similarly, for trigonal alkali metal nitrates $RbNO_3$ IV and $CsNO_3$ II the frequencies are [56]: Rb^+ (1057 cm^{-1}) > Cs^+ (1051 cm^{-1}). The covalent interactions in $AgNO_3$ II cause directional polarization which lowers the vibrational energy of ν_1 to 1044 cm^{-1} [57].

The non-degenerate ν_1 mode may manifest multiplet features when there is more than one crystallographic site for the nitrate group in the unit cell. Three components of about equal intensity and 1 cm^{-1} apart were observed [58] in the Raman spectra of $RbNO_3$ IV and $CsNO_3$ II, corresponding to the three sets of nonequivalent crystallographic C_1 sites of the nitrate ion. Disordered sites of the nitrate ion in the unit cell may cause an asymmetric bandshape of ν_1 in the Raman spectra of $LiNO_3$, $NaNO_3$ II and KNO_3 II [56,59]. Band analysis revealed a broad second component about 3-5 cm^{-1} lower than the dominant peak that increased in intensity with increased temperature.

The Raman spectra of $AgNO_3$ differ from the spectra of alkali metal nitrates in that the normally Raman forbidden ν_2 mode has much greater intensity. Two components at 809 and 810 cm^{-1} were observed [57] in the oriented single crystal spectra.

Vibrational spectroscopy may be used to follow the phase transitions of a crystal. Theoretically a change in the structure will bring about a corresponding change in the spectrum, such as the appearance of new bands, the fade-out of the old bands, and/or a variation in relative intensities.

The position and halfwidth of the ν_1 vibration in the Raman spectra have been used to investigate the phase transitions in $LiNO_3$, $NaNO_3$ and KNO_3 [55] over a wide range of temperature up to the melting points. A plot of the two parameters versus temperature shows a discontinuity in the curve at the transition temperature (401 K) from KNO_3 II to KNO_3 I. Unlike KNO_3, the position and width changed smoothly with the temperature and no clear-cut discontinuity was detected in the case of the $NaNO_3$ II to $NaNO_3$ I transition. This observation was in agreement with the fact that $NaNO_3$ undergoes a continuous phase transition.

For $RbNO_3$ and $CsNO_3$, the transitions from the room temperature phases to the high temperature phases are characterized by a definite degree of reorientational disorder of the nitrate ion. Consequently, beside the main band of ν_1 with intensity I in the Raman spectra, a secondary band with intensity I′ was observed [60]. The orientational disorder parameter for the phase transitions of the second kind was defined as:

$$\eta = (I - I')/(I + I') \qquad (1.4)$$

A plot of η versus the temperature gave a curve which had a sudden change of slope near the phase transition temperature [60]: 427 K for $CsNO_3$ II to $CsNO_3$ I and 437 K for $RbNO_3$ IV to $RbNO_3$ III.

The changes in orientational order in $RbNO_3$ and $CsNO_3$ are also reflected in the external modes of the nitrates. It was found [61] that the librational mode of the nitrate ion shifted to low wavenumber and broadened as the temperature increased.

Infrared spectroscopy has been used [62] to study the effect of partial replacement of Ag^+ by Na^+ on the order-disorder transition II to I in the mixed crystals of $AgNO_3$-$NaNO_3$. As the mole fraction of Na^+ increased, there was a gradual change in the spectra. The band features of the mixed crystals were not the simple average of those of the two components. The intensity and halfwidth of ν_3 were found not to change linearly with the mole fraction of Na^+ and maxima were observed on the curves of intensity versus $x(Na^+)$ for the ν_2 and $2\nu_2$ bands.

1.6 Objectives of the Program

The above survey shows that the structural chemistry of the pure nitrates has been studied in detail by most of the techniques for structure determination. The structures and thermodynamic properties of the molten binary nitrates are also known with fair accuracy. However, due attention has not been paid to the structures of the binary nitrate solids. To our knowledge, vibrational spectroscopy has not been systematically applied to investigate the structures and structural phase transitions of the mixed crystals of nitrates. Only the IR studies [62] of the mixed crystals of $AgNO_3$-$NaNO_3$ and the Raman studies [63] of the phase transitions of the NH_4NO_3-KNO_3 system have been reported. It is interesting to note that shortly after its discovery, the Raman effect was used to investigate the solid of equimolar $NaNO_3$-KNO_3 [64]. It was found [65] that the ν_1 vibration in the equimolar mixture of $NaNO_3$-KNO_3 was a

single band at high temperature while at room temperature it split to two, corresponding to $NaNO_3$ II and KNO_3 II respectively.

Most of the knowledge about the structures of the solids of mixed nitrates comes from an analysis of the phase diagrams obtained by thermal methods which are normally based on the macroscopic properties of the system. The structural details associated with solid solutions can be inferred, but not proved, from a knowledge of the structures and structural phase transitions of the pure components [66]. The explanations are not always correct. In addition, thermal analysis is a dynamic process and it may fail to detect the phase transitions of small enthalpies or phases existing in a small temperature range. Phase transitions in the solid state sometimes take place slowly and the phase diagrams determined by thermal analysis may not represent an equilibrium state, as was noted in the discussion of the phase diagram of $AgNO_3$-KNO_3 (Section 1.5). Our Raman studies of the $NaNO_3$-KNO_3 system (Chapter 5) indicated a new disordered state for which the transition was too slow to be detected by a single DSC run. The slow transition of the new disordered state accounted for the quenchable properties of the $R\bar{3}m$ solid solution while the DSC studies [4] indicated that the solid solution was unquenchable.

Among the spectroscopic techniques XRD is used most frequently in the phase diagram studies. The diffraction patterns of powder samples provide a sensitive identification of the crystal phases in a system. In favourable cases lattice parameters can be derived and the influence of the guest atoms on the molar volume of the host crystal can be measured [67]. Care must be taken when X-ray techniques are used to investigate metastable systems since high energy X-rays may cause decomposition of the sample. The X-ray investigations [4,8] of

the $NaNO_3$-KNO_3 system indicated an unquenchable disordered state and always gave a diffraction pattern of a mixture of KNO_3 II and $NaNO_3$ II. Our Raman studies indicated that the disordered state could be quenched. The decomposition of the quenched disordered state may have been caused by the X-rays or by handling the samples in air. In Raman studies the samples can be kept in glass or quartz tubes and investigated under controlled conditions. The samples were not disturbed during the measurements.

Raman spectroscopy is being developed as a complementary tool to thermal and X-ray methods for phase equilibrium studies of new materials. Special efforts have been made to evaluate the structures of the binary nitrate solids to gain a better understanding of the trend in the structures and structural phase transitions in the series of alkali metal nitrates. Substitutional crystals may create an intermediate situation for a given type of structure and to explore the influences of a second component on the properties and temperature range of a given phase. Substitutional crystals are widely used in practice because chemical substitution can bring about changes in properties and stability to satisfy various needs. A major object of chemistry is to learn how to change the components to modify a given property or to stabilize a desired phase (e.g., ferroelectric potassium nitrate). It is as important as synthesizing a new compound. The structural chemistry of substitutional crystals is the key to the problem.

Table 1.1 The phases, their space groups and stable temperature ranges of alkali metal nitrates and silver nitrate at atmospheric pressure.

MNO_3	phase	space group	Z	stable temperature range (K)
$LiNO_3$		$R\bar{3}c$	2	up to melting point
$NaNO_3$	I	$R\bar{3}m$	1	548 – 580
	II	$R\bar{3}c$	2	< 548
KNO_3	I	$R\bar{3}m$	1	401 – 607
	II	Pmcn	4	< 401
	III	R3m	1	373 – 397
$RbNO_3$	I	Fm3m	4	564 – 583
	II	$R\bar{3}m$	1	492 – 564
	III	Pm3m	8	437 – 492
	IV	$P3_1$	9	< 437
$CsNO_3$	I	Pm3m	8	434 – 687
	II	$P3_1$	9	< 434
$AgNO_3$	I	$R\bar{3}m$	1	433 – 485
	II	Pbca	8	< 433

Table 1.2 Ionic radii of alkali metals, silver and the nitrate ion (in pm) [52,54].

Li^+	Na^+	K^+	Rb^+	Cs^+	Ag^+	NO_3^-
60	95	133	148	169	126	219

Table 1.3 Heats of mixing in equimolar $LiNO_3$-MNO_3 binary liquids [52].

MNO_3	$NaNO_3$	KNO_3	$RbNO_3$	$CsNO_3$
ΔH^M (kJ/mol)	-0.510	-1.96	-2.72	-3.91

Table 1.4 Heats of mixing in equimolar $AgNO_3$-MNO_3 binary liquids [54].

MNO_3	$NaNO_3$	KNO_3	$RbNO_3$	$CsNO_3$
ΔH^M (kJ/mol)	0.607	-0.519	-1.17	-2.19

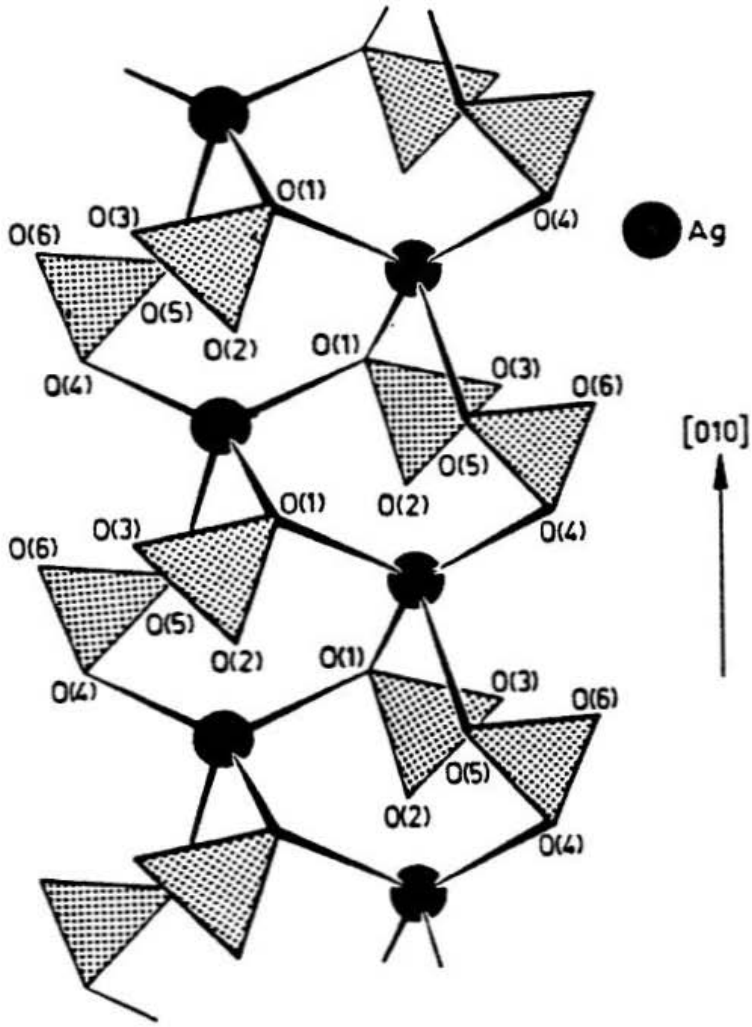

Fig. 1.1 The structure of the infinite chain $[Ag_2(NO_3)_4]_n^{2n-}$. The silver ions are tetrahedrally coordinated to the nitrate ions, half of which act as unidentate ligands and the other half act as bidentate ligands [26].

CHAPTER 2

THEORY

2.1 Theory of Molecular Vibrations

The features in the vibrational spectrum, such as the number, frequency, intensity, polarization and shape of the bands are determined by the structure of the sample. The theory of molecular vibrations correlates the spectroscopic findings to the microscopic structure of the substance. This section contains an outline of the theory required to understand and discuss the spectroscopic results.

2.1.1 Vibrations of Isolated Molecules

The complicated vibrations of a polyatomic molecule in the gas phase may be represented by the superposition of a number of normal vibrations. The number, symmetry and activity of the normal vibrations are determined by the geometry of the molecule. Group theory provides a simple and quick way to predict all these features from the structure of the molecule [68]. Free nitrate ions belong to point group D_{3h} and should have four fundamental vibrational bands: ν_1 A′ (P), ν_2 A″(IP), ν_3 E' (IR,R) and ν_4 E' (IR,R).

In the normal mode description of vibrations all the nuclei move in phase with the same frequency. The normal vibrations are independent of each other. For the ith normal vibration

there is a normal coordinate Q_i so that the kinetic (T) and potential (V) energies of the molecule can be written as:

$$2T = \sum_i \dot{Q}_i^2 \qquad (2.1)$$

$$2V = \sum_i \lambda_i Q_i^2 \qquad (2.2)$$

λ is a variable proportional to the force field for normal vibration and reciprocal of the mass. λ is related to the observed frequency ν of the normal vibration by:

$$\nu_i = \sqrt{\lambda_i / 2\pi} \qquad (2.3)$$

Since the normal coordinates are independent of each other, the wavefunction Ψ and energy E of the system may be expressed as:

$$\Psi = \psi_1 \psi_2 \psi_3 \cdots \qquad (2.4)$$

$$\mathbf{E} = \sum_i \mathbf{E}_i \qquad (2.5)$$

Here:

$$E_i = h\nu_i(v_i + 1/2) \qquad (2.6)$$

Internal coordinates and the FG matrix method are used to evaluate λ from the secular equation:

$$| GF - \lambda I | = 0 \qquad (2.7)$$

F is a matrix whose components are force constants and G is a matrix involving the reciprocal of the mass of the atoms. I is unit matrix.

When light of a given polarization impinges on a molecule, it induces a dipole moment which subsequently radiates:

$$\boldsymbol{\mu}_i = \tilde{\alpha}\mathbf{E} \qquad (2.8)$$

The induced dipole moment μ_i is generally not parallel to the applied electric field vector **E**. Consequently, the polarizability $\tilde{\alpha}$ is a symmetric tensor:

$$\tilde{\alpha} = \begin{bmatrix} \alpha_{xx} & \alpha_{xy} & \alpha_{xz} \\ \alpha_{yx} & \alpha_{yy} & \alpha_{yz} \\ \alpha_{zx} & \alpha_{zy} & \alpha_{zz} \end{bmatrix} \qquad (2.9)$$

The polarizability tensor is often considered to be a combination of a symmetric and an asymmetric part. The symmetric part is described by the invariant mean polarizability $\bar{\alpha}$:

$$\bar{\alpha} = \frac{1}{3}(\alpha_{xx} + \alpha_{yy} + \alpha_{zz}) \qquad (2.10)$$

The asymmetric part is described by the polarizability anisotropy β:

$$2\beta^2 = [(\alpha_{xx} - \alpha_{yy})^2 + (\alpha_{yy} - \alpha_{zz})^2 + (\alpha_{zz} - \alpha_{xx})^2 + 6(\alpha_{xy}^2 + \alpha_{yz}^2 + \alpha_{zx}^2)] \qquad (2.11)$$

The intensity of a normal vibration in the Raman spectrum is related to the molecular properties by the following equation [69]:

$$I = KI_0 \frac{(\omega_0 - \omega)^4}{\mu\omega[1 - \exp(-h\omega/kT)]}[45\bar{\alpha}^2 + 7\beta^2] \qquad (2.12)$$

K is a constant, I_0 and ω_0 are the intensity and frequency of the incident light, μ is the reduced mass. ω is the frequency of the normal mode.

The scattered light intensity may be divided into two parts [70,71], polarized and depolarized:

$$I_\alpha(\omega) = I_{pol}(\omega) = I_{iso}(\omega) = I_{\parallel}(\omega) - \frac{4}{3}I_{\perp}(\omega) \qquad (2.13a)$$

$$I_\beta(\omega) = I_{depol}(\omega) = I_{aniso}(\omega) = I_{\perp}(\omega) \qquad (2.13b)$$

$I_{\parallel}$ and $I_{\perp}$ are intensities for two geometries of the polarization of the light. In the 90° scattering geometry, $I_{\parallel}$ is measured when both the incident and the analysed scattered light are polarized in the vertical plane and $I_{\perp}$ is measured when the scattered light is analysed for polarization in the horizontal plane (Fig. 2.1). A notation widely used to describe the experiment of polarized Raman scattering from gases, liquids or clear oriented crystals consists of four letters which indicate from left to right: the direction of incident radiation,

incident polarization, scattered polarization and direction of observation respectively. For example, the usual conditions for measurement of $I_{\parallel}$ and $I_{\perp}$ in Fig. 2.1 are x(zz)y and x(zx)y.

Reduced procedures for Raman spectra have been proposed to provide the necessary quantitative data treatment in the low frequency region [72,73]. The measured Raman intensity may be expressed as:

$$I(\omega) = C(\omega_0 - \omega_i)^4 \omega_i^{-1} B^{-1} S_i \qquad (2.14)$$

C is a constant which depends on the instrument response, slit width, solid collection angle and absorption due to colour. ω_0 is the frequency of the incident light, ω_i is the frequency difference of the scattered light (Raman shifts), B is a temperature factor for which the Boltzmann distribution gives a good approximation:

$$B = 1 - \exp(-h\omega_i c/kT) \qquad (2.15)$$

and S_i is the intrinsic molar scattering coefficient at frequency ω_i (Eq. 2.14) and is related to the term $[45\bar{\alpha}^2 + 7\beta^2]$ in Eq. (2.12) with:

$$S_i = \left(\frac{\partial \tilde{\alpha}}{\partial Q_i}\right)^2 \qquad (2.16)$$

The reduced function is defined as:

$$R(\omega_i) = I(\omega_i)(\omega_0 - \omega_i)^{-4} \omega_i B = CS_i \qquad (2.17)$$

As shown in Eqs. (2.14) and (2.17), the temperature and frequency dependent terms can

be removed from the experimentally measured intensity so that the reduced spectrum is directly proportional to the intrinsic molar scattering coefficient.

Application of the reduction procedure to $I_{\parallel}$ and $I_{\perp}$ respectively gives $R_{\parallel}$ and $R_{\perp}$ and the isotropic reduced spectra $R_{\alpha}(\omega)$ or R_{iso} may be obtained as for Eq. (2.13):

$$R_{iso} = R_{\parallel} - \frac{4}{3}R_{\perp} \qquad (2.18)$$

Raman spectra may be presented in either the I or R format. The R format is most useful in the low frequency region.

The $I_{\alpha}(\omega)$ Raman spectrum depends on vibrational motion only, while $I_{\beta}(\omega)$ depends on both vibrational and reorientational motions of the molecule. Quantitative analysis of I_{α} and I_{β} may give detailed information about vibrational and reorientational relaxation. This is done through time correlation functions [71,72]. Correlation functions provide a concise method of expressing the degree to which dynamical properties are correlated as a function of time.

The vibration correlation function $G_v(t)$ can be obtained from the Fourier transformation of the normalized isotropic Raman profile:

$$G_{iso} = G_v(t) = \int I_{\alpha}(\omega)\exp(-i\omega t)d\omega \qquad (2.19)$$

Here ω is the frequency measured from the band centre ω_0. $G_v(t)$ is a direct probe of vibrational dephasing.

The Raman correlation function G_{2R} may be obtained by deconvolution of the vibration contribution with the G_{aniso} function:

$$G_{aniso} = G_v(t) \cdot G_{2R}(t) = \int I_\beta(\omega) \exp(i\omega t)\, d\omega \qquad (2.20)$$

Assuming that the band profile has a Lorentzian shape, the correlation function will decay exponentially with time:

$$G(t) = A \exp(-\frac{t}{\tau}) \qquad (2.21)$$

The correlation time which is defined as:

$$\tau = \int_{-\infty}^{\infty} G(t)dt \qquad (2.22)$$

will have a simple relationship to the full width at half height Γ (in cm^{-1}):

$$\Gamma^{-1} = \pi c \tau \qquad (2.23)$$

Then the vibrational and reorientational relaxation time τ_v and τ_R can be determined from the half widths of the isotropic spectra:

$$\tau_v^{-1} = \pi c \Gamma_{iso}$$

$$\tau_R^{-1} = \pi c (\Gamma_{aniso} - \Gamma_{iso}) \qquad (2.24)$$

2.1.2 Molecular Vibrations in Condensed Matter

Ordered crystals

Many of the principles described above for isolated molecules apply to crystals. However, since the molecules are fixed in a lattice, the vibrational spectrum of a crystal differs from that of the free molecule. The frequencies due to external rotatory and translatory lattice modes appear at low wavenumbers. In addition, the selection rules are affected by the crystal symmetry as well as the molecular symmetry.

Crystals are characterized by long range order: a large number of repeat units (primitive unit cell) related by translation symmetry. The combination of the translational operations with rotational operations creates the 230 "three-dimensional" space groups. All crystalline materials have a structure which belongs to one of these groups. Translation symmetry makes it possible to factor vibrations in the crystal by the wave vector **k** which is defined as:

$$\mathbf{k} = 2\pi/\lambda$$

where λ is the wavelength of the crystal wave motions and corresponds to the distance over which motions of atoms are in phase.

If in the crystal there are N unit cells, each of which contains n atoms, then there will be 3nN normal modes in all. In these modes there are N factors, each corresponding to one of the allowed values of **k**.

It has been found that symmetry coordinates defined by **k** and $\mathbf{k} + \bar{\mathbf{k}}$, where $\bar{\mathbf{k}}$ is a vector of the reciprocal lattice, are identical, and that symmetry coordinates defined by **k** and **-k** are degenerate. The problem is thus reduced to the choice of the primitive unit cell in **k**-

space. Vibrational analysis of a crystal is based on one primitive cell which has all the distinctive features of the structure. Because the dimensions of a unit cell are small compared with the wavelengths of the radiation used in vibrational spectroscopy, all unit cells can be considered as experiencing the same electric field, i.e., only $\mathbf{k} \approx 0$ wavevector phonons scatter light. For the approximation of $\mathbf{k} \approx 0$ and first order spectra, group theory provides a simple and quick approach to deduce the selection rules for crystals.

The symmetry of the unit cell is called the factor group, which is the subgroup of the corresponding space group with the translations between unit cells considered as identity operations. The distribution of normal modes for the crystal can be established by factor group analysis. This procedure is similar to that used to deduce the selection rules for isolated molecules but includes the screw axis and glide plane symmetry operations [75]. The symmetry properties are determined by studying the effect of each symmetry operation in the factor group on each type of atom in the unit cell.

A more convenient procedure is the correlation method [76]. This method is based on an analysis of the symmetry and the number of atoms, molecules or ionic groups in the primitive unit cell. The number of equivalent atoms in the unit cell determines which set of sites the atoms occupy. The set of sites has its own symmetry and is called the site group (site symmetry), which is a subgroup of the factor group of the crystal. The site symmetry may be ascertained from crystallographic data or the site symmetry table [77]. In this technique the symmetry properties are determined first for atomic or molecular groups of interest as isolated species. These results are then analysed (or correlated) to species of the site symmetry and finally to species of the factor group symmetry. Infrared and Raman activities are predicted

from the symmetry species of the factor group. For crystals containing molecular groups, the correlation method has the advantage of mapping the effects of the static field and the correlation field on the free ion spectrum. This results in the separation of modes into internal and external modes. Internal modes of molecular species have a stationary centre of mass while external modes involve relative motion of the mass centres of atoms (translatory) or molecular groups (translatory and rotatory).

Molecules are fixed in the crystal. Polarized light may be employed to excite certain particular modes in clear, oriented single crystals. Polarized infrared radiation with its electric vector along the x, y or z axis will activate vibrations that change the dipole moment in the same direction, thus differentiating differently polarized modes.

Polarized Raman spectra of single crystals are more common and more information about the symmetry properties of the normal modes may be obtained, because there are six polarizability components (α_{xx}, α_{yy}, α_{zz}, α_{xy}, α_{yz}, α_{zx}) associated with normal modes, the excitation geometries are flexible and it is easer to sample. By deliberate arrangement of the light path only those modes linked with a unique polarizability component change can be measured in the Raman spectrum.

For nonlinear (piezoelectric) crystals the polar modes (IR active modes) may undergo TO-LO splittings. In the crystal, atoms move against each other with wavelike disturbances that propagate at the speed of light (phonons). There are two kinds of the optical modes: longitudinal (the atomic displacements are along the propagation direction) and transverse (the atom displacements are normal to the propagation direction). Polar modes carry an electric dipole moment. The oscillating dipole generates a local polarization which in turn

generates a macroscopic electric field. The long range dipole-dipole interaction couples similar transition moments throughout the crystal. As a result, polar mode frequencies depend on the orientation and magnitude of the wave vectors of the phonon relative to electric field. TO-LO splittings occur because the induced electric field reinforces the effect of the ionic displacement for longitudinal modes but has zero effect on the transverse modes. The magnitude of the splitting is given by the Lyddane-Sachs-Teller relation [78]:

$$\omega_l / \omega_t = \sqrt{\epsilon_0 / \epsilon_\infty} \qquad (2.25)$$

Where ω_t is the frequency of the transverse mode, ω_l is the frequency of the longitudinal mode, ε_0 is the static dielectric constant and ε_∞ is the dielectric constant at high frequency. Since $\varepsilon_0 > \varepsilon_\infty$, so $\omega_l > \omega_t$. TO-LO splitting may be observed in Raman spectra for modes which are simultaneously active in the infrared. This can only occur for noncentric crystals and provides a convenient technique for identification of non-linear crystals.

Disorder in crystals

The above discussion is based on the assumption of perfect order in the crystal, i.e., the complete invariance of the structure under all symmetry operations of the space group. In fact most crystals have imperfections which can lead to different degrees of disorder. In addition to defects, dislocations and grain boundaries which are mostly packing irregularities, there are intrinsic chemical problems. Few crystals like NaF have long phonon mean-free-paths because they are isotopically pure and do not have easily substituted look-alike ions of the same

charge and size. For molecules or ions with isotopic variations due to natural isotope distribution, the vibrational modes will have different frequencies in accord with $(1/\mu)^{1/2}$ and may decouple from the main lattice frequencies.

The lattice modes of a crystal at 0 K will correspond to ground state vibrations but when the crystals are warmed there will be vibrational modes associated with excited vibrational states. Hot bands become common even at room temperature. The anharmonicity and increased thermal amplitudes of vibrations associated with the hot bands will lead to crystal expansion and greater freedom of movement. Increased rotational degrees of freedom often lead to positional disorder. The oxygen atoms become disordered in high temperature nitrate solids. This is just a partial disorder because the metal ions and the nitrogen atoms remain on the crystal sites with long range order. In the X-ray analysis of $NaNO_3$ the reflections from the O planes go to zero intensity but the reflections from K and N planes remain [79]. Such thermal disorder was observed in the Raman spectra of KNO_3 and $NaNO_3$ as an anomalous component in the symmetric stretching region [55].

The vibrational spectrum of a crystal will be modified by small changes in the crystal structure owing to impurity ions. In isomorphic substitution, the intruding ions (guest) are of a similar size and charge to the substituted ions (host) and a solid solution is formed. In the solid solution the foreign ion randomly substitutes in the crystal. Each equipoint can be considered as occupied by an average atom whose mass, X-ray scattering factor, and force constants are weighted averages of the host and guest atoms. There is no change in the space group and therefore no change in the number of infrared or Raman bands. For instance a considerable mole fraction of rubidium can occupy potassium sites in KNO_3 but the crystal

structure of KNO_3 remains unchanged [80]. The X-ray diffraction pattern of KNO_3 does not change while the lattice parameters shift proportionally with the amount of the guest rubidium ion.

Frequency shifts in the vibrational spectra of substitutional solid solutions are more complicated than in the case of isotopic substitution since there are changes in force constants due to changes in lattice parameters as well as the change in mass. For the simple case where all the chemical bonds between the atoms are of equal strength, the interatomic potentials may be approximated by the Born potential for ionic lattice:

$$\phi = \frac{N\alpha Z_+ Z_- e^2}{r}\left(1 - \frac{1}{n}\right) \qquad (2.26)$$

N is the number of primitive unit cells in the crystal, α is the Madelung constant, Z_+ and Z_- are charges of the cations and anions respectively, n is the Born exponent and r is the equilibrium interatomic distance.

There are two force constants associated with each pair of atoms. The radial force constant K_r acts along the separation distance and is related to the interatomic potential ϕ by:

$$K_r = \frac{\partial^2 \phi}{\partial r^2} = \frac{N\alpha Z_+ Z_- e^2}{r^3}\left(1 - \frac{1}{n}\right) \qquad (2.27)$$

The tangential force constant K_t acts perpendicularly to the separation distance and is related to the interatomic potential by:

$$K_t = \frac{1}{r} \cdot \frac{\partial \phi}{\partial r} \tag{2.28}$$

The first derivative of the lattice energy at equilibrium is zero and so is K_t.

In the harmonic approximation the frequency is related to the force constant and the reduced mass μ of the oscillator by:

$$\nu = A\sqrt{\frac{K_r}{\mu}} \tag{2.29}$$

Combining Eqs. (2.27) and (2.29), we have:

$$\nu = B\sqrt{\frac{1}{r^3\mu}} \tag{2.30}$$

Where A and B are constants. This equation correlates the frequency shifts to changes in lattice parameters due to ion substitution. It may be applied in the case of the translatory motions of the atoms against each other.

As the difference between the guest ion and the host ion increases, the crystal may become unstable with respect to phase separation. Like atoms will be enriched in certain volumes of the crystal separated by regions enriched in the other kind of atoms. If the scale of the separated phases is large, the measured spectra will be merely a superposition of the spectra of the individual phases (mechanical mixtures). However, for phase separation on a microscopic or submicroscopic scale, changes in spectra may still be observed. Lamellar structures on a scale of tens to hundred of nanometers may cause the crystal vibrations to

depart from those predicted for a model based on infinite repetition of the unit cell. The infrared spectrum is influenced mainly by short-range order and is relatively insensitive to long-range order. The Raman spectrum, on the other hand, is more sensitive to intermediate or long range order. Our Raman studies (Chapters 5 and 6) suggest that a new disordered state exists in $NaNO_3$-KNO_3 which is caused by phase separation on a microscopic or submicroscopic scale.

Glasses

Glasses differ from crystals in that the former do not have long range order. Consequently, the rigorous theory based on the analysis of one definite size unit cell in the crystal is no longer valid for glasses. Glasses may be considered to have such a large unit cell (containing ~ 10^{23} atoms) that they cannot have a well defined **k** vector. Because of the disorder broadening, directional averaging, and large number of phonon branches, it is impossible to define these branches experimentally as in the case of crystals. One measures the vibrational density of states, i.e., the number of oscillators with a given frequency in a given volume element.

Glasses give spectra very similar to the liquid from which they are formed because the glass and liquid have the same distribution of atomic positions. In contrast, there are distinct differences between the Raman spectra of the glassy and crystalline state of the same material. The spectra of glasses usually exhibit weak broad Raman bands with no fine structures.

2.2 Thermodynamic Consideration of Binary Nitrate Solid Solutions

A combination of thermodynamic and microstructural characterization of solids of the same thermal history may be fruitful. The systematic variation of thermodynamic properties with chemical compositions may help to judge on an atomic basis the reasons for the stability of a given structure. Usually four structures may exist for a binary nitrate: a real crystal with a new structure; a single crystal with the host structure (solid solution); a disordered solid; and a glass. Among these structures the thermodynamics of solid solution formation has been studied most systematically. An energetic analysis of the various contributions from the mixing of the components with different volumes and crystal structures lays the foundation for a quantitative treatment of solid solutions.

A solid solution in a binary nitrate system is stable thermodynamically only if its free energy is less than that of an equivalent mechanical mixture of its components or any other possible exsolution products.

For the formation of the solid solution $A_{1-x}B_xNO_3$:

$$(1 - x) ANO_3 + x\, BNO_3 \rightarrow A_{1-x}B_xNO_3$$

the free energy change ΔG^{ss} is composed of two terms:

$$\Delta G^{ss} = \Delta H^{ss} - T\Delta S^{ss} \qquad (2.31)$$

The entropy change ΔS^{ss} is generally positive. For random substitution it can be expressed by:

$$\Delta S^{ss} = -R[x\ln x + (1-x)\ln(1-x)] \qquad (2.32)$$

x is the mole fraction of one component.

If the enthalpy ΔH^{ss} is zero, the solution is ideal. However, the formation of a solid solution from two ionic salts (as in the case of $A_{1-x}B_xNO_3$) usually involve a positive excess enthalpy, indicating an energetically unfavourable situation.

Regular or subregular solution models have been used to account for the positive enthalpy [81]. A regular solution is assumed to have the ideal mixing entropy of a random distribution (Eq. (2.32)). The heat of mixing of a binary regular solid solution may be expressed as:

$$\Delta H^{ss} = Wx(1-x) \tag{2.33}$$

Here W is the interaction parameter which is a measure of the effects of the structural features of the end members on the solid solution formation. The above equation holds for solutions with symmetric behaviour. Otherwise, a two-parameter subregular solution may be used:

$$\Delta H^{ss} = x(1-x)[W_1x + W_2(1-x)] \tag{2.34}$$

The nitrates studied in this work may be regarded as isostructural systems at solidified temperatures (see Chapter 1). For such systems four effects determine the range and stability of the solid solution: the size difference of the ions or atoms, the charges of the ions, the difference in the bonding character of the two compounds and the electron configuration. The first two factors are the most important. They have formed the basis of most theoretical models for calculation of the interaction parameter W.

According to the Born theory of ionic lattice, the electrostatic energy of the crystal

lattice may be expressed as:

$$U = -M/d \tag{2.35}$$

M is a constant determined by the crystal structure and d is the distance from any ion to the nearest neighbour. Assuming that the dominant term in ΔH^{xs} is the lattice energy change and that the coordination number does not change on mixing, the following relationship between W and the size difference has been deduced [53]:

$$W = U[(d_1 - d_2)/(d_1 + d_2)]^2 \equiv U\delta^2 \tag{2.36}$$

Where d_1 and d_2 are lattice parameters of the pure components. The equation is valid in the case of complete miscibility and where Vegard's law (the lattice parameters change linearly with composition in the solid solution) is valid.

This model successfully gives a quantitative account for the observed trend in the solubility of alkali halide solid solutions. For $\delta < 8\%$ complete miscibility at room temperature was predicted. For larger δ the predicted critical mixing temperature is in accord with the experimental data obtained at that time.

It was noted that the radius difference was not always an adequate criterion for the formation of solid solutions even in the simplest binary mixtures of alkali metal halides [82]. The relative differences of lattice energies (ΔU) and polarization coefficients of cations (ω) were suggested as a more sensitive criterion for binary systems with a common anion:

$$\Delta U = \frac{U_2 - U_1}{U_2} \times 100$$
$$\omega = \frac{\alpha_2 - \alpha_1}{\alpha_2} \times 100 \qquad (2.37)$$

α_1 and α_2 are polarization coefficients of the smaller and larger cations respectively. The relative difference in the radii of Na^+ and K^+ is as large as 26.3%. However the $NaNO_3$-KNO_3 system is still considered to form a continuous series of solid solutions [4]. This was attributed to the similarity in the lattice energies of $NaNO_3$ and KNO_3 [82].

It was also pointed out that there was some difficulty in applying Eq. (2.36) to more complicated binary systems [83]. The arbitrariness of the assignment of an ionic radius was noted. In addition, the mixed species may only occupy a small fraction of the total volume.

A term representing the difference in molar volume between the two end members was suggested to correlate with the thermodynamic mixing parameters W_1 and W_2 or W. The volume mismach was defined as:

$$\Delta V_1 = \frac{V_2 - V_1}{V_2} \quad \text{and} \quad \Delta V_2 = \frac{V_2 - V_1}{V_1}$$
$$\text{or:} \qquad \Delta V = \frac{V_2 - V_1}{V_{\bar{12}}} \qquad (2.38)$$

Here V_1, V_2 and $V_{\bar{12}}$ are the molar volumes of the small component, the larger component and the mean of the two respectively. ΔV_1 is associated with W_1, ΔV_2 is associated with W_2

and ΔV is associated with W. A plot of W (W_1, W_2) versus ΔV (ΔV_1, ΔV_2) for several rock salt alkali halides shows a quadratic relationship:

$$W = 124.6(\Delta V)^2 + 10.9(\Delta V) \qquad \text{(kJ/mol)} \tag{2.39}$$

Such correlations were believed to be valid for a wide range of binary systems with similar structures and charges, regardless of the type of cation or anion. They have been used with success to predict solid solubility, deviation from ideality and the energetics of phase transitions for oxide, chalcogenide and alkali halide systems.

The correlation for alkali halides was used to calculate the solid solubility in the binary nitrate systems in this work. The molar volumes were computed from the crystallographic data of the nitrates [21]. Except for $CsNO_3$ which has no rhombohedral structure at atmospheric pressure, all calculations were based on the structure of $LiNO_3$. For $CsNO_3$ the molar volume of the high temperature Pa3 structure was first obtained. Then it was used to deduce the molar volume of the rhombohedral structure (Table 2.1).

Subregular mixing parameters W_1 and W_2 were calculated for the binary systems $LiNO_3$-MNO_3 and KNO_3-MNO_3, here M represents the other alkali metals. From W_1 and W_2 the critical mixing temperature T_c and composition x_{1c} (or x_{2c}) can be calculated by:

$$RT_c = 2x_{1c}A - 2x_{1c}^2B + 6x_{1c}^3C \tag{2.40}$$

$$x_{1c} = 1 - x_{2c} = \frac{B \pm \sqrt{B^2 - 9AC}}{9C} \tag{2.41}$$

Here:

$$A = 2W_1 - W_2$$
$$B = 5W_1 - 4W_2 \qquad (2.42)$$
$$C = W_1 - W_2$$

For regular solutions the following relationship holds:

$$x_{1c} = x_{2c} = 0.5$$
$$RT_c = 0.5W \qquad (2.43)$$

The calculations are only a first order approximation. They cannot predict the formation of solid solutions in binary nitrates quantitatively. However, the calculations do suggest the general tendency of solid solution formation in alkali metal nitrates. As shown in Tables 2.2 and 2.3, it is very difficult for lithium nitrate to form solid solutions with other alkali metal nitrates. All the systems containing lithium nitrate have critical temperatures higher than the melting temperature. Except for $LiNO_3$-$NaNO_3$, the binary systems of the other alkali metal nitrates with lithium nitrate have incredibly high critical temperatures. Other processes may occur besides the random mixing for the systems with large size differences. If the attractions between ions are sufficiently different, ordering may take place and complexes result. The fact that potassium nitrate, rubidium nitrate and cesium nitrate form congruently melting compounds with lithium nitrate is consistent with the above theoretical treatment.

The systems containing potassium nitrate may form solid solutions with other alkali metal nitrates but not lithium nitrate. The KNO_3-$RbNO_3$ system has a critical temperature

much lower than room temperature but it forms continuous solid solutions at high temperature. Cesium nitrate is generally believed to form limited solid solutions with potassium nitrate. The solubility would be greater than that of sodium nitrate in potassium nitrate if cesium nitrate had the same structure as potassium nitrate. The $NaNO_3$-KNO_3 system has a critical temperature higher than the melting point of sodium nitrate. It should be difficult for these two nitrates to form solid solutions. Recent studies [4,66] suggested that $NaNO_3$-KNO_3 can form solid solutions at relatively low temperature with comparable amounts of both nitrates. This concept is questionable.

Eq. (2.34) for subregular solutions expresses the energetic asymmetry in a binary system with size difference in cations or anions. The asymmetry parameter η is defined as:

$$\eta = \frac{W_1}{W_2} = \left[\frac{R_2}{R_1}\right]^2 \tag{2.44}$$

This relationship shows that it is energetically favourable for a larger ion to be replaced by a smaller one, but it is much more difficult to replace a small ion by a large one. Application of Eq. (2.41) to predict the solubility of an asymmetric binary system revealed the same trend in solubility [85]. The calculated mole fractions for the smaller cations (x_{1c}) are greater than 0.5.

In deducing Eqs. (2.34) and (2.44), spherical ions were assumed or implied. There was satisfactory agreement between the theoretical predictions and experimental observations for alkali halides, rock salt oxides, chalcogenides, tungstates and molybdates [83,84]. In all these systems the ions may be safely regarded as spheres. However, care must be taken when the

theory is applied to nitrates because the nitrate ion is definitely not spherical. In formation of solid solutions of nitrates the shape and orientation of the nitrate groups must be taken into consideration. A new theory (or a modification of the present ones) is needed to account for the abnormal observation [67] that the larger Rb^+ dissolves much more readily in KNO_3 than the smaller K^+ in $RbNO_3$.

The above theories dealt with solid solutions of isostructural systems. When the crystal structures of the end members are different, an additional term has been suggested [85] to account for the contribution of the phase transition enthalpy to the mixing enthalpy in Eq. (2.34):

$$(\Delta H^{ss})' = \Delta H^{ss} + x_2 \Delta H_{tr} \qquad (2.45)$$

$(\Delta H^{ss})'$ is the mixing enthalpy of the solids with different structures. ΔH^{ss} is the mixing enthalpy of the solids when both have the structure of component 1. ΔH_{tr} is the enthalpy of phase transition of component 2 to the structure of component 1. It was assumed that component 2 must undergo the phase transition before it can dissolve in component 1. The extra enthalpy $x_2 \Delta H_{tr}$ makes it unfavourable for nonisostructural salts to form solid solutions. Usually only mutually terminal solubility occurs in such systems. Identical structures were assumed to be a necessary requirement for the formation of a continuous series of solid solutions [66]. However, this is not always the case. Complete miscibility occurs between high temperature phases of potassium nitrate and rubidium nitrate, although the crystal structure of KNO_3 I is $R\bar{3}m$ and that of $RbNO_3$ I is $Fm3m$ [17,22]. One of the explanations may be that ΔH_{tr} for the transition of rubidium nitrate from Fm3m structure to $R\bar{3}m$ structure is very

small (Chapter 4). It was noted [67] that the heat for the transitions of $RbNO_3$ from phase III to II and from phase II to I was very small when the composition of KNO_3 was more than 10 mol%.

The theory of solid solutions of inorganic compounds has not been fully developed. Most of the rules and generalizations are based on investigations of the simple halide or oxide salts which may be safely regarded as consisting of spherical ions. In general these generalities can be applied to nitrates [82]. Since the nitrate ions are oblate in the crystals, it would not be a surprise if deviations are found. There seems to be a need to develop a theory which will account for the shapes of inorganic ions. The theory of the mixed crystals of organic molecules has made some success in this respect [86]. Alkali metal nitrates are the simplest ionic crystals with nonspherical ions. A systematic study of the solid solutions of the salts may help the development of the theory of solid solutions.

2.3 A Brief Description of the Structural Chemistry of Alkali Metal Nitrates

Alkali metal nitrates show interesting changes in crystal structures and phase transitions and in some of the physical properties such as molar volumes, melting points and solubilities in water. These changes can be explained by the structure of the nitrate ion and the gradual increase in the radius of the cations.

The structures and the numbers of phase transitions of alkali metal nitrates are a function of the radii of the cations [87]. The smaller ions Li^+ (69 pm) and Na^+ (98 pm) adopt the calcite structure ($R\bar{3}c$) at room temperature. The larger ions Rb^+ (148 pm) and Cs^+ (167

pm) adopt the trigonal structure ($P3_1$). The potassium ion as the intermediate of the series has a unique orthorhombic structure, Pmcn, at room temperature. As the temperature is raised, $LiNO_3$ remains unchanged. $NaNO_3$ and KNO_3 (and perhaps $RbNO_3$) transform to the disordered calcite structure, $R\bar{3}m$, and $RbNO_3$ and $CsNO_3$ transform to the cubic structure, Pm3m. Potassium nitrate has one additional transition which can only be achieved by cooling phase I and rubidium nitrate has two additional transitions.

The unique structure of potassium nitrate at room temperature and the extra transitions for potassium nitrate and rubidium nitrate are consistent with the fact that the sizes of K^+ and Rb^+ lie between those of the cations in the two structures of $LiNO_3$ and $CsNO_3$ and that nitrate ions have triangular planar shape with strong orientational preference. Lu and co-workers [88] found that an approach which worked well for highly symmetric molecular ions SeO_4^{2-} or SO_4^{2-} was not very good for NO_3^-. The calculated structures of potassium nitrate had a much shorter c axis due to the planarity of the nitrate ions. In crystals, nitrate groups usually form planes between which the cations are located and the different structures or phase transitions mainly involve orientational disorder of the nitrate ions in the plane and /or positional shift of the cations [22,89].. The transition of KNO_3 II to KNO_3 I involves a complete rearrangement of the cation and anion positions. The transition is not directly reversible. When KNO_3 I is cooled from 433 K or above, a new phase III is formed. Phase III and I are closely related and the transition between them is completely reversible and involves an order-disorder process of orientation-switching of the nitrate ions and a positional adjustment of the potassium ions. The transition between phase III and I is similar to the transition between

phase II and I of $NaNO_3$. The intermediate phase III of KNO_3 may serve as an indication that there is a tendency to retain the calcite structure. The large potassium ion forces the crystal to have another structure when the temperature is lower than 383 K. The lattice is a little strained since the transition from R3m to Pmcn is accompanied by a volume increase.

The rubidium ion can be accommodated in the $CsNO_3$ structure, although $RbNO_3$ has a tendency to adopt the structures suitable for the smaller ions, as is illustrated by the two additional transitions at high temperature. This is supported by the following experimental observations. (a) Most of the recent studies on the structural phase transitions of $RbNO_3$ showed that the experimental data (neutron, X-ray, dilatometry) could best be explained by assuming that the transition of $RbNO_3$ III to $RbNO_3$ II involved a change in structure from cubic (Pm3m) to rhombohedral ($R\bar{3}m$)[22,90,91]. (b) Rubidium nitrate was found to form continuous solid solutions with potassium nitrate which indicated readiness for $RbNO_3$ to have the KNO_3 I structure at high temperature. (c) The disappearance of the transitions of the high temperature phases $RbNO_3$ I and $RbNO_3$ II in the mixtures of KNO_3-$RbNO_3$ may also be due to changes in the structure [67].

The changes in the physical properties in the series of alkali metal nitrates also suggest that KNO_3 and $RbNO_3$ occupy an intermediate state between one stable structure of nitrate and another (Table 2.4). There is a general increase in the molar volumes as the radii of the cations increase from Li^+ to Cs^+. The increase is not smooth. From $NaNO_3$ ($R\bar{3}c$) to KNO_3 (Pmcn) the volume jumps by 10 cm^3/mol while from KNO_3 (Pmcn) to $RbNO_3$ ($P3_1$) the volume shrinks although Rb^+ is larger than K^+. Obviously the arrangement of the nitrate ions in the crystal KNO_3 II cannot be regarded as a close packing of spheres [87]. Otherwise there

would have been a smooth increase in molar volumes from $NaNO_3$ through KNO_3 to $RbNO_3$.

The extraordinarily large molar volume of KNO_3 II means that there is room to accommodate larger ions. It also means that if ions smaller than K^+ entered into the crystal, the structure would become unstable and a change would take place. It may be impossible to change the size of the potassium ion itself; however, a similar situation may be created by partly substituting potassium ions with larger or smaller ions. The KNO_3-$RbNO_3$ and $NaNO_3$-KNO_3 would be suitable systems.

The change in melting points (Table 2.4) also reveals abnormalities around KNO_3 and $RbNO_3$. The melting points increase gradually from 537 K of $LiNO_3$ to 607 K of KNO_3, it drops to 583 K for $RbNO_3$ and rises again dramatically to 687 K for $CsNO_3$.

The melting process is complicated because it involves the structures of both solid and liquid. The enthalpy of fusion ΔH_m may be expressed as [92]:

$$\Delta H_m = T_m \Delta S_m \qquad (2.46)$$

ΔS_m is the entropy of fusion. Fusion is associated with positional randomization and orientational randomization. For compounds of similar structure, ΔH_m may be regarded as a measure of the bond strength of the crystal before melting.

Near the melting point, $RbNO_3$ has a lattice structure similar to the high temperature phases of $NaNO_3$ and KNO_3, as discussed above. Thus, $LiNO_3$ through $RbNO_3$ have similar solid structures. The enthalpy of fusion decreases gradually from $LiNO_3$ to $RbNO_3$ and the

lattice energy decreases as the radius of the cation increases. The low melting point of $LiNO_3$ is mainly due to the high entropy of fusion. $LiNO_3$ maintains the ordered calcite structure up to the melting point, while $NaNO_3$ and KNO_3 transform to the disordered calcite structure before melting. $RbNO_3$ has the lowest entropy of fusion, indicating a disordered solid state similar to the melt. It was noted [93] that $RbNO_3$ had a negative volume change on melting. The large rubidium ions greatly distort the calcite structure and can hardly hold the framework together. So the low melting point of $RbNO_3$ is mainly due to the low enthalpy of fusion.

Cesium nitrate has an entropy of fusion comparable to that of KNO_3. However, the enthalpy of fusion is larger. This accounts for the dramatic rise in the melting point. $CsNO_3$ has a different structure. The framework of nitrate ions in $CsNO_3$ can easily accommodate the large cation. The lattice energy of $CsNO_3$ is larger than that of KNO_3, although the larger cesium ion has less favourable electrostatic attraction.

In general the solubilities in water of alkali metal nitrates decrease as the radii of the cations increase (Table 2.4) and again the general trend is interrupted at $RbNO_3$. $RbNO_3$ can dissolve in water more than either KNO_3 or $CsNO_3$ can. The situation is complicated because it is necessary to consider the structure of solid and liquid, and solvation of the ions. Nevertheless the larger solubility of $RbNO_3$ can at least partly be attributed to the smaller lattice energy resulting from the strained structure.

Changes in the structures and physical properties pertaining directly to the structure with the size of the cations indicate that the crystal structures of alkali metal nitrates can be best understood if the nitrate ion is regarded as a nonspherical group with strong orientation. The

nonspherical nitrate ions form a planar framework in the crystals. The framework of the $LiNO_3$ structure type is stable for smaller cations and the framework of the $CsNO_3$ structure type is stable for larger cations. There is strain in the lattices of KNO_3 and $RbNO_3$ because the intermediate size of K^+ or Rb^+ does not quite fit either framework.

Table 2.1 Molar volumes of the nitrates (in cm^3 /mol) [a].

$AgNO_3$ (423 K)	$LiNO_3$ (524 K)	$NaNO_3$ (548 K)	KNO_3 (401 K)	$RbNO_3$ (523 K)	$CsNO_3$ (> 434 K)
39.240	30.279	39.229	49.276	55.947	60.683

a. Calculated for unit cell volumes in the high temperature disordered phase $R\bar{3}m$.

Table 2.2 Calculated critical temperatures and compositions of mixing for binary nitrate systems $LiNO_3$-MNO_3.

MNO_3	ΔV_1	ΔV_2	ΔR [a] (%)	W_1 (kJ)	W_2 (kJ)	T_c (K)	x_{1c}
$NaNO_3$	0.2281	0.2955	30.6	8.969	14.1	759	0.632
KNO_3	0.3856	0.6275	48.8	22.73	55.90	2996	0.686
$RbNO_3$	0.4588	0.8476	54.4	31.23	98.75	5330	0.701
$CsNO_3$	0.5010	1.004	62.4	36.74	136.54	7406	0.708

a The relative percentage differences in the cation radii from reference 81.

Table 2.3 Calculated critical temperatures and compositions of mixing for binary nitrates KNO_3-MNO_3.

MNO_3	ΔV_1	ΔV_2	ΔR [a] (%)	W_1 (kJ)	W_2 (kJ)	T_c (K)	x_{1c}
$LiNO_3$	0.3856	0.6275	48.8	22.73	55.90	2996	0.686
$NaNO_3$	0.2039	0.2561	26.3	7.403	10.97	593	0.620
$RbNO_3$	0.1192	0.1354	10.7	3.071	3.759	210	0.571
$CsNO_3$	0.1880	0.2315	19.6	6.452	9.200	500	0.612

a The relative percentage differences in the cation radii from reference 81.

Table 2.4 Some physicochemical properties of alkali metal nitrates.

MNO_3	V [a] (cm^3 /mol)	T_m [b] (K)	solubility [c] (mol/dm^3)	ΔS_m [d] (J/mol·K)	ΔH_m [e] (kJ/mol)
$LiNO_3$	29.0	537	10.2	49.0	26.3
$NaNO_3$	37.6	580	10.3	25.5	19.0
KNO_3	47.9	607	3.13	19.2	11.7
$RbNO_3$	47.5	583	3.58	9.2	5.4
$CsNO_3$	52.9	687	1.18	19.7-20.9	14.2

a. Molar volumes at 298 K from reference 93.

b. Melting points from reference 93.

c. Solubilities at 298 K from reference 94.

d. Entropy of fusion from reference 92.

e. Calculated enthalpy of fusion by Eq. (2.46).

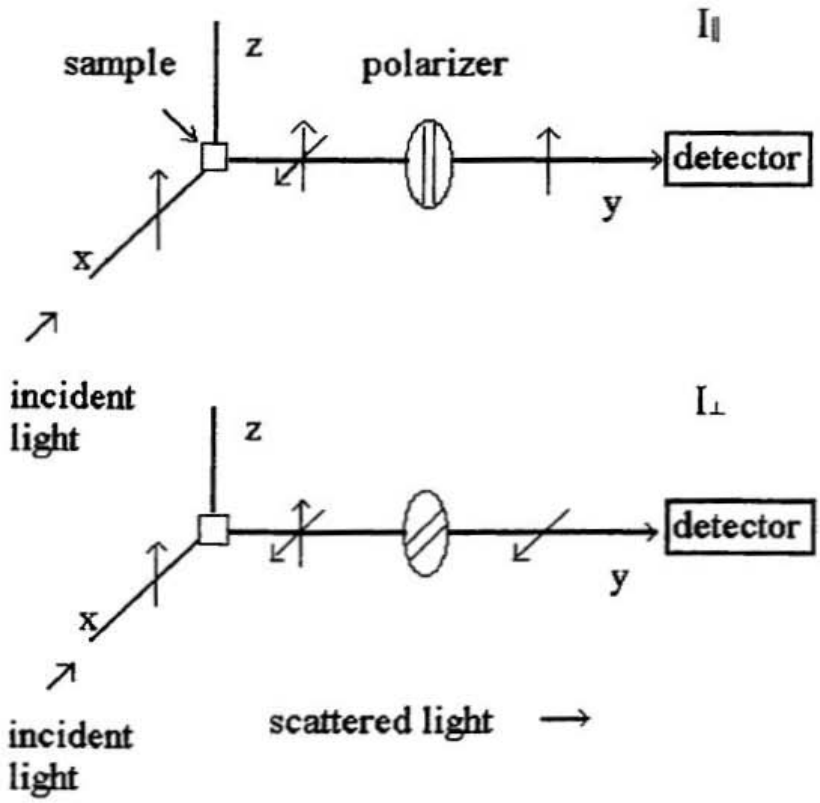

Fig. 2.1 Excitation and light-collection geometries for polarization measurements of Raman scattering.

CHAPTER 3

EXPERIMENTS

3.1 Preparation of Samples

All the chemicals were analytical grade reagents and were usually used without further purification since identical results were obtained with recrystallized solids.

3.1.1 The $LiNO_3$-MNO_3 Systems

The nitrates were dried in an oven at 393 K over night. The dried chemicals were handled in a dry nitrogen filled dry box which was dried by P_2O_5. The solids were weighed at definite ratios, mixed well in a mortar and transferred to 6 mm id quartz tubes. The mixtures were dried under vacuum for 72 hours, first at 333, then at 378, and finally at 403 K. Then the temperature was raised gradually until the nitrates melted completely. The samples of $LiNO_3$-$RbNO_3$ and $LiNO_3$-$CsNO_3$ were prepared by cooling the mixtures after 12 hours in the molten state. The samples of $LiNO_3$-KNO_3 were cooled under different conditions. The molten samples were left in the oven and cooled naturally as in the case of $LiNO_3$-$RbNO_3$. After the Raman measurements, the samples were reheated at 333 K for 24 hours and the Raman spectra were measured again. The quenched sample of equimolar $LiNO_3$-KNO_3 was obtained when the molten mixture was taken out of the oven and allowed to cool quickly without any

disturbance.

3.1.2 The $NaNO_3$-KNO_3 and KNO_3-$RbNO_3$ Systems

The nitrates were dried in an oven at 393 K for a day. The dried chemicals were weighted at definite ratios and mixed well. The mixtures of $NaNO_3$-KNO_3 were transferred to 6 mm id quartz tubes and the mixtures of KNO_3-$RbNO_3$ were transferred to 5 mm id Pyrex glass tubes. The mixtures were dried under vacuum at about 403 K for three days. Then the samples were melted and kept in molten state for about eight hours before sealing the tubes.

3.1.3 The $AgNO_3$-MNO_3 Systems

Crystals of the compounds $KAg(NO_3)_2$, $RbAg(NO_3)_2$ and $CsAg(NO_3)_2$ were prepared by slow evaporation in a desiccator of aqueous solutions of equimolar $AgNO_3$-MNO_3 (M = K, Rb, Cs). The preparation was performed in a darkened room.

3.2 Raman Spectroscopic Measurements

Raman spectra of the solids at room temperature were recorded on a Coderg PHO Raman spectrometer with the standard 90° scattering geometry. The 488.0 nm line of the argon ion laser was used as the source of excitation. The power level was about 300 mW except for $AgNO_3$-MNO_3 systems for which the power level was kept below 80 mW. The slits were set

at 2 cm^{-1} , the scanning rate was 50 cm^{-1} /min, and two data points per wavenumber were collected for all the measurements except for the ν_1 region. For studies of the ν_1 region the slits were 0.25 cm^{-1} , the scanning rate was 25 cm^{-1} /min and eight data points were collected per wavenumber. The scattering light was detected by a PMT cooled to 253 K. The signals in the form of photon counts were stored and processed with the MUN VAX 11/780 computer.

Raman spectra for the samples at different temperatures were obtained in an insulated furnace. The temperature was monitored with a chromal-alumel thermocouple. The temperature at the samples was accurate to about one degree.

A vacuum cryostat was used to obtain spectra at liquid nitrogen temperature.

CHAPTER 4

RAMAN SPECTROSCOPIC STUDIES OF THE SOLID SOLUTIONS OF POTASSIUM AND RUBIDIUM NITRATE

4.1 Introduction

Both potassium nitrate and rubidium nitrate can exist in several phases at atmospheric pressure and above room temperature [15,22]. Due to their special position in the series of alkali metal nitrates, KNO_3 and $RbNO_3$ have more alternative structures at atmospheric pressure [87]. Their structures represent the transition from the structure stable for small cations ($R\bar{3}c$) to the structure stable for large cations ($P3_1$). It seemed worth while to determine how the polymorphism of potassium nitrate and rubidium nitrate manifests itself in the mixed crystals. The dependence of the structure of the solid solution on the composition will shed light on the trend in the structural changes of alkali metal nitrates.

Two substitutional solid solutions have been reported [95,96] for solids grown from room temperature aqueous solutions of KNO_3 and $RbNO_3$ mixtures with variable concentrations. In the potassium rich solution the $K_{1-x}Rb_xNO_3$ crystal grows with the KNO_3 II structure (denoted as $K_{1-x}Rb_xNO_3$ (KII)) for x = 0 to 0.50 and in the rubidium rich solution the $K_{1-x}Rb_xNO_3$ crystal grows with the $RbNO_3$ IV structure (denoted as $K_{1-x}Rb_xNO_3$ (RbIV)) for x = 0.98 to 1.0. The two phase region was determined by solubility [95] and XRD [96] to extend

from 50 to 98 mol% $RbNO_3$. Similar solid-solid solubility was observed [67] for crystals grown from fused mixtures of KNO_3-$RbNO_3$. For up to 52 mol% $RbNO_3$ in KNO_3 only the diffraction pattern of KNO_3 II was detected. Electrical conductivity and X-ray measurements indicated [97] that as much as 4 mol% KNO_3 could dissolve in $RbNO_3$ IV at room temperature. For samples quenched from the melt or from the solid solution at temperature above 433 K, complications arose because of the formation of solids with the metastable KNO_3 III structure. The presence of the KNO_3 III structure was identified from the X-ray diffraction pattern, ferroelectric behaviour and marked volume changes [80].

Phase transition studies by thermal analysis [67,98] gave different results for the cooling and heating runs. When cooled from the melts, the transition of potassium nitrate from phase I to III was observed for mixtures up to 42 mol% $RbNO_3$ [98]. The two step transition I → III → II of potassium nitrate was observed only for mixtures containing up to 10 mol% $RbNO_3$. It was assumed that it was difficult for KNO_3 II to dissolve $RbNO_3$. However, the heating studies [67] indicated that the solubility of $RbNO_3$ in KNO_3 II was about 50 mol%. The solid solutions with 50 mol% $RbNO_3$ had only the transition of KNO_3 II to KNO_3 I. The sample containing 95 mol% $RbNO_3$ had only the three transitions of rubidium nitrate. Between 60 and 90 mol% $RbNO_3$ transitions of KNO_3 II to KNO_3 I and $RbNO_3$ IV to $RbNO_3$ III were observed while the other two transitions of rubidium nitrate were absent.

The binary system of potassium and rubidium nitrate is unusual and interesting because it is one of the few examples in which nonisostuctural components form a continuous series of solid solutions. It has been generally accepted [83] that isostructure was a necessary condition for complete miscibility between the end members. Solid solutions of KNO_3-$RbNO_3$

are also one of the few examples in which larger guest ions can replace many more smaller host ions than vice versa. The general rule [83] is that it is easier to put a smaller atom into a larger host lattice. The difference in solubilities is striking: larger rubidium ions can replace more than half of the smaller potassium ions in potassium nitrate while smaller potassium ions can only replace about 5 mol% rubidium ions. Finally, it was noted [67] that the two high temperature transitions of rubidium nitrate disappeared between 60 and 90 mol% $RbNO_3$ in the thermal analysis heating run. An independent study was suggested.

When rubidium ion is substituted for potassium ion in the crystals of potassium nitrate, the crystal structures of KNO_3 II and KNO_3 III remain unchanged even for high concentrations of rubidium ion. Chemical substitution of this kind may be used as an experimental technique for lattice dynamic studies. In the substitutional crystals rubidium ion will change the lattice parameters because the equipoint site is occupied by an average atom whose mass and force constants are the weighted average of rubidium and potassium atoms. Chemical substitution is more complicated than isotopic substitution in which only mass is changed. However, under favourable circumstances chemical substitution may be very helpful in band assignment. The KNO_3-$RbNO_3$ system seemed quite promising.

The present work was undertaken in an attempt to apply Raman spectroscopy of chemically substituted solids for lattice dynamic studies. Raman spectroscopy was also used to explain the phase diagram of KNO_3-$RbNO_3$ through a study of the structures of the solid solutions from fused mixtures of rubidium and potassium nitrate. The solid solutions were found to keep the main Raman features of the host crystal and the Raman bands due to the solute did not appear. The solid solubilities were determined by the first appearance of the

Raman bands due to the solute. Slight frequency shifts could be attributed to the changes in lattice constants due to the guest ions. The frequency shifts served as a sensitive probe for structural changes.

4.2 Raman Spectra of the Solid Solutions of KNO_3-$RbNO_3$

Potassium nitrate undergoes different phase transitions for heating and cooling processes and KNO_3 III may be kept in metastable state at room temperature if it is cooled fast enough. Thus, two kinds of samples were prepared. The quenched samples were obtained when the molten mixtures were taken out of the oven and cooled to room temperature quickly in the air. The annealed samples were obtained from the quenched samples (after Raman measurements) reheated to 403 K overnight and then cooled to room temperature very slowly (over about a 24 hours period).

Tables 4.1 and 4.2 summarize the main Raman features of the solids from the molten mixtures of KNO_3 and $RbNO_3$. The Raman spectrum of pure $RbNO_3$ was measured for comparison. The Raman data for KNO_3 II and KNO_3 III are taken from the work by Brooker [55,99]. There are distinct differences in the Raman spectra of the same sample with different thermal histories (Fig. 4.1). Raman data from the spectra of the quenched samples are collected in Table 4.1 and Raman data from the spectra of the annealed samples are collected in Table 4.2.

4.2.1 Raman Spectra of the Quenched Samples

The quenched samples with a content of rubidium nitrate up to 80 mol% have the typical Raman features of KNO_3 III, indicating the formation of $K_{1-x}Rb_xNO_3$ (KIII). The ν_1 vibration appears at about 1054 cm^{-1}. There is a single peak at 717 cm^{-1}. The Raman profile in the ν_3 region is in good agreement with the literature [55]. The antisymmetric stretching mode presents the typical transverse and longitudinal optic Raman features of KNO_3 III: a relative high and sharp peak at 1350 cm^{-1} (TO) and a lower and broad peak at 1440 cm^{-1} (LO). The band at about 1430 cm^{-1} is due to the $2\nu_4$ vibration. A single distinct band appears at 1664 cm^{-1} in the $2\nu_2$ region.

There is a small but unambiguous frequency shift in the internal vibrational region of the nitrate ion as the amount of $RbNO_3$ in the solid solutions increases. The ν_1 appears to shift to lower wavenumbers: from 1055 cm^{-1} for $K_{0.95}Rb_{0.05}NO_3$ (KIII) to 1052 cm^{-1} for $K_{0.20}Rb_{0.80}NO_3$ (KIII). The ν_3 vibration also shifts to lower frequencies and the TO-LO splitting seems to decrease a little: 1351 and 1442 cm^{-1} for $K_{0.95}Rb_{0.05}NO_3$ (KIII) and 1348 and 1435 cm^{-1} for $K_{0.20}Rb_{0.80}NO_3$ (KIII). It seems that as more potassium ions are replaced by rubidium ions, the lattice expands and there is a decrease in the strength of intermolecular coupling.

The expansion of the KNO_3 III structure due to the existence of larger rubidium ions is more obvious in the external vibrational region. There is only one strong peak at 125 cm^{-1} in this region for KNO_3 III. It is due to the rotatory motion of the nitrate ion in the crystal. The peak centred at 125 cm^{-1} for $K_{0.95}Rb_{0.05}NO_3$ (KIII) shifted to 116 cm^{-1} for $K_{0.20}Rb_{0.80}NO_3$ (KIII) (Fig. 4.2).

The sample with 95 mol% $RbNO_3$ presents an entirely different Raman pattern (Fig. 4.3). It has the characteristic Raman bands of $RbNO_3$ IV alone (Table 4.1), suggesting the formation of $K_{0.05}Rb_{0.95}NO_3$ (RbIV). There are two peaks instead of one in the external vibrational region: 61 and 110 cm^{-1}. The bands in the internal vibrational region also have different profiles and positions from those of $K_{1-x}Rb_xNO_3$ (KIII). The ν_1 vibration appears at 1057 cm^{-1} which is 5 cm^{-1} higher than would be expected if the sample were a solid solution with the KNO_3 III structure. The frequency of $2\nu_2$ at 1674 cm^{-1} is also higher than that of $K_{1-x}Rb_xNO_3$ (KIII) (1664 cm^{-1}). There are two distinct bands with very nearly the same intensity in the ν_4 region: 707 and 721 cm^{-1}. Three bands may be distinguished in the ν_3 region: 1349, 1410 and 1440 cm^{-1}. The profile is quite different from that of KNO_3 III. Compared with the bands of KNO_3 III in the same region, the band at 1349 cm^{-1} is flatter and broader and the band at 1440 cm^{-1} is not so distinct. The very broad feature centred at 1410 cm^{-1} has no corresponding band in KNO_3 III. The 5 mol% impurity of smaller potassium ion causes the external and ν_1 vibrations in $K_{0.05}Rb_{0.95}NO_3$ (RbIV) to shift to higher wavenumbers.

The Raman spectrum of $K_{0.10}Rb_{0.90}NO_3$ may be regarded as a mixture of those of $K_{1-x}Rb_xNO_3$ (KIII) and $K_{0.05}Rb_{0.95}NO_3$ (RbIV) (Table 4.1). There are two bands in the ν_1 and $2\nu_2$ regions. The stronger bands at 1056 and 1674 cm^{-1} are due to $K_{0.05}Rb_{0.95}NO_3$ (RbIV) and the weaker ones at 1049 and 1661 cm^{-1} are assigned to vibrations of $K_{1-x}Rb_xNO_3$ (KIII). The three bands in the ν_4 region may also be attributed to $K_{1-x}Rb_xNO_3$ (KIII) (714 cm^{-1}) and $K_{0.05}Rb_{0.95}NO_3$ (RbIV) (707 and 721 cm^{-1}). In the ν_3 and external vibrational regions the features due to $K_{1-x}Rb_xNO_3$ (KIII) are too weak to be distinguished from the much stronger features due to $K_{0.05}Rb_{0.95}NO_3$ (RbIV) in the vicinity (Fig. 4.3). To judge from the relative

intensities there seems to be more $K_{0.05}Rb_{0.95}NO_3$ (RbIV) which may suggest that the solubility of KNO_3 in $RbNO_3$ is slightly more than 5 mol%.

4.2.2 Raman Spectra of the Annealed Samples

The situation is similar for the Raman spectra of the annealed samples (Fig. 4.4) and three types of solid can also be classified by the Raman spectra (Table 4.2): $K_{1-x}Rb_xNO_3$ (KII), $K_{0.05}Rb_{0.95}NO_3$ (RbIV) and a mixture of the two. The major difference is that the Raman features of KNO_3 III are replaced by those of KNO_3 II (Fig. 4.1). The ν_1 and ν_4 vibrations shift a little lower to 1050 and 715 cm^{-1}. The $2\nu_2$ bands become much weaker and obscure between 1650 and 1680 cm^{-1}. The most characteristic features are in the ν_3 and the external vibrational regions. There are two peaks with similar intensity at 1345 and 1358 cm^{-1} which are the typical bands of the ν_3 vibration for KNO_3 II. In the external vibrational region three relatively strong bands may be distinguished at about 45, 80 and 121 cm^{-1}. The Raman bands agree well to those reported for KNO_3 II [55].

The presence of rubidium ions in the lattice seems to have little effect on the internal vibrations of nitrate ions in $K_{1-x}Rb_xNO_3$ (KII). The frequency of bands in the ν_1, ν_3, ν_4, and $2\nu_2$ are quite constant from $K_{0.95}Rb_{0.05}NO_3$ (KII) to $K_{0.33}Rb_{0.67}NO_3$ (KII). On the other hand, the lattice expansion due to the larger rubidium ions in $K_{1-x}Rb_xNO_3$ (KII) crystal caused the external modes to vibrate at lower frequencies (Fig. 4.5).

The solubility range for $K_{1-x}Rb_xNO_3$ (KII) reduced a little to $x = 0.67$ from $x = 0.80$ for $K_{1-x}Rb_xNO_3$ (KIII) and the Raman features of $K_{0.05}Rb_{0.95}NO_3$ (RbIV) began to appear for x

= 0.80 (Table 4.2). As was the case for the quenched samples, the first addition of the smaller potassium ions caused the external vibrations to shift to slightly higher wavenumbers but then the frequencies seem unaffected by the small additional amount of potassium ion.

4.3 Discussion

4.3.1 Lattice Dynamical Studies of $K_{1-x}Rb_xNO_3$

It is interesting to notice that the 52 cm^{-1} band in $K_{1-x}Rb_xNO_3$ (KII) shifted 9 cm^{-1} for x = 0.05 to x = 0.67, while the 84 cm^{-1} band only shifted half this value, about 4 cm^{-1} for the same composition span (Fig. 4.6). A reverse shift has been reported [55] for thermal expansion effects. When the temperature was raised from 298 K to 390 K, the 52 cm^{-1} band decreased by 2 cm^{-1} while the 84 cm^{-1} band decreased by 5 cm^{-1}, doubled the shift of the 52 cm^{-1} band. This is consistent with the assignments by Brooker [99] that the 52 cm^{-1} band in KNO_3 II is due to translatory motion of the K^+ sublattice against the NO_3^- sublattice and the 84 cm^{-1} band involves rotatory motions of the nitrate ion about the a and b axes. These two modes are influenced differently by thermal expansion or by introduction of larger ions.

According to vibrational theory, frequency is proportional to the restoring force and inversely proportional to the reduced mass of the vibrating particles. The expansion of the lattice by thermal motion or by introduction of larger ions will cause the restoring force to decrease. Thermal expansion is more favourable for the rotatory motion of the nitrate ions than the expansion by large ion substitution because the larger ions will occupy extra space

and make less room for the rotatory motion. On the other hand thermal expansion has little influence on the mass while addition of larger, heavier rubidium ions will increase the average mass of the cation. Cations do not take part in the rotatory motions of NO_3^- but they are directly involved in the translatory motions of cations against anions. Substitution of the heavier rubidium ions caused the frequency of the translatory mode to decrease more quickly than did the effect of lattice expansion.

The rotatory motion of the nitrate ion in KNO_3 III is associated with the doubly degenerate E centred at 125 cm^{-1} [55]. As x increased from 0.05 to 0.80, the frequency of this libration of the nitrate ion in $K_{1-x}Rb_xNO_3$ (KIII) shifted from 125 to 118 cm^{-1} (Table 4.1). The relative shift rate (0.056) of the 125 cm^{-1} band was similar to the relative shift rate (0.048) of the 84 cm^{-1} band in $K_{1-x}Rb_xNO_3$ (KII). This is consistent with the fact that both bands have the same origin: rotatory motions of the nitrate ion about the a and b axes. Larger rubidium ions expand the lattice of the crystal so that the nitrate ion is less confined. The relaxed nitrate ion librates at lower frequency.

The 52 cm^{-1} band in $K_{1-x}Rb_xNO_3$ (KII) shifted much more rapidly (relative shift rate is 0.18) because it has a different origin. It is due to the translatory motion of cations against anions. Larger and heavier rubidium ions redouble the effect on this lattice vibration mode by actually participating in the vibration. Potassium nitrate is an ionic crystal and the interatomic potentials between K^+ and NO_3^- are mainly due to columbic interaction. Assuming that all the chemical bonds between cations and anions are of equal strength, the equation deduced in Section 2.1.2:

$$\nu = B\sqrt{\frac{1}{\mu r^2}} \qquad (2.30)$$

may be used to predict the frequency shifts of this translatory mode due to substitution of Rb^+ for K^+ in $K_{1-x}Rb_xNO_3$ (KII).

The translatory motion of the K^+ sublattice against the NO_3^- sublattice in KNO_3 II has the B_{2g} symmetry. The nitrate ions in the crystal form planes perpendicular to the c axis. The potassium ions are located between the planes of the nitrate ions. Therefore changes in the separation distance r in Eq. (2.30) may be replaced by the expansion along the c axis due to substitution of Rb^+ for K^+ (by 2.86% for $K_{0.44}Rb_{0.56}NO_3$ (KII) [80]) without introducing serious errors. Table 4.3 presents the results of the calculation. The calculated frequencies are in general agreement with the observed. For higher concentrations of rubidium ions, the agreement is not so good. This is partly because the expansion along the c axis no longer obeys Vegard's law when the mole fraction of Rb^+ equals or exceeds 0.37 [80]. Subsequently the linear relationship between the concentration of rubidium ions and the separation distance fails.

This model is only a first order approximation. Nevertheless, the agreement between the observed frequencies and the predicted ones by Eq. (2.30) is reasonablely good and provides semi-quantitative support for the assignment of the 52 cm^{-1} band in KNO_3 II to the translatory motion of the cations against the anions.

There is disagreement about the assignment of the 52 cm^{-1} band. Shortly after the work of Brooker [99], Akiyama *et al* [100] used a rigid ion model to perform a lattice dynamical

analysis of the optical active vibrations of KNO_3 II. They found that the best fit was obtained if the 52 cm^{-1} band was assigned to the rotatory mode of the nitrate ion around the b axis and the 84 cm^{-1} band was assigned to the rotatory mode around the a axis. Recently Liu *et al* [101] performed lattice dynamical calculations with the rigid ion approximation and empirical potentials and concluded that the 52 cm^{-1} band was a combination of translatory and rotatory motions. It must be pointed out that Brooker's assignment was consistent with the measured ^{15}N isotopic shifts and single crystal depolarization measurements. The present experimental study corroborates the assignment of Brooker and suggests that the theoretical calculations based on rigid ion models are inadequate. The rigid ion model may not properly deal with the non-spherical (planar) NO_3^-.

4.3.2 Structural Consideration of $K_{1-x}Rb_xNO_3$

Raman studies of the KNO_3-$RbNO_3$ system indicated that two kinds of room temperature solid solutions crystallized from the mixed melts. One had the structure of potassium nitrate and the other had the structure of rubidium nitrate. Rubidium ion can substitute for potassium ion up to 80 mol% in $K_{1-x}Rb_xNO_3$ (KIII) and up to 67 mol% in $K_{1-x}Rb_xNO_3$ (KII). The two step transition I to III to II of KNO_3 on cooling held true for $K_{1-x}Rb_xNO_3$ when $x \leq 0.67$. Potassium ion can only replace about 5 mol% rubidium ion in $K_{1-x}Rb_xNO_3$ (RbIV). The solid solubility determined by Raman spectroscopy is consistent with the observations by other techniques [67,80,97], especially the thermal analysis heating run. The three transitions of rubidium nitrate alone were detected by thermal method for the sample

$K_{0.05}Rb_{0.95}NO_3$ and the Raman spectra of this sample, whether quenched or annealed, had only the features of rubidium nitrate. Both the II to I transition of potassium nitrate and the three transitions of rubidium nitrate were detected in the heating run for the sample $K_{0.10}Rb_{0.90}NO_3$ and the spectrum of the sample, whether quenched or annealed, had Raman features of both nitrates.

KNO_3 III has the R3m structure with three formula units per hexagonal cell. On a statistical basis this means that for x = 0.80 at least half of the microstructure of R3m in $K_{1-x}Rb_xNO_3$ (KIII) has unit cells with only rubidium ions. When annealed, this sample presented a Raman spectrum containing characteristic bands of both $K_{1-x}Rb_xNO_3$ (KII) and $K_{1-x}Rb_xNO_3$ (RbIV). This appears to be due to ion diffusion. Given enough time for the transition to the stable phase at room temperature, the sublattice with one-third potassium ions changed to $K_{1-x}Rb_xNO_3$ (KII) while the sublattice with only rubidium ions changed to $K_{1-x}Rb_xNO_3$ (RbIV). The Raman spectra of $K_{0.33}Rb_{0.67}NO_3$ (containing one-third potassium ions) indicated that it had only the transition of $K_{1-x}Rb_xNO_3$ (KIII) to (KII). The R3m unit cell with only Rb^- in $K_{0.20}Rb_{0.80}NO_3$ (KIII) seemed less stable. Without sufficient K^-, the quenched sample $K_{0.10}Rb_{0.90}NO_3$ became a mixture of $K_{0.05}Rb_{0.95}NO_3$ (RbIV) and $K_{1-x}Rb_xNO_3$ (KIII) saturated with Rb^-. The fact that the ν_1 vibration of $K_{1-x}Rb_xNO_3$ (KIII) shifted more to lower frequency in $K_{0.10}Rb_{0.90}NO_3$ (1049 cm^{-1}) than in $K_{0.20}Rb_{0.80}NO_3$ (KIII) (1051 cm^{-1}) indicated that there were more R3m unit cells with only rubidium ions in the former than in the latter.

It is worthwhile to compare the Raman spectra of the quenched and annealed $K_{0.10}Rb_{0.90}NO_3$. The spectrum of the quenched sample was measured first. The spectrum was

measured again after annealing. The distinct Raman features in the ν_1 and ν_4 regions due to $K_{1-x}Rb_xNO_3$ (KIII) in the quenched sample (Fig. 4.3) seemed to disappear completely and there appeared to be only the Raman bands of $K_{1-x}Rb_xNO_3$ (RbIV) in the annealed sample (Fig. 4.4). It appears that, after annealing, $K_{1-x}Rb_xNO_3$ (KIII) in the quenched $K_{0.10}Rb_{0.90}NO_3$ transformed to $K_{1-x}Rb_xNO_3$ (RbIV) instead of (KII), as one might expect. A more detailed scan in the ν_1 region indicated that the band due to the KNO_3 structure greatly decreased in intensity after the thermal treatment (Fig. 4.7). The remaining small peak due to $K_{1-x}Rb_xNO_3$ (KII) shifted to higher frequency so that it became a shoulder on the band due to $K_{1-x}Rb_xNO_3$ (RbIV). Usually the transition of the KNO_3 III structure to the KNO_3 II structure causes ν_1 to shift to lower frequency. The weak feature appeared more like that due to thermal disordered energy states in $K_{1-x}Rb_xNO_3$ (RbIV) [59] than due to $K_{1-x}Rb_xNO_3$ (KII). Obviously most of the $K_{1-x}Rb_xNO_3$ (KIII) in the quenched sample $K_{0.10}Rb_{0.90}NO_3$ did not transform to $K_{1-x}Rb_xNO_3$ (KII) but to (RbIV).

Raman studies offer a possible explanation for the disappearance of the two transitions of rubidium nitrate at high temperature in the composition range between 60 and 90 mol% $RbNO_3$. This region represented the structural change from a mixture of $K_{1-x}Rb_xNO_3$ (K) and (Rb) to $K_{1-x}Rb_xNO_3$ (K) alone. Under the influence of the coexisting KNO_3 structure, $K_{1-x}Rb_xNO_3$ (Rb) manifested some new structural features. The metastable R3m phase with only rubidium ions was detected by Raman technique for the quenched $K_{1-x}Rb_xNO_3$ (x = 0.80 and 0.90). On annealing, the R3m phase transformed to phase IV of rubidium nitrate. It would be expected that the reverse process should take place when the mixtures were heated and that part of $K_{1-x}Rb_xNO_3$ (RbIV) transformed to (RbII) which had the same structure as KNO_3

I. Electrical conductivity studies also indicated that $K_{1-x}Rb_xNO_3$ (RbII) transformed directly to (RbIV) on cooling when the potassium content was more than 6 mol% [97]. We have measured the temperature dependence of $K_{0.20}Rb_{0.80}NO_3$ and found that the mixture became one phase ($R\bar{3}m$) above 423 K. Thus, the missing transitions of rubidium nitrate were phase IV to III and phase II to I. Phase II of rubidium nitrate and phase I of potassium nitrate have the same $R\bar{3}m$ structure and they form continuous solid solutions below the solidus. In a sense the potassium rubidium nitrate system might well be regarded as a system of limited solid solutions. There seemed to be two kinds of solid solution below the solidus: $K_{1-x}Rb_xNO_3$ (Rb) for $x \geq 0.95$ and $K_{1-x}Rb_xNO_3$ (K) for $x \leq 0.67$, between the two limits were mixtures of the two kinds of solid solutions.

The direct transition between the $P3_1$ and $R\bar{3}m$ phases and the appearance of the metastable R3m unit cell with only rubidium ions indicated a greater tendency for rubidium nitrate to have the structure of potassium nitrate. This tendency at least partly explains the strikingly different solubilities. It is energetically unfavourable for mixtures of different structures to form solid solutions. A positive transition enthalpy ΔH_{tr} must be added to the formation enthalpy expression of the solid solution for nonisostructural components because the guest member is forced to have the structure of the host member. Usually only limited solubilities are observed for nonisostructural systems and ΔH_{tr} may be regarded as the site preference energy. For rubidium nitrate to have the structure of potassium nitrate the enthalpy ΔH_{tr} must be rather small and the enthalpy for potassium nitrate to transform to the structures of rubidium nitrate must be very large. As a result, rubidium ions can dissolve in potassium nitrate a greater extent than potassium ions can in rubidium nitrate.

The solid solutions formed from mixtures of KNO_3-$RbNO_3$ are contrary to the usual rule that it is easier to put a smaller atom into a large host lattice than vice versa. Larger rubidium ions replace many more smaller potassium ions in the potassium nitrate crystal while smaller potassium ions can hardly dissolve in the rubidium nitrate crystal. The difference in coordination numbers between the potassium ion in potassium nitrate and the rubidium ion in rubidium nitrate was believed [96] to account for this paradoxical phenomenon. For an ionic crystal the coordination of cations and anions depends in some way on the ionic radii of the component ions and the relative size may be the more fundamental factor. In the series of alkali metal nitrates the relative size of the alkali metal ions and the nitrate ion causes potassium nitrate to have an intermediate structure between those of lithium nitrate and cesium nitrate (Section 2.3). The rubidium ion seems to locate near the boundary size for the cesium nitrate structure. A few percent of a smaller cation may destabilize the structure of rubidium nitrate.

The general rule for solid solubility of ions of different size was based on the observations for systems of halides, oxides and chalcogenides which may be safely regarded as consisting of spherical ions. The theoretical models for energetics of solid solution formation mainly involved some manner of packing the spherical anions and placing the cations in the vacancies [83,84]. The size parameter for calculating the asymmetric solubility relations was introduced on the underlying assumption that ions are spherical. Care must be taken when applying these theories to nitrate systems because the spherical approximation is too rough an for nitrate ions. The trend of alkali metal nitrates for the physical properties directly pertaining to the structure, such as molar volumes or melting points, may be best

understood if planarity of the nitrate ion is taken into consideration. Even lattice dynamic calculations based on *ab initio* potentials only resulted in a shortening of the c axis of the potassium nitrate structure [88]. Failure to obtain better agreement with experiments was attributed to the fact that sufficient attention had not been paid to the planarity of the nitrate ions. The extraordinary solubilities in the KNO_3-$RbNO_3$ solid solutions may serve as further evidence that the planarity of the nitrate ion plays an important part in the structural chemistry of nitrates.

The metastable KNO_3 III structure accommodated more rubidium ions and the lattice seemed to be more expanded than the KNO_3 II structure for the same amount of rubidium ions. It was noted that the internal vibrations of the nitrate ion shifted to lower frequencies with the addition of rubidium ions in $K_{1-x}Rb_xNO_3$ (KIII) while they remained almost unchanged in $K_{1-x}Rb_xNO_3$ (KII). The ν_1 mode of the nitrate ion shifted about 3 cm^{-1} to lower frequency in $K_{1-x}Rb_xNO_3$ (KIII) while it was practically unchanged in $K_{1-x}Rb_xNO_3$ (KII). The nitrate ions appeared more sensitive to substitution of rubidium ions in KNO_3 III than in KNO_3 II. In crystals the nitrate ion experiences a symmetrical polarization of the cations which causes the ν_1 vibration to shift to higher energy. For the same crystal structure the larger cation will produce less perturbation and the frequency will shift to lower value. The sensitivity of the ν_1 vibration in KNO_3 III to substitution of rubidium ions indicated that its lattice parameters changed considerably.

The Raman spectra in the external vibrational region also indicated that the lattice parameters changed more in $K_{1-x}Rb_xNO_3$ (KIII) than in $K_{1-x}Rb_xNO_3$ (KII) when potassium ions were substituted by rubidium ions. The Raman band at about 85 cm^{-1} of KNO_3 II and the

Raman band at about 125 cm^{-1} of KNO_3 III involve similar rotatory modes of the nitrate group [55,99]. The frequencies are inversely proportional to the space available for the rotatory motion. For the same amount of rubidium ions the rotatory modes of the nitrate ion shifted more to the lower frequency in $K_{1-x}Rb_xNO_3$ (KIII) than in (KII). When x increased from 0.05 to 0.67, the frequency of the rotatory modes decreased by 7 cm^{-1} for the former and by 4 cm^{-1} for the latter.

The more sensitive response of the KNO_3 III structure to substitution of larger rubidium ions is consistent with the crystallographic studies of the structures and structural phase transitions of potassium nitrate. It was found [80] that both the molar volume and the distance between successive K planes were smaller in KNO_3 III than in KNO_3 II. The transition of phase III to II of potassium nitrate was accompanied with volume expansion instead of contraction. The more compact KNO_3 III would expand even more when larger rubidium ions replace smaller potassium ions. The more expanded KNO_3 III would cause larger frequency shifts in the Raman spectrum. Furthermore, the arrangement of the nitrate ions and the cations makes KNO_3 III more sensitive than KNO_3 II to substitution of larger cations. In the KNO_3 III crystal, the potassium ion and nitrate ion alternatively line along the same c axis. In the KNO_3 II crystal they are located on different c axes, each of which carries only one kind of ion. It is expected that the nitrate ion would experience the perturbation of the cations more directly in KNO_3 III crystal than in KNO_3 II crystal. This may also bring about larger frequency shifts.

The greater expansion in the lattice of KNO_3 III due to larger rubidium ions may partly account for the reported deterioration of ferroelectricity in $K_{1-x}Rb_xNO_3$ (KIII) [80]. It was

noted that the ferroelectric hysteresis loop was disfigured and the spontaneous polarization decreased as the content of rubidium ions increased. These features disappeared almost completely when the mole fraction of rubidium ions increased to 0.56. The changes were not considered to be due to the appearance of another crystallographic structure. In this work the Raman spectra of the solid solutions containing $RbNO_3$ up to 80 mol% had practically the same pattern as KNO_3 III (Table 4.1) even in the most characteristic ν_3 region. The well separated and sharp TO-LO Raman features for the nitrate asymmetric stretching mode were in good agreement with the literature [55,102]. It has been reported [102] that the substitution of 30 mol% potassium ions by rubidium ions only brought about a very slight broadening of the TO-LO features and about 2 cm^{-1} shift to lower frequencies for both features, which was also in good agreement with our observations. Since Raman studies indicated no crystallographic change in the solid solutions, the deterioration in ferroelectricity must be due to some change in the R3m lattice because of the larger rubidium ions. Compared with phase II, phase III of potassium nitrate has a looser structure along the c axis but a more compact unit cell [88]. The larger expansion in $K_{1-x}Rb_xNO_3$ (KIII) must be along the a and b axes, with the c axis relatively unchanged. The spontaneous polarization, which is along the c axis, will decreases as a result of expansion in the a- and b-direction without a corresponding expansion in the c-direction.

The ferroelectricity of $K_{1-x}Rb_xNO_3$ (KIII) deteriorated most rapidly when x was more than 0.40 and $K_{0.44}Rb_{0.56}NO_3$ was found to be almost paraelectric [80]. The disappearance of ferroelectricity may be due to the presence of sufficient number of rubidium ions to overturn the ordering of ferroelectric microdomains in KNO_3 III, to give a structure that resembles

KNO_3 I. Both Raman and infrared studies [55,103] have indicated that it was not appropriate to describe the vibrational spectrum of KNO_3 I on the basis of the average $R\bar{3}m$ structure determined crystallographically. The R3m structure appears to be the most possible one for the paraelectric phase I of potassium nitrate. The TO-LO splitting has been reported [104] in the ν_3 region of the Raman spectrum of KNO_3 I and infrared studies [105] suggested that the local environment of the nitrate ion was practically identical in phases I and III of potassium nitrate. The frequency shift was found to be extremely small and the ν_3 region was essentially unchanged between phases I and III in the IR spectra. It was suggested that the transition of phase I to III involved ordering of dipoles already existing in phase I. This was supported by the study of X-ray diffuse scattering [106] of potassium nitrate above the ferroelectric Curie point. The thermal transition of KNO_3 III to I was accompanied by large expansion along the c axis [88]. Assuming that the expansion of the c axis in the solid solutions due to larger rubidium ions had the same effect as the thermal expansion, an addition of 60 mol% $RbNO_3$ would have the same result as a temperature increase of 100 K. It is reasonable to assume that at high concentrations of $RbNO_3$ the ordering of the R3m microstructures in $K_{1-x}Rb_xNO_3$ (KIII) was disrupted and resulted in the paraelectric property similar to KNO_3 I.

Recently theoretical and experimental studies [5,88,105] have been directed toward methods to stabilize ferroelectric ordering in KNO_3. The work has focused on thin films of KNO_3 because of their potential applications in random access memory devices. Several mechanisms have been suggested to improve the stability of KNO_3 films in phase III, based on changes in physical properties such as hydrostatic pressure [107] and film thickness [108]. The present work might shed light from the view point of structure. The nitrates of sodium, potassium and

rubidium all have the same $R\bar{3}m$ structure at high temperature but only KNO_3 gives rise to a ferroelectric structure on cooling. The size of the cation must be one of the important factors and insertion of small amounts of rubidium ion may lead to stabilized ferroelectric KNO_3 III films.

4.4 Conclusions

Raman spectroscopic studies of the KNO_3-$RbNO_3$ system revealed the following structural features of the nitrates and their solid solutions:

1. The 52 cm^{-1} band is primarily due to the translatory motion of the K^+ sublattice against the NO_3^- sublattice. Reported calculations based on hard sphere models are not consistent with experimental measurements.
2. The solubility of $RbNO_3$ was 67 mol% in KNO_3 II and 80 mol% in KNO_3 III. The solubility of KNO_3 in $RbNO_3$ IV was 5 mol%.
3. The transition from R3m to $P3_1$ was observed for samples containing 90 and 80 mol% $RbNO_3$. The tendency of $RbNO_3$ to have the structure of KNO_3 appears to explain why the larger Rb^+ has much greater solubility in KNO_3 than smaller K^+ in $RbNO_3$.
4. $K_{1-x}Rb_xNO_3$ (KIII) was expanded more than $K_{1-x}Rb_xNO_3$ (KII) by larger Rb^+. The greater and uneven expansion in $K_{1-x}Rb_xNO_3$ (KIII) could partly account for the reported deterioration of ferroelectricity as larger rubidium ions were introduced in the crystal.

Table 4.1 Observed wavenumbers for Raman bands of mixed crystals of $K_{1-x}Rb_xNO_3$ (KIII) and $K_{0.05}Rb_{0.95}NO_3$ (RbIV) at 298 K.

$K_{1-x}Rb_xNO_3$ [a]	external	ν_4	ν_1	ν_3	$2\nu_2$
x = 1.00	95,108	706,720	1055	1350,1407,1440	1673
x = 0.95	61,110	707,721	1057	1349,1410,1440	1674
x = 0.90	61,110	707,721	1056	1347,1412,1435	1674
		714	1049		1661
x = 0.80	116	717	1052	1348,1424,1435	1662
x = 0.67	118	717	1052	1349,1428,1437	1663
x = 0.50	120	717	1053	1350,1430,1438	1664
x = 0.33	121	717	1053	1349,1430,1439	1663
x = 0.80	124	718	1054	1351,1430,1441	1665
x = 0.10	124	718	1054	1350,1430,1440	1664
x = 0.05	125	719	1055	1351,1430,1442	1664
KNO_3 III [b]	125	717	1053	1348,1431,1440	1664

a. Samples were quenched from the melts and measured at 298 K.

b. Data from reference 55.

Table 4.2 Observed wavenumbers for Raman bands of mixed crystals of $K_{1-x}Rb_xNO_3$ (KII) and $K_{0.05}Rb_{0.95}NO_3$ (RbIV) at 298 K.

$K_{1-x}Rb_xNO_3$ [a]	external	ν_4	ν_1	ν_3	$2\nu_2$
x = 1.00	59,108	706,720	1055	1350,1407,1440	1673
x = 0.95	62,112	708,722	1057	1350,1410,1438	1675
x = 0.90	62,111	707,721	1057	1348,1410,1437	1674
x = 0.80	62,114	707,721	1057	1348,1437	1674
		715	1051		1662
x = 0.67	41,79,120	714	1050	1345,1357	1650,1677 [c]
x = 0.50	43,80,121	715	1051	1346,1358	1650,1680 [c]
x = 0.33	45,81,121	715	1051	1345,1359	1650,1672 [c]
x = 0.20	47,82,122	715	1051	1345,1359	1654,1682 [c]
x = 0.10	49,82,123	714	1050	1344,1358	1650,1685 [c]
x = 0.05	50,83,123	714	1050	1344,1358	1651,1675 [c]
KNO_3 II [b]	52,84,123	715	1050.5	1344,1359	1652,1679 [c]

a. Samples were annealed and measured at 298 K.

b. Data from reference 55.

c. Broad and weak features from about 1650 to 1680 cm^{-1}.

Table 4.3 Frequency shift of the 52 cm^{-1} band in $K_{1-x}Rb_xNO_3$ (KII) as a function of the mole fraction of Rb^+.

x [a]	0.05	0.1	0.2	0.33	0.5	0.67
ν_{obs} (cm^{-1})	50	49	47	45	43	41
ν_{cal} (cm^{-1}) [b]	50	49	47	46	44	42

a. Mole fraction of rubidium ion for the annealed samples and measured at 298 K.

b. Calculated frequencies by Eq. (2.30).

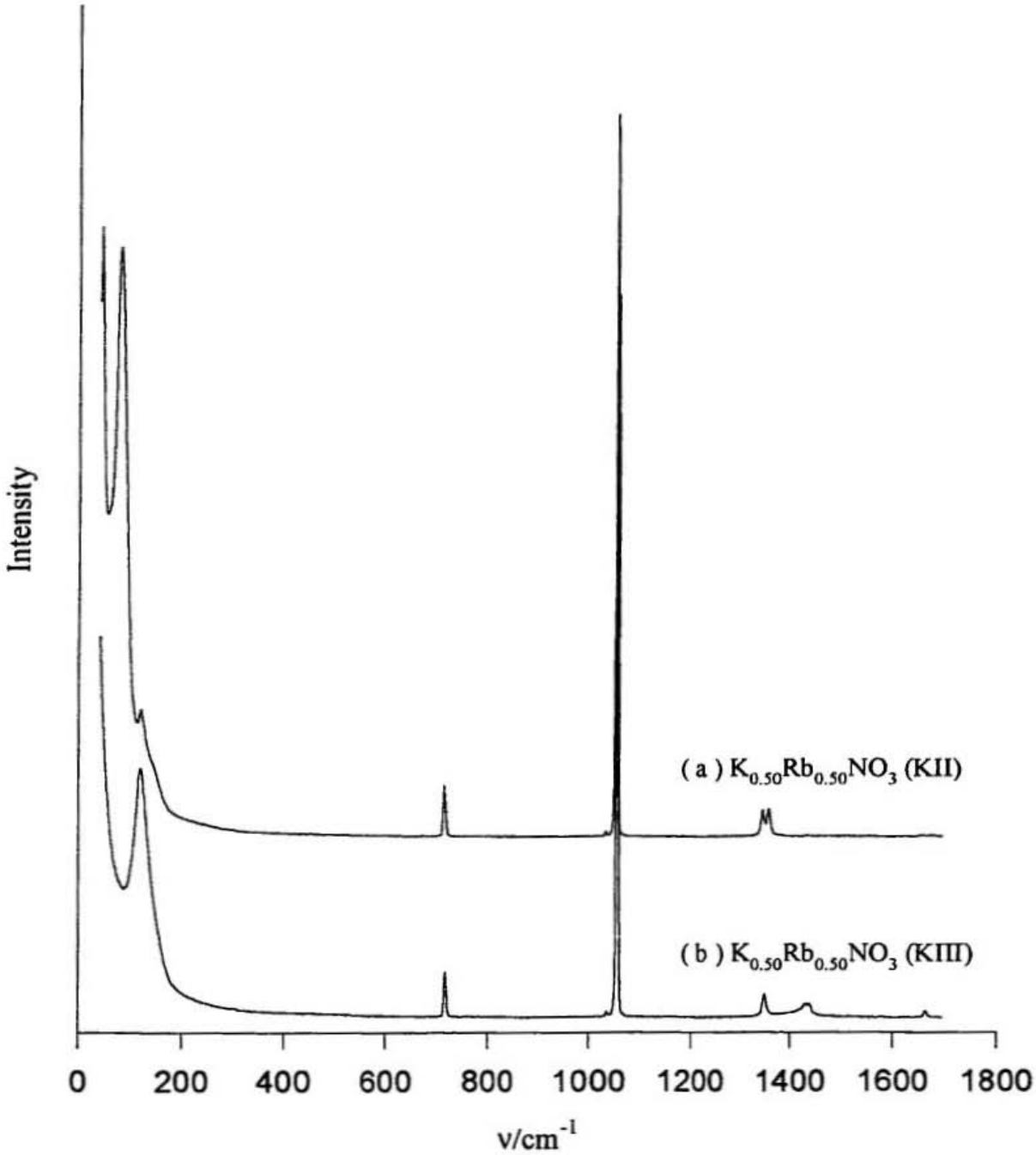

Fig 4.1 Raman spectra of the annealed (a) and quenched (b) sample of equimolar KNO_3-$RbNO_3$ at 298 K.

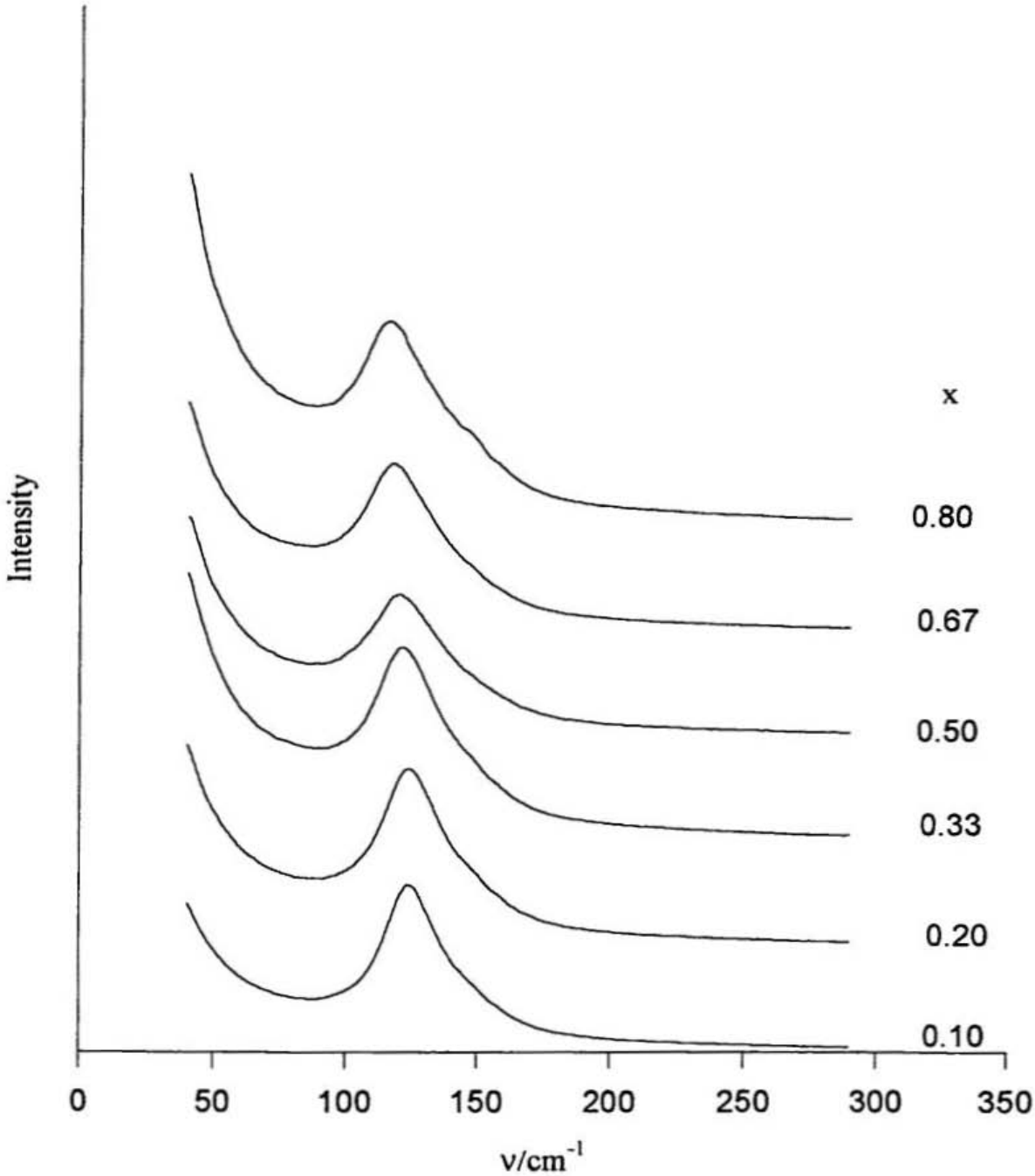

Fig. 4.2 Raman spectra in the external vibrational region of $K_{1-x}Rb_xNO_3$ (KIII) at 298 K. X is the mole fraction of $RbNO_3$.

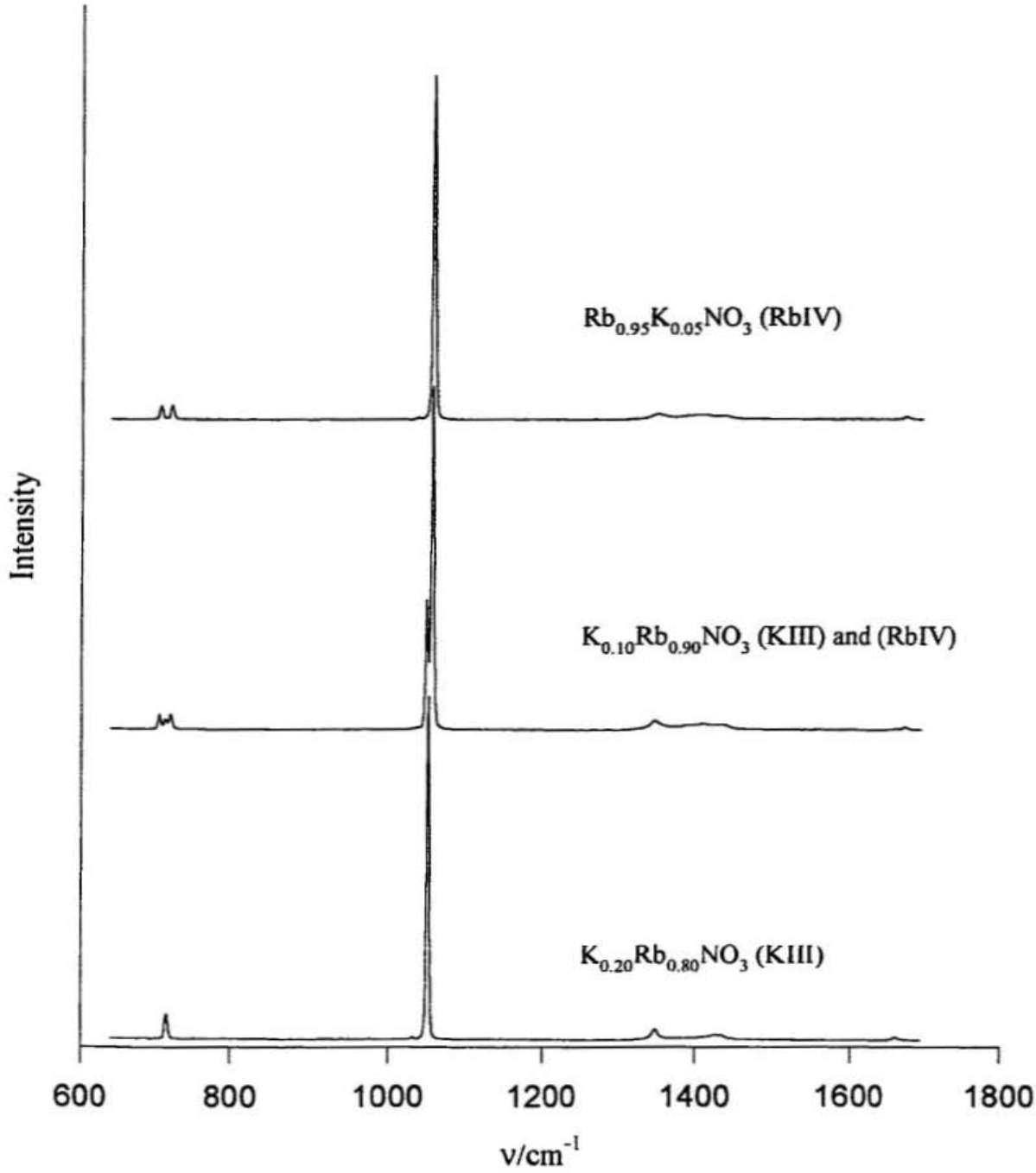

Fig. 4.3 Raman spectra in the internal vibrational region of the quenched $K_{1-x}Rb_xNO_3$ at 298 K. $K_{0.10}Rb_{0.90}NO_3$ is a mixture of the $K_{1-x}Rb_xNO_3$ (KIII) and (RbIV).

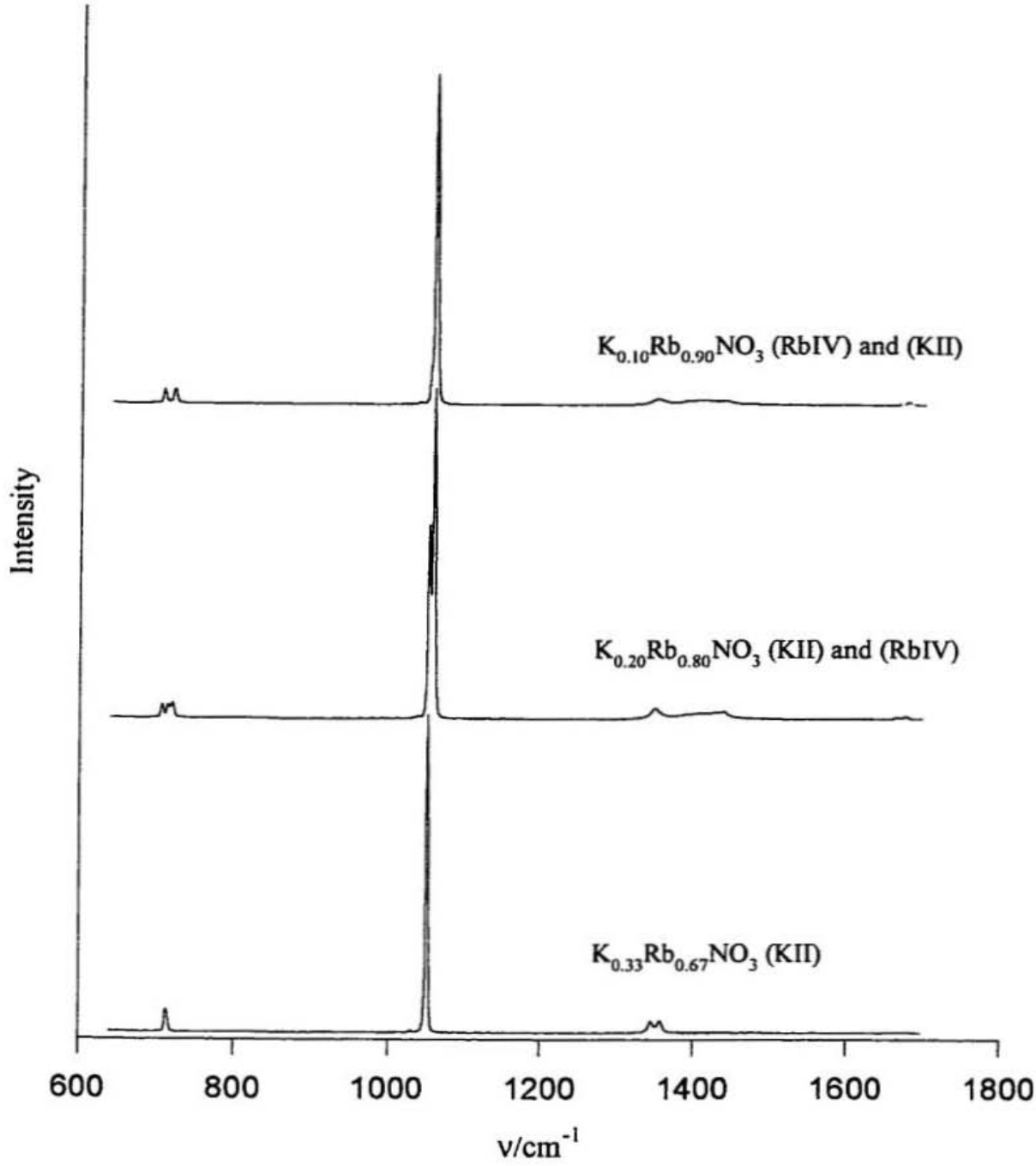

Fig. 4.4 Raman spectra in the internal vibrational region of the annealed $K_{1-x}Rb_xNO_3$ at 298 K.

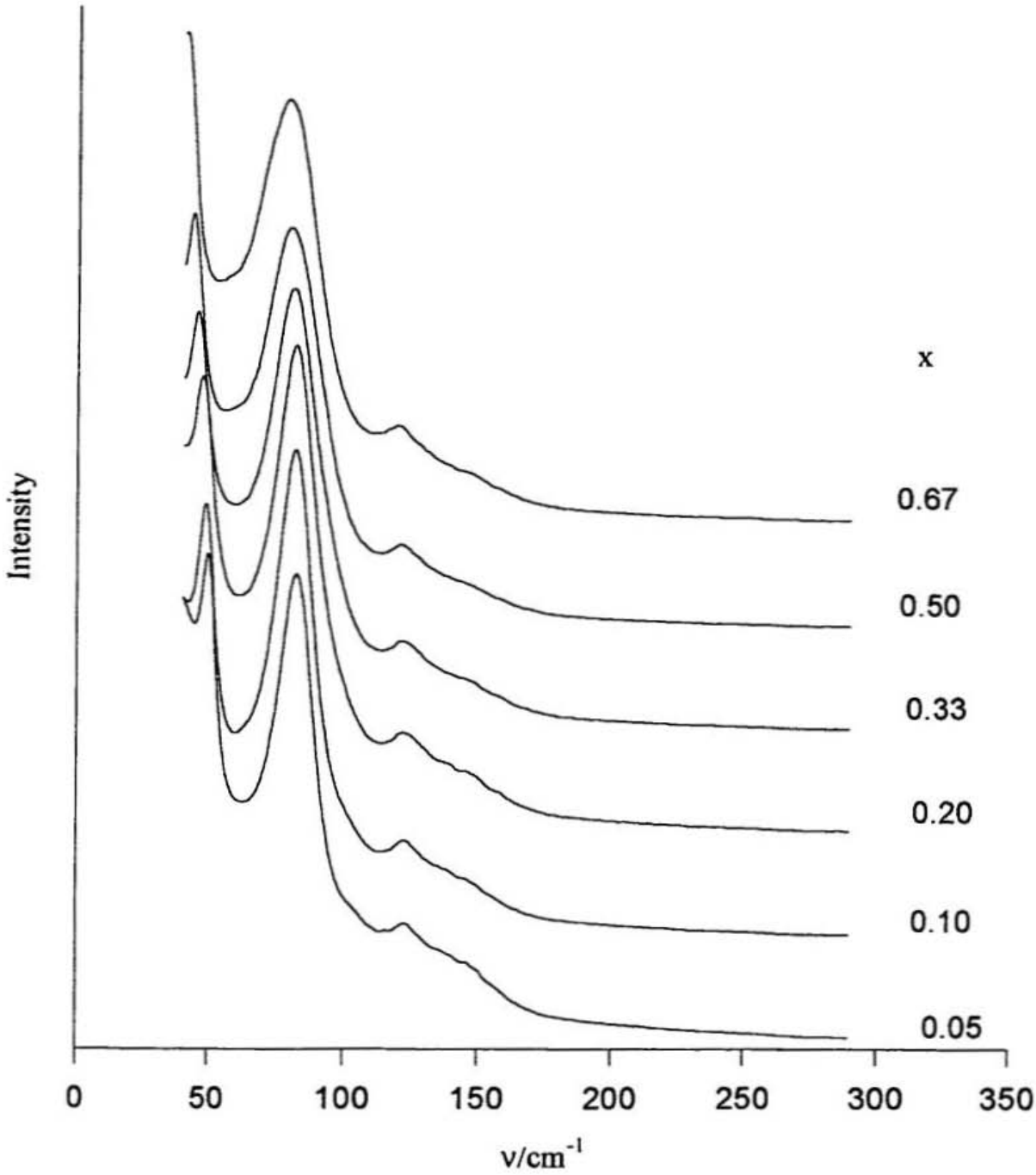

Fig. 4.5 Raman spectra in the external vibrational region of $K_{1-x}Rb_xNO_3$ (KII) at 298 K. X is the mole fraction of $RbNO_3$.

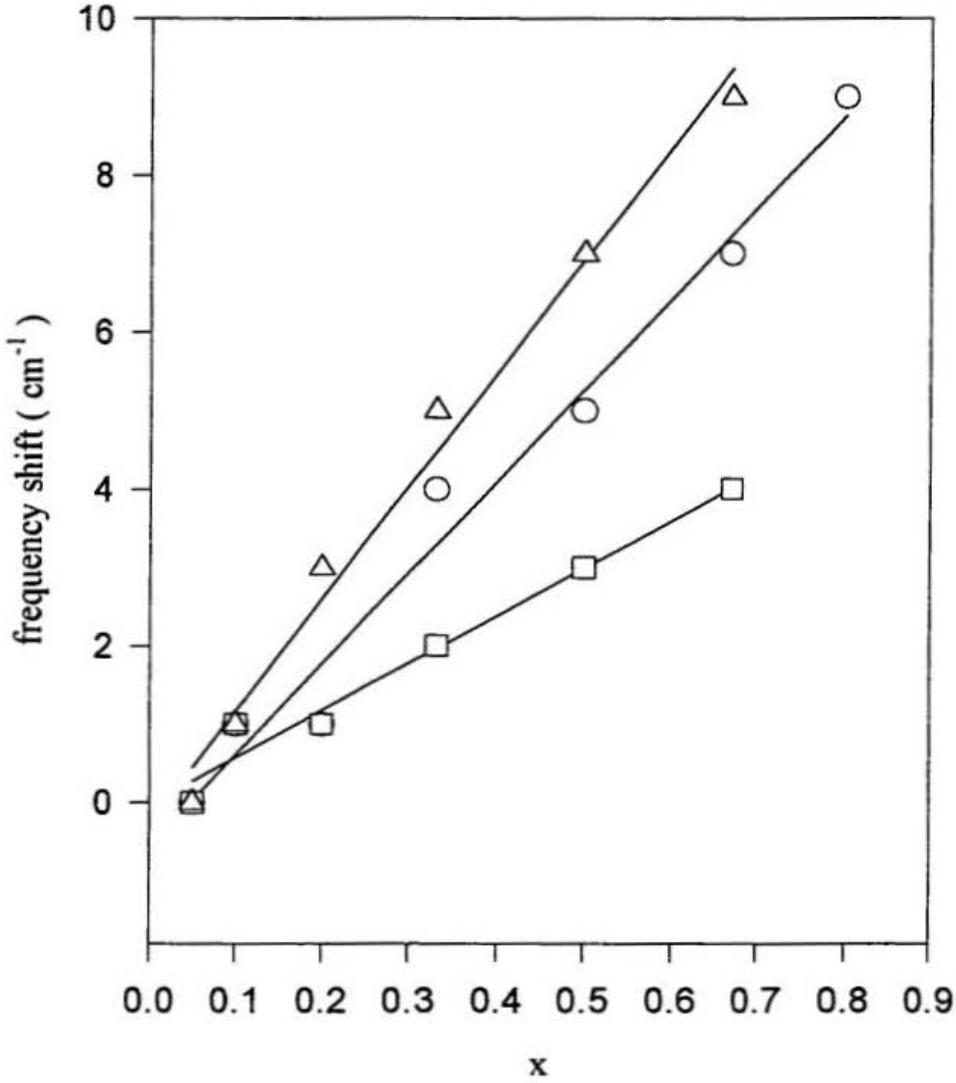

Fig. 4.6 Relative frequency shifts of $K_{1-x}Rb_xNO_3$ at 25 ^{0}C for the 84 cm^{-1} band (□) and the 52 cm^{-1} band (Δ) of KNO_3 II, and the 125 cm^{-1} band (o) of KNO_3 III . X is the mole fraction of $RbNO_3$.

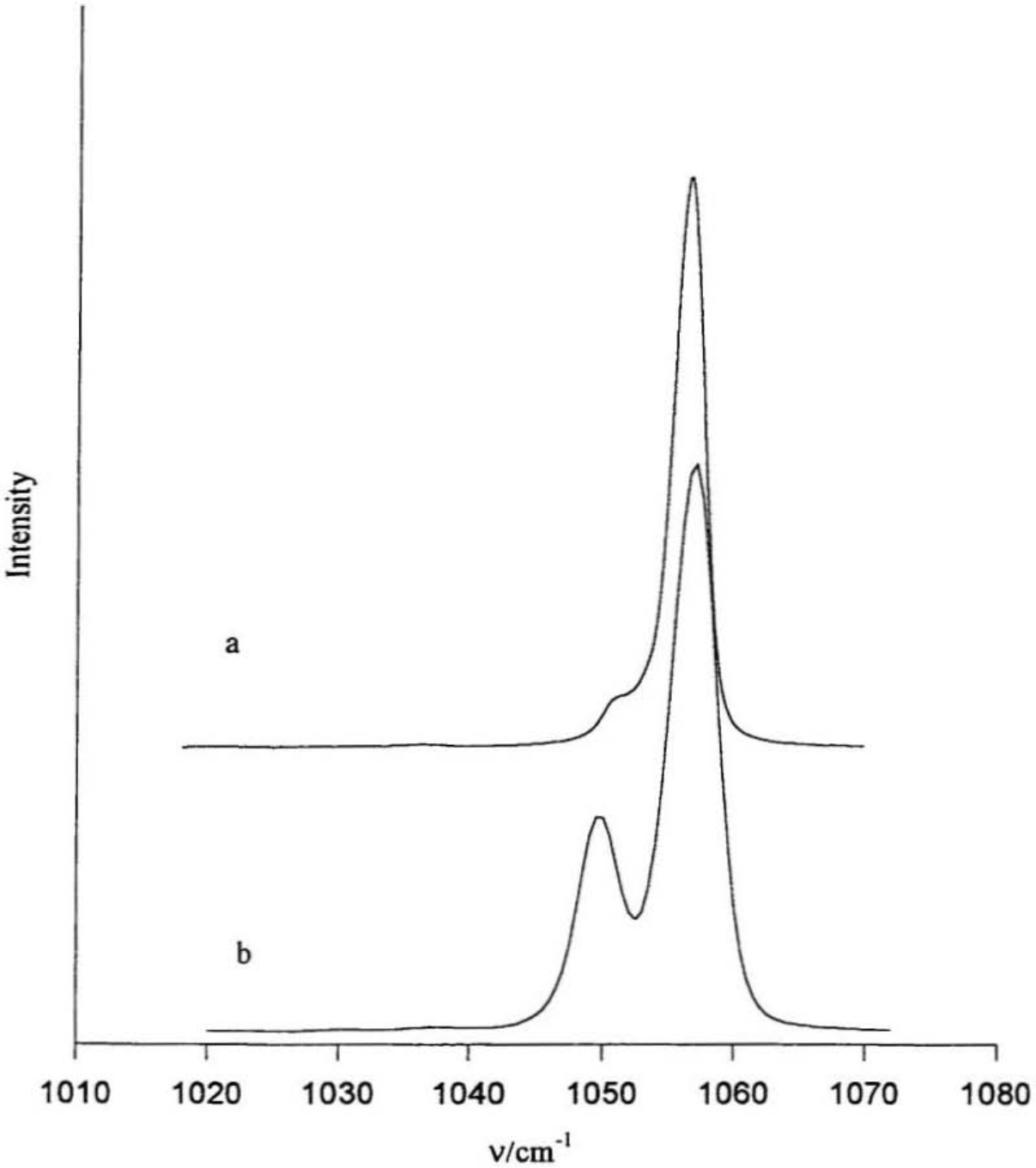

Fig. 4.7 Raman spectra in the ν_1 region of $K_{0.10}Rb_{0.90}NO_3$ at 298 K. The band due to substitutional KNO_3 in the quenched sample (b) becomes much weaker and shifts to higher frequency after annealing (a).

CHAPTER 5

RAMAN SPECTROSCOPIC STUDIES OF THE MIXED CRYSTALS OF SODIUM AND POTASSIUM NITRATE

5.1 Introduction

The sodium-potassium nitrate system is one of the most extensively investigated binary inorganic salt systems. These cheap and easily available salts are widely used as model compounds for theoretical studies and as solvents in industrial processes. A survey of the literature from 1884 to 1955 [109] gave 20 reports on phase diagram studies of the system. The number has now more than doubled and reports for the $NaNO_3$-KNO_3 system continue to appear [110]. Most recently, advanced thermal analysis techniques were used to obtain more accurate liquidus and solidus data [4]. Thermodynamic properties were also measured to gain a better understanding of the system [111]. Models based on regular solution theory were suggested to calculate the solidus and liquidus and to provide a microscopic insight for the thermodynamic properties [8].

Some of the earliest work [112] indicated a limited range of solid solutions and a eutectic for the $NaNO_3$-KNO_3 system because the observed solidus was quite flat in the intermediate concentration range. Later it was found by microscopic examination [113] that the solids below the solidus appeared homogeneous. Most published phase diagrams had a curved solidus in

the intermediate concentration region and the system was regarded as a continuous solid solution. Recently, DSC has been used to investigate the $NaNO_3$-KNO_3 system [4] and it has been estimated that the solidus actually appears flat in the intermediate concentration region. Nevertheless, the system is still considered to form a continuous series of solid solutions because of the homogeneous appearance of the crystals under the optical microscope. It seems that the horizontal solidus from 20 to 80 mol% KNO_3 is not necessarily due to limited solid solutions. Several attempts have been made [4,8,114] to use X-ray diffraction to investigate the solids below the solidus without any positive results. In one study [114] it was reported that the solid solution of equimolar $NaNO_3$-KNO_3 at 473 K had a different X-ray diffraction pattern from either $NaNO_3$ or KNO_3 at the same temperature, which was inconsistent with the accepted phase diagram.

Compared with the solidus and liquidus measurements, much less work has been done on the equilibria of solid states of the $NaNO_3$-KNO_3 system. Among the early studies, Kofler's phase diagram [113] was cited most frequently. The hot-stage-microscope technique was used in the investigation. Part of the subsolidus was only obtained by extrapolation and the intermediate transition involving KNO_3 III was not observed. Recently Greis *et al.* [66] examined the system carefully by differential scanning calorimetry. Special attention was paid to separate the cooling and heating runs. A complete phase diagram for the whole composition range was constructed. The thermal investigation was combined with a knowledge of phase transitions of the pure nitrates to deduce the structural chemistry of the solids of binary $NaNO_3$-KNO_3 system.

There are only a few examples of direct measurement of the structures of the mixed

crystals of $NaNO_3$-KNO_3 by spectroscopic methods. These were mostly for the equimolar mixture. Shortly after its discovery, Raman scattering was applied to study the equimolar $NaNO_3$-KNO_3 solid [64]. The structure of the solid solution seemed to be quenchable. The freshly prepared solid had only one sharp band in the ν_1 region. Four days later it became two sharp lines due to $NaNO_3$ II and KNO_3 II respectively. In another report [65] it was found that there was only one peak in the ν_1 region due to the solid solution of equimolar $NaNO_3$-KNO_3 when measured at 463 K. The band split into two when measured at room temperature, obviously due to decomposition of the solid solution to the components.

A knowledge of the microscopic structures of the solids is essential for a correct explanation of the flatness of the solidus in the phase diagram. The suggestion that $NaNO_3$-KNO_3 mixtures form continuous solid solutions is based on the homogeneous appearance of the mixed crystals under an optical microscope alone. X-ray diffraction has not offered any unambiguous support to this suggestion. In this work Raman studies of the $NaNO_3$-KNO_3 system are reported for the whole composition region in order to reveal the structural features of the binary solids and to offer a possible explanation for the horizontal solidus from 20 to 80 mol% KNO_3 observed by DSC.

Quenching was used in this study to obtain metastable phases of the binary solids. When quenched, the high temperature phase of sodium nitrate goes to the low temperature phase instantly, while the high temperature phase of potassium nitrate transforms to the ferroelectric phase which may be preserved infinitely in vacuum in a metastable state. The quenched mixtures may fully or partially retain the high temperature structures and new metastable phases may appear. The study of rapid solidification and metastable structures is of theoretical

and practical importance. Both metastable and stable states represent minima in the potential curve of the system. Knowledge of the action of dopants on metastability can help to find the stabilizing or destabilizing agents for a given phase [115]. Many materials are used in metastable state. Glasses and diamond are well-known examples. According to an estimate [116], more than 20,000 publications were available on various aspects of rapidly solidified materials.

Three temperatures were chosen for quenching: 493, 393, 358 K. Raman spectra were measured for both the quenched and annealed solids. The choice of the temperatures was based on the cooling runs of DSC reported by Greis *et al.* (Fig. 5.1) [66]. They represent temperatures of stability for the important structures of the phase diagram.

5.2 Raman Spectra of Mixed Crystals of $NaNO_3$-KNO_3

The most distinct Raman features of the solids of mixed $NaNO_3$-KNO_3 quenched from 493, 393 and 358 K and the annealed samples are summarized in Tables 5.1-5.4. For comparison Raman data of $NaNO_3$ II, KNO_3 II and KNO_3 III [55] are also included in the tables. Six kinds of solids can be classified by their spectra: a solid solution $Na_{0.95}K_{0.05}NO_3$ (NaII); a solid solution $Na_{1-x}K_xNO_3$ (KIII); a mixture of (NaII) and (KIII); a mixture of $Na_{1-x}K_xNO_3$ (KIII) and KNO_3 II; a mixture of $NaNO_3$ II and KNO_3 II; a new disordered state $Na_{1-x}K_xNO_3$ (D).

Since potassium nitrate has different structural phase transitions for heating and cooling procedures, care has been taken to ensure that the present samples represented the same states as in the DSC cooling runs [66] at the given temperature:

1. The 493 K quenched samples – The prepared samples were reheated at 493 K overnight and then quenched in liquid nitrogen.
2. The 393 K quenched samples – After the measurement of the Raman spectra, the samples were reheated at 493 K overnight. Then the temperature of the oven was set at 393 K. The mixtures were cooled to this temperature in the oven and kept there for 8 hours then quenched in liquid nitrogen.
3. The 358 K quenched samples – After the measurement of the Raman spectra, the samples were reheated to 493 K, cooled to 393 K in the oven and kept at this temperature for 8 hours, and then gradually cooled to 358 K (about one day). The samples were kept at 358 K for 8 hours and quenched in liquid nitrogen.
4. The annealed samples – After the measurement of the Raman spectra, the samples were reheated at 403 K overnight and then cooled to 343 K very slowly (about two days) before they were taken out of the oven and allowed to cool to room temperature.

5.2.1 Raman Spectra of the Annealed Samples

At room temperature, phase II of sodium nitrate is stable and the structure is $R\bar{3}c$. The stable phase of potassium nitrate is phase II with the structure of Pmcn. The DSC investigation [66] indicated mechanical mixtures of $NaNO_3$ II and KNO_3 II in the whole composition region at room temperature. Raman studies indicated that the annealed samples had spectra of mechanical mixtures of $NaNO_3$ II and KNO_3 II for all the compositions studied except for $Na_{0.95}K_{0.05}NO_3$ (Table 5.1).

The $Na_{0.95}K_{0.05}NO_3$ solid gave the spectrum of the $NaNO_3$ II structure alone [1]: the typical bands at 100 and 186 cm^{-1} and a single band in each of the three internal vibrational regions: ν_1 (1068 cm^{-1}), ν_3 (1386 cm^{-1}) and ν_4 (725 cm^{-1}) respectively. Even in the most sensitive ν_1 region there was no detectable evidence of the existence of KNO_3 II (Fig. 5.2). In the Raman spectrum of $Na_{0.90}K_{0.10}NO_3$ a small band at 1053 cm^{-1} due to KNO_3 II was detected along with the strong band at 1069 cm^{-1} due to $Na_{0.95}K_{0.05}NO_3$ (NaII). Therefore the Raman studies indicated a solid solution $Na_{0.95}K_{0.05}NO_3$ (NaII) not previously reported. The spectra of all the other compositions indicated a eutectic mixture of $NaNO_3$ II (really $Na_{0.95}K_{0.05}NO_3$ (NaII)) and KNO_3 II. In the external vibrational region the strong bands due to KNO_3 II at 52 and 85 cm^{-1} and the strong band of $NaNO_3$ II at 186 cm^{-1} appeared in most of the spectra. The 52 cm^{-1} band, which is most sensitive to substitution of cations because it involves the translatory motion of the cations [99], remained essentially constant in the Raman spectra of all the mixtures.

In the internal vibrational region, there coexisted the bands due to $NaNO_3$ II (725, 1069, 1387 and 1670 cm^{-1}) and the bands due to KNO_3 II (716, 1052, 1346 and 1361 cm^{-1}). The frequencies of the Raman bands were independent of composition. As the composition of potassium nitrate increased from 10 to 95 mol%, the characteristic Raman bands of KNO_3 II increased in intensity gradually and those of $NaNO_3$ II decreased accordingly until all the Raman features of $NaNO_3$ II disappeared except the most sensitive ν_1 mode in $Na_{0.05}K_{0.95}NO_3$

---

[1] Later it was found that this might not represent an equilibrium state. After cooling a sample from 403 to 333 K over an interval of two weeks, a small peak appeared at about 1054 cm^{-1} .

(Fig. 5.2).

5.2.2 Raman Spectra of the 358 K Quenched Samples

Phase III of potassium nitrate, if cooled quickly, may be preserved in a metastable state at room temperature. The Raman spectra of the 358 K quenched samples may be used to indicate the range within which the KNO_3 III structure exists in the vicinity of 358 K. Greis *et al.* [66] deduced from the DSC cooling run that the solids in the whole composition region were simply a mixture of pure $NaNO_3$ II and pure KNO_3 III between 353 and 361 K. The Raman studies detected four kinds of solid for the 358 K quenched samples (Table 5.2): the solid solution $Na_{0.95}K_{0.05}NO_3$ (NaII); mixtures of $Na_{0.95}K_{0.05}NO_3$ (NaII) and a solid solution $Na_{1-x}K_xNO_3$ (KIII); mixtures of $Na_{1-x}K_xNO_3$ (KIII) and KNO_3 II; a new disordered state $Na_{1-x}K_xNO_3$ (D). $Na_{0.95}K_{0.05}NO_3$ (NaII) had the characteristic bands of the $NaNO_3$ II structure alone (Table 5.2).

$Na_{0.95}K_{0.05}NO_3$ (NaII) coexisted with $Na_{1-x}K_xNO_3$ (KIII) in $Na_{1-x}K_xNO_3$ (x = 0.10, 0.20, 0.33). The differences in frequencies between the two solid solutions were large enough for easy distinction. In the Raman spectrum of $Na_{0.90}K_{0.10}NO_3$, the features of $Na_{0.95}K_{0.05}NO_3$ (NaII) were predominant. In the external vibrational region, the characteristic band of $Na_{1-x}K_xNO_3$ (KIII) at about 125 cm^{-1} was just detectable (Fig. 5.3) and in the ν_3 region the characteristic profile of (KIII) was barely observed. In the ν_1 region there was a small peak at 1055 cm^{-1} due to $Na_{1-x}K_xNO_3$ (KIII) beside the strong band at 1068 cm^{-1} due to $Na_{0.95}K_{0.05}NO_3$ (NaII). The ν_4 vibration of $Na_{1-x}K_xNO_3$ (KIII) appeared as a low frequency tail

to the 725 cm^{-1} band of $Na_{0.95}K_{0.05}NO_3$ (NaII). As the content of KNO_3 increased to 33 mol%, the bands due to $Na_{0.95}K_{0.05}NO_3$ (NaII) gradually decreased in intensity and the intensities of the Raman bands due to $Na_{1-x}K_xNO_3$ (KIII) increased accordingly. From 40 to 1700 cm^{-1} distinct bands due to both solid solutions were observed throughout the whole Raman spectrum of $Na_{0.67}K_{0.33}NO_3$, clearly indicating the coexistence of the two phases (Figs. 5.3 and 5.4).

At the KNO_3 rich end, $Na_{1-x}K_xNO_3$ (KIII) coexisted with KNO_3 II. The Raman spectrum of $Na_{0.10}K_{0.90}NO_3$ was almost entirely that of the KNO_3 III structure, with only very weak features of KNO_3 II observed in the external vibrational region. The strong bands at 52 and 83 cm^{-1} of KNO_3 II were just observable (Fig. 5.3). In both the ν_1 and ν_4 regions only one band was detected due to the similar energies of these vibrations in both phases. The ν_3 vibration of KNO_3 II was too weak to be detected in the Raman spectrum of $Na_{0.10}K_{0.90}NO_3$.

The Raman features of KNO_3 II increased dramatically when the mole fraction of KNO_3 increased from 0.90 to 0.95. In the external vibrational region, the two bands of KNO_3 II at 52 and 85 cm^{-1} appeared more strongly than the libration of the nitrate ion in $Na_{1-x}K_xNO_3$ (KIII) at 125 cm^{-1} (Fig. 5.3). The ν_1 and ν_4 vibrations were still inseparable for the two phases but shifted 1 cm^{-1} to the lower frequencies due to the increasing amount of KNO_3 II. In the ν_3 region one of the doublet peaks of KNO_3 II was strong enough to produce a distinct band at 1360 cm^{-1} (Fig. 5.4) but the other band (1344 cm^{-1}) overlapped with the band at 1348 cm^{-1} of $Na_{1-x}K_xNO_3$ (KIII) to give an asymmetric band near 1351 cm^{-1}, which then appeared stronger than the other band of (KIII) at 1444 cm^{-1}. To judge by the relative strengths of the bands due to $Na_{1-x}K_xNO_3$ (KIII) and KNO_3 II in the external and ν_3 regions,

both phases were present in $Na_{0.05}K_{0.95}NO_3$ in comparable amounts.

In the intermediate concentration region (x = 0.50, 0.67, 0.80), the Raman spectra had features dissimilar to any known spectrum of pure KNO_3 or $NaNO_3$ in any phase. The bands in both external and internal vibrational regions were broad. To judge by the profile in the ν_1 region, which was much broader than the band of a single pure nitrate, there must be more than one state of the nitrate ion in these solids. The maxima in the ν_1 and external vibrational regions shifted noticeably to lower wavenumbers as the mole fraction of $NaNO_3$ decreased: from 1067 and 152 cm^{-1} for $Na_{0.50}K_{0.50}NO_3$ to 1056 and 127 cm^{-1} for $Na_{0.20}K_{0.80}NO_3$. In the ν_3 region there was a broad band which extended from 1340 to 1450 cm^{-1} (Fig. 5.4). These features are typical for Raman spectra of disordered or amorphous [71] substances and indicated a new disordered state $Na_{1-x}K_xNO_3$ (D) in this composition region.

5.2.3 Raman Spectra of the 393 K Quenched Samples

When quenched from 393 K, the structure of potassium nitrate in the solid solutions $Na_{1-x}K_xNO_3$ will normally have the KNO_3 III structure. In Greis' phase diagram determined from DSC cooling runs there were two kinds of solid at 393 K. One was the $R\bar{3}m$ solid solution for x > 0.40 and the other was a mixture of the $R\bar{3}m$ solid solution and $NaNO_3$ II ($R\bar{3}c$) for x < 0.40 (Fig. 5.1). Raman studies indicated that there were four kinds of solid for the 393 K quenched samples (Table 5.3): the solid solution $Na_{0.95}K_{0.05}NO_3$ (NaII); mixtures of $Na_{0.95}K_{0.05}NO_3$ (NaII) and a metastable state of the residual $R\bar{3}m$ solid solution $Na_{1-x}K_xNO_3$ (RSS); the solid solution $Na_{1-x}K_xNO_3$ (KIII); the new disordered state

$Na_{1-x}K_xNO_3$ (D). As in the case of the annealed or the 358 K quenched sample, $Na_{0.95}K_{0.05}NO_3$ (NaII) had the Raman features of the $NaNO_3$ II structure alone.

A metastable state of the residual $R\bar{3}m$ solid solution $Na_{1-x}K_xNO_3$ (RSS) after exsolution of $Na_{0.95}K_{0.05}NO_3$ (NaII) coexisted with (NaII) for $0.10 \leq x \leq 0.33$. This was the two phase region ($R\bar{3}m$ and $R\bar{3}c$) at 393 K in Greis' phase diagram. Since the residual $R\bar{3}m$ solid solution was unquenchable, it transformed to a metastable state (RSS). The samples in this composition region had two sets of bands: in addition to bands due to $Na_{0.95}K_{0.05}NO_3$ (NaII) there were bands due to $Na_{1-x}K_xNO_3$ (RSS). In the Raman spectrum of $Na_{0.90}K_{0.10}NO_3$ there were small shoulders at 717 cm^{-1} in the ν_4 region and at about 1062 cm^{-1} in the ν_1 region. The intensities of these shoulders increased as x increased. A broad feature from 1350 to 1450 cm^{-1} also appeared (Fig. 5.5). In the external vibrational region there was a diffuse feature between the two lattice vibrations of $Na_{0.95}K_{0.05}NO_3$ (NaII) at 102 and 188 cm^{-1}. This feature became a broad band at 150 cm^{-1} in $Na_{0.67}K_{0.33}NO_3$ (Fig. 5.6).

From comparison of the spectra of the same sample quenched from 393 and 358 K (Fig. 5.7), it was clear that the metastable state in $Na_{1-x}K_xNO_3$ (RSS) did not have the KNO_3 III structure. In the ν_3 region the broad profile was evidently different from the TO-LO features of KNO_3 III. In the 393 K quenched samples the ν_1 vibration of $Na_{1-x}K_xNO_3$ (RSS) had a frequency close to the ν_1 band of $Na_{0.95}K_{0.05}NO_3$ (NaII) so that it appeared as a shoulder in $Na_{1-x}K_xNO_3$ for $x = 0.10, 0.20$ and merged to one band for $x = 0.33$ (Fig. 5.7). On the other hand, the 358 K quenched samples had two well-separated bands in the ν_1 region due to $Na_{1-x}K_xNO_3$ (KIII) and $Na_{0.95}K_{0.05}NO_3$ (NaII) respectively. The Raman features in the external vibrational region were broader and at lower frequencies for $Na_{1-x}K_xNO_3$ (RSS) in the 393 K

quenched sample than the libration of NO_3^- in $Na_{1-x}K_xNO_3$ (KIII) in the 358 K quenched sample (Figs 5.3 and 5.6).

The fact that a metastable state (RSS) rather than KNO_3 III was frozen implied that the residual $R\bar{3}m$ solid solution had not decomposed into KNO_3 and $NaNO_3$ in the process of quenching. As $Na_{0.95}K_{0.05}NO_3$ (NaII) separated from the $R\bar{3}m$ solid solution, the residual solid solution became more concentrated with KNO_3 and transformed to the intermediate concentration region to be discussed later. In the external vibrational region the broad features of $Na_{1-x}K_xNO_3$ (RSS) in the samples with $0.10 \leq x \leq 0.33$ was centred at about 150 cm^{-1} and appeared quite like the band due to the sample with $x = 0.50$ (Fig. 5.6).

The samples with $x \geq 0.90$ presented almost the same Raman spectra as the KNO_3 III structure alone in every sensitive region (Table 5.3). These crystals were solid solutions of $Na_{1-x}K_xNO_3$ (KIII). To judge by the small changes in the spectra, the lattice of (KIII) seemed to change little with the replacement of potassium ions by smaller sodium ions at less than 10 mol%. The symmetrical single band at 128 cm^{-1}, attributed to the rotatory motion of the nitrate ion in $Na_{1-x}K_xNO_3$ (KIII) (Fig. 5.6), shifted to slightly higher frequency when the smaller sodium ion replaced the larger potassium ion. The bands at 718 and 1055 cm^{-1} were typical for the KNO_3 III structure and were also symmetric. In the ν_3 region the transverse and longitudinal optical mode Raman features of the KNO_3 III structure [55] appeared distinctly: the weaker band at 1352 cm^{-1} (TO) and the stronger band at 1444 cm^{-1} (LO) and the $2\nu_4$ vibration at 1435 cm^{-1}. No detectable features due to other structures were observed between the TO and LO modes (Fig. 5.5).

It is interesting to notice that the TO-LO pattern of $Na_{1-x}K_xNO_3$ (KIII) was a little

different from that in pure KNO_3 III [55] and $K_{1-x}Rb_xNO_3$ (KIII) (Fig. 5.8). When compared to the intensity of the ν_4 band, the relative intensity of the TO mode in $K_{1-x}Rb_xNO_3$ (KIII) and in $Na_{1-x}K_xNO_3$ (KIII) may be regarded as the same while the intensity of the LO mode in $Na_{1-x}K_xNO_3$ (KIII) becomes much larger. TO-LO splitting occurs for polar vibrational modes. The large increase in the intensity of the LO mode indicated a significant change in the lattice polarization when a small amount of $NaNO_3$ was added.

Just as in the case of the 358 K quenched samples, in the intermediate concentration region ($0.50 \leq x \leq 0.80$) there was the new disordered state $Na_{1-x}K_xNO_3$ (D) in the 393 K quenched samples (Fig. 5.9). Broad features were observed over the whole spectrum. The spectrum of $Na_{0.20}K_{0.80}NO_3$ (D) had the same spectral pattern as that of $Na_{0.10}K_{0.90}NO_3$ (KIII) in both external and internal vibrational regions. However, there were several notable differences. The frequency of the ν_1 band was 3 cm^{-1} higher in the former than in the latter, which was beyond the instrumental error. It was too large a shift to be caused by introduction of the extra 10 mol% of KNO_3 when compared to the frequency difference in ν_1 between $Na_{0.10}K_{0.90}NO_3$ (KIII) and $Na_{0.05}K_{0.95}NO_3$ (KIII). The band in the ν_1 region, as well as in the ν_4 and external vibrational regions, was considerably broader in $Na_{0.20}K_{0.80}NO_3$ (D) than in $Na_{0.10}K_{0.90}NO_3$ (KIII). In the ν_3 region the well-separated TO-LO bands of KNO_3 III at 1352 and 1444 cm^{-1} superimposed on a broad background from about 1350 to 1450 cm^{-1}.

The broadened bands were also observed in the Raman spectra of $Na_{0.33}K_{0.67}NO_3$ (D) and $Na_{0.50}K_{0.50}NO_3$ (D). The three samples had very similar Raman spectra. They all had a broad band in the ν_1 region, the maximum of which shifted from 1066 cm^{-1} for $Na_{0.50}K_{0.50}NO_3$ to 1058 cm^{-1} for $Na_{0.20}K_{0.80}NO_3$. The O-18 form of the nitrate ion, $N\,^{18}O\,^{16}O_2^-$, gave a peak

at a position about 20 cm^{-1} lower than that of $N^{16}O_3^-$. The two bands do not overlap in the Raman spectrum of the crystalline nitrates, while in the three disordered samples there was a serious overlap and the band due to $N^{18}O^{16}O_2^-$ could hardly be observed (Fig. 5.5). The bands in the external vibrational region were broad and asymmetric (Fig. 5.6). As the amount of KNO_3 increased from 50 to 80 mol%, the band became more symmetrical and the maximum shifted from 152 to 127 cm^{-1}. The symmetrical band at 718 cm^{-1} in the ν_4 region appeared unchanged with the different compositions of $Na_{1-x}K_xNO_3$ (D). It was much broader than the band at 718 cm^{-1} of $Na_{0.10}K_{0.90}NO_3$ (KIII) or the band at 725 cm^{-1} of $Na_{0.95}K_{0.05}NO_3$ (NaII) quenched from the same temperature of 393 K. The change of the profile in the ν_3 region with the change of the composition was most interesting. All the three samples had a broad feature extending from about 1350 to 1450 cm^{-1}. In $Na_{0.50}K_{0.50}NO_3$ (D) there was a small maximum at 1385 cm^{-1} on the broad background. The maximum disappeared in $Na_{0.33}K_{0.67}NO_3$ (D), replaced by a rather flat plateau from 1358 to 1445 cm^{-1}. The plateau got lower and its edges grew into distinct bands at 1354 and 1447 cm^{-1} in the spectrum of $Na_{0.20}K_{0.80}NO_3$ (D) to give a profile quite like that of KNO_3 III in the ν_3 region.

5.2.4 Raman Spectra of the 493 K Quenched Samples

It has usually been assumed [66] that sodium nitrate and potassium nitrate form a continuous series of solid solutions of the $R\bar{3}m$ structure just below the solidus. The disordered calcite structure $R\bar{3}m$ is unquenchable and can only be investigated at high temperature. Thus, the quenched samples represent new metastable states brought about in

the course of quenching. The Raman spectra of the 493 K quenched samples indicated that three states may be frozen from the $R\bar{3}m$ solid solutions: the solid solutions $Na_{1-x}K_xNO_3$ (NaII), (D) and (KIII). As x increased from 0.05 to 0.95, the Raman spectra changed from that of $Na_{1-x}K_xNO_3$ (NaII) to that of $Na_{1-x}K_xNO_3$ (KIII) (Table 5.4).

The features in the external vibrational region revealed an interesting change due to the formation of the solid solutions of different ratios of sodium ions to potassium ions (Fig. 5.10). The characteristic bands at 100 and 187 cm^{-1} of $Na_{0.95}K_{0.05}NO_3$ (NaII) shifted to lower frequency as smaller sodium ions were replaced by larger potassium ions. At x = 0.33, only one distinct band remained at 170 cm^{-1} and the 100 cm^{-1} band was replaced by a small shoulder at about 80 cm^{-1} on the Rayleigh wing. The 170 cm^{-1} band continued to shift to lower frequency as more potassium ions were added until at x = 0.90 the characteristic band of the KNO_3 III structure appeared at 127 cm^{-1} and the weak shoulder disappeared.

The gradual change in the ν_3 region was also quite notable (Fig. 5.11). There was one peak at 1386 cm^{-1} in the Raman spectra of $Na_{0.95}K_{0.05}NO_3$ and $Na_{0.90}K_{0.10}NO_3$. It was assigned to the ν_3 vibration of the nitrate ion in the $NaNO_3$ II structure. The intensity of the peak decreased and a broad feature appeared from 1350 to 1450 cm^{-1} when x = 0.20. The intensity of the 1386 cm^{-1} band continued to decrease and the broad feature grew stronger as the content of K^+ increased until x = 0.67 when the band at 1386 cm^{-1} disappeared and the broad feature developed into two small peaks at 1355 and 1448 cm^{-1}. Finally, at x = 0.90, these two peaks became the characteristic TO-LO features of the KNO_3 III structure in the ν_3 region.

Only one peak appeared in the ν_1 region with a relatively constant frequency at about 1068 cm^{-1} for x up to 0.50 (Table 5.4). Then it shifted to lower wavenumbers as additional

K^+ was added: 1065 cm^{-1} for $Na_{0.33}K_{0.67}NO_3$ and 1057 cm^{-1} for $Na_{0.20}K_{0.80}NO_3$. At the same time the band became broad and the peak due to $N^{18}O^{16}O_2^-$ was obscured. Eventually the peak became the ν_1 vibration of the KNO_3 III structure at 1055 cm^{-1} and was sharp again in $Na_{0.10}K_{0.90}NO_3$ (Fig. 5.12).

There was also a single band in the ν_4 region (Table 5.4). The shift from the typical frequency of $Na_{1-x}K_xNO_3$ (NaII) (725 cm^{-1}) to the typical frequency of (KIII) (718 cm^{-1}) started at $x = 0.33$, which was a little different from the shift of the ν_1 vibration. The band appeared rather symmetric for all the compositions while it was obviously broader in $Na_{0.80}K_{0.20}NO_3$ through $Na_{0.20}K_{0.80}NO_3$ than in the other compositions (Fig. 5.12).

The samples with $x \leq 0.20$ may be regarded as solid solutions with the $NaNO_3$ II structure ($R\bar{3}c$) alone. The Raman spectra had the characteristic pattern of $NaNO_3$ II. Single bands were observed in the ν_1 and ν_4 regions, which shifted a little from the typical values of $NaNO_3$ II (1068 and 725 cm^{-1}) as x increased from 0.05 to 0.20. The band width and profiles in the internal vibrational region were consistent with an assignment to a solid solution with the crystal structure of $NaNO_3$, $Na_{0.80}K_{0.20}NO_3$ (NaII) (Fig. 5.12). The two bands in the external vibrational region at about 100 and 180 cm^{-1} also indicated that $Na_{0.80}K_{0.20}NO_3$ (NaII) consisted of a single crystal structure (Fig. 5.10). On the contrary, in the Raman spectra of the same sample quenched from 393 K there were other features between the two bands (Fig. 5.6), which suggested an additional metastable phase.

$Na_{0.67}K_{0.33}NO_3$ may also be regarded as a solid solution with the $NaNO_3$ II structure. However, the great number of potassium ions caused the crystal to possess considerable disorder. There was only one distinct band in the external vibrational region (Fig. 5.10) and

the bands in the internal vibrational region were a bit broader than the bands of the samples with less KNO_3. The samples $Na_{1-x}K_xNO_3$ (x = 0.50, 0.67, 0.80) had the same Raman features of the disordered phase as those described for the 358 and 393 K quenched samples (Fig. 5.9). The samples with x = 0.90, 0.95 had practically the same Raman spectra as the same samples quenched from 393 K and appear to have the KNO_3 III structure.

5.3 Discussion

The $NaNO_3$-KNO_3 system is rather interesting. The size difference between sodium and potassium ions is large, yet the nitrates are reported [4,66] to form continuous solid solutions. At high temperature (above 548 K) both nitrates adopt the same $R\bar{3}m$ structure, at moderate temperature (above 373 K) they have similar structures ($R\bar{3}c$ and $R\bar{3}m$ or R3m), and at room temperature their structures are quite different ($R\bar{3}c$ and Pmcn).

Raman spectroscopic studies of the mixed crystals of sodium and potassium nitrate were in general agreement with the phase diagram by DSC. It is expected that the different treatments of the samples and the different basic principles between DSC and Raman can account for minor discrepancies in the observations. The quenched samples measured by Raman spectroscopy may have different microstructures, different solid solubilities and non-equilibrium crystalline phases or amorphous structures. Furthermore, Raman spectra are measured for samples under vacuum. In principle, DSC is based on macroscopic properties of the system while Raman gives information about the microscopic structure of the system. Raman may provide justification of atomic level for the structures of the solids deduced from

DSC.

5.3.1 Limited Solid Solutions in $NaNO_3$-KNO_3

In Greis' phase diagram of $NaNO_3$-KNO_3 established by DSC cooling runs, only one kind of solid solution – the continuous solid solutions of $R\bar{3}m$ was reported [66]. Exsolution of the pure components from the $R\bar{3}m$ solid solution was the only explanation to account for the subsolidus in the phase diagram. No other kinds of solid solution and no structural phase transitions of one kind of solid solution to another kind of solid solution were observed. Our Raman studies of the $NaNO_3$-KNO_3 mixtures quenched from different temperatures suggested some alternative explanations for the phase diagram.

The same Raman spectrum of the $NaNO_3$ II structure alone was observed for $Na_{0.95}K_{0.05}NO_3$ quenched from different temperatures, indicating that there existed the solid solution $Na_{0.95}K_{0.05}NO_3$ (NaII) over the whole investigated temperature range. We have measured the Raman spectrum of the sample quenched directly from the melt and found that it also had the Raman bands of the $NaNO_3$ II structure alone. According to the phase diagram, $Na_{0.95}K_{0.05}NO_3$ was in the diphasic region below the λ transition temperature at 526 K. The phases coexisting with pure $NaNO_3$ II would be the $R\bar{3}m$ solid solution or low temperature phases of pure KNO_3. The relative amounts of pure $NaNO_3$ II and the $R\bar{3}m$ solid solution at 493 and 393 K would be different. All these conditions would cause different Raman features in the spectra of the samples undergoing different heat treatments. However, no detectable variations in the Raman spectra were observed. On the other hand, $Na_{0.90}K_{0.10}NO_3$ had four

different Raman spectra in response to the four different treatments: the Raman spectrum of $Na_{0.90}K_{0.10}NO_3$ (NaII) for the 493 K quenched sample; the spectrum of $Na_{0.95}K_{0.05}NO_3$ (NaII) and (RSS) for the 393 K quenched sample; the spectrum of $Na_{0.95}K_{0.05}NO_3$ (NaII) and (KIII) for the 358 K quenched sample; and the spectrum of $NaNO_3$ II and KNO_3 II for the annealed sample.

Raman studies suggested that $Na_{0.95}K_{0.05}NO_3$ (NaII) existed in the temperature range between 526 and about 353 K. Decomposition of this solid solution proceeded very slowly. When cooled down from 403 to 343 K in two days, the solid solution did not show any exsolution while all samples with higher K^+ contents became mechanical mixtures of the two components (Table 5.1). Exsolution of KNO_3 was detected only after the solid solution was annealed to 333 K in two weeks. Therefore Raman studies suggested that there should be a vertical line at x = 0.05 and from 526 to 353 K to indicate the solid solution $Na_{0.95}K_{0.05}NO_3$ (NaII). This is supported by the discontinuity at x = 0.063 (point Y in Fig. 5.1) on the curve that indicated the phase separation of $R\bar{3}c$ from $R\bar{3}m$. Greis neglected the dramatic drop of the transition temperature at x = 0.063 and simply assigned areas a and b in Fig. 5.1 as the diphasic region of $R\bar{3}c$ and $R\bar{3}m$.

With the vertical line at x = 0.05 to indicate $Na_{0.95}K_{0.05}NO_3$ (NaII), there should be two areas below the boundary. Area a (Fig. 5.1) is the uniphasic region of $Na_{1-x}K_xNO_3$ (NaII) and the upper boundary of the area is for the λ transition of $Na_{1-x}K_xNO_3$ (NaI) to (NaII). Area b (Fig. 5.1) should be diphasic of $Na_{0.95}K_{0.05}NO_3$ (NaII) and the $R\bar{3}m$ solid solution and the upper boundary indicates the exsolution of the solid solution $Na_{0.95}K_{0.05}NO_3$ (NaII) from the $R\bar{3}m$ solid solutions. The need to include this vertical line has been confirmed by the temperature

dependent Raman spectra of $Na_{0.95}K_{0.05}NO_3$ (Chapter 6).

Transitions of the $R\bar{3}m$ solid solution to other structures of the solid solution may be brought about by quenching. Raman studies of the 493 K quenched samples suggested that the $R\bar{3}m$ solid solutions transformed to $Na_{1-x}K_xNO_3$ (NaII) for $x \leq 0.20$ or to (KIII) for $x \geq 0.90$. The 493 K quenched $Na_{0.80}K_{0.20}NO_3$ had the characteristic Raman bands of $NaNO_3$ II ($R\bar{3}c$) alone and the 493 K quenched $Na_{0.10}K_{0.90}NO_3$ had the characteristic Raman bands of KNO_3 III (R3m) alone. The structural phase transition of the $R\bar{3}m$ solid solutions to the $R\bar{3}c$ solid solutions was similar to the transition of pure $NaNO_3$ I quenched from high temperature. The structural phase transition of the $R\bar{3}m$ solid solutions to the R3m solid solutions was similar to the transition of pure KNO_3 I quenched from high temperature. For these reasons the $R\bar{3}m$ solid solutions for $x \leq 0.20$ may well be regarded as limited solid solutions $Na_{1-x}K_xNO_3$ (NaI) and the $R\bar{3}m$ solid solutions for $x \geq 0.90$ may well be regarded as limited solid solutions $Na_{1-x}K_xNO_3$ (KI), presuming that $NaNO_3$ I and KNO_3 I have different structures. Support for this interpretation can be found from Raman studies [55] of the pure nitrates which indicated that $NaNO_3$ I and KNO_3 I did not have identical structures.

Thus, based on information about the microscopic structures of the system, Raman studies suggested that there were limited solid solutions $Na_{1-x}K_xNO_3$ (NaII) and (KIII) in addition to the $R\bar{3}m$ solid solutions and that there were transitions of the $R\bar{3}m$ solid solutions to the limited solid solutions in addition to exsolution of the pure components. These two important observations appear to offer a more reasonable explanation for the phase diagram established by DSC cooling runs.

5.3.2 The Solids Between 353 and 361 K

Thermal effects were observed by DSC cooling run [66] at 353 K in the composition range $0.20 \leq x \leq 0.95$ and attributed to the transition of phase III to II of pure potassium nitrate. These authors extended the range and a horizontal line was drawn across the phase diagram at 353 K along with another horizontal line at 361 K. Mechanical mixtures of pure $NaNO_3$ II and KNO_3 III were deduced for the solids in areas c and d (Fig. 5.1). Area e was regarded as the diphasic region $R\bar{3}m$ and R3m and its upper boundary corresponded to exsolution of KNO_3 and the transition of KNO_3 I to KNO_3 III. Raman studies of the 358 K quenched samples indicated that this was not necessarily the case.

Raman studies indicated that the 358 K quenched $Na_{0.05}K_{0.95}NO_3$ and $Na_{0.10}K_{0.90}NO_3$ were mixtures of KNO_3 II and $Na_{1-x}K_xNO_3$ (KIII) instead of $NaNO_3$ II and KNO_3 III. It is not likely that quenching had brought about a structural change of $NaNO_3$ II to KNO_3 II. It seems more likely that at 358 K some of the potassium nitrate exsolved from the solid solution and transformed to phase II. The sodium nitrate dissolved in the remaining potassium nitrate to form the solid solution $Na_{1-x}K_xNO_3$ (KIII) which is quenchable. In the small range between the horizontal lines at 353 and 361 K, there should be a vertical line at x a bit less than 0.90 indicating the solid solution (KIII) because the 358 K quenched $Na_{0.10}K_{0.90}NO_3$ sample had a Raman spectrum dominated by $Na_{1-x}K_xNO_3$ (KIII). The weak bands at 52 and 84 cm^{-1} due to KNO_3 II (Fig. 5.3) indicated that only a small fraction of KNO_3 II had exsolved from the 358 K quenched $Na_{0.10}K_{0.90}NO_3$. As the content of $NaNO_3$ halved, the amount of $Na_{1-x}K_xNO_3$ (KIII) appeared to be approximately halved and the relative intensity

of the bands due to KNO_3 II and $Na_{1-x}K_xNO_3$ (KIII) appeared to be nearly equal in the spectrum of $Na_{0.05}K_{0.95}NO_3$ (Fig 5.3).

The Raman spectra of the 393 and 493 K quenched samples also indicated that the composition limit for $Na_{1-x}K_xNO_3$ (KIII) was at x between 0.90 and 0.80. The Raman spectra of the 393 and 493 K quenched $Na_{0.10}K_{0.90}NO_3$ had the same characteristic bands of KNO_3 III alone while the spectra of $Na_{0.20}K_{0.80}NO_3$ represented the new disordered state.

The KNO_3 rich end of the phase diagram from the DSC cooling run may be properly explained by the assumption that there should be a vertical line for $Na_{1-x}K_xNO_3$ (KIII) with x between 0.90 and 0.80. The upper boundary of area e ended at x = 0.85 (Fig. 5.1). This may be the indication for the vertical line. The existence of the vertical line at $Na_{0.15}K_{0.85}NO_3$ (KIII) provides another interpretation for the observed thermal effects in this region. Area e (Fig. 5.1) should be a uniphasic region of $Na_{1-x}K_xNO_3$ (KIII) instead of a diphasic region of a mixture of KNO_3 III and the $R\bar{3}m$ solid solution its upper boundary should be due to the transition of the $R\bar{3}m$ solid solution (KI) to the R3m solid solution (KIII) instead of exsolution of KNO_3 III from the $R\bar{3}m$ solid solution and. The thermal effects at 361 K in this region should be due to exsolution of KNO_3 II from $Na_{1-x}K_xNO_3$ (KIII) instead of $NaNO_3$ II from the $R\bar{3}m$ solid solution.

The existence of $Na_{0.15}K_{0.85}NO_3$ (KIII) was justified by the dramatic lowering of the transition temperature of phase III to II of potassium nitrate. The transition temperature was found to be 353 K [66] while the literature values for pure potassium nitrate are 397 K for the transition of phase I to III and 383 K for transition of phase III to II [117]. The lowering of the transition temperature may be due to formation of solid solution or due to impurities. The

former was more likely because the transition temperature remained practically constant over the whole composition region. If it had been due to the impurities, the transition temperature would have changed with compositions. The horizontal line at 353 K in Greis' phase diagram indicated that the thermal effect was related to the same structural change no matter the composition. Greis and the co-workers deduced that the structural change was the transition of phase III to II of pure KNO_3. Therefore the mixtures between 353 and 361 K were those of KNO_3 III and $NaNO_3$ II. The vertical line for $Na_{0.15}K_{0.85}NO_3$ (KIII) provides another explanation. The constant thermal effect was due to the same structural phase transition involving $Na_{0.15}K_{0.85}NO_3$ (KIII). Because of formation of this solid solution, the transition temperature was lowered. On the right of the vertical line (area c), KNO_3 II coexisted with $Na_{0.15}K_{0.85}NO_3$ (KIII) and on the left (area d), Na $_{0.85}$K $_{0.15}$NO $_3$ (NaII) coexisted with $Na_{0.15}K_{0.85}NO_3$ (KIII), as was observed in the Raman studies of the 358 K quenched samples.

5.3.3 The Disordered State in the Intermediate Concentration Region

Raman studies indicated that a new disordered state (area f in Fig. 5.1) was quenched to room temperature. The three samples with x = 0.50, 0.67, 0.80 had almost the same broadened Raman spectrum, when quenched from 358, 393 or 493 K (Fig. 5.9). The bands in the ν_3 region were very similar, in both band position and profile. The bands in the external vibrational region and in the ν_4 and $2\nu_2$ regions were also similar (Fig. 5.3). However the ν_1 bands displayed slight differences. The frequency of the 358 K quenched sample was lower than those of the other two and the band appeared sharper at the top (Fig. 5.9). A low

frequency component was almost resolved from the broad band.

The separation of the ν_1 band was more distinct in the 358 K quenched $Na_{0.33}K_{0.67}NO_3$ and $Na_{0.50}K_{0.50}NO_3$. There was a shoulder at 1055 cm^{-1} in the spectrum of the latter and at 1060 cm^{-1} in the former (Fig. 5.13). The low frequency shoulder increased in intensity as x increased until it became the major component of the band in $Na_{0.20}K_{0.80}NO_3$.

In the Raman spectrum of the 358 K quenched $Na_{0.50}K_{0.50}NO_3$, minor band separations were also observed in the external vibrational region (Fig. 5.3) and the ν_4 and ν_3 regions (Fig. 5.14). The shoulder at about 125 cm^{-1} and the shoulder at 1055 cm^{-1} may be due to $Na_{1-x}K_xNO_3$ (KIII). The shoulder at 724 cm^{-1} and the peak at 1386 cm^{-1}, which looked sharper and higher than those of the same sample quenched from 393 or 493 K, indicated the existence of $Na_{1-x}K_xNO_3$ (NaII).

The Raman spectra of the quenched samples with x = 0.50, 0.67 and 0.80 had the typical Raman features of disordered solids: broad bands over the whole spectrum with large frequency shifts in the external vibrational region (from 152 to 127 cm^{-1}) and in the ν_1 region (from 1068 to 1058 cm^{-1}) when x increased from 0.50 to 0.80. To judge by the frequency of the ν_1 vibration, the solids in this composition range corresponded to a transition from the $NaNO_3$ II-dominant structure to the KNO_3 III-dominant structure. The regular change of the profile in the ν_3 region also indicated this transition. The small peak at 1386 cm^{-1} in $Na_{0.50}K_{0.50}NO_3$ was characteristic of the $NaNO_3$ II structure and the two bands at 1353 and 1447 cm^{-1} in $Na_{0.20}K_{0.80}NO_3$ were characteristic of the KNO_3 III structure. In this regard the solids appeared to be mixtures of $Na_{1-x}K_xNO_3$ (NaII) and (KIII) with different ratios. The domain of $Na_{1-x}K_xNO_3$ (NaII) and (KIII) must be on a scale of dozens of nanometers since

they produced a broadened Raman spectrum instead of a spectrum of distinct bands of ordinary mixtures.

In Greis' phase diagram from the DSC cooling run there was a eutectoid line at 361 K in the composition region $0.55 \leq x \leq 0.85$. The sample $Na_{0.50}K_{0.50}NO_3$ exhibited phase separation because it is located slightly outside the region. Above 361 K the solids in this region were the $R\bar{3}m$ solid solutions. The same structure should result from the solid solutions quenched from 393 or 493 K, as was observed in the Raman study. The 358 K quenched samples should have had different structures and be a mixture of $NaNO_3$ II and KNO_3 III according to the DSC study. However, broad Raman bands of the similarly disordered states were observed. There were hardly any band separations. It would appear that structural phase transitions of the samples in the eutectoid region took place so slowly that they were hardly detectable under present experimental conditions.

Kinetically hindered transformation at the eutectoid temperature is typical for disordered solids or glasses. Indeed the glassy state was observed in an early work on the $NaNO_3$-KNO_3 system [118]. The transparent mass was almost indistinguishable from the liquid by microscope. On one occasion in the present study we obtained the glass of equimolar $NaNO_3$-KNO_3. The Raman spectrum was almost the same as the spectrum of the melt but quite different from the spectrum of the quenched sample. The broader and smoother Raman bands of the glass suggested that the ions were in a more randomly mixed state than in the quenched disordered sample. There was no distinct peak at about 1386 cm^{-1} in the Raman spectrum of the glass. A slow transformation is a necessary precondition for a disordered or amorphous state to be quenchable. On the other hand, the manifestation of slow kinetics may be an indication of the

existence of a disordered or amorphous state. It seems likely that the new disordered state existed in the samples with $0.50 \leq x \leq 0.80$ before quenching. Usually the amorphous state which is frozen in already exists at the instant of quenching [115,116].

Raman studies suggested that the $R\bar{3}m$ solid solutions in area f (Fig. 5.1) were in a new disordered state which was quenchable. This disordered state was different from the disordered state in $Na_{1-x}K_xNO_3$ (NaI) or (KI) of the terminal phases which was unquenchable. Disorder in KNO_3 I or $NaNO_3$ I is caused by random orientation of the nitrate ion. Disorder in the new disordered state appear to have different origin. The new disordered state appears to be caused by phase separation. Raman studies indicated that the nitrate distribution in the new disordered state was not entirely random as in the melt or glass. The Raman spectra of the new disordered solids have the appearance of admixtures of very small particles of $Na_{1-x}K_xNO_3$ (NaII) and (KIII). Such phase separation on a microscopic or submicroscopic scale may be caused by the large size difference between sodium and potassium ions (26%). It would be difficult for these ions to form homogeneous solid solutions with large solubility at relatively low temperature. Moreover, $NaNO_3$ I and KNO_3 I have slightly different structures although both belong to the same space group $R\bar{3}m$ [55]. Phase separation between $Na_{1-x}K_xNO_3$ (NaI) and (KI) may already exist in the $R\bar{3}m$ solid solutions. When quenched, a mixture of $Na_{1-x}K_xNO_3$ (NaII) and (KIII) resulted.

It is now generally accepted that sodium and potassium nitrate form a continuous series of solid solutions under the solidus [4,8,66,110,111,113,114]. The suggestion of a eutectic system with limited solid solutions (10 and 76 mol% $NaNO_3$) proposed by Hussink [112] in 1900 has been rejected by most authors. It must be pointed out that the previous arguments for rejecting the

limited solid solution interpretation were not quite correct. It was argued [113,119] that the discrepancies resulted from different rates of cooling or heating. Definite eutectic pauses might be observed in a fairly broad interval on the heating curves when the rate was not sufficiently slow. A phase diagram based on cooling curves did not have a flat solidus and indicated the formation of a continuous series of solid solutions. All the early reports of phase diagrams [109,113,119] which supported the formation of a continuous series of solid solutions had a curvature at the minimum of the solidus. However, since 1980 when DSC studies were applied to the $NaNO_3$-KNO_3 system [4], it was found that the solidus was flat from 20 to 80 mol% KNO_3. The calculated solidus based on continuous solid solutions was not so flat and did not fit the experimental data very well. The discrepancies were as large as 30 K for x = 0.1 and 0.9. Still $NaNO_3$-KNO_3 was regarded as a system of continuous solid solutions. A hypothetical relationship [4] between the free energy curves of solid and liquid solutions was given to illustrate that a horizontal solidus may correspond a continuous series of solid solution.

The present Raman studies of the quenchable disordered state of the solid solutions offer an explanation for the horizontal solidus in the phase diagram of $NaNO_3$-KNO_3 from the view point of structural chemistry of the solids. There were basically three different kinds of structure in the $R\bar{3}m$ solid solutions. For $x \leq 0.20$ the $R\bar{3}m$ solid solutions behaved like $NaNO_3$ I. For $x \geq 0.90$ the $R\bar{3}m$ solid solutions behaved like KNO_3 I. For $0.50 \leq x \leq 0.80$ the $R\bar{3}m$ solid solutions were in the quenchable disordered state which seemed to be an admixture of $Na_{1-x}K_xNO_3$ (NaI or NaII) and (KI). If the $R\bar{3}m$ solid solutions in the terminal regions were regarded as two different phases $Na_{1-x}K_xNO_3$ (NaI) and (KI), and the solid

solutions in the intermediate concentration region were regarded as a eutectic mixture of (NaI) and (KI), $NaNO_3$-KNO_3 might well be regarded as a system of limited solid solutions. It is interesting to notice that the solid solubility limits suggested by the present Raman studies is consistent with the work in 1900 [112]. A system with limited solid solutions usually has a flat solidus in the intermediate concentration region. This is what has been observed by DSC. A theory based on limited solid solutions would account for the flatness and the calculated solidus would fit better to the experimental data than the calculated solidus [4] based on a continuous solid solution.

The most important experimental evidence supporting the theory of continuous solid solutions was the homogeneous appearance under microscope [113]. However, light microscopes are inappropriate for mixtures on a microscopic or submicroscopic scale. A eutectic mixture is believed to form if the percent of atoms within the interphase boundaries is negligible small. Usually the effective thickness of the interphase boundaries is about one or two atomic dimensions. When the particle size of a mixture exceeds 100 to 200 atomic dimensions, the percent of atoms in the boundaries become negligible. This size is well below the best possible resolution with optical microscope. The $NaNO_3$-KNO_3 system is complicated because the disordered calcite structures of $NaNO_3$ I and KNO_3 I are very similar under microscope and the mixture of the two structures must also be very similar. It is difficult for an optical microscope to distinguish different phases on a microscopic or submicroscopic scale.

5.4 Conclusions

Raman studies of $NaNO_3$-KNO_3 quenched from different temperatures revealed the following structural features which have been overlooked by DSC studies.

1. There existed limited solid solutions $Na_{1-x}K_xNO_3$ (NaII) and (KIII) as well as the $R\bar{3}m$ solid solutions and there existed structural phase transitions of the $R\bar{3}m$ solid solutions to these limited solid solutions in addition to exsolution of the components from the $R\bar{3}m$ solid solutions.
2. Two vertical lines were suggested to be added to Greis' phase diagram obtained by cooling runs. One indicated the solid solution $Na_{0.95}K_{0.05}NO_3$ (NaII) and the other indicated the solid solution $Na_{0.15}K_{0.85}NO_3$ (KIII).
3. A quenchable disordered state was detected by Raman spectroscopy for the $R\bar{3}m$ solid solutions in the intermediate concentration region. The disorder seemed to be due to phase separation of $Na_{1-x}K_xNO_3$ (NaI) and (KI). The existence of the new disordered state suggested that $NaNO_3$-KNO_3 might well be regarded as a system of limited rather than continuous solid solutions.

Table 5.1 Observed wavenumbers for Raman bands of the annealed $Na_{1-x}K_xNO_3$ measured at 298 K.

samples	external	ν_4	ν_1	ν_3	$2\nu_2$
$NaNO_3$ II [a]	102,199	724	1068	1386	1670
x = 0.05	100,186	725	1068	1386	1670
x = 0.10	85,100,187	717,725	1053,1069	1350,1386	1670
x = 0.20	52,85,100,125, 188	716,725	1052,1069	1346,1361,1387	1670
x = 0.33	52,85,100,126, 188	716,726	1052,1069	1346,1361,1387	1671
x = 0.50	52,85,100,125, 188	716,725	1052,1069	1346,1361,1387	1650,1670,1687
x = 0.67	52,85,125,187	716,725	1052,1069	1346,1361,1387	1650,1670,1683
x = 0.80	52,85,126,187	711,726	1052,1069	1346,1361,1387	1652,1670,1685
x = 0.90	51,84,124,186	715,725	1051,1068	1345,1360,1386	1650,1670,1685
x = 0.05	51,84,124	715	1051,1063	1345,1359	1650,1685
KNO_3 III [a]	52,84,125	715	1050	1344,1359	1652,1686

a. Data from reference 55.

Table 5.2 Observed wavenumbers for Raman bands of the $Na_{1-x}K_xNO_3$ samples quenched from 358 K and measured at 298 K.

samples	external	ν_4	ν_1	ν_3	$2\nu_2$
$NaNO_3$ II [a]	102,199	724	1068	1386	1670
x = 0.05	100,187	725	1069	1386	1670
x = 0.10	101,120,188	717,725	1055,1069	1387	1670
x = 0.20	101,125,187	717,725	1054,1068	1352,1386,1444	1668
x = 0.33	101,125,187	717,725	1054,1068	1351,1386,1444	1669
x = 0.50	(84) [b],152	718,724	1055,1067	1350,1386,1450	1667
x = 0.67	143	717	1060,1065	1360,1444	1667
x = 0.80	127	718	1056	1353,1447	1667
x = 0.90	52,86,128	718	1055	1352,1435,1446	1665
x = 0.95	52,84,125	717	1054	1351,1360,1433,1444	1664
KNO_3 II [a]	52,84,125	715	1050	1344,1359	1652,1682
KNO_3 III [a]	125	717	1053	1348,1436,1440	1664

a. Data from reference 55.

b. Weak feature on the Rayleigh wing.

Table 5.3 Observed wavenumbers for Raman bands of the $Na_{1-x}K_xNO_3$ samples quenched from 393 K and measured at 298 K.

samples	external	ν_4	ν_1	ν_3	$2\nu_2$
$NaNO_3$ II [a]	102,199	724	1068	1386	1670
x = 0.05	100,186	725	1069	1386	1670
x = 0.10	100,187	717,725	1060,1069	1386	1670
x = 0.20	102,188	717,726	1061,1069	1340-1450 [b],1387	1670
x = 0.33	100,150,184	716,724	1067	1340-1450 [b],1385	1668
x = 0.50	152	718	1066	1340-1450 [b],1385	1667
x = 0.67	138	717	1065	1358,1445	1667
x = 0.80	127	718	1058	1354,1447	1667
x = 0.90	128	718	1055	1351,1435,1445	1665
x = 0.95	127	719	1055	1352,1434,1444	1665
KNO_3 III [a]	125	717	1053	1348,1436,1440	1664

a. Data from reference 55.

b. Broad diffuse features from 1340 to 1450 cm^{-1}.

Table 5.4 Observed wavenumbers for Raman bands of the $Na_{1-x}K_xNO_3$ samples quenched from 493 K and measured at 298 K.

samples	external	ν_4	ν_1	ν_3	$2\nu_2$
$NaNO_3$ II [a]	102,199	724	1068	1386	1670
x = 0.05	100,187	725	1068	1386	1670
x = 0.10	99,186	725	1068	1386	1670
x = 0.20	96,181	724	1067	1340-1450 [c],1385	1669
x = 0.33	(80) [b],170	720	1067	1340-1450 [c],1385	1669
x = 0.50	(80) [b],151	719	1068	1340-1450 [c],1386	1668
x = 0.67	(80) [b],135	718	1065	1355,1448	1667
x = 0.80	(80) [b],128	718	1057	1353,1433,1447	1666
x = 0.90	128	718	1055	1352,1435,1446	1665
x = 0.95	127	718	1055	1351,1434,1444	1665
KNO_3 III [a]	125	717	1053	1352,1436,1440	1664

a. Data from reference 55.

b. Weak features on the Rayleigh wing which decrease in frequency and intensity as x increases.

c. Broad and diffuse features from 1340 to 1450 cm^{-1} .

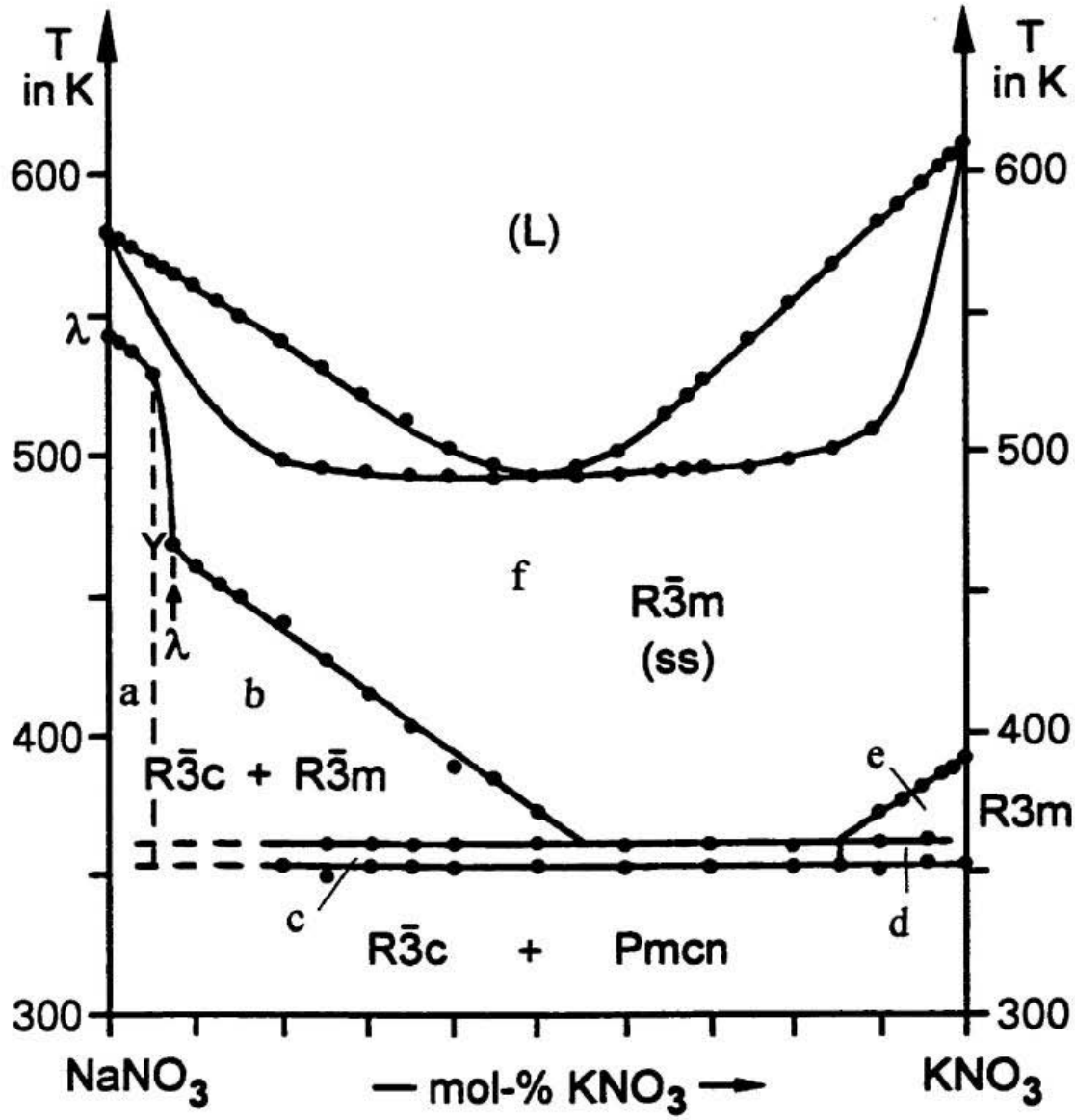

Fig. 5.1 The Greis' phase diagram [66] of $NaNO_3$-KNO_3 established from DSC cooling runs. Two additional vertical lines are suggested to indicate $Na_{0.95}K_{0.05}NO_3$ (NaII) and $Na_{0.15}K_{0.85}NO_3$ (KIII). Raman studies offer different explanations from Greis' in the areas a, b, c, d, e and f.

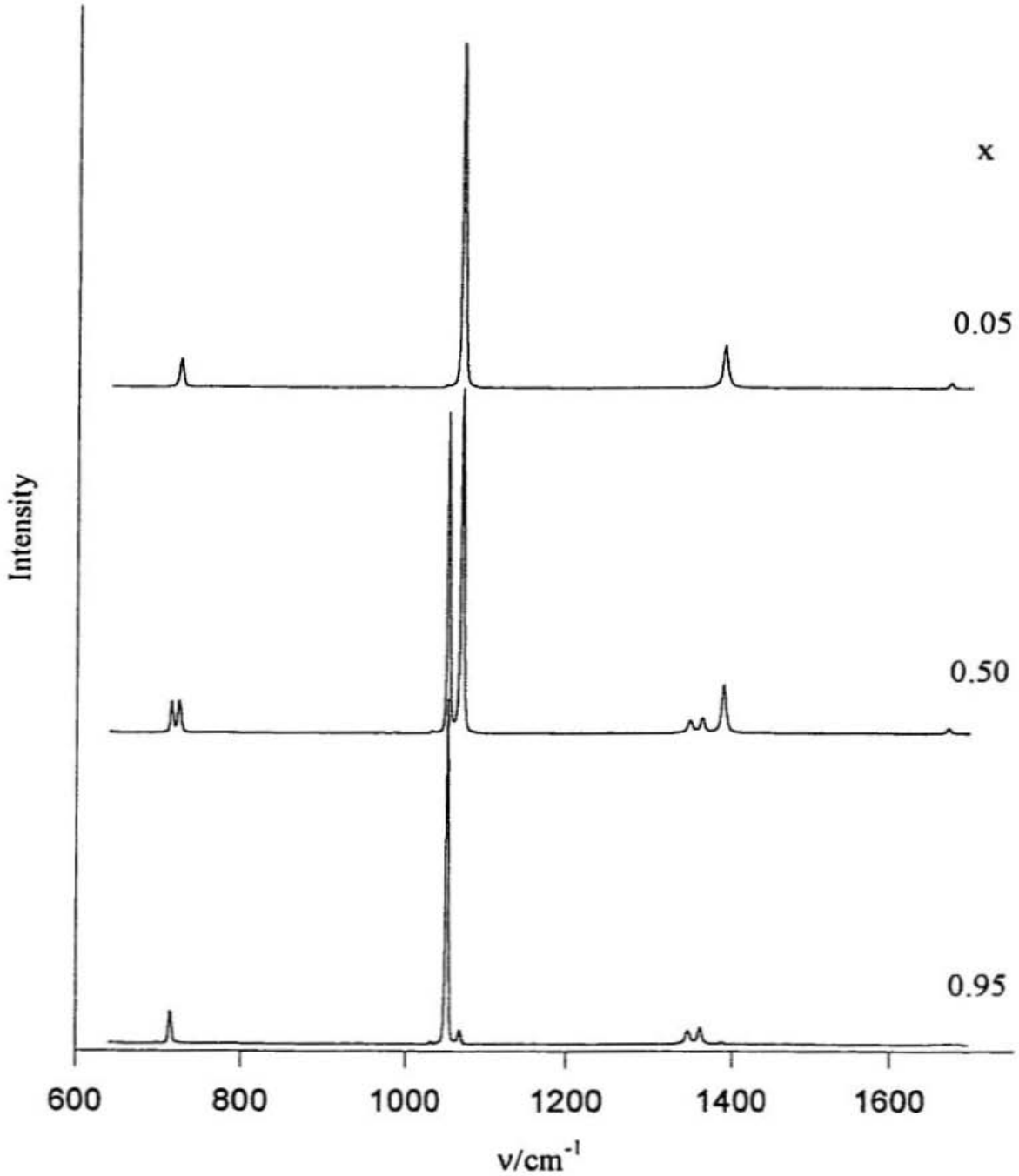

Fig. 5.2 Raman spectra in the internal vibrational region of the annealed $Na_{1-x}K_xNO_3$ at 298 K. X is the mole fraction of KNO_3.

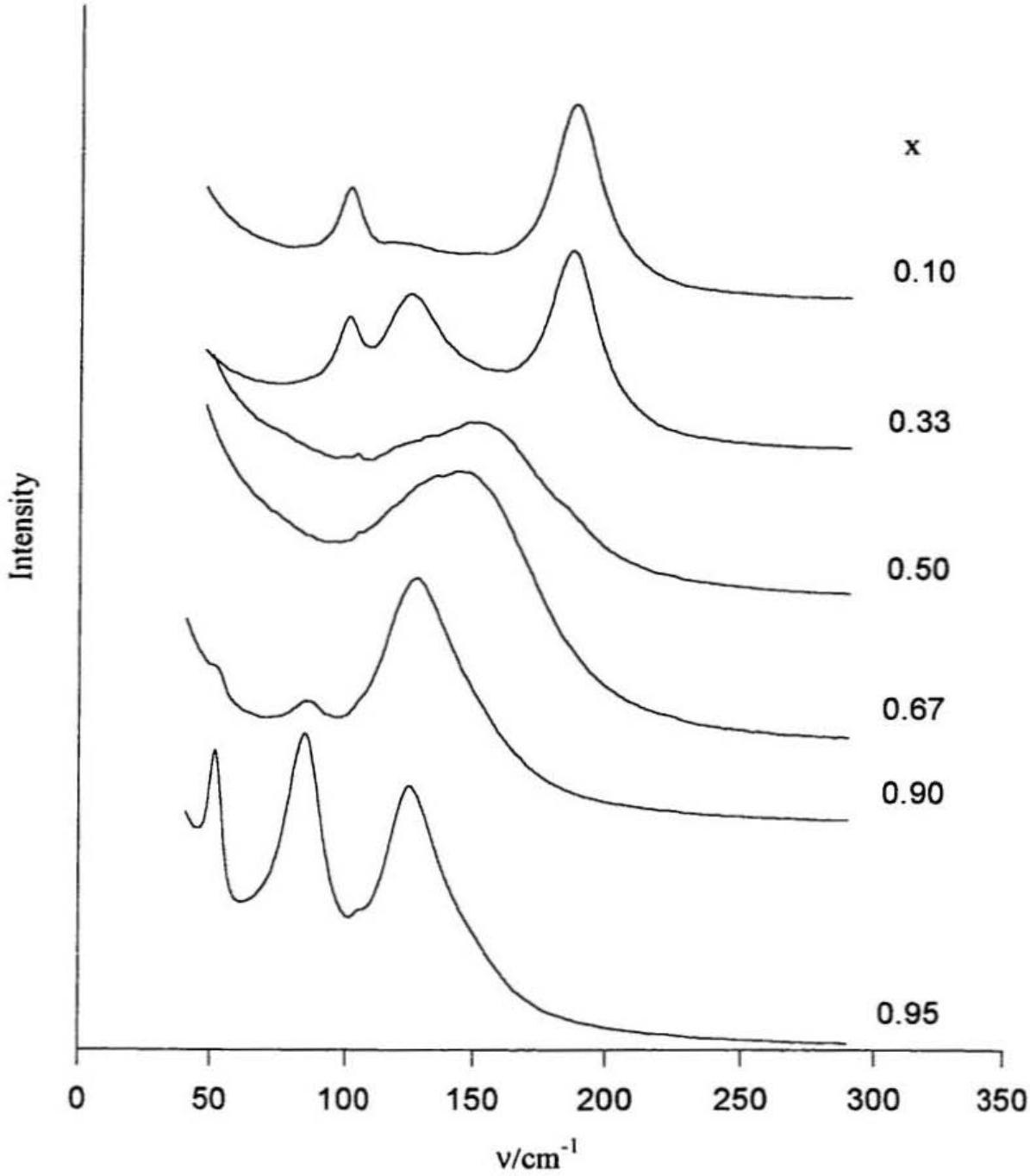

Fig. 5.3 Raman spectra in the external vibrational region of $Na_{1-x}K_xNO_3$ quenched from 358 K and measured at 298 K. X is the mole fraction of KNO_3.

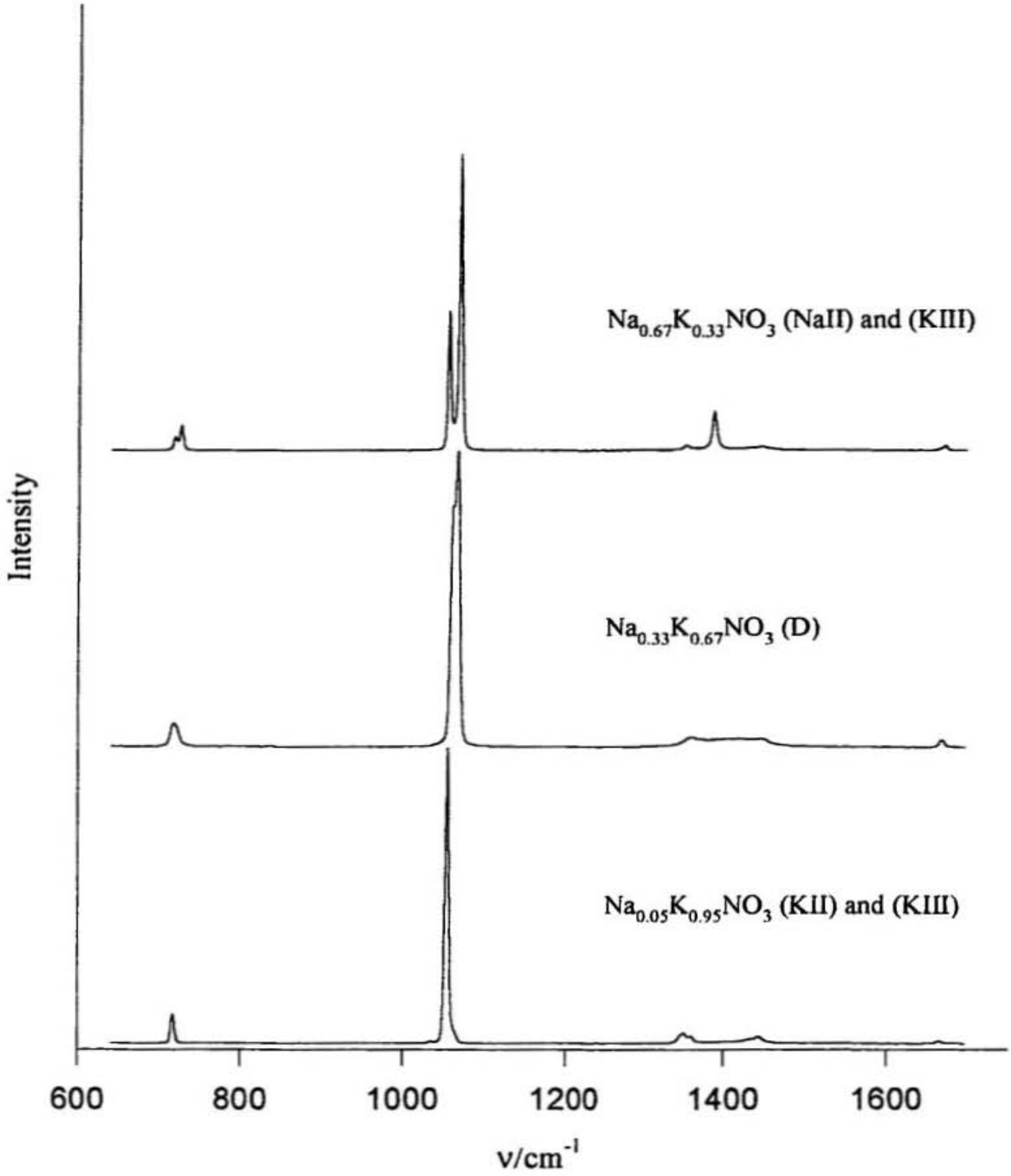

Fig. 5.4 Raman spectra in the internal vibrational region of $Na_{1-x}K_xNO_3$ quenched from 358 K and measured at 298 K.

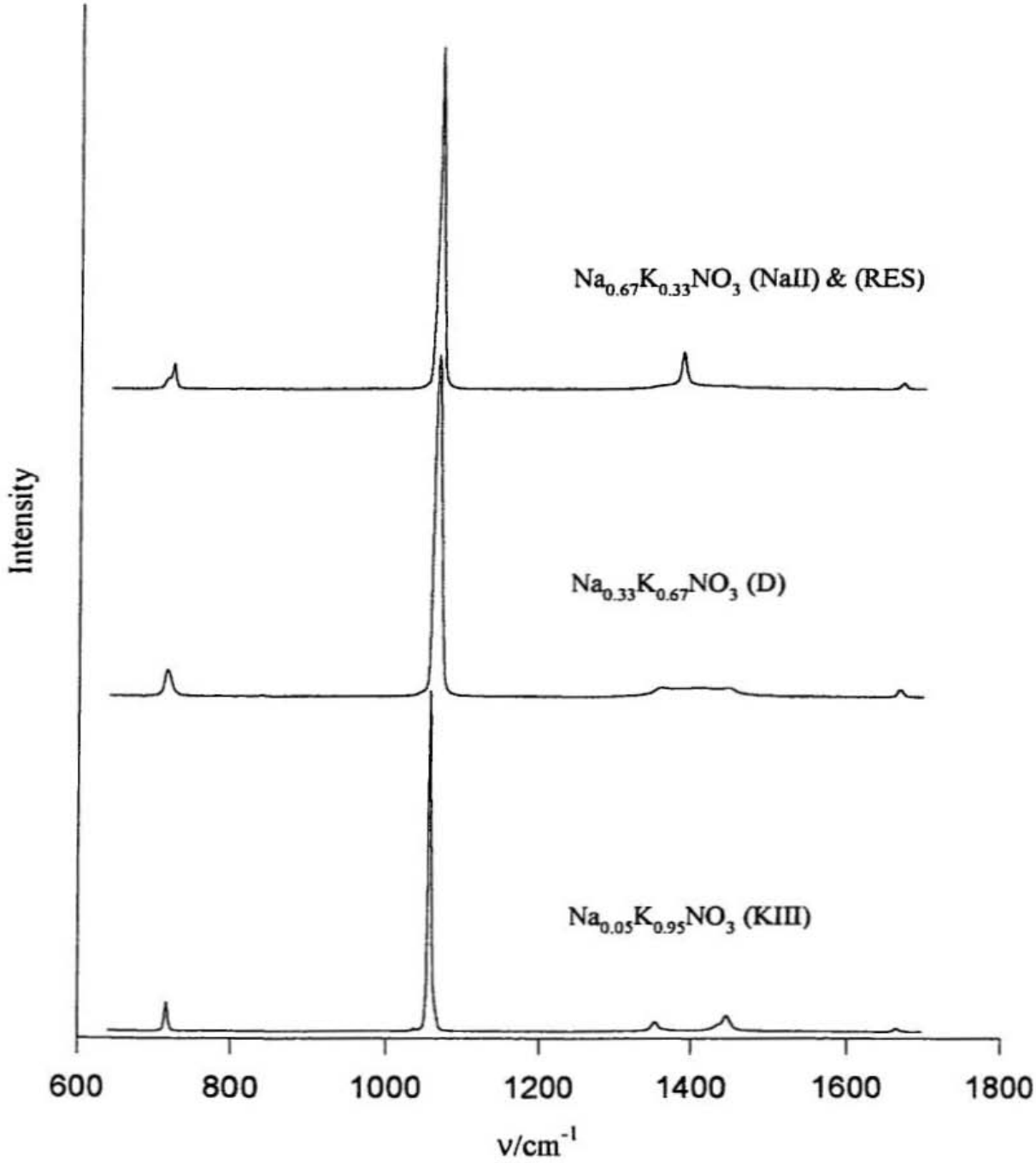

Fig. 5.5 Raman spectra in the internal vibrational region of $Na_{1-x}K_xNO_3$ quenched from from 393 K and measured at 298 K.

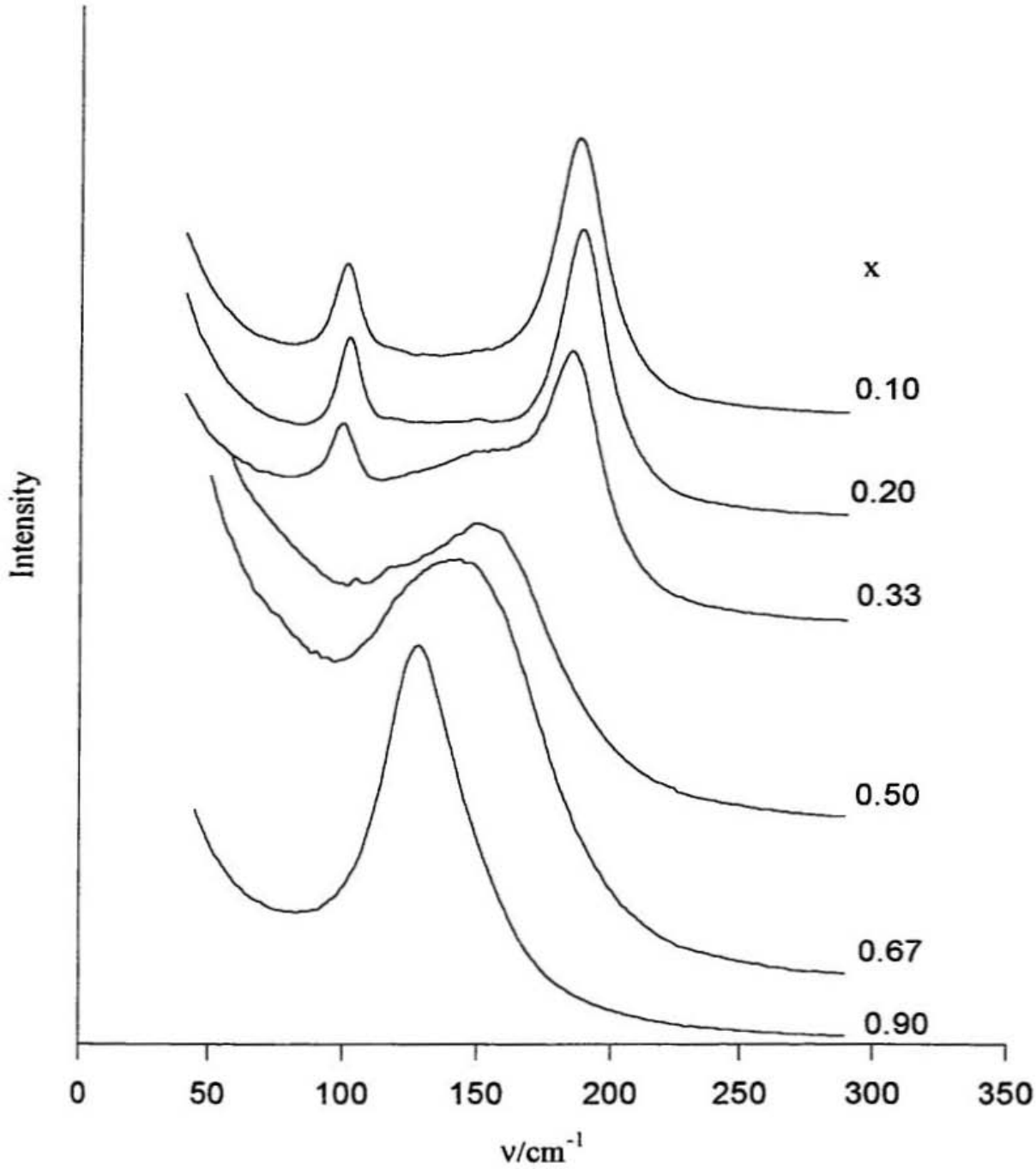

Fig. 5.6 Raman spectra in the external vibrational region of $Na_{1-x}K_xNO_3$ quenched from 393 K and measured at 298 K. X is the mole fraction of KNO_3.

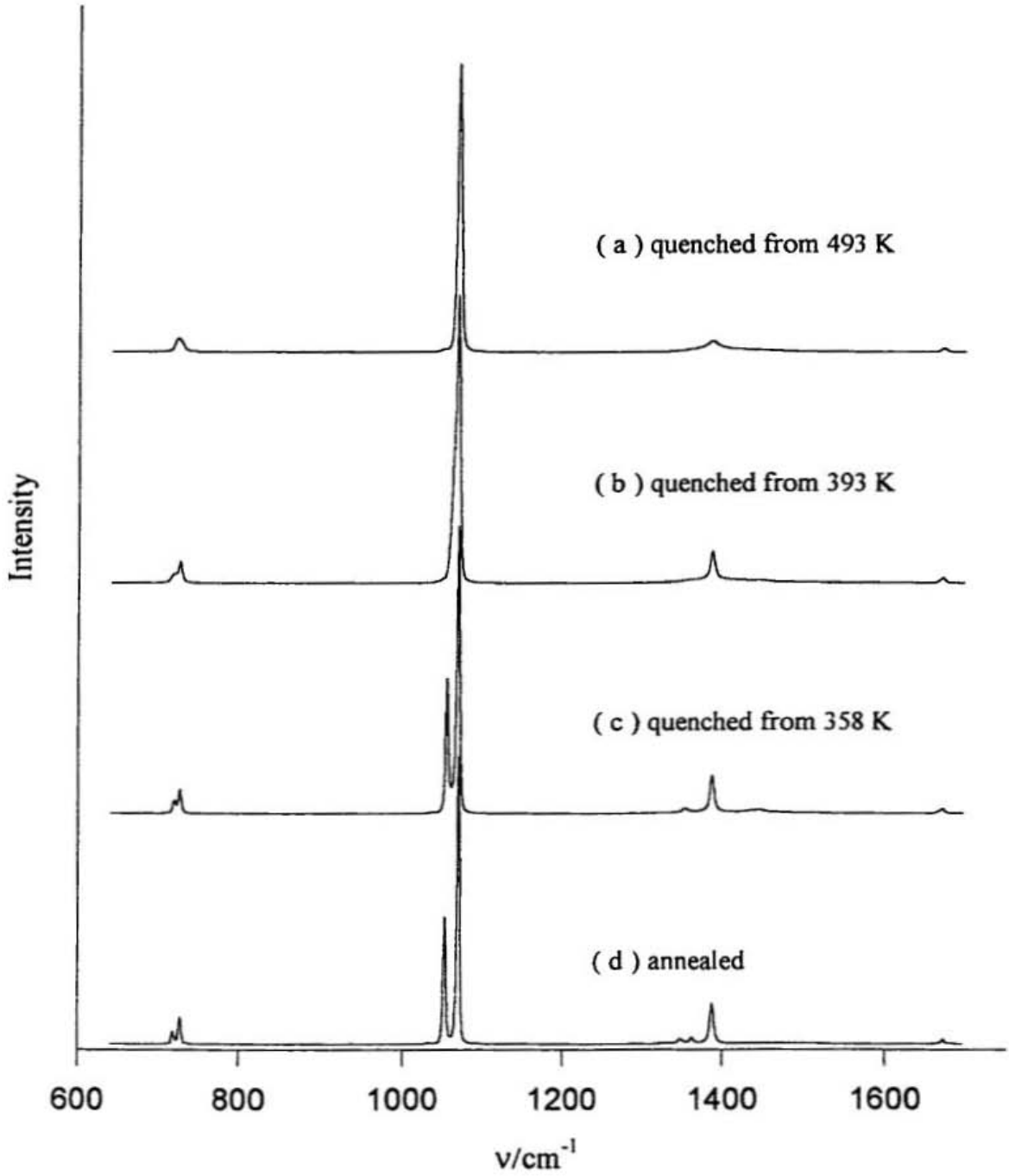

Fig. 5.7 Raman spectra in the internal vibrational region of $Na_{0.67}K_{0.33}NO_3$ at 298 K after different heat treatments.

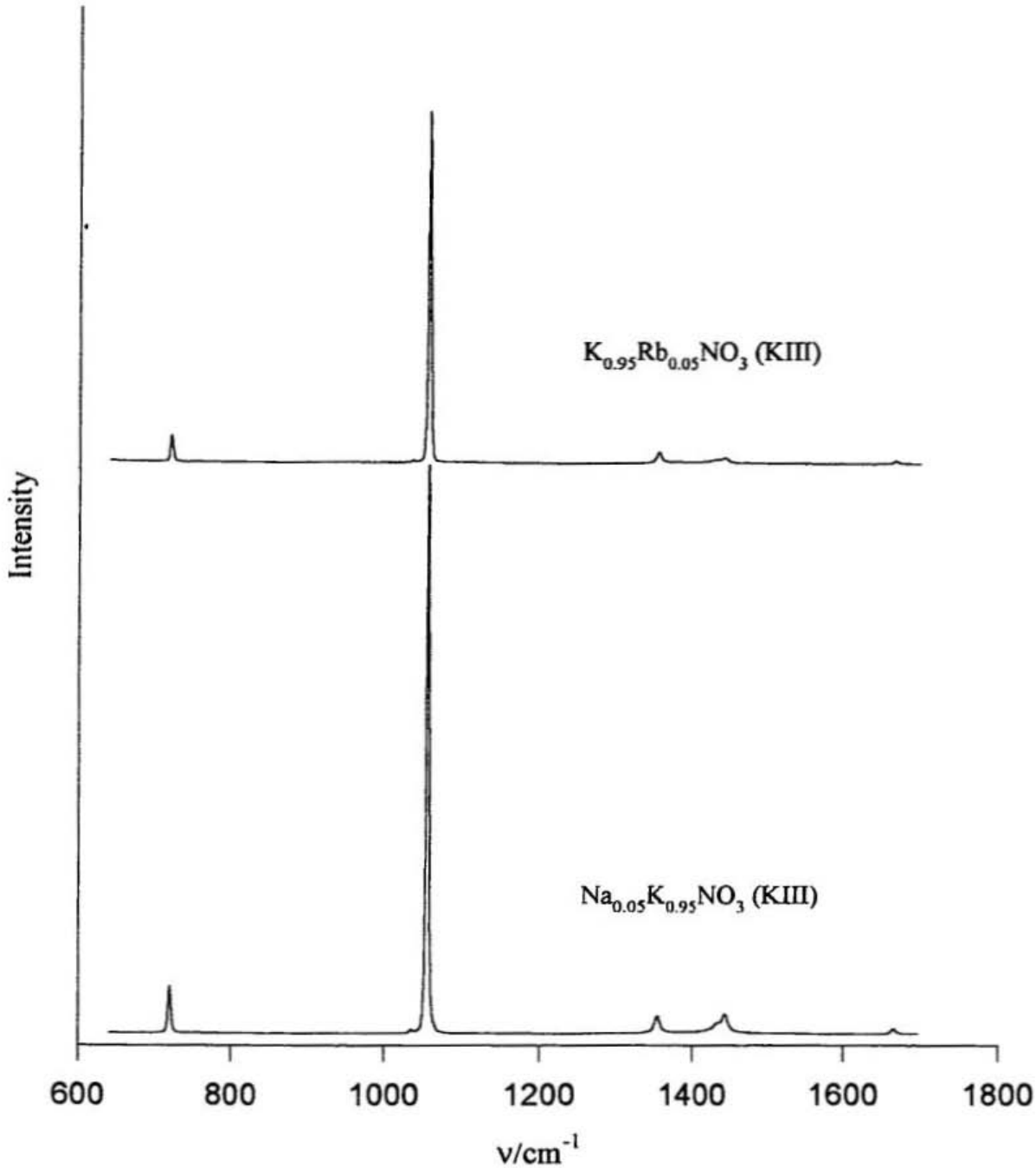

Fig. 5.8 Raman spectra of $K_{0.95}Rb_{0.05}NO_3$ (KIII) and $Na_{0.05}K_{0.95}NO_3$ (KIII) at 298 K. The relative intensities of the TO-LO ν_3 bands are different.

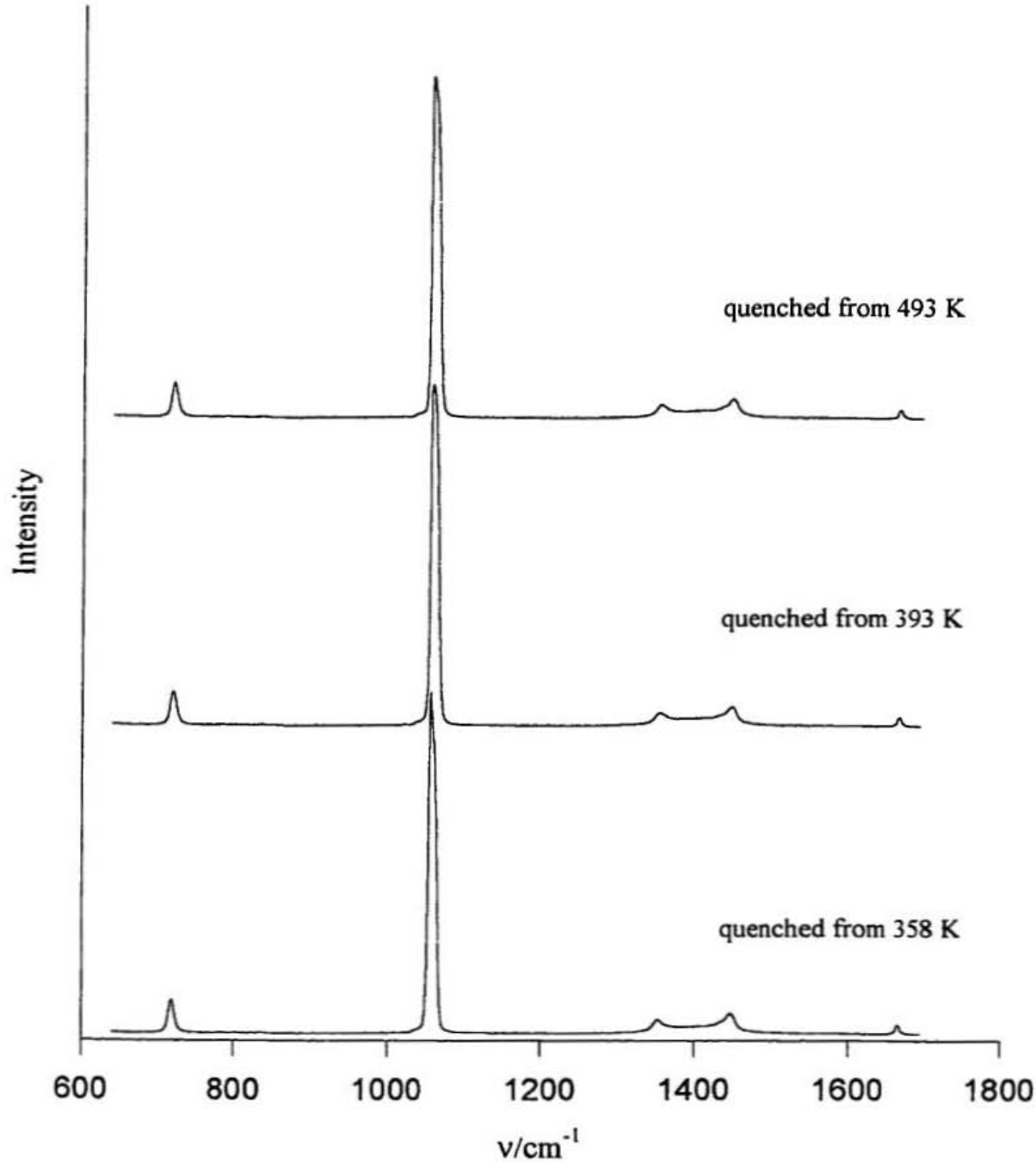

Fig. 5.9 Raman spectra of $Na_{0.20}K_{0.80}NO_3$ quenched from different temperatures and measured at 298 K. The Raman spectra are essentially the same.

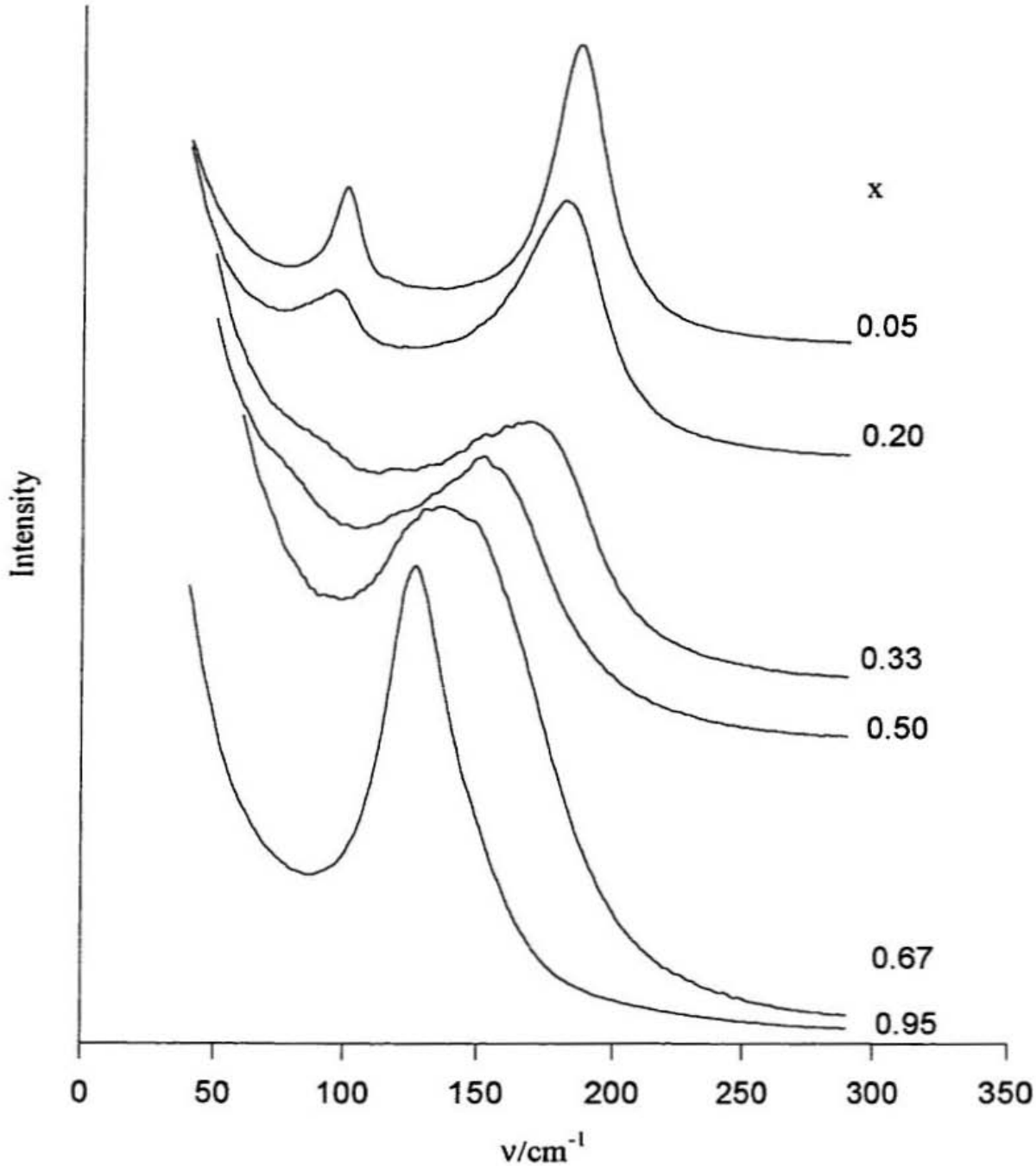

Fig. 5.10 Raman spectra in the external vibrational region of $Na_{1-x}K_xNO_3$ quenched from 493 K and measured at 298 K. X is the mole fraction of KNO_3.

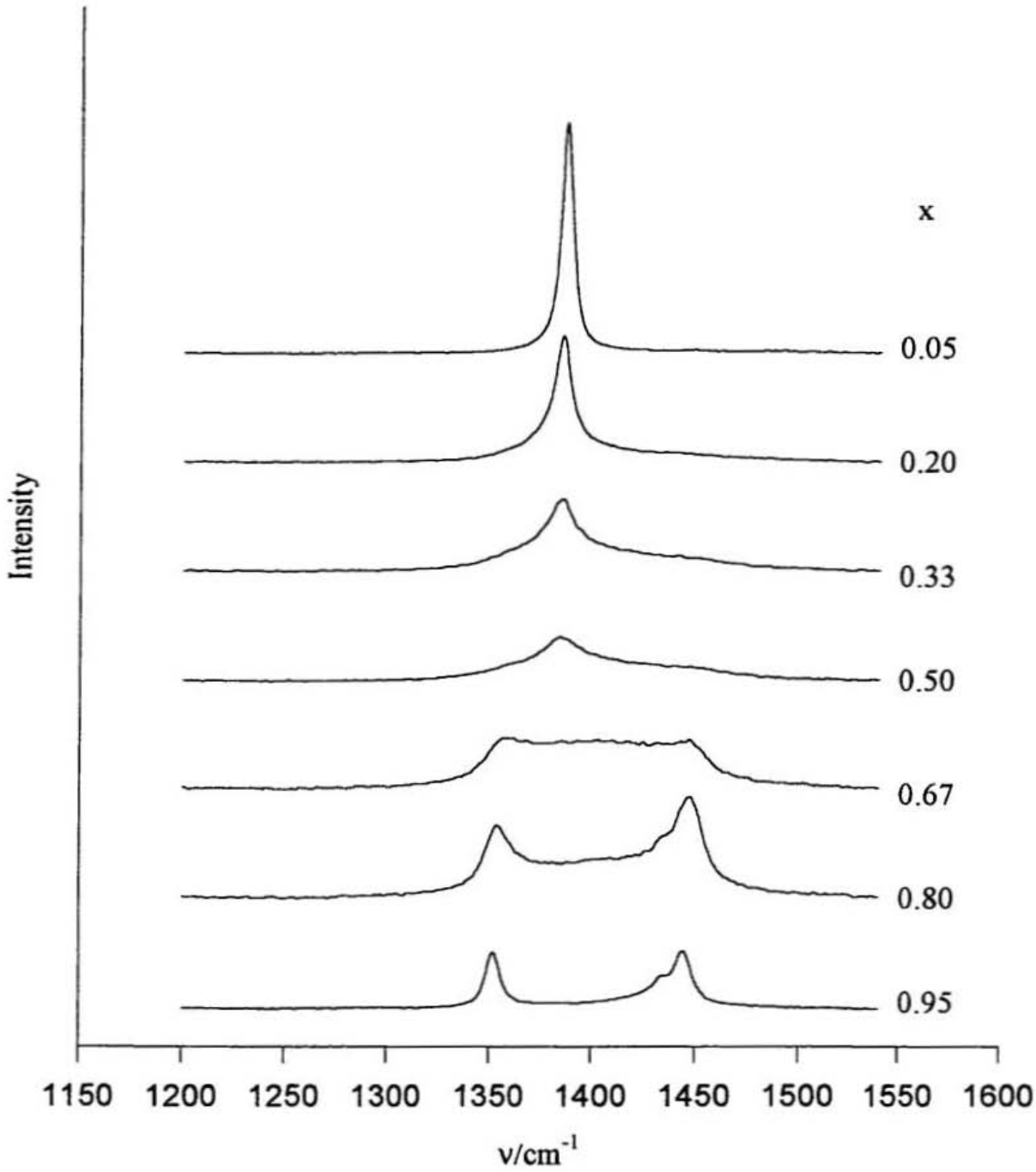

Fig. 5.11 Raman spectra in the ν_3 region of NaKNO quenched from 220 ^{0}C and measured at 298 K. X is the mole fraction of KNO_3.

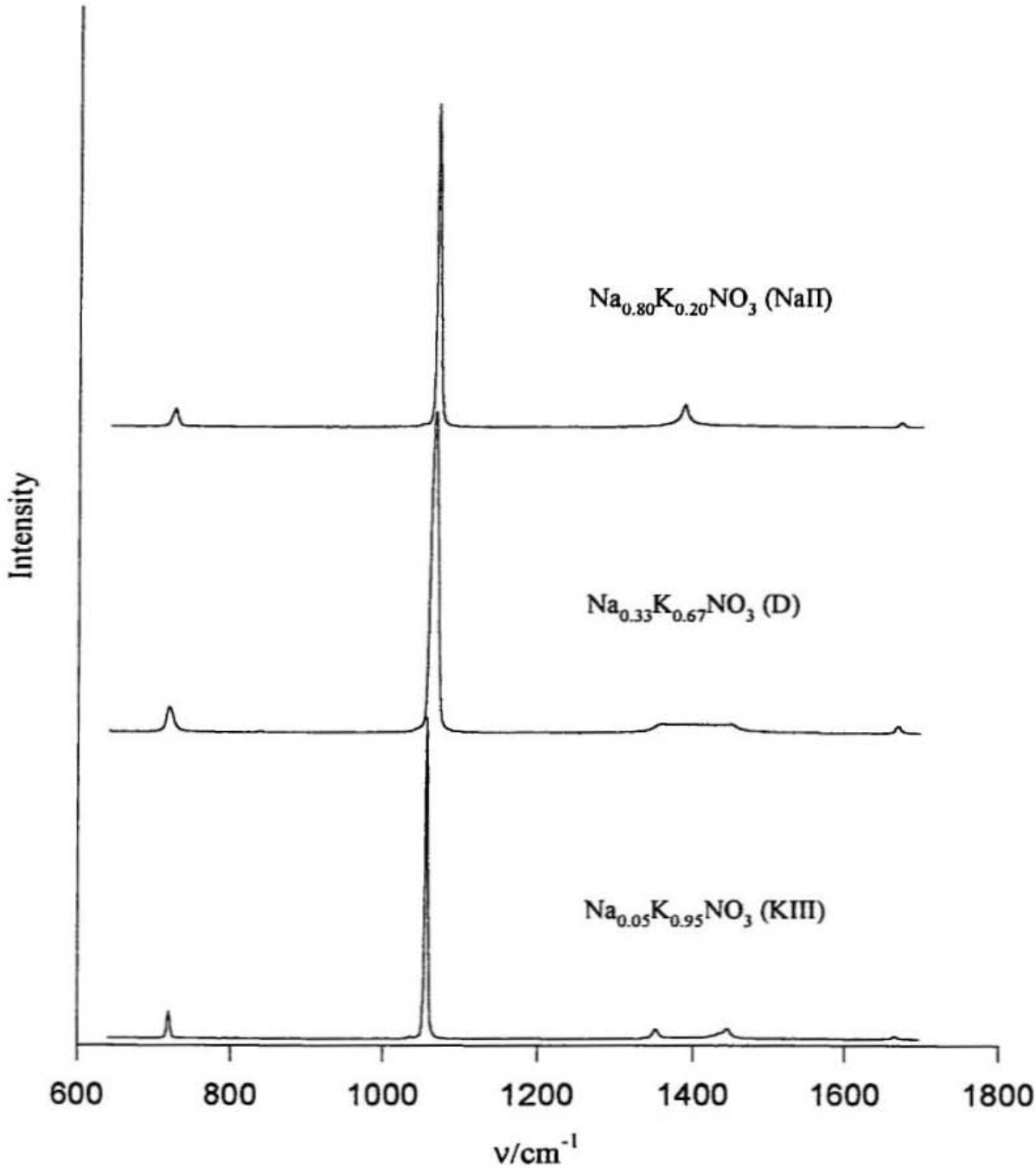

Fig. 5.12 Raman spectra in the internal vibrational region of $Na_{1-x}K_xNO_3$ quenched from 493 K and measured at 298 K. Three kinds of spectrum represent three different structures of the solids.

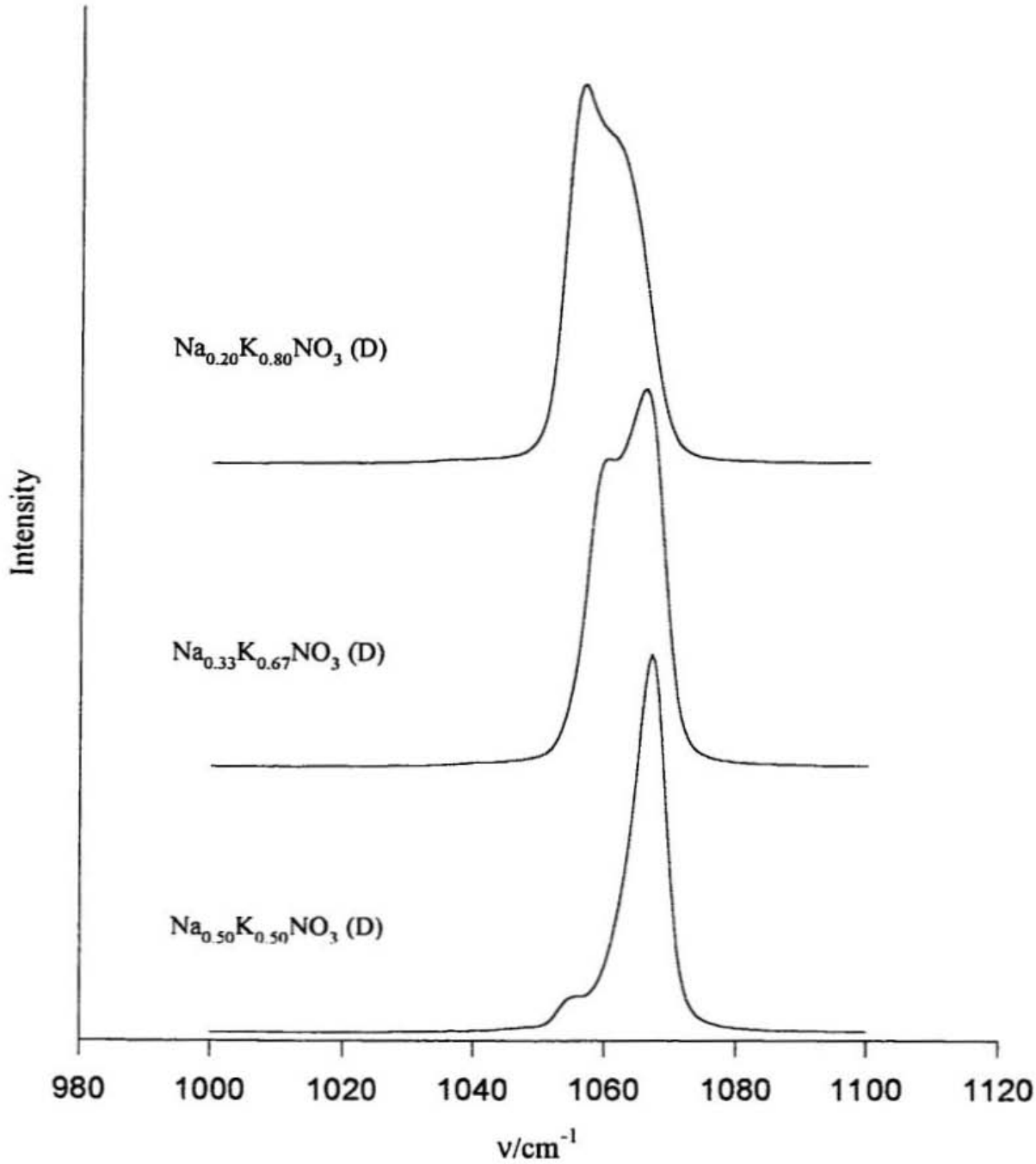

Fig. 5.13 Raman spectra in the ν_1 region of $Na_{1-x}K_xNO_3$ quenched from 358 K and measured at 298 K. The band profiles are different for different compositions.

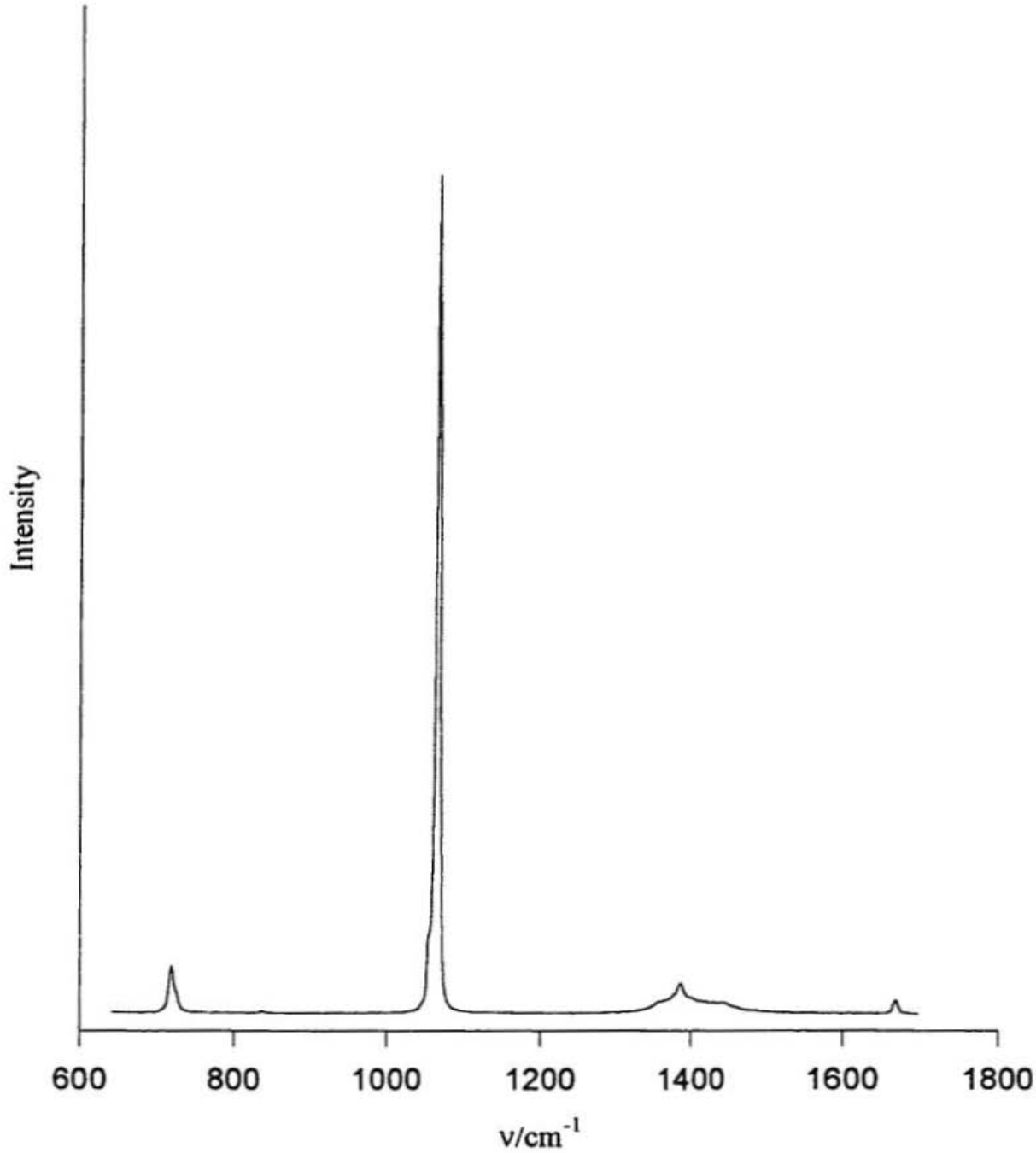

Fig. 5.14 Raman spectra in the internal vibrational region of $Na_{0.50}K_{0.50}NO_3$ quenched from358 K and measured at 298 K.

CHAPTER 6

TEMPERATURE DEPENDENCE OF MIXED CRYSTALS OF SODIUM AND POTASSIUM NITRATE

6.1 Introduction

Sodium and potassium nitrate is one of the binary systems which has been studied in great detail. Attention has been focused chiefly on the thermodynamical properties. After so many careful observations and thorough discussions [4,8,66,109-114], both theoretical and experimental, little doubt is left about the solidus and liquidus of the $NaNO_3$-KNO_3 system. Now it is widely accepted that a continuous series of solid solutions forms just below the solidus which is nearly horizontal in the composition region between 20 and 80 mol% KNO_3.

However, much less is known about the structural chemistry of the mixed crystals of $NaNO_3$-KNO_3 and our knowledge about the solids is far from satisfactory. Among the early researchers, Kofler [113] made the most extensive observations of the structures and structural phase transitions of the solids from the mixed melts with a hot-stage microscope. Greis and co-workers [66], based on Kofler's diagram and the structural phase transitions of pure sodium nitrate and potassium nitrate, constructed a complete phase diagram from melts to solids at room temperature from DSC cooling runs and heating runs. Greis *et al.* gave a most detailed description about the structural chemistry of the mixed crystals of $NaNO_3$-KNO_3 in the whole

composition region. Most of the structural details deduced by Greis and co-workers have not been examined by spectroscopic techniques.

There were several attempts to apply X-ray diffraction techniques to the study of the structures of the mixed crystals. Kamimoto [114] examined the solid of equimolar $NaNO_3$-KNO_3 by DSC and XRD. The X-ray pattern of the sample was found to be different from that of either $NaNO_3$ or KNO_3 at the same temperature of 473 K, which indicated a different structure from $NaNO_3$ I or KNO_3 I. This observation was not in agreement with Greis' phase diagram [66] which suggested that the solid solution at 473 K should have the same structure as $NaNO_3$ I or KNO_3 I. Kamimoto's observation that the annealed sample consisted of a mixture of solid solutions was also inconsistent with Greis' phase diagram which indicated a mixture of the pure nitrates at room temperature. Finally, Kamimoto found that the quenched sample of equimolar $NaNO_3$-KNO_3 had a unique X-ray diffraction pattern and so the solid had a unique structure, which is contrary to other XRD investigations [4,8]. Kramer and Wilson [4] analysed several DSC samples by XRD and found that the mixtures, no matter whether they were quenched from above or below the liquidus, had two distinct and sharp crystal patterns corresponding to rhombohedral $NaNO_3$ II and orthorhombic KNO_3 II. High temperature XRD was suggested as a means to study the solid solutions.

It seems that XRD may not give unambiguous information of the structures of all mixed crystals. Raman methods may have more promise. Shortly after its discovery, the Raman effect was used to investigate the solid of equimolar $NaNO_3$-KNO_3 [64]. The freshly prepared sample only gave one sharp line in the ν_1 region. One day later the line became diffuse and after four days two sharp lines appeared. The X-ray examination showed no difference

between the sample of different ages. Unfortunately, the work was not continued. Recently we have studied the quenched mixtures of $NaNO_3$-KNO_3 over the whole composition region by Raman spectroscopy (Chapter 5). The Raman observations agreed with Greis' phase diagram in general but with three notable differences in structural details about the solids below the solidus: (1) There were limited solid solutions $Na_{1-x}K_xNO_3$ (NaII) and (KIII) in addition to the $R\bar{3}m$ solid solutions. (2) Two vertical lines at x = 0.05 and x = 0.85 were added to the Greis' phase diagram for $Na_{0.95}K_{0.05}NO_3$ (NaII) and $Na_{0.15}K_{0.85}NO_3$ (KIII) respectively. (3) There was a new disordered state in the intermediate concentration region. The importance of these suggestions makes it necessary to reexamine the structural changes at different temperatures and to make sure that the structural details were not brought about by quenching.

This work reports the Raman spectra for the temperature dependence of the mixed crystals $Na_{1-x}K_xNO_3$. Four samples with x = 0.95, 0.67, 0.20, 0.05 were investigated. The four samples present the four kinds of structural phase transitions of the binary nitrate observed in the quenched samples.

6.2 Raman Spectra of Mixed Crystals of $NaNO_3$-KNO_3

The Raman bands of the mixed crystals at high temperature were not so sharp as those of the quenched samples due to interference by hot bands. The external vibrations were sometimes obscured by the strong Rayleigh wing, and irregular peaks in the external vibrational region (due to reflection of the bulk samples) added difficulties for the band

assignment. Nevertheless, the spectra had all the main Raman features in both external and internal vibrational regions and were sufficiently distinct for structural determination. For $Na_{0.05}K_{0.95}NO_3$ and $Na_{0.95}K_{0.05}NO_3$, the spectra were measured at 473, 393, 366, 361 and 356 K. Ten-hour intervals were taken for the samples to reach equilibrium. For $Na_{0.33}K_{0.67}NO_3$ and $Na_{0.80}K_{0.20}NO_3$, the spectra were measured at 473, 393, 366, 361, 356, 351 and 346 K. Ten-hour intervals were taken for 473, 393 and 366 K. For lower temperatures the intervals were 22 hours. Another 22 hours were taken at the lowest temperature to observe whether new features appeared in the spectrum.

6.2.1 Temperature Dependence of $Na_{0.05}K_{0.95}NO_3$

The most important Raman features of $Na_{0.05}K_{0.95}NO_3$ are summarized in Table 6.1. Raman features of potassium nitrate in phase I, II or III [55] are also included for comparison.

The Raman spectra at 473 and 393 K had the typical Raman features of the KNO_3 I structure, indicating that the sample was the $R\bar{3}m$ solid solution. There was one broad band in the external vibrational region at about 110 cm^{-1} which was on the strong Rayleigh wing (Fig. 6.1). In the ν_1 and ν_4 regions, there was also one band at 1055 and 716 cm^{-1} respectively. The bands were broad and symmetrical. The doublet structure in the ν_3 region was similar in details to KNO_3 I [55]: a broad feature from 1320 to 1450 cm^{-1} with small peaks at 1352 and 1428 cm^{-1}. The former appeared a bit weaker than the latter (Fig. 6.2). One or two wavenumbers shift to higher frequency was reasonable for a temperature decrease from 473 to 393 K.

When the temperature was lowered to 366 K, some notable changes occurred in Raman features. The ν_1 vibration was now at 1054 cm^{-1}, 2 cm^{-1} lower instead of higher than it was at 393 K. This is the value for the ν_1 band of the KNO_3 III structure [55]. The band profile in the ν_3 region was also typical for the KNO_3 III structure. The transverse and longitudinal optical Raman features of KNO_3 III [55] appeared distinctly at 1350 and 1439 cm^{-1} (Fig. 6.2). Beside the LO mode was the $2\nu_4$ vibration at 1432 cm^{-1}. The bands became much sharper during the structural phase transition from disordered $R\bar{3}m$ to ordered R3m. The ν_1 band due to the O-18 form of nitrate ion, $N\,^{18}O\,^{16}O_2^-$, appeared distinctly at a position about 20 cm^{-1} lower than the band due to $N\,^{16}O_3^-$. In the external vibrational region the Rayleigh wing was depressed greatly and the libration of the nitrate group appeared distinctly at 121 cm^{-1} (Fig. 6.1). Only one sharp symmetrical band in the ν_1 or ν_4 region and the characteristic profile in the ν_3 region indicated that the mixture had the KNO_3 III structure alone. The sample was the solid solution $Na_{0.05}K_{0.95}NO_3$ (KIII). The transition from $Na_{0.05}K_{0.95}NO_3$ (KI) to (KIII) was gradual. The features in the external vibrational region were similar (Fig. 6.1) and in the ν_3 region the doublet structure of $Na_{0.05}K_{0.95}NO_3$ (KI) at 393 K was similar to the precursor of the characteristic TO-LO pattern of (KIII) at 366 K (Fig. 6.2).

Further changes in Raman features took place at 361 K. The most notable one was in the external vibrational region. In addition to the band at 120 cm^{-1}, there were two bands at 50 and 82 cm^{-1}. They involved the translatory motion of cations against anions and the rotatory motions of the nitrate ion about the a and b axes in the lattice of KNO_3 II [99]. The existence of KNO_3 II was also evident in the ν_3 region. On the well-separated TO-LO bands of $Na_{1-x}K_xNO_3$ (KIII) at 1350 and 1439 cm^{-1} were superimposed the doublet peaks of KNO_3

II at 1343 and 1359 cm^{-1}. As a result, the TO mode overlapped with the 1343 cm^{-1} band to form an asymmetric band at 1347 cm^{-1} (Fig. 6.2). The ν_1 and ν_4 were one wavenumber lower than corresponding bands at 366 K. This may be regarded as the result of KNO_3 II in $Na_{1-x}K_xNO_3$ (KIII) because both bands are a little lower in the former than in the latter [55]. The Raman spectrum of $Na_{0.05}K_{0.95}NO_3$ at 361 K was a mixture of $Na_{1-x}K_xNO_3$ (KIII) and KNO_3 II.

The spectrum at 366 K had exactly the same Raman features of the KNO_3 III structure as the spectrum of the 493 or 393 K quenched sample in the ν_3 and external vibrational regions which are most sensitive to structural changes (Figs. 6.3 and 6.4). The Raman bands were similar except that the bands in the high temperature spectra were a bit broader and shifted to lower frequencies. Therefore, the $R\bar{3}m$ solid solution $Na_{0.05}K_{0.95}NO_3$ (KI) behaved like pure KNO_3 at high temperatures and was unquenchable. When quenched, $Na_{0.05}K_{0.95}NO_3$ (KI) transformed to (KIII) which can be preserved in a metastable state in vacuum. At 361 K, the spectrum had the same Raman bands of both KNO_3 II and $Na_{1-x}K_xNO_3$ (KIII) as those of the 358 K quenched sample (Figs. 6.3 and 6.4). This is consistent with the assumption that KNO_3 II exsolved from $Na_{1-x}K_xNO_3$ (KIII) instead of $NaNO_3$ II exsolving from the $R\bar{3}m$ solid solutions in the temperature range between 361 and 353 K in Greis' phase diagram [66] (Section 5.3.2).

At 356 K the Raman features due to $Na_{1-x}K_xNO_3$ (KIII) disappeared almost completely in both external and internal vibrational regions. The dominant features were due to KNO_3 II. In the external vibrational region, two strong bands at 51 and 82 cm^{-1} and a medium one at 123 cm^{-1} were typical for KNO_3 II. The ν_1 and ν_4 vibrations further lowered to 1051 and

716 cm^{-1} respectively because of disappearance of the KNO_3 III structure. The doublet peaks at 1345 and 1359 cm^{-1} (Fig. 6.2) and very weak features in the $2\nu_2$ region were also typical for KNO_3 II. However, the 5 mol% $NaNO_3$ did not dissolve in KNO_3 II. There was a small peak at 1058 cm^{-1} in the ν_1 region and a diffuse feature extending from 1350 to 1450 cm^{-1} in the ν_3 region (Fig. 6.2). The frequency of this ν_1 band was much lower than that of pure $NaNO_3$ II and compared to the 1051 cm^{-1} band of KNO_3 II, this band was much stronger than it would be if it had arisen from only 5 mol% $NaNO_3$. Furthermore there were no characteristic Raman bands in any spectral regions sensitive to $NaNO_3$ II. The band at 1058 cm^{-1} may be attributed to the residual solid solution (RSS). As more and more KNO_3 exsolved, the concentration of $NaNO_3$ in the solid solution increased till it reached to the composition of the eutectoid ($0.55 \leq x \leq 0.85$). In the study of the quenched mixtures of $NaNO_3$-KNO_3, it has been noted that the eutectoid mixtures were in a disordered state and the transition of eutectoid mixtures was much slower than for the non-eutectoid ones. The value of 1058 cm^{-1} was in agreement with the quenched $Na_{0.20}K_{0.80}NO_3$ (D). The sample $Na_{0.05}K_{0.95}NO_3$ at 356 K may be regarded as mixed crystals of KNO_3 II and the metastable $Na_{0.20}K_{0.80}NO_3$ (RSS).

6.2.2 Temperature Dependence of $Na_{0.95}K_{0.05}NO_3$

All the Raman spectra of $Na_{0.95}K_{0.05}NO_3$ at the temperatures between 473 and 356 K had the same spectral profiles of the $NaNO_3$ II structure in every sensitive region (Table 6.2). The solid in this temperature range was the solid solution $Na_{0.95}K_{0.05}NO_3$ (NaII) alone.

In the external vibrational region the translatory vibration at 97 cm^{-1} and the rotatory vibration of the nitrate ion at 183 cm^{-1} shifted to lower wavenumbers gradually as the temperature was raised from 356 to 473 K (Fig. 6.5). For pure sodium nitrate the shift rate of the rotatory mode is comparable to the translatory mode [55,121,122]. When the temperature was increased from 298 to 523 K, the rotatory mode of the nitrate ion shifted from 189 to 173 cm^{-1} ($\Delta\nu$ = 16 cm^{-1}) and the translatory mode shifted from 102 to 88 cm^{-1} ($\Delta\nu$ = 14 cm^{-1}) [55]. The rotatory mode in $Na_{0.95}K_{0.05}NO_3$ (NaII) had a similar shift rate: from 183 to 173 cm^{-1} ($\Delta\nu$ = 10 cm^{-1}) for a temperature rise from 356 to 473 K. However, the translatory mode shifted much faster in the solid solution than in pure sodium nitrate at the same temperature interval: from 97 to 78 cm^{-1} ($\Delta\nu$ = 19 cm^{-1}). At 473 K the translatory vibration almost merged into the strong Rayleigh wing (Fig. 6.5). The 97 cm^{-1} band is closely related to the order-disorder phenomenon in sodium nitrate. The progressive disappearance of this band was associated with the transition of the ordered calcite to the disordered calcite lattice as the transition temperature was approached [122]. Above the transition temperature a continuous Rayleigh wing induced by disordering was observed in the place of this translatory band. In the Raman spectra of the solid solution the progressive disappearance of the band at 97 cm^{-1} seemed to be enhanced by addition of larger potassium ions in the crystal of sodium nitrate. Complete disorder was observed at lower temperature in the solid solution.

Parallel Raman measurements of pure sodium nitrate were made to examine the effect of potassium ions on the order-disorder transition in sodium nitrate (Table 6.2). At 393 K or lower the effect of temperature was small: a shift of one or two wavenumbers to lower frequency in the external and internal vibrational regions. The frequency difference between

the translatory and rotatory modes (86 cm^{-1} for $Na_{0.95}K_{0.05}NO_3$ (NaII) and 85 cm^{-1} for pure $NaNO_3$ II) appeared not to change when the temperature was decreased from 393 to 356 K. When the temperature was increased to 473 K, all the Raman bands in $Na_{0.95}K_{0.05}NO_3$ (NaII) showed small frequency shifts except the translatory vibration which shifted to lower frequency at a greater rate. The difference between translatory and rotatory modes was 87 cm^{-1} for the pure $NaNO_3$ II while it was 95 cm^{-1} for $Na_{0.95}K_{0.05}NO_3$ (NaII). The presence of the larger potassium ion seemed to have more effect on the ordered calcite structure of $NaNO_3$ at higher temperature than at lower temperature (Fig. 6.6).

In the internal vibrational region, band shifts due to temperature changes were much smaller - one or two wavenumbers or less (Table 6.2). The whole spectral profile was typical for the $NaNO_3$ II structure: only one fairly symmetrical band in the ν_1, ν_3, ν_4 and $2\nu_2$ regions. Nevertheless, notable disorder was deduced from the Raman spectrum at 473 K. The ν_1 vibration due to the naturally abundant $N^{18}O^{16}O_2^-$ was easily resolved about 20 cm^{-1} lower than the band due to $N^{16}O_3^-$ in the 393 K spectrum while it could hardly be detected on the broad bottom of the ν_1 band of $N^{16}O_3^-$ in the 473 K spectrum. At 473 K the ν_3 band was broader than at lower temperatures and there was a diffuse feature from 1350 to 1450 cm^{-1} (Fig. 6.7). The disorder was partly due to the higher temperature and partly due to introduction of larger potassium ions. It was noted [121] that when the crystal of $NaNO_3$ was heated to 486 K there was only an appreciable decrease in peak intensity of the ν_3 band. At higher temperature the line broadened rapidly and a diffuse feature appeared. In the case of $Na_{0.95}K_{0.05}NO_3$ (NaII), band broadening and the diffuse features were already obvious at 473 K. At 393 or 356 K, the ν_3 band of $Na_{0.95}K_{0.05}NO_3$ (NaII) looked the same as that of pure

$NaNO_3$ II while at 473 K it was broader and the diffuse feature was stronger for (NaII) than for pure $NaNO_3$ II (Fig. 6.7).

6.2.3 Temperature Dependence of $Na_{0.33}K_{0.67}NO_3$

The Raman spectra of $Na_{0.33}K_{0.67}NO_3$ had practically the same pattern at temperatures between 473 and 356 K. The spectral pattern was typical for disordered solids and indicated the new disordered state $Na_{0.33}K_{0.67}NO_3$ (D). There was a strong Rayleigh wing extending to 200 cm^{-1}, on which was a band centred at about 130 cm^{-1}. The top of the band was flat (from 110 to 140 cm^{-1}) and there were irregular peaks (Fig. 6.8). The bands in the internal vibrational region were also broad. The ν_1 and ν_4 bands were quite symmetrical. There was a very broad feature in the ν_3 region which extended from 1300 to 1500 cm^{-1} with a rather flat plateau between 1350 and 1450 cm^{-1}. The profile of ν_3 and its intensity related to ν_1 seemed hardly to change with the change of temperature (Fig. 6.9). Since there was no notable change in all the sensitive spectral regions, $Na_{0.33}K_{0.67}NO_3$ (D) may be regarded as unchanged and in the same disordered structure at the temperatures between 473 and 356 K.

When the temperature was decreased to 351 K, new Raman features appeared. In the external vibrational region, two sharp bands at 51 and 83 cm^{-1} appeared on the strong Rayleigh wing. These two bands are the most characteristic lattice vibrations of KNO_3 II. The broad band at about 130 cm^{-1} remained and on its high frequency side was a small discontinuity at about 170 cm^{-1} which may be an indication of the presence of $NaNO_3$ II (Fig. 6.8). Raman features of KNO_3 II and $NaNO_3$ II were also observed in the internal vibrational

region. A sharp band at 1051 cm^{-1} in the ν_1 region and two bands at 1345 and 1359 cm^{-1} in the ν_3 region were typical for KNO_3 II. The band at 725 cm^{-1} in the ν_4 region and a band at 1384 cm^{-1} in the ν_3 region suggested the $NaNO_3$ II structure in the sample. However it was clear that $Na_{0.33}K_{0.67}NO_3$ (D) only partly decomposed to KNO_3 II and $NaNO_3$ II. There remained characteristic Raman bands of $Na_{1-x}K_xNO_3$ (D). The peaks due to $NaNO_3$ II and KNO_3 II in the ν_3 region appeared superimposed on the broad feature of $Na_{1-x}K_xNO_3$ (D) from 1300 to 1500 cm^{-1} (Fig. 6.9). The broad ν_1 band at 1061 cm^{-1} was a mixture of the bands due to $NaNO_3$ II and $Na_{1-x}K_xNO_3$(D), and the broad ν_4 band at 716 cm^{-1} may be regarded as a combination of the bands due to KNO_3 II and (D).

When annealed at 351 K for another 22 hours, $Na_{1-x}K_xNO_3$ (D) in $Na_{0.33}K_{0.67}NO_3$ decomposed to $NaNO_3$ II and KNO_3 II almost completely. In the external vibrational region, the predominant Raman features were the two strong bands at 52 and 84 cm^{-1} and a medium band at 125 cm^{-1} due to KNO_3 II and a band at 183 cm^{-1} due to $NaNO_3$ II (Fig. 6.8). In the internal vibrational region two sets of Raman bands were well separated, one standing for $NaNO_3$ II and the other standing for KNO_3 II (Table 6.3). The intensity of the former was lower than the latter (Figs. 6.8 and 6.9), and was approximately consistent with the ratio of 1 to 2 of $NaNO_3$ to KNO_3. The weak diffuse feature in the ν_3 region and a small shoulder at about 130 cm^{-1} suggested residual $Na_{1-x}K_xNO_3$ (D) in the sample (Figs 6.8 and 6.9). The asymmetry in the low frequency side of the 1068 cm^{-1} band may also be due to $Na_{1-x}K_xNO_3$ (D).

The temperature dependent Raman spectra of $Na_{0.33}K_{0.67}NO_3$ suggested a disordered state existing at a temperature down to 356 K. At lower temperature the disordered solid

decomposed directly to $NaNO_3$ II and KNO_3 II.

6.2.4 Temperature Dependence of $Na_{0.80}K_{0.20}NO_3$

The Raman spectra of $Na_{0.80}K_{0.20}NO_3$ exhibited the greatest variation with temperature because this sample has three two-phase regions and because the transition rate slowed down as the composition of the solid solution reached 50 mol% KNO_3 as a result of exsolution of $Na_{0.95}K_{0.05}NO_3$ (NaII). In fact the Raman spectra below 366 K did not represent an equilibrium state of the system at the measured temperature. Nevertheless, the temperature dependent Raman spectra gave an *in situ* presentation of the procedure of structural phase transitions of the mixed crystal from 473 to 346 K. Table 6.4 is a summary of the spectra.

The Raman spectrum for the sample at 473 K was typical for the disordered state: one broad band with irregular peaks in the external vibrational region and one broad band in the ν_1, ν_3, ν_4 and $2\nu_2$ region. The solid solutions $Na_{0.05}K_{0.95}NO_3$, $Na_{0.33}K_{0.67}NO_3$ and $Na_{0.80}K_{0.20}NO_3$ were reported [66] to have the same $R\bar{3}m$ structure at 473 K. However, there were notable differences among the Raman spectra of the three solids. The band in the external vibrational region shifted to high wavenumbers as the content of $NaNO_3$ increased and the band profiles were a little different (Fig. 6.10). In the ν_3 region, the doublet profile of $Na_{0.05}K_{0.95}NO_3$ was similar to that of KNO_3 I and the small peak at 1380 cm^{-1} in the spectrum of $Na_{0.80}K_{0.20}NO_3$ indicated features due to $NaNO_3$ I (Fig. 6.11). The frequencies of the ν_1 and ν_4 vibrations were notably higher in the latter than in the former (Tables 6.1 and 6.4). The Raman spectrum of $Na_{0.33}K_{0.67}NO_3$ at 473 K appeared to be a mixture of the spectra

of $Na_{0.80}K_{0.20}NO_3$ and $Na_{0.05}K_{0.95}NO_3$ in both band positions and profiles (Figs. 6.10 and 6.11). When compared with the Raman spectra of the pure nitrates [55], the Raman spectrum of $Na_{0.80}K_{0.20}NO_3$ at 473 K suggested a solid solution with the $NaNO_3$ I structure and the spectrum of $Na_{0.05}K_{0.95}NO_3$ at 473 K suggested a solid solution with the KNO_3 I structure. Brooker [55] has reported the difference between the Raman spectra of $NaNO_3$ I and KNO_3 I although they have the same space group of $R\bar{3}m$. He suggested that there might be a slight difference in structure between the two disordered nitrates.

At 393 K the spectrum was dominated by features of the $NaNO_3$ II structure (Table 6.4). $Na_{0.95}K_{0.05}NO3$ (NaII) exsolved from $Na_{0.80}K_{0.20}NO_3$ (NaI). In the external vibrational region there were two distinct bands at 95 and 180 cm^{-1} which are the translatory and rotatory modes in the $NaNO_3$ II structure (Fig. 6.12). The bands in the internal vibrational region were also characteristic for the $NaNO_3$ II structure (Table 6.4). Nevertheless the sample was found to be a mixture. Between the two lattice vibrations of the $NaNO_3$ II structure there was a broad feature centred at about 150 cm^{-1} (Fig. 6.12) which was not present in the spectrum of $Na_{0.95}K_{0.05}NO_3$ (NaII) (Fig. 6.5). The ν_1 band was broader and asymmetric on the low frequency side (Fig. 6.13). On the 724 cm^{-1} band due to the $NaNO_3$ II structure there was a small shoulder at 715 cm^{-1} and the 1382 cm^{-1} band of the $NaNO_3$ II structure located on a broad feature from 1300 to 1500 cm^{-1} (Fig. 6.14). All these additional Raman features suggested the existence of a residual solid solution (RSS) after exsolution of $Na_{0.95}K_{0.05}NO_3$ (NaII). This is consistent with Greis' phase diagram [66] which indicated a diphasic region of $R\bar{3}m$ and $R\bar{3}c$ for $Na_{0.80}K_{0.20}NO_3$ at 393 K.

When the temperature decreased to 366 K, more $Na_{0.95}K_{0.05}NO_3$ (NaII) exsolved and the

residual solid solution (RSS) was near the composition of the eutectoid in Greis' phase diagram. The increased content of KNO_3 in $Na_{1-x}K_xNO_3$ (RSS) caused the broad feature between the two lattice vibrations of $Na_{0.95}K_{0.05}NO_3$ (NaII) to shift to a lower wavenumber centred at about 130 cm^{-1} (Fig. 6.12). The asymmetry on the low frequency side of the ν_1 band of $Na_{0.95}K_{0.05}NO_3$ (NaII) now became a shoulder at 1060 cm^{-1} (Fig. 6.13).

A further decrease in the temperature brought about new features in the Raman spectrum. At 361 K, a diffuse band appeared at about 120 cm^{-1} (Fig. 6.12). Beside the 1060 cm^{-1} shoulder there was a small peak at 1054 cm^{-1} (Fig. 6.13). On the broad feature in the ν_3 region, there were two small peaks at 1351 and 1439 cm^{-1} (Fig. 6.14). All these features indicated that $Na_{1-x}K_xNO_3$ (KIII) had begun to separate from (RSS). At 356 K the diffuse feature at 120 cm^{-1} became a distinct band and at 351 K it was the dominant feature between the two lattice bands due to $Na_{0.95}K_{0.05}NO_3$ (NaII) (Fig. 6.12). In the internal vibrational region, features due to $Na_{1-x}K_xNO_3$ (RSS) were also mostly replaced by features of $Na_{1-x}K_xNO_3$ (KIII). Raman bands due to $Na_{1-x}K_xNO_3$ (KIII) and $Na_{0.95}K_{0.05}NO_3$ (NaII) coexisted in the spectrum of $Na_{0.80}K_{0.20}NO_3$ at 351 K (Figs. 6.13 and 6.14).

Finally at 346 K, $Na_{1-x}K_xNO_3$ (KIII) decomposed to KNO_3 II and $NaNO_3$ II. In the external vibrational region, the characteristic translatory and rotatory modes of KNO_3 II appeared at 51 and 86 cm^{-1} (Fig. 6.12). The ν_1 band at 1053 cm^{-1} was one wavenumber lower than that at 351 K because the replacement of $Na_{1-x}K_xNO_3$ (KIII) by KNO_3 II. The doublet peaks of KNO_3 II in the ν_3 region were just distinguishable at 1354 and 1360 cm^{-1} (Fig. 6.14). Only part of $Na_{1-x}K_xNO_3$ (KIII) decomposed to KNO_3 II and $NaNO_3$ II although the solid was kept at 346 K for two days. Features due to $Na_{1-x}K_xNO_3$ (KIII) still existed. The

band at 123 cm^{-1} looked a bit stronger than the same band in the spectrum at 356 K, taking the band at 82 cm^{-1} as the standard (Figs. 6.1 and 6.12). In the ν_3 region the TO-LO features may be distinguished and the LO mode may be observed at 1444 cm^{-1} (Fig. 6.14).

6.3 Discussion

The studies of temperature dependent Raman spectra of mixed crystals of $NaNO_3$-KNO_3 confirmed the Raman spectroscopic studies of the quenched samples. Moreover, some additional details about the structural phase transitions were revealed as the Raman technique was used to actually follow the transitions.

6.3.1 Limited Solid Solutions in $NaNO_3$-KNO_3

Raman studies indicated that $Na_{0.95}K_{0.05}NO_3$ (NaII) had the same characteristic temperature dependence as pure $NaNO_3$ II [121,122] down to 353 K. No changes in Raman features due to other processes were detected. The presence of 5 mol% KNO_3 in the solid solution appeared only to speed up the order-disorder transition of sodium nitrate. This was in good agreement with the Raman studies of the quenched sample which indicated that $Na_{0.95}K_{0.05}NO_3$, whether quenched from 493, 393 or 358 K, produced practically the same spectrum of the $NaNO_3$ structure. The temperature dependent studies supported the suggestion that there should be a vertical line near x = 0.05 and at 526 through 353 K in Greis' phase diagram for $Na_{0.95}K_{0.05}NO_3$ (NaII) (Fig. 5.1).

In Greis' phase diagram by DSC cooling runs, the subsolidus for the exsolution of $NaNO_3$ broke into three parts (areas a and b in Fig. 5.1). The λ transition temperature of sodium nitrate decreased slowly and rather linearly when potassium nitrate was added up to 5 mol% (13 K in all). More KNO_3 caused a dramatic drop of the transition temperature, and from 5 to 10 mol% KNO_3 the temperature decreased by 62 K. Then followed another linear and gradual decrease of the transition temperature, almost parallel to that from 0 to 5 mol% KNO_3. Greis and co-workers offered no explanation for the dramatic changes in the transition temperature and attributed all the three parts to exsolution and the λ transition of pure sodium nitrate. If this were so, there should also be DSC peaks due to structural phase transitions of potassium nitrate. DSC seemed to have failed to detect the exothermic effects due to KNO_3 for the mixtures with $x < 0.10$.

Raman studies of the subsolidus for $x \leq 0.05$ (area a in Fig. 5.1) indicated the λ transition of $Na_{1-x}K_xNO_3$ (NaI) to (NaII). The large potassium ions in the crystal increased the rate of disorder in $Na_{1-x}K_xNO_3$ (NaII) and thus lowered the λ transition temperature. The effect was proportional to the amount of potassium ions present in the crystal and the λ transition temperature decreased linearly with increased x. The dramatic temperature drop at $0.05 < x < 0.10$ indicated a change in the mechanism. Then followed a linear boundary (area b in Fig. 5.1) indicating the temperature for exsolution of $Na_{0.95}K_{0.05}NO_3$ (NaII) from the $R\bar{3}m$ solid solutions which decreased proportionally to the content of $Na_{0.95}K_{0.05}NO_3$ (NaII) in the $R\bar{3}m$ solid solutions.

A DSC study [123] of variation of the λ transition temperature in $NaNO_3$-based binary alloys supports our results for $Na_{0.95}K_{0.05}NO_3$ (NaII). In this study the solid solutions with the

$NaNO_3$ II were reported for x up to 0.10. However, the uncertainty for $Na_{0.90}K_{0.10}NO_3$ (NaII) was much greater than for $Na_{0.95}K_{0.05}NO_3$ (NaII) because fast runs had to be used in the former to avoid smearing out of the DSC signals. Thus the temperature at which thermal effects were observed in the DSC study did not likely correspond to the λ transition of $Na_{0.90}K_{0.10}NO_3$ (NaII). It was more likely to reflect several complicated processes. Exsolution of $Na_{0.90}K_{0.10}NO_3$ (NaII) from the $R\bar{3}m$ solid solution was detected in the Raman spectrum of the 393 K quenched $Na_{0.90}K_{0.10}NO_3$. The genuine λ transition of $Na_{1-x}K_xNO_3$ (NaI) to (NaII) must be somewhere just below x = 0.10.

On the KNO_3 rich part of Greis' phase diagram, the upper boundary of area e in Fig. 5.1 was for the temperature of exsolution of pure KNO_3 III from the $R\bar{3}m$ solid solution. This line must now be explained otherwise. The temperature dependence for the Raman spectra of $Na_{0.05}K_{0.95}NO_3$ did not indicate exsolution of any components down to 366 K. If this line were for exsolution of KNO_3 III, Raman features due to the residual solid solution would have been observed. However, there were only the characteristic Raman bands due to the KNO_3 III structure. Therefore, area e was the uniphasic region of $Na_{1-x}K_xNO_3$ (KIII) instead of diphasic region of KNO_3 III and a residual $R\bar{3}m$ solid solution, and its upper boundary was for the phase transition of $Na_{1-x}K_xNO_3$ (KI) to (KIII), as was evident by examination of the Raman spectra of $Na_{0.05}K_{0.95}NO_3$ at 393 K and 366 K.

Exsolution in $Na_{0.05}K_{0.95}NO_3$ occurred at 361 K. Raman studies indicated that it was not $NaNO_3$ II that separated from the $R\bar{3}m$ solid solution, which was suggested in Greis' phase diagram. It was KNO_3 II that exsolved from $Na_{0.05}K_{0.95}NO_3$ (KIII), as was clear from the Raman spectrum at 361 K (Figs. 6.1 and 6.2). Raman bands due to KNO_3 II and $Na_{1-x}K_xNO_3$

(KIII) appeared in the spectrum with comparable intensity. The sample was in a diphasic region. As some of KNO_3 exsolved, the remaining $Na_{1-x}K_xNO_3$ (KIII) must contain KNO_3 less than 95 mol%. Raman studies of the 358 K quenched $Na_{0.10}K_{0.90}NO_3$ indicated the existence of $Na_{1-x}K_xNO_3$ (KIII) containing KNO_3 slightly less than 90 mol%. In Greis' phase diagram, the boundary for the transition of $Na_{1-x}K_xNO_3$ (KI) to (KIII) ended at $x = 0.85$ (Fig. 5.1). It was reasonable to continue the boundary with a vertical line to indicate the solid solution $Na_{0.15}K_{0.85}NO_3$ (KIII). The region between 361 and 353 K and for $x \geq 0.85$ in Greis' phase diagram (area d) would be the diphasic region of KNO_3 II and $Na_{0.15}K_{0.85}NO_3$ (KIII).

The transition of $Na_{1-x}K_xNO_3$ (KI) to (KIII) was observed by hot-stage microscopy for $NaNO_3$ up to 10 w% [113]. The transition temperature with 5 w% $NaNO_3$ was 385 K. In Kofler's phase diagram there was an indication of formation of $Na_{1-x}K_xNO_3$ (KIII) containing 2 w% $NaNO_3$. The diagram was referred to by Kramer and Greis [4,66]. However, the formation of solid solutions other than $R\bar{3}m$ seems to have been neglected. Zamaly and Jemal[46] presented a phase diagram which was similar to Kofler's in the KNO_3 rich part. The formation of $Na_{1-x}K_xNO_3$ (KIII) extended to about 10 mol% KNO_3. In Zamaly's phase diagram there was also a small region for $Na_{1-x}K_xNO_3$ (NaII) (up to 5 mol% KNO_3). Zamaly and Jemal examined the $NaNO_3$-KNO_3 system down to 373 K. Their results concerning limited solid solutions were in good agreement with our Raman studies.

6.3.2 The Disordered State

At high temperature both sodium nitrate ($NaNO_3$ I) and potassium nitrate (KNO_3 I)

adopt the disordered calcite structure. The space group is $R\bar{3}m$. The isostructure is the key argument that the two nitrates form continuous solid solutions. The space group $R\bar{3}m$ was based on XRD studies which may lead to an apparent symmetry higher than actual because X-ray diffraction gives an average structure. Raman spectroscopy is a much faster technique than X-ray diffraction. Raman studies suggested [55] that on a shorter time scale the crystal symmetry of KNO_3 I was lower than $R\bar{3}m$ and $NaNO_3$ I and KNO_3 I had slightly different crystal structures.

In fact $NaNO_3$ I and KNO_3 I have quite different structural chemistry. The order-disorder transition ($R\bar{3}c$ to $R\bar{3}m$) in sodium nitrate is a typical λ transition. The transition temperature (548 K) is near the melting point. The transition involves orientational disordering of the nitrate groups in the crystal and it is reversible. When cooled down the disordered $R\bar{3}m$ structure in $NaNO_3$ I goes back to the ordered $R\bar{3}c$ structure in $NaNO_3$ II. The disordered state in $NaNO_3$ I is unquenchable. When quenched, disordered $NaNO_3$ I transforms to ordered $NaNO_3$ II. On the other hand, the order-disorder transition (Pmcn to $R\bar{3}m$) in potassium nitrate is of first order. The transition takes place at a much lower temperature (401 K). The transition involves rearrangement of cations and anions and it is not directly reversible. When cooled, the disordered $R\bar{3}m$ structure in KNO_3 I first changes to the ordered R3m structure of KNO_3 III then to the Pmcn structure in KNO_3 II. The disordered state in KNO_3 I is unquenchable. When quenched, KNO_3 I goes to the intermediate ordered phase KNO_3 III.

It is expected that the $R\bar{3}m$ solid solutions of $NaNO_3$-KNO_3 with different compositions would have slightly different disordered structures. The temperature dependence for the

Raman spectrum of $Na_{0.95}K_{0.05}NO_3$ was found to be quite similar to that of pure sodium nitrate: as the temperature increased, the two external vibrations of the $NaNO_3$ II structure shifted to lower frequencies and the 100 cm^{-1} band gradually vanished as the transition temperature was approached. $Na_{0.95}K_{0.05}NO_3$ (NaI) was unquenchable. When quenched, $Na_{0.95}K_{0.05}NO_3$ (NaI) went directly to (NaII). The temperature dependence for the Raman spectrum of $Na_{0.05}K_{0.95}NO_3$ was found to be similar to that of pure potassium nitrate: as the temperature decreased the disordered $R\bar{3}m$ structure in $Na_{0.05}K_{0.95}NO_3$ (KI) first transformed to the ordered R3m structure in (KIII) and then to the structure Pmcn in (KII). $Na_{0.05}K_{0.95}NO_3$ (KI) was unquenchable. When quenched, $Na_{0.05}K_{0.95}NO_3$ (KI) went to the intermediate ordered phase (KIII). The temperature dependence for the Raman spectrum of $Na_{0.33}K_{0.67}NO_3$ was unique and indicated that the solid solution had a disordered structure different from either $Na_{0.95}K_{0.05}NO_3$ (NaI) or $Na_{0.05}K_{0.95}NO_3$ (KI).

There were four notable features which distinguished the disordered state in $Na_{0.33}K_{0.67}NO_3$ from the disordered state in $Na_{0.95}K_{0.05}NO_3$ (NaI) or $Na_{0.05}K_{0.95}NO_3$ (KI). The transition from disordered state to ordered state was slower for the former than for the latter. It took less than 10 hours for $Na_{0.95}K_{0.05}NO_3$ (NaI) or $Na_{0.05}K_{0.95}NO_3$ (KI) to complete the order-disorder transition while it took more than two days for $Na_{0.33}K_{0.67}NO_3$ (D) under similar conditions. Because of the slowness of the order-disorder transition of the intermediate concentration phase, the disordered state may be kept metastably when exsolution of a component caused the residual solid solution of the terminal phases to have a composition of the intermediate concentration phase, as was noted in the discussion of the temperature dependence for the Raman spectra of $Na_{0.80}K_{0.20}NO_3$ and $Na_{0.05}K_{0.95}NO_3$. The

order-disorder transition in $Na_{0.33}K_{0.67}NO_3$ (D) led to decomposition directly to its components $NaNO_3$ II and KNO_3 II, unlike $Na_{0.95}K_{0.05}NO_3$ (NaI) or $Na_{0.05}K_{0.95}NO_3$ (KI) in which the disordered solid solution (NaI) or (KI) transformed to the ordered solid solution (NaII) or (KIII).

The order-disorder transition in $Na_{0.33}K_{0.67}NO_3$ (D) was of a quite sudden feature. The Raman spectra before the transition were very similar and there was no precursor of the coming structural change (Fig. 6.8 and 6.9). On the other hand, the temperature dependence for the Raman spectra of $Na_{0.95}K_{0.05}NO_3$ and $Na_{0.05}K_{0.95}NO_3$ suggested a gradual phase transition. In the external region (Figs 6.1 and 6.5) and the ν_3 region (Figs. 6.2 and 6.7), the spectra taken above the transition had features of the upcoming ordered phases. Finally, the disordered state in $Na_{0.33}K_{0.67}NO_3$ (D) could be frozen by quenching while the disordered state in $Na_{0.95}K_{0.05}NO_3$ (NaI) or $Na_{0.05}K_{0.95}NO_3$ (KI), just like $NaNO_3$ I or KNO_3 I, was unquenchable.

The new disordered features in $Na_{0.33}K_{0.67}NO_3$ (D) suggested a cause other than the orientational disorder of the nitrate ions, as in the disordered calcite structure, because the disordered orientation of the planar anions cannot be frozen by quenching. The disordering in $Na_{0.33}K_{0.67}NO_3$ (D) was caused by the existence of two different cations and it may remain even without the disordered orientation of the nitrate group. The temperature dependent Raman spectra of $Na_{0.33}K_{0.67}NO_3$ suggested that the new disordered state existed in the whole temperature range where Greis' phase diagram [66] indicated the continuous solid solution of the disordered $R\bar{3}m$ structure.

The large size difference between sodium and potassium ions made it difficult for the

$R\bar{3}m$ solid solutions to have a uniform structure over a wide composition region and at a relatively low temperature. The difficulty was aggravated by the slight difference in the disordered calcite structure of $NaNO_3$ I and KNO_3 I. Raman studies suggested that the slight difference remained between the solid solutions $Na_{1-x}K_xNO_3$ (NaI) and (KI) of the terminal phases. The new disorder in the mixtures of the intermediate concentration phase may be regarded as a balance between the two slightly different disordered calcite structures when the contents of $NaNO_3$ and KNO_3 were comparable in the solid solutions. The new disordered state may be the result of phase separation of $Na_{1-x}K_xNO_3$ (NaI) and (KI) on a microscopic or submicroscopic scale. In this respect, the new disordered state in the intermediate concentration range of $NaNO_3$-KNO_3 might well be regarded as an indication of eutectic mixtures of $Na_{1-x}K_xNO_3$ (NaI) and (KI) in the terminal phases.

Although it is now widely accepted [4,66,113] that sodium and potassium nitrate forms a continuous series of solid solutions, the idea of limited solid solutions [112] should not be abandoned. Two observations are inconsistent with the continuous solid solution model. The solidus was found almost horizontal from 20 to 80 mol% KNO_3 [4] and the X-ray diffraction pattern of the solid solution of equimolar $NaNO_3$-KNO_3 was different from either KNO_3 or $NaNO_3$ at the same temperature of 473 K [114]. The new disordered state in the solid solutions of intermediate concentration region offers a possible explanation. The new disordered state in the solid solutions in the intermediate concentration region had a slightly different microscopic structure from the $R\bar{3}m$ structure of the terminal phases, so a different X-ray diffraction pattern was observed. If the disordered structures of $Na_{1-x}K_xNO_3$ (NaI) and (KI) in the terminal phases are regarded as two different phases and the new disordered state in

the solid solutions of intermediate concentrations is regarded as a mixture of the two, the $NaNO_3$-KNO_3 system might well be regarded as one of limited solid solutions. A system of limited solid solutions usually has a flat solidus in the intermediate concentration region.

The sole direct evidence for continuous solid solutions in $NaNO_3$-KNO_3 was the appearance of the mixed crystals under hot-stage microscope [113]. Since the terminal phases were in such similar disordered states that they could not be distinguished by light microscope, a mixture of such disordered states on a microscopic scale in the intermediate concentration region might well be indistinguishable. It is necessary to reconsider the $NaNO_3$-KNO_3 system in the light of Raman evidence in this work.

The study of order-disorder in $NaNO_3$ is also of great interest for earth science [124-128]. Recently Salje and co-workers [125-127] made a systematic study of sodium nitrate by X-ray intensity, excess birefringence, Raman spectroscopy and molecular dynamics. The disorder transition in sodium nitrate served as a model to investigate the disorder in calcite, an important component of the earth's crust. At 1250 K calcite has a transition similar to the order-disorder transition in sodium nitrate. It was suggested [125] that this transition accounted for the non-linearity of the boundary between the stability fields of calcite and aragonite in a P-T phase diagram. According to present Raman studies, it seems that sodium nitrate alone cannot fully simulate the process. Sodium nitrate can only have the calcite structure. The aragonite structure is adopted by potassium nitrate. Raman studies of the limited solid solutions in $NaNO_3$-KNO_3 indicated that it was very difficult, if not impossible, for sodium nitrate to have the aragonite structure. There appear three disordered structures in the nitrates corresponding to the disordered calcite structure: $NaNO_3$ I, KNO_3 I and the new disordered

state in $NaNO_3$-KNO_3 with comparable amounts of both components. Parallel studies of the disordering in KNO_3 and mixed $NaNO_3$-KNO_3 may be of help to obtain a better understanding of the order-disorder phenomena in carbonates.

6.4 Conclusions

Raman studies of $NaNO_3$-KNO_3 at different temperatures were in good agreement with the studies of the quenched samples. The suggestions about the phase diagram that were made in Chapter 5 were fully confirmed.

1. The discontinuous subsolidus on the $NaNO_3$ rich part of Greis' phase diagram suggested three processes for different compositions: the structural phase transition of $Na_{1-x}K_xNO_3$ (NaI) to (NaII) for $x \leq 0.05$; a mechanism change for $0.05 < x < 0.10$; exsolution of $Na_{0.95}K_{0.05}NO_3$ (NaI) from the $R\bar{3}m$ solid solutions for $0.10 \leq x \leq 0.55$. The subsolidus on the KNO_3 rich part indicated the structural phase transition of $Na_{1-x}K_xNO_3$ (KI) to (KIII).
2. Two vertical lines should be added to Greis' phase diagram: one for $Na_{0.95}K_{0.05}NO_3$ (NaII) between 526 and 353 K, the other for $Na_{0.15}K_{0.85}NO_3$ (KIII) between 361 and 353 K.
3. The $R\bar{3}m$ solid solutions just below the solidus may adopt one of the three slightly different disordered structures: $Na_{1-x}K_xNO_3$ (NaI) or (KI) in the terminal phases, or a new disordered state in the intermediate concentration phase which appeared to be similar to a mixture of (NaI) and (KI). The existence of the three disordered structures

suggested that $NaNO_3$-KNO_3 was a system of limited solid solutions instead of continuous solid solutions.

Table 6.1 Observed wavenumbers for Raman bands of $Na_{0.05}K_{0.95}NO_3$ measured at different temperatures.

T (K)	external	ν_4	ν_1	ν_3	$2\nu_2$
473	~ 110 [d]	716	1055	1352-1428 [e]	1664
393	114	717	1056	1356-1428 [e]	1664
366	121	717	1054	1350,1432,1439	1663
361	50,82,123	717	1053	1347,1359,1431,1440	1665
356	51,82,123	715	1051,1058	1345,1359	~ 1670 [f]
405 [a]	120	716	1055	1365,1421	1664
390 [b]	50,79,120	715	1050	1343,1359	1652,1679
385 [c]	120	717	1053	1348,1428,1438	1663

a. Data from reference 55 for pure KNO_3 I.

b. Data from reference 55 for pure KNO_3 II.

c. Data from reference 55 for pure KNO_3 III.

d. Broad features with irregular small peaks.

e. Broad features with small peak on both ends.

f. Very weak, diffuse features from 1650 to 1680 cm^{-1} .

Table 6.2 Observed wavenumbers for Raman bands of $Na_{0.95}K_{0.05}NO_3$ measured at different temperatures.

T (K)	external	ν_4	ν_1	ν_3	$2\nu_2$
473	78,173	723	1065	1380	1665
473 [a]	86,173	724	1066	1381	1666
393	94,180	724	1066	1382	1667
393 [a]	96,181	725	1067	1384	1668
366	95,181	724	1066	1383	1667
361	96,182	724	1067	1384	1669
356	97,183	725	1067	1384	1668
356 [a]	99,184	725	1068	1385	1669

a. Data for pure sodium nitrate.

Table 6.3 Observed wavenumbers for Raman bands of $Na_{0.33}K_{0.67}NO_3$ measured at different temperatures.

T (K)	external	ν_4	ν_1	ν_3	$2\nu_2$
473	110-140 [b]	717	1058	1300-1500 [c]	1664
393	110-140 [b]	717	1060	1300-1500 [c]	1665
366	110-140 [b]	717	1060	1300-1500 [c]	1665
361	110-140 [b]	717	1061	1300-1500 [c]	1665
356	110-140 [b]	716	1060	1300-1500 [c]	1664
351	51,83,123	716,725	1051,1061	1345,1359,1384 [d]	1666
351 [a]	50,82,123,181	715,724	1050,1066	1344,1359,1383 [d]	1667

a. The Raman spectrum was measured after the sample was kept at 351 K for another 22 hours.

b. Broad feature with small irregular peaks.

c. Broad features from 1300 to 1500 cm^{-1} .

d. Bands located on the broad features from 1300 to 1500 cm^{-1} .

Table 6.4 Observed wavenumbers for Raman bands of $Na_{0.80}K_{0.20}NO_3$ measured at different temperatures.

T (K)	external	ν_4	ν_1	ν_3	$2\nu_2$
473	~ 140 [a]	722	1064	1380	1664
393	95,180	715,724	1066	1382	1667
366	96,181	715,724	1060,1067	1383	1667
361	97,183	717,724	1054,1067	1351,1384,1439	1668
356	98,123,184	718,725	1054,1067	1351,1384,1444	1668
351	98,120,184	718,725	1054,1068	1350,1385,1444	1668
346	51,86,98,184	718,726	1053,1068	1354,1360,1385,1444	1669

a. Broad features with irregular small peaks.

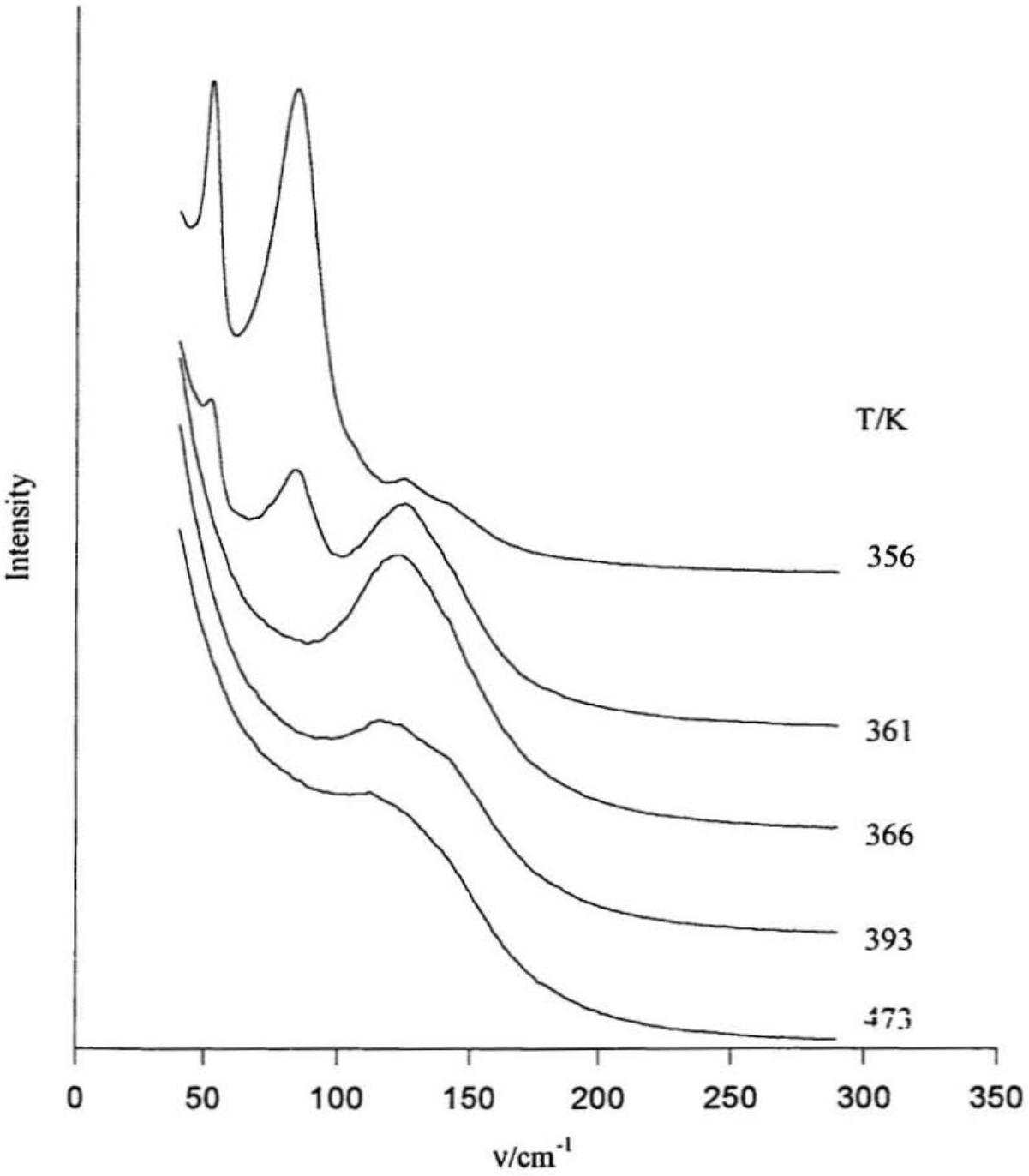

Fig. 6.1 Raman spectra in the external vibrational region of $Na_{0.05}K_{0.95}NO_3$ at different temperatures.

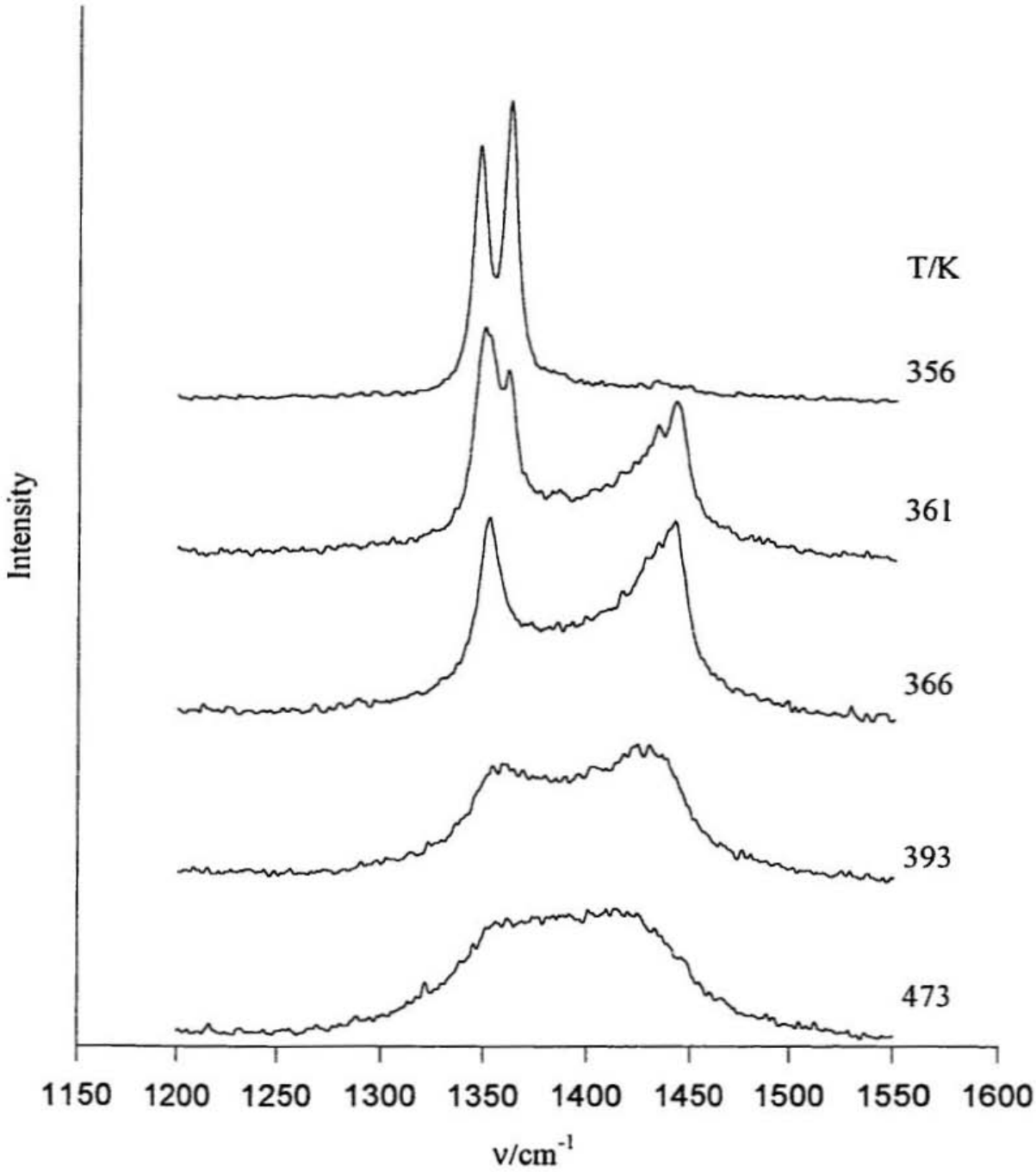

Fig. 6.2 Raman spectra in the ν_3 region of $Na_{0.05}K_{0.95}NO_3$ at different temperatures.

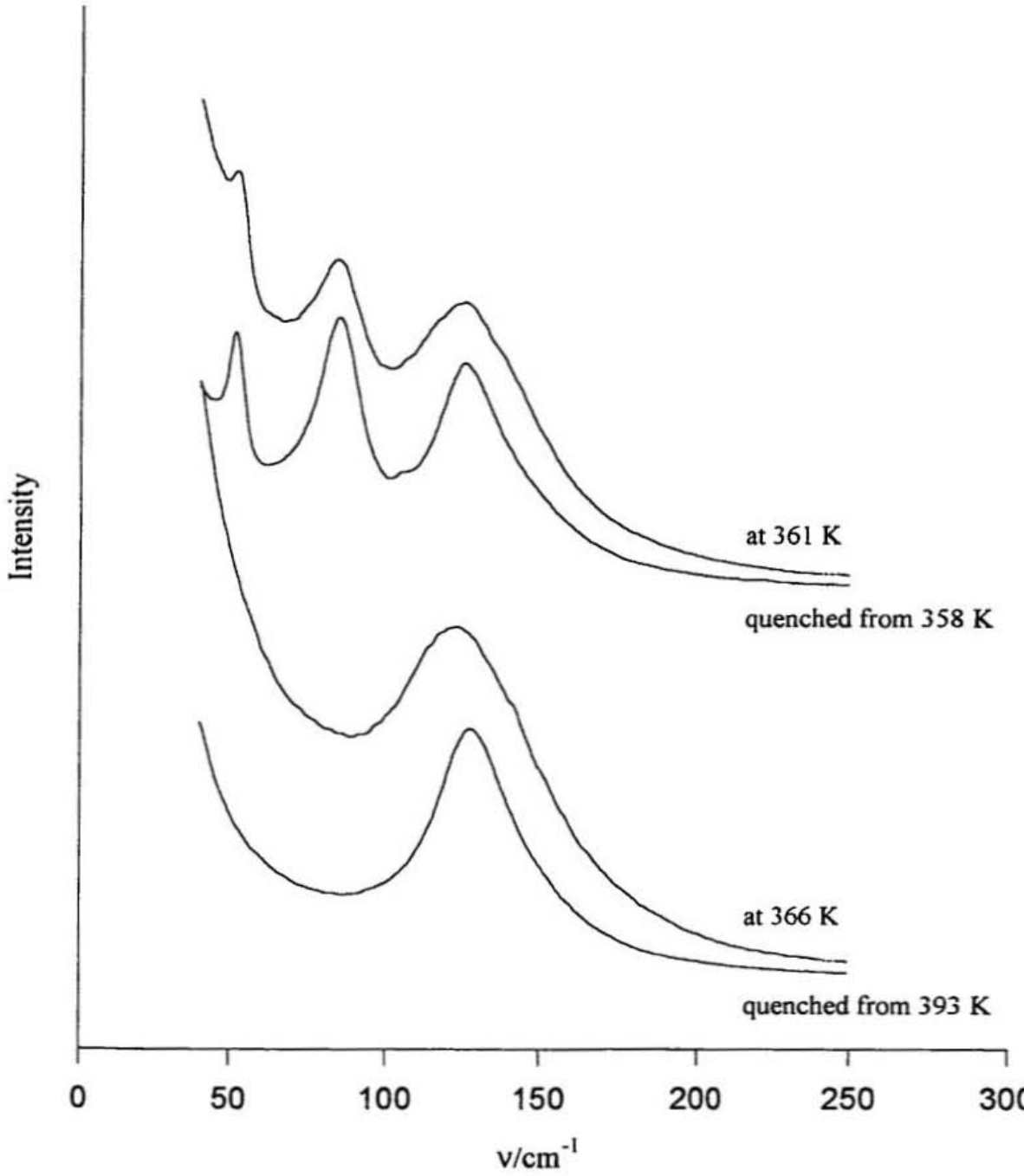

Fig. 6.3 Raman spectra in the external vibrational region of $Na_{0.05}K_{0.95}NO_3$ for quenched sample at 298 K and unquenched sample at indicated temperatures.

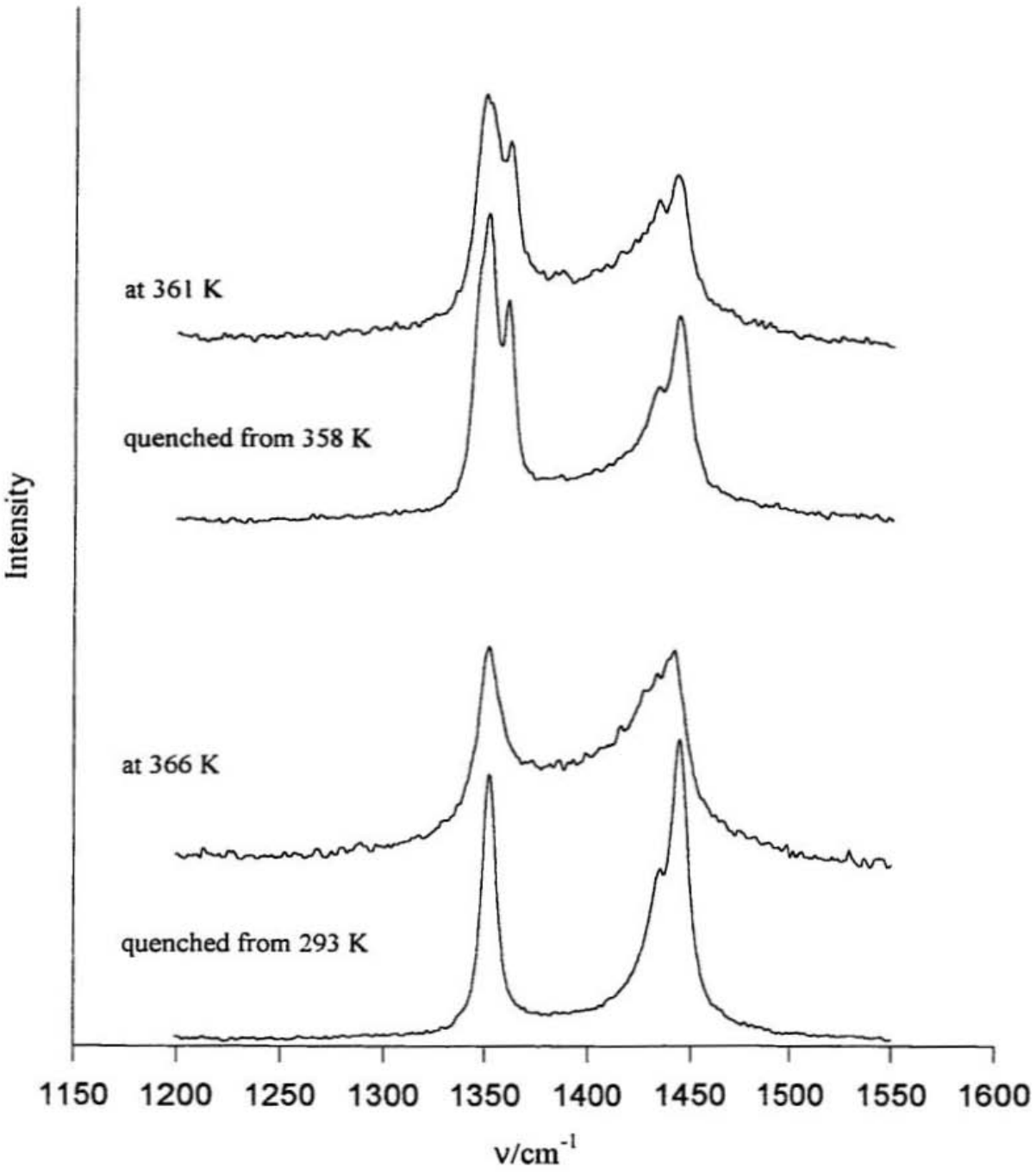

Fig. 6.4 Raman spectra in the ν_3 region of $Na_{0.05}K_{0.95}NO_3$ for quenched sample at 298 K and unquenched sample at indicated temperatures.

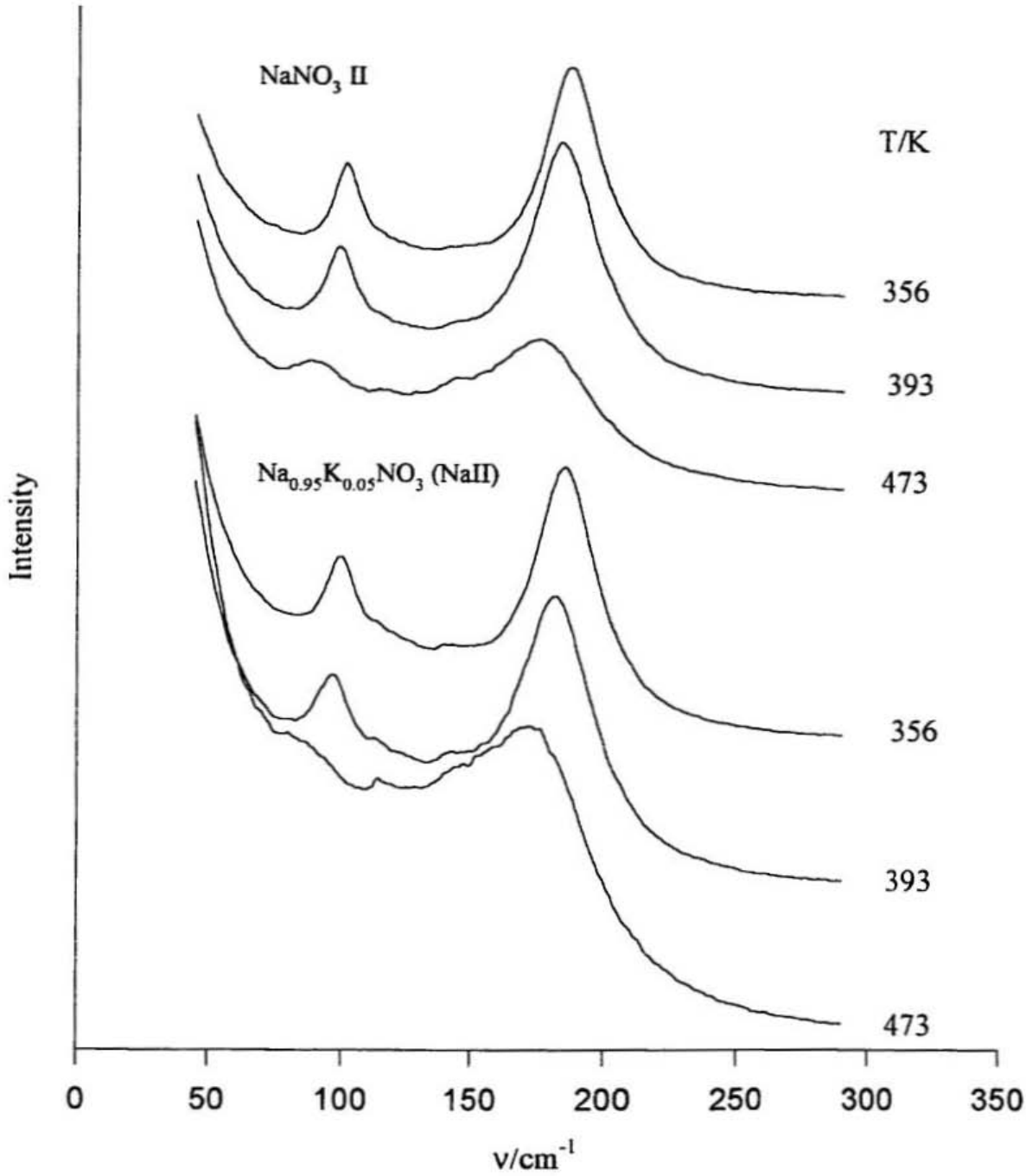

Fig 6.5 Raman spectra in the external vibrational region of pure $NaNO_3$ II and $Na_{0.95}K_{0.05}NO_3$ (NaII) at different temperatures.

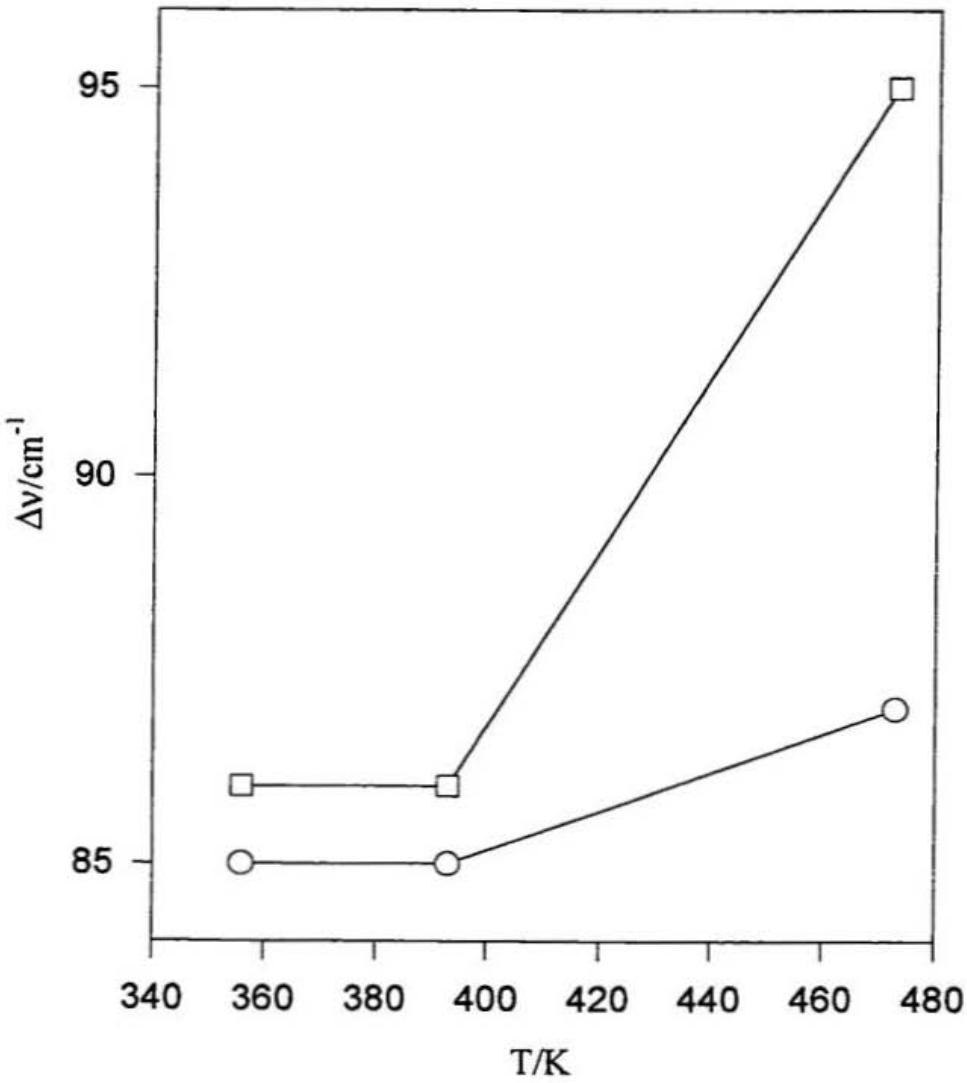

Fig. 6.6 Frequency difference between the two lattice modes of $NaNO_3$ II (o) and $Na_{0.95}K_{0.05}NO_3$ (NaII) (❑) at different temperatures.

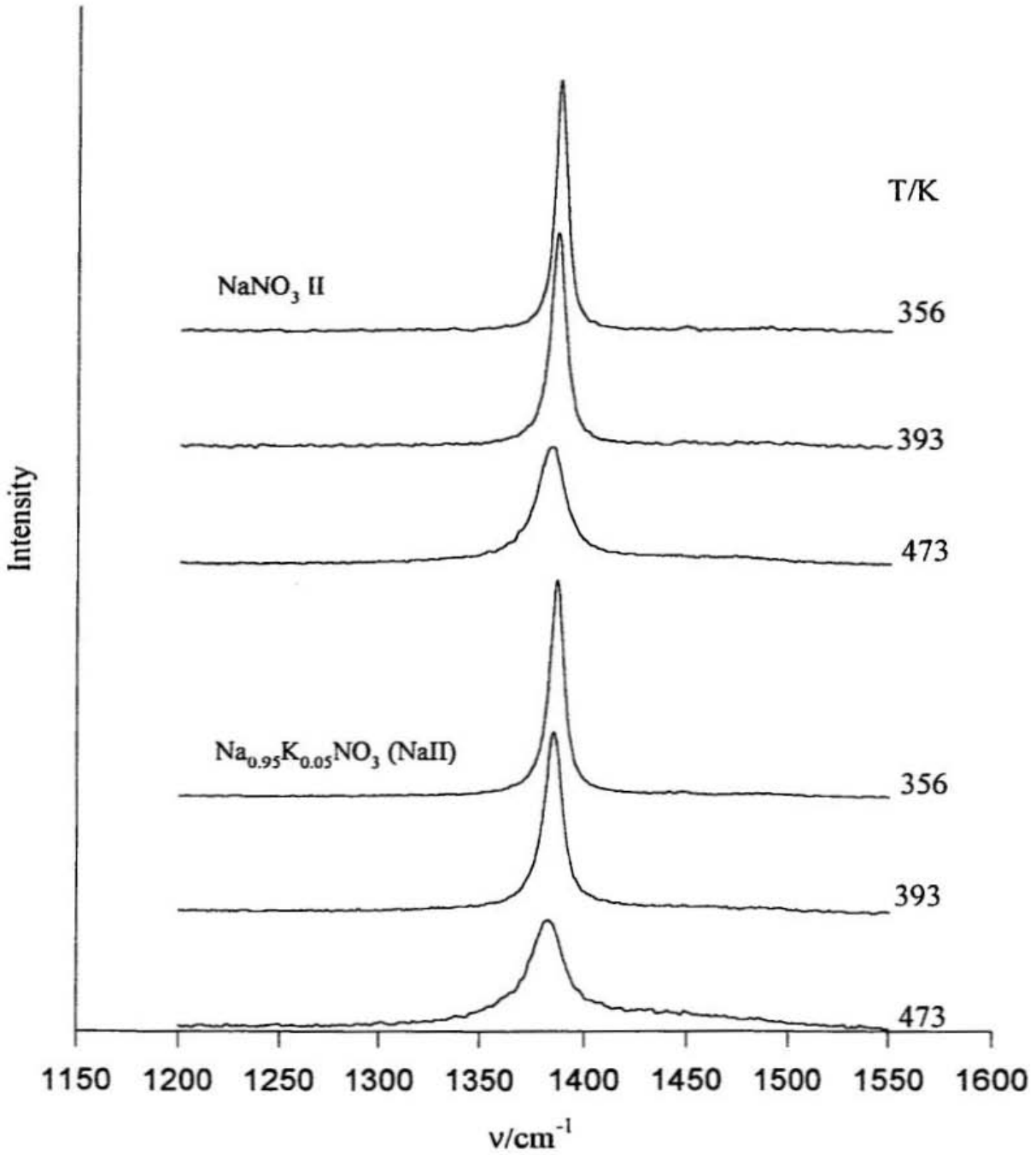

Fig. 6.7 Raman spectra in the ν_3 region of pure $NaNO_3$ II and $Na_{0.95}K_{0.05}NO_3$ (NaII) at different temperatures.

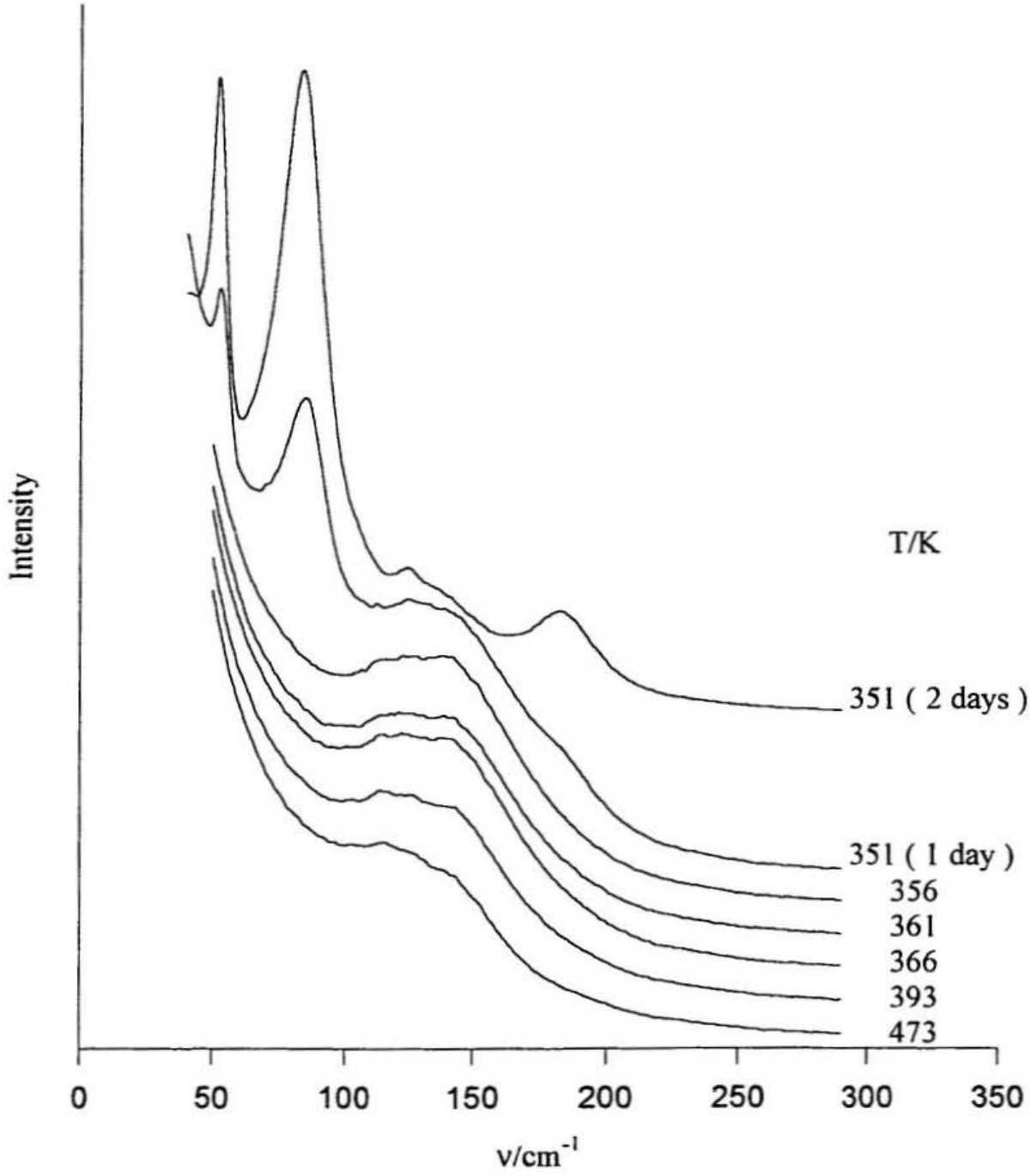

Fig. 6.8 Raman spectra in the external vibrational region of $Na_{0.33}K_{0.67}NO_3$ at different temperatures.

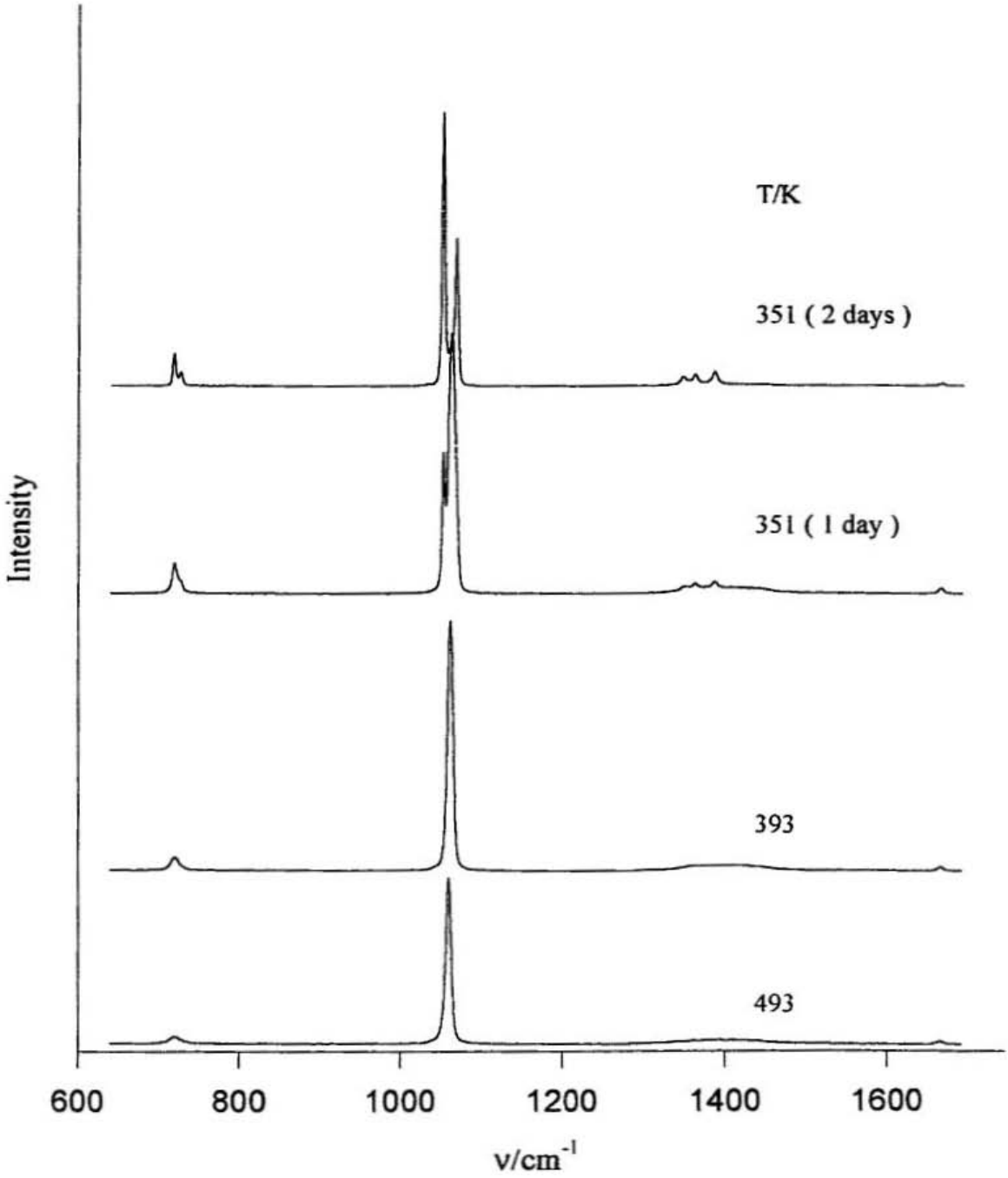

Fig. 6.9 Raman spectra in the internal vibrational region of $Na_{0.33}K_{0.67}NO_3$ at different temperatures.

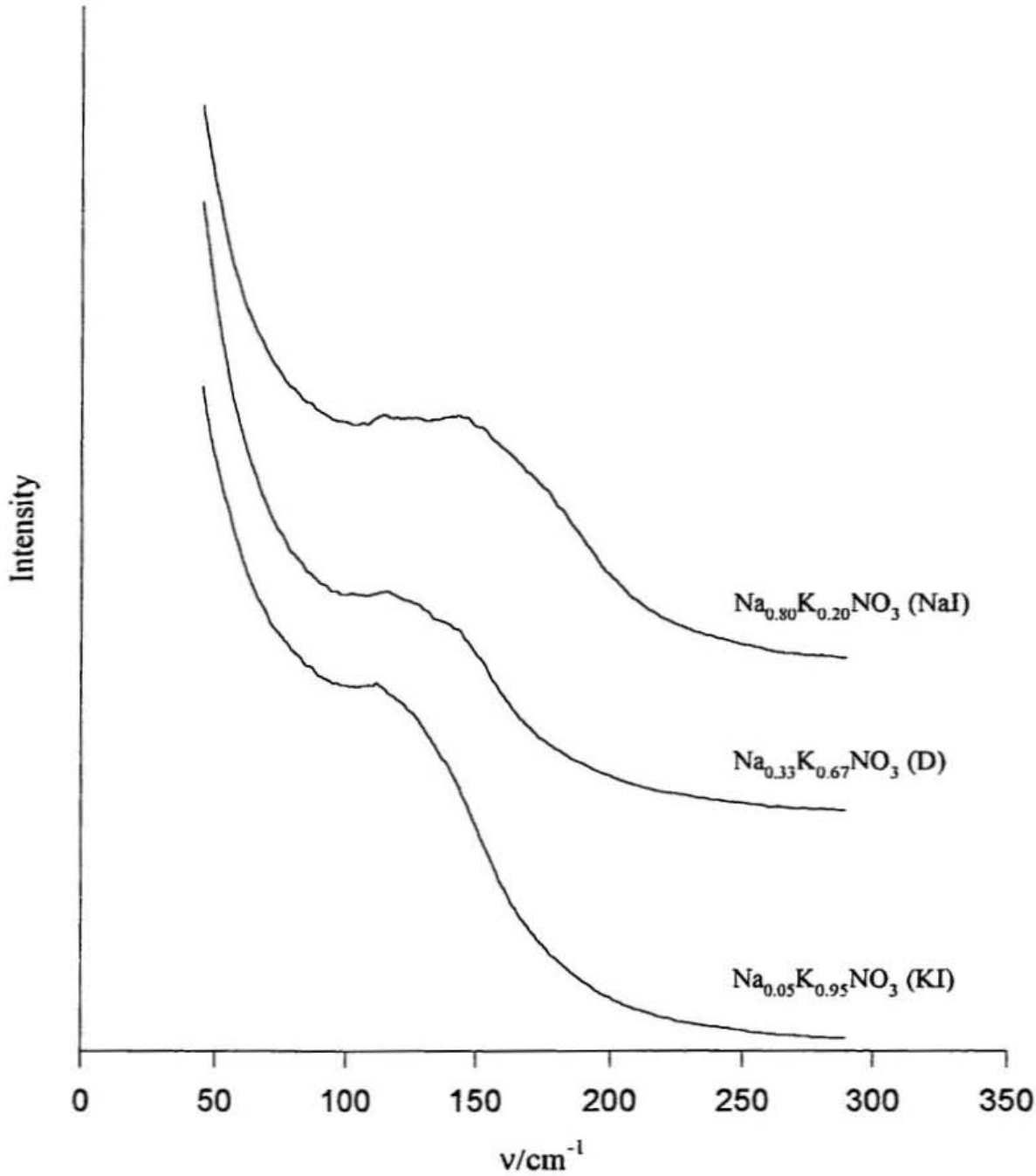

Fig. 6.10 Raman spectra in the external vibrational region of $Na_{1-x}K_xNO_3$ at 473 K.

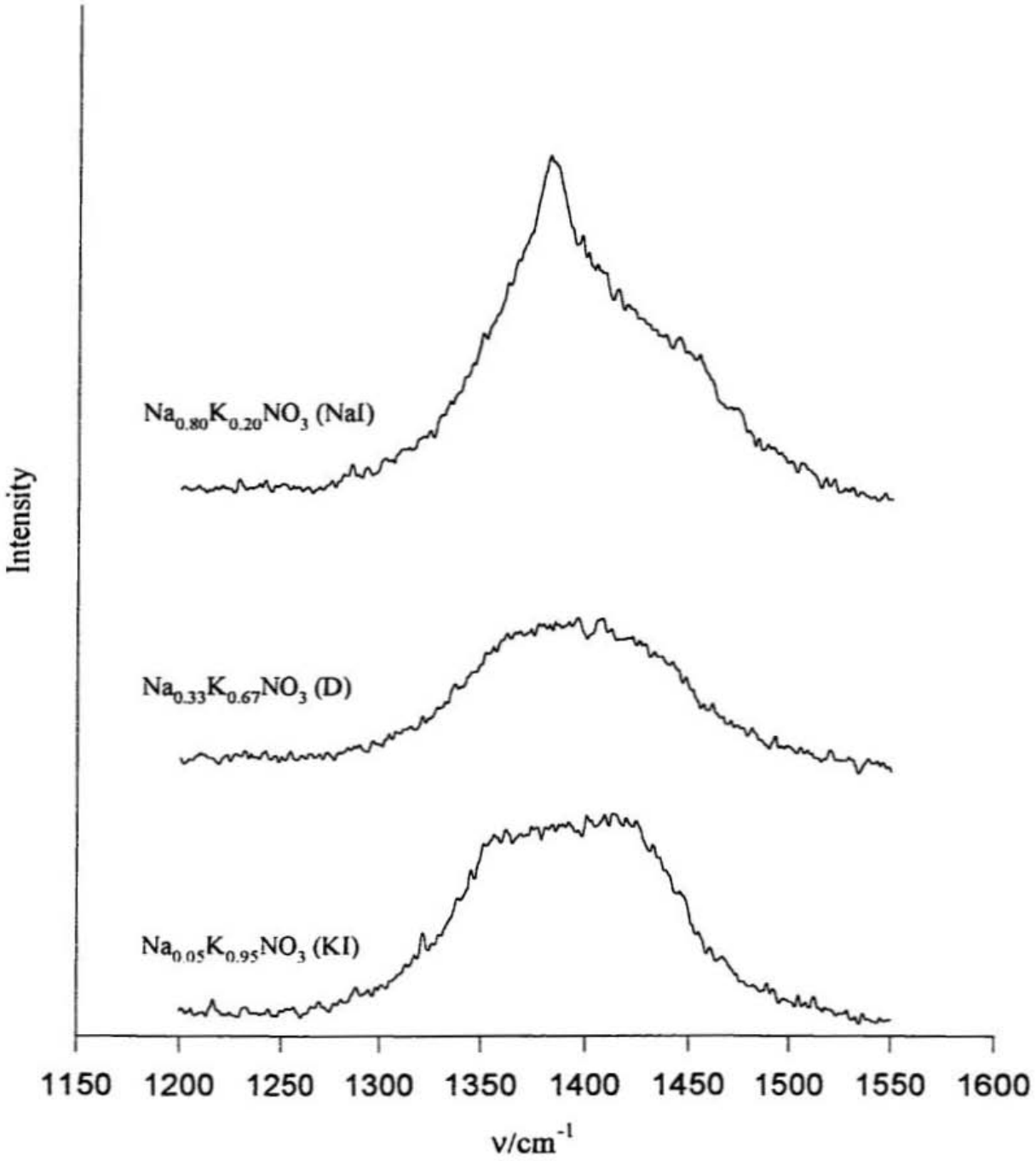

Fig. 6.11 Raman spectra in the ν_3 region of $Na_{1-x}K_xNO_3$ at 473 K.

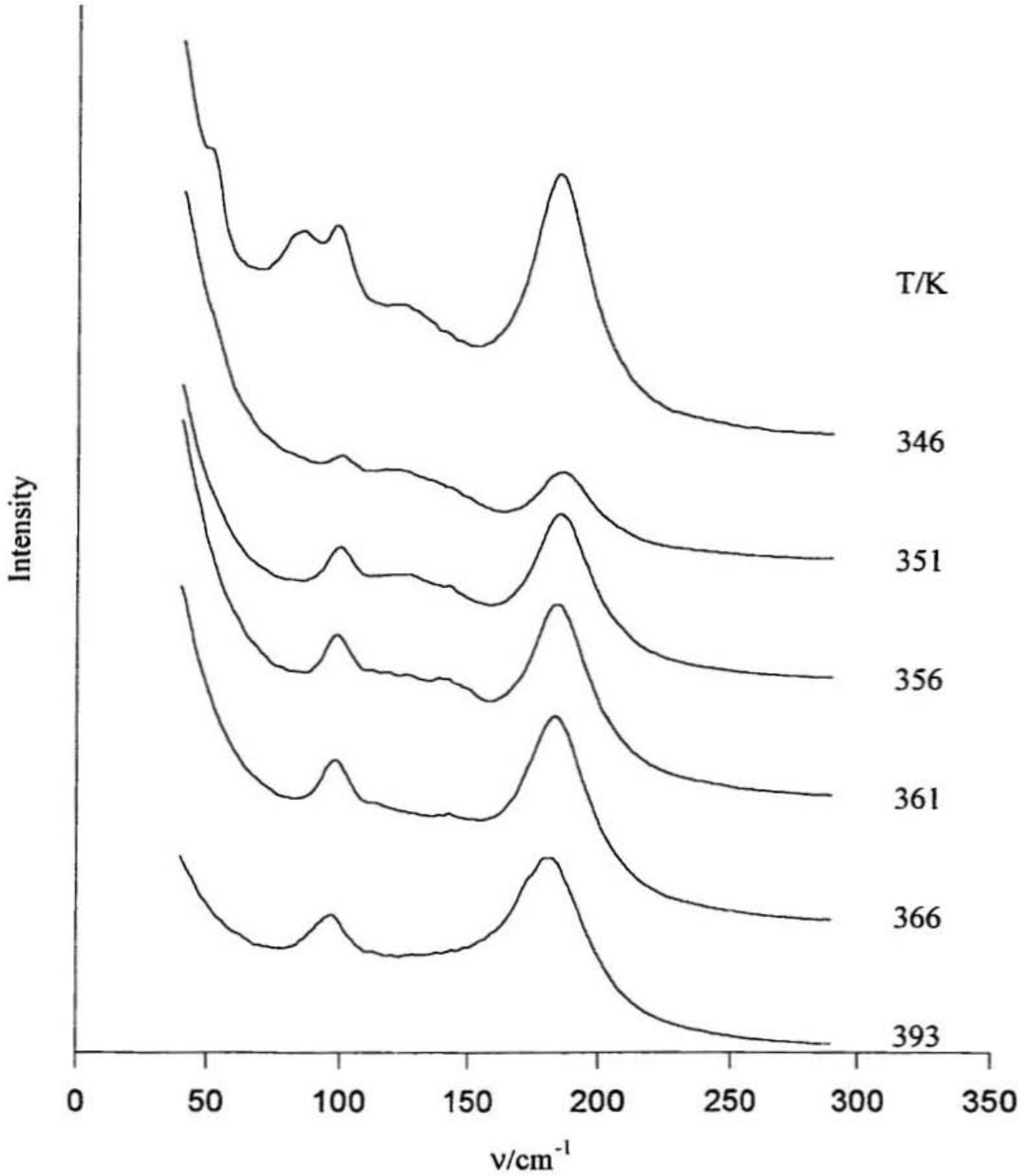

Fig. 6.12 Raman spectra in the external vibrational region of $Na_{0.80}K_{0.20}NO_3$ at different temperatures.

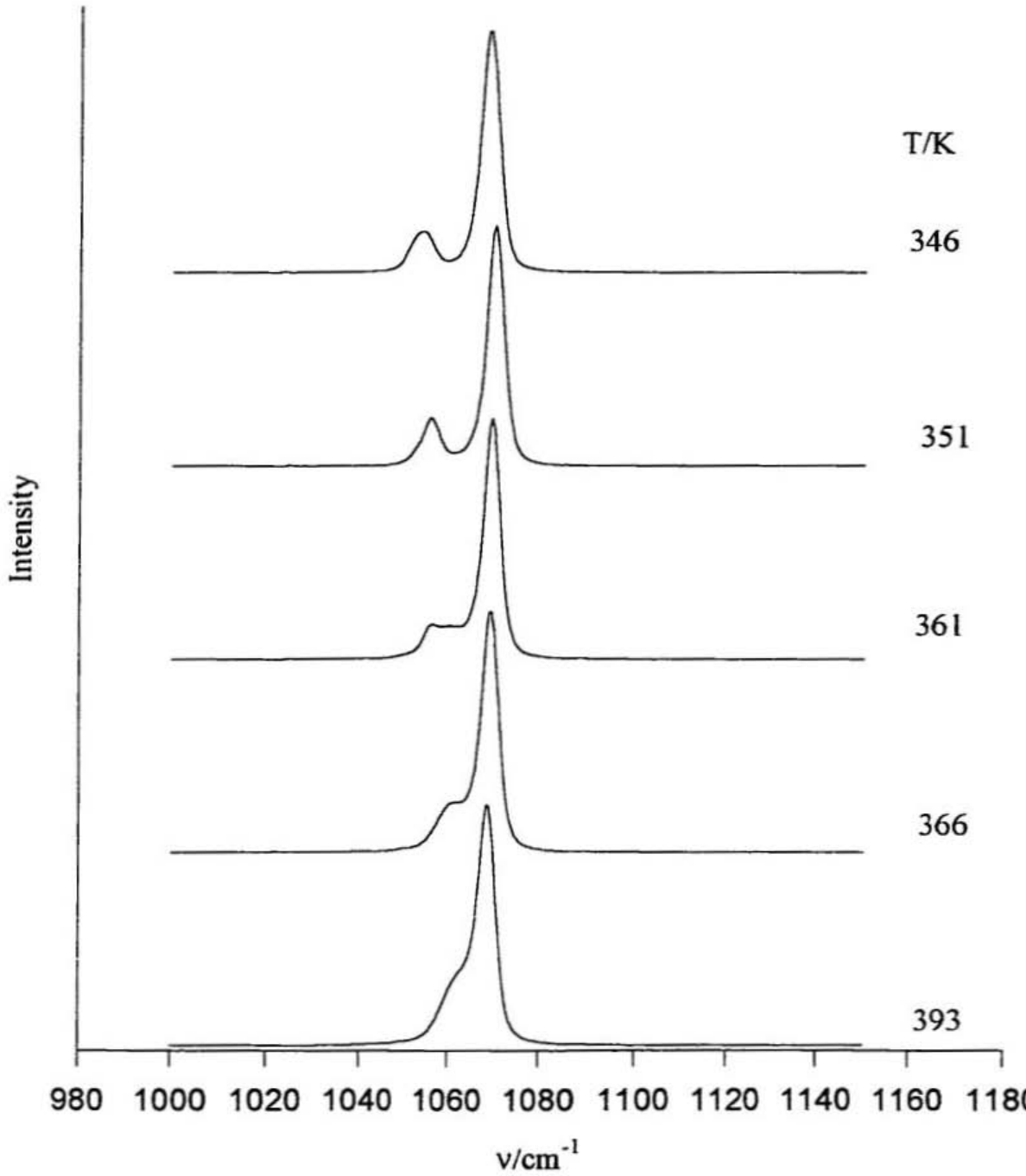

Fig. 6.13 Raman spectra in the ν_1 region of $Na_{0.80}K_{0.20}NO_3$ at different temperatures.

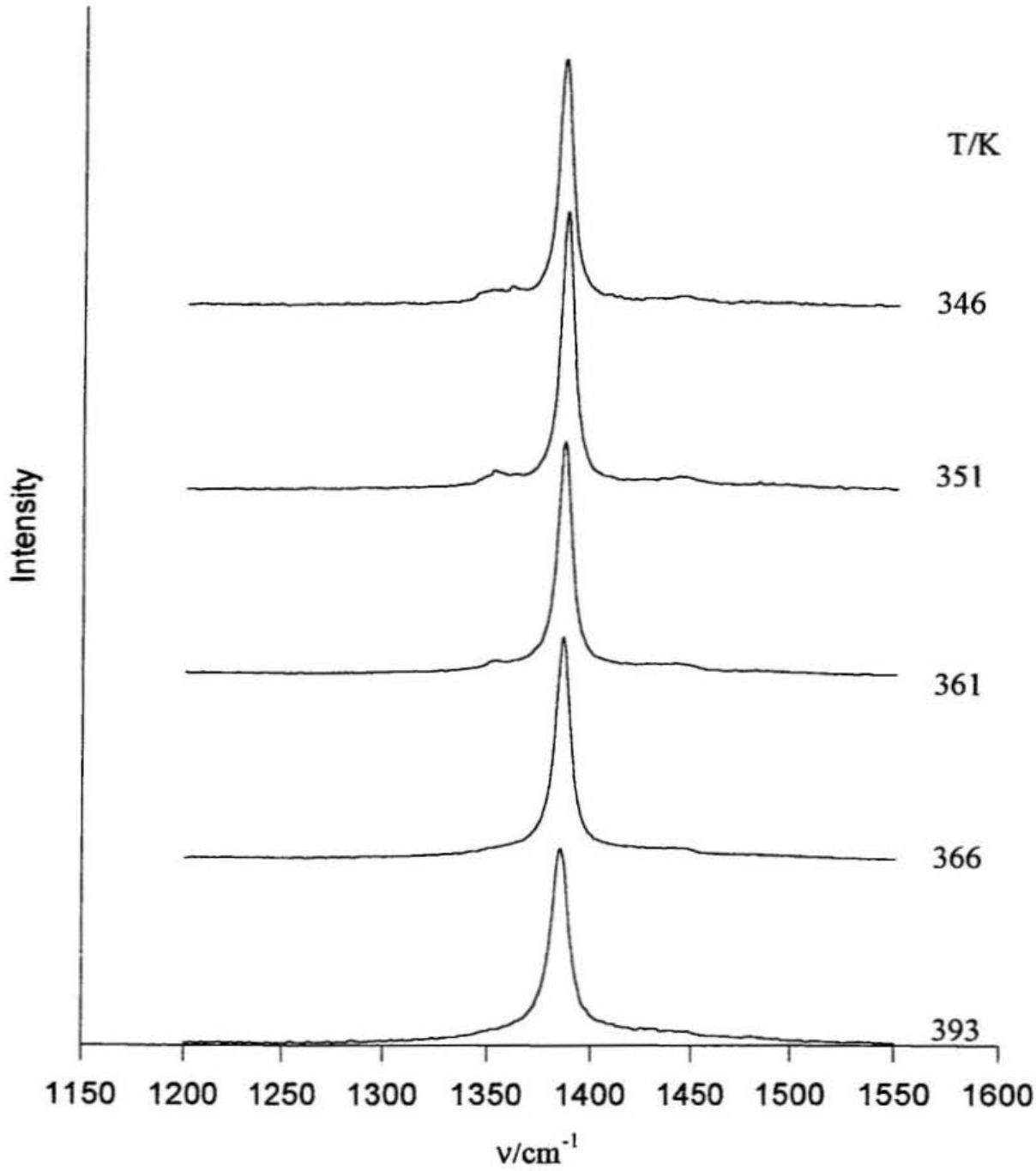

Fig. 6.14 Raman spectra in the ν_3 region of $Na_{0.80}K_{0.20}NO_3$ at different temperatures.

CHAPTER 7

RAMAN SPECTROSCOPIC STUDIES OF THE STRUCTURE AND COMPOSITION OF THE COMPOUNDS $MLi(NO_3)_2$ (M = K, Rb, Cs) FORMED FROM THE MELTS

7.1 Introduction

Systems of binary alkali metal nitrates have been much investigated. Phase diagrams for all possible combinations of binary nitrates have been constructed, checked and rechecked because of the ease with which the low melting point nitrates can be handled. The general features of the binary systems are well established and the dependence of the mixed crystals on the nature of alkali metals has been summarized [43]. As the size difference of the two cations gradually increases, the phase diagrams get successively more complicated, from solid solutions and eutectic mixtures to incongruently and congruently melting compounds.

For the series of lithium nitrate with the other alkali metal nitrates, $LiNO_3$-$NaNO_3$ and $LiNO_3$-KNO_3 are usually regarded as eutectic systems [43,109], although a discontinuity at $x(Li^+)$ = 0.45 in the liquidus was observed in the phase diagram of $LiNO_3$-KNO_3 by some early researchers [129,130]. It was tentatively attributed to an intermediate compound with an incongruently melting point. This observation seems to have been neglected by current investigators [1,131]. No further studies have been attempted to explore the origin of the

discontinuity.

The size difference between the cations in $LiNO_3$-$RbNO_3$ is sufficiently large to permit formation of the congruently melting compound $RbLi(NO_3)_2$ [43,109]. The compound forms solid solutions or eutectics with the end components. There seems to be little debate about the phase diagram $LiNO_3$-$RbNO_3$. For $LiNO_3$-$CsNO_3$ the early investigations [109] indicated eutectic or solid solution formation but these suggestions were questioned [43] since the congruently melting compound had already been observed for $LiNO_3$-$RbNO_3$. Bolshakov and co-workers [43] reinvestigated the binary nitrates and a congruently melting compound $CsLi(NO_3)_2$ was detected at 467 K. The existence of the compound was confirmed by other authors [44,45].

The binary systems have been investigated primarily by thermal analysis. They have not been studied by Raman spectroscopy. Compared with thermal methods, the Raman technique has two advantages. Firstly, thermal analysis is a dynamic procedure while the Raman technique is usually static. Intermediate entities which can only exist in a very short interval of temperature or which have very small enthalpy changes may occur without being detected by thermal techniques. Such short lived species may be frozen by quenching and then investigated easily by Raman spectroscopy. On the other hand, some processes are so slow that it is impractical for a single run of thermal experiment to detect the effect of an equilibrium transition. Under such circumstances the Raman technique can be used to follow the slow progress of the structural changes in the system.

Secondly, Raman features are directly related to the microscopic structure of the system. The nitrate ion is a good Raman scatterer and is sensitive to its environment. The vibrational

spectra of the nitrate group and the variation of the bands with changing environments have been well established for crystalline states, aqueous solutions, matrix isolated ion pairs or melts [20,55,70,71,132]. The nitrate ion can thus serve as a probe of the structure in a binary nitrate system. The three components of the symmetric stretching vibration of the nitrate ion have been used to confirm the existence of the three distinct C_1 sites of the anion in the crystal $RbNO_3$ and $CsNO_3$ [58]. The energy of the ν_1 mode is sensitive to the perturbing force fields and the frequency shift of this band may be a useful indication of changes in the environments of nitrate ions [7a,11]. Coordination of cations to the nitrate group may lower the symmetry of the nitrate ion and thus lift the degeneracy of the ν_3 vibration. The frequency difference and the relative intensity of the component bands give information about the coordination state of the nitrate ions [133]. Raman spectra in the low frequency region can be easily obtained. Bands of the lattice vibrations also provide additional information for structural evaluation.

In this work Raman spectroscopy has been applied to study the systems of $LiNO_3$-KNO_3, $LiNO_3$-$RbNO_3$ and $LiNO_3$-$CsNO_3$. Special attention has been paid to the possible existence of the compound $KLi(NO_3)_2$ in the $LiNO_3$-KNO_3 system and an alternative explanation for the small discontinuity on the solidus is offered. Raman spectra of the congruently melting compounds $RbLi(NO_3)_2$ and $CsLi(NO_3)_2$ have been measured and a tentative structure is deduced for the compounds.

7.2 Raman Spectra of the Solids from the Melts

Three samples were prepared for each system so that comparison may be made and the

Raman bands for every entity in the specimen may be distinguished. The molar ratios of the mixed $LiNO_3$-MNO_3 (M = K, Rb, Cs) were 2:1, 1:1 and 1:2 (hereafter these ratios always represent lithium nitrate to the other nitrates).

7.2.1 Raman Spectra of $LiNO_3$-KNO_3

The Raman spectra of $LiNO_3$-KNO_3 were most variable because the system has a unique phase diagram and because KNO_3 III can be preserved in a metastable state at room temperature if the conditions are not favourable for equilibrium transition of phase III to II of potassium nitrate. Different preparations of the same sample gave different Raman spectra.

Naturally cooled samples were prepared from the melts by just turning off the oven to permit the samples to crystallize in a manner that would be similar to the calorimetric studies. Samples cooled naturally outside the oven gave similar Raman bands (Table 7.1). The bands were classified into two sets, the intensities of which varied as the relative amount of each of the nitrates varied (Figs. 7.1 and 7.2). In fact these bands were found to be the characteristic Raman bands of $LiNO_3$ and KNO_3 III respectively.

In the external vibrational region the most distinct features are the strong band at 125 cm^{-1} and a very strong band at 238 cm^{-1} (Fig. 7.1). The former is the characteristic band for libration of the nitrate ion in KNO_3 III and the latter is due to the rotatory motion of the nitrate ion in $LiNO_3$. The translatory motion of the nitrate ion in $LiNO_3$ also produces a medium band at 123 cm^{-1} which is overlapped by the strong and broad band of KNO_3 III in the vicinity. The variation of the intensities of the bands at 125 and 238 cm^{-1} agrees roughly

with the variation of the ratio between the two types of nitrate. The positions of the two bands remain constant for different compositions. (Table 7.1).

In the internal vibrational region the two sets of bands for the two nitrates separate from one other distinctly and it is easy to assign each band (Fig. 7.2). The crystal structure of lithium nitrate belongs to the space group $R\bar{3}c$ and the nitrate group occupies the D_3 site. No band splitting is expected and there are three Raman active fundamental bands in the internal vibrational region. In addition, the overtone $2\nu_2$ appears in the Raman spectrum. The bands at 1072, 1386, 737 and 1676 cm^{-1} are in good agreement with the ν_1, ν_3, ν_4 and $2\nu_2$ bands in pure lithium nitrate [134]. The other bands give excellent agreement with those of KNO_3 III of the R3m structure [55]. The bands at 719 and 1055 cm^{-1} are due to the ν_4 and ν_1 vibrations of the nitrate ion in KNO_3 III. A weak band at 1665 cm^{-1} in the $2\nu_2$ region indicates that potassium nitrate in the sample is not in phase II and the well separated TO-LO Raman features in the ν_3 region confirm the presence of phase III [102]. The profile is also the same as phase III: a sharp and strong ν_3 (E) TO component at 1351 cm^{-1} and the broad and weaker ν_3 (E) LO component at 1442 cm^{-1} along with $2\nu_4$ at 1431 cm^{-1}.

Phase III of potassium nitrate was metastable at room temperature and it was converted to phase II by reheating the samples at 333 K for 24 hours. The spectrum changed dramatically (Fig. 7.3). Careful examination of the spectra revealed that the change was caused by structural changes in potassium nitrate alone because the characteristic Raman bands of lithium nitrate remain unaltered by reheating (Table 7.1). In the external vibrational region the translatory motion of K^+ sublattice against NO_3^- sublattice at 52 cm^{-1} and the rotatory motions of the nitrate group at 85 cm^{-1} in KNO_3 II replaced the libration of the

nitrate ion in KNO_3 III at 125 cm^{-1}. There is a medium band at 125 cm^{-1}. It is due to the translatory motion of the nitrate ions in $LiNO_3$ and KNO_3 II [55].

In the internal vibrational region the characteristic Raman bands of KNO_3 III were also completely replaced by the bands due to KNO_3 II (Fig. 7.4). The ν_1 and ν_4 vibrations of the nitrate ion (at 717 and 1052 cm^{-1} respectively) shifted to lower wavenumbers because of the transition of phase III to II of potassium nitrate. The unique TO-LO splitting of ν_3 in KNO_3 III disappeared and the doublet feature of ν_3 in KNO_3 II appeared at 1346 and 1361 cm^{-1}. Only one band due to $LiNO_3$ at 1676 cm^{-1} was detected in this region because the broad $2\nu_2$ feature of KNO_3 II was too weak to be detected.

The Raman studies of $LiNO_3$-KNO_3 indicated that under natural cooling conditions, the two nitrates separated on crystallization. The solids were mechanical mixtures of lithium nitrate and potassium nitrate. No compounds or solid solutions were detected. The characteristic frequencies remain unchanged as the ratio of the two nitrates changed. Potassium nitrate in the mixtures exhibited its unique structural phase transitions. Phase III was preserved at room temperature when the cooling rate was sufficiently fast and it transformed to phase II when reheated. These results are in agreement with the phase diagram studied by thermal analysis [43,109] which showed a eutectic mixture for the system. Samples cooled in the oven experienced an environment similar to that in thermal analysis.

When the molten sample of equimolar $LiNO_3$-KNO_3 was taken out of the oven and quenched to room temperature without any disturbances, the Raman spectrum was entirely different from the spectrum of the same sample cooled inside the oven (Table 7.2).

In the external vibrational region the strong band at 125 cm^{-1} due to KNO_3 III and the

strong band at 238 cm^{-1} due to $LiNO_3$ disappeared almost completely. The predominant features were two new bands at 63 and 106 cm^{-1} on a strong Rayleigh wing (Fig. 7.5). These bands cannot be due to $LiNO_3$ or KNO_3 III.

The frequencies and band profiles of the internal modes of the nitrate ion were also distinctly different from those of $LiNO_3$ and KNO_3 III. Although there were two peaks in the ν_1 and ν_4 regions, the relative intensities were different (Fig. 7.6) and, more important, the frequencies were different. The values of 1046 and 1068 cm^{-1} did not correspond to the ν_1 vibration of the nitrate ion in either $LiNO_3$ (1071 cm^{-1}) or KNO_3 III (1054 cm^{-1}). The two bands at 724 and 739 cm^{-1} were also different from those of KNO_3 III at 718 cm^{-1} and $LiNO_3$ at 736 cm^{-1}.

The most notable differences were observed for the bands in the ν_3 region. The medium intensity band of $LiNO_3$ at 1386 cm^{-1} and the characteristic TO-LO pattern of ν_3 in KNO_3 III were replaced by three bands at 1323, 1424 and 1467 cm^{-1}. The band in the middle was a little weaker than those at both ends. The two bands in the $2\nu_2$ region (1642 and 1660 cm^{-1}) were also different in frequencies and band profiles from those in the mechanical mixture of KNO_3 III and $LiNO_3$ (1664 and 1676 cm^{-1}).

Complete disappearance of the Raman features of the two components implies absence of the separate structures of $LiNO_3$ and KNO_3. The entirely new features in the Raman spectrum of the quenched sample mean that an entirely new structure has been created in the equimolar $LiNO_3$-KNO_3 solid which has been overlooked by thermal analysis. The new structure corresponds to the compound $KLi(NO_3)_2$. The compound was found to be unstable at room temperature. When the sample in the sealed tube was left at the ambient environment

for about a month, the Raman bands associated with the new compound decreased in intensity while the bands due to pure $LiNO_3$ and KNO_3 II appeared. The Raman spectrum of the aged quenched sampled showed the features of a mixture of $LiNO_3$ and KNO_3 II together with the new compound $KLi(NO_3)_2$ (Table 7.2).

In the aged sample the characteristic lattice modes of KNO_3 II at 52 and 85 cm^{-1} and the strong libration band of the nitrate group in $LiNO_3$ at 237 cm^{-1} can be seen along with the two external modes of the new compound $KLi(NO_3)_2$ at 63 and 106 cm^{-1} (Fig. 7.7). Three peaks can be distinguished in the ν_1 region: one at 1046 cm^{-1} due to the new compound, the second one at 1052 cm^{-1} attributed to KNO_3 II, and the third peak at 1069 cm^{-1} due to a combination of the two closely situated bands: 1068 cm^{-1} of $KLi(NO_3)_2$ and 1071 cm^{-1} of $LiNO_3$. The situation is similar in the ν_4 region and similar assignment was made. The 716 cm^{-1} band was assigned to KNO_3 II, the 724 cm^{-1} band to the new compound and the 738 cm^{-1} band to a mixture of the bands at 736 cm^{-1} due to $LiNO_3$ and 739 cm^{-1} due to the new compound. The bands in the ν_3 region clearly indicated that the quenched sample of equimolar $LiNO_3$-KNO_3 was a mixture of the new compound, $LiNO_3$ and KNO_3 II after one month's standing. All the bands characteristic of the three compounds appear separately: 1324, 1426 and 1467 cm^{-1} for the new compound, 1386 cm^{-1} for $LiNO_3$ and 1346 and 1361 cm^{-1} for KNO_3 II. In the $2\nu_2$ region the 1676 cm^{-1} band was assigned to $LiNO_3$ and the double bands at 1645 and 1661 cm^{-1} to the new compound. Raman features due to KNO_3 II were too weak in this region to be detected.

When the sample of the new compound in the sealed tube was heated at 333 K for 24 hours, the compound $KLi(NO_3)_2$ decomposed to the pure components almost completely.

The Raman spectrum was dominated by characteristic bands of $LiNO_3$ and KNO_3 II in both external and internal vibrational regions (Table 7.2). Weak features of the new compound were still detected in the external and ν_3 regions. The small shoulder at 102 cm^{-1} (Fig. 7.7) and the typical three peaks at 1323, 1426 and 1466 cm^{-1} (Fig 7.8) were attributed to residual $KLi(NO_3)_2$.The spectrum was almost the same as the naturally cooled sample after 24 hours at 333 K except for the remaining weak features of the new compound.

It was essential not to disturb the melt when it was cooled. If the sample was shaken violently during the solidification, the Raman spectrum was similar to that for samples cooled naturally in the oven, i.e., $LiNO_3$ and KNO_3 crystallized separately because of the disturbance.

Judged by the stability conditions, it seems more likely that $KLi(NO)_2$ is a congruently melting compound rather than an incongruently melting compound. It can be obtained directly from the melt on fast solidification. It appears to exist only in a narrow temperature region just below the solidus and in a narrow composition range near equimolar $LiNO_3$-KNO_3. Decomposition occurs when the cooling rate is not fast enough, or with mechanical or thermal disturbance. The narrow temperature range of existence partly accounts for the failure to detect the new compound by thermal methods. Attempts have been made to obtain the compound by quenching the 1:2 or 2:1 samples. The non-equimolar samples, even when quenched in liquid nitrogen, produced essentially the same Raman spectra as the naturally cooled samples except for very weak features of the new compound in the external and ν_3 regions. This fact suggests that the eutectic points of the new compound with the end members should be located in the vicinity of the equimolar point of $LiNO_3$ and KNO_3 so that the major end members in the non-equimolar samples was much more than the new

compound. The amount of the new compound in the non-equimolar mixtures was further reduced by the short temperature range of existence.

The composition of the new compound is $KLi(NO_3)_2$. The quenched equimolar sample, when freshly prepared, had the Raman spectrum of the new compound alone and no other features due to separate $LiNO_3$ and KNO_3 were present. When the new compound decomposed, Raman bands due to potassium nitrate and lithium nitrate appeared simultaneously. The relative intensity of the ν_3 vibrations due to $LiNO_3$ and KNO_3 II remained unchanged when the new compound partly decomposed one month later, or nearly completely after reheating at 333 K for 24 hours. In fact it was found that the new compound has the same structure as the congruently melting compounds $RbLi(NO_3)_2$ and $CsLi(NO_3)_2$ (Section 7.3).

Thus, Raman studies indicated that a congruently melting compound $KLi(NO_3)_2$ forms in the $LiNO_3$-KNO_3 system and the discontinuity at $x(Li^+) = 0.45$ in the phase diagram [129,130] may be a eutectic point for the compound and potassium nitrate.

Quenching may be the origin of the new compound. It has been reported [116] that quenching may bring about new metastable crystalline phases. The prototype of the new compound may already exist in the melt of equimolar $LiNO_3$-KNO_3. A neutron diffraction study [36] suggested the lithium ions in molten $LiNO_3$ were tetrahedrally surrounded by four nearest nitrate ions, one oxygen in each nitrate ion facing towards the lithium ion. The coordination number four is different from the nearest oxygen atoms around the lithium ion in the crystal $LiNO_3$ which are six. The estimated Li-O distance was shorter in the melt than in the crystal [36]. In molten KNO_3, the potassium ions experience a different cationic

environment [27]. The interionic interaction is not so strong and the coordination between potassium and nitrate ions is of a random nature. The complex structure of lithium and nitrate ions in the equimolar melt of $LiNO_3$-KNO_3 may have been frozen in by the quenching process to form the new compound.

7.2.2 Raman Spectra of $LiNO_3$-$RbNO_3$ and $LiNO_3$-$CsNO_3$

The main Raman features of the solid $LiNO_3$-$RbNO_3$ mixtures at different mole ratios are summarized in Table 7.3. Raman spectra of pure $LiNO_3$ and $RbNO_3$ IV are also included for comparison.

According to the phase diagram, the solid of equimolar $LiNO_3$-$RbNO_3$ is a congruently melting compound $RbLi(NO_3)_2$. The Raman bands of the equimolar solid were assigned to this compound alone. The most distinct feature in the external vibrational region was a band at 110 cm^{-1} with a shoulder at 63 cm^{-1}. The strong band at 239 cm^{-1} and the medium band at 124 cm^{-1} of the lattice modes of pure $LiNO_3$ were undetectable (Fig. 7.9 (b)). The frequencies of the two bands were almost the same as those of the external vibrations of $RbNO_3$ IV but the band profiles were quite different. The bands in the compound $RbLi(NO_3)_2$ were located on a strong Rayleigh wing which extended to 200 cm^{-1}, and thus appeared rather weak. The bands in rubidium nitrate were sharper and much stronger. The 1:2 sample was found to be a mixture of $RbLi(NO_3)_2$ and $RbNO_3$ IV. The medium band at 111 cm^{-1} was obviously a mixture of the weaker 110 cm^{-1} band in $RbLi(NO_3)_2$ and the stronger 111 cm^{-1} band in $RbNO_3$ IV (Fig. 7.9 (c)). The 2:1 sample was found to be a mixture of $RbLi(NO_3)_2$

and $LiNO_3$. The strong band of $LiNO_3$ at 239 cm^{-1} appeared and the 110 cm^{-1} band had the same band profile as in the Raman spectrum of $RbLi(NO_3)_2$ (Fig. 7.9 (a) and (b)).

In the internal vibrational region, doublet features appeared in all the four Raman active vibrations in the spectrum of the compound $RbLi(NO_3)_2$: 722 and 739 cm^{-1} for ν_4, 1047 and 1069 cm^{-1} for ν_1, 1324 and 1463 cm^{-1} between which was a weak and diffuse feature around 1420 cm^{-1} for ν_3, and 1644 and 1659 cm^{-1} for $2\nu_2$ (Fig. 7.10 (b)). The doublets had comparable intensities except for that of the $2\nu_2$ for which the 1644 cm^{-1} band was much weaker.

In the ν_4 region the band at 722 cm^{-1} was assigned to $RbLi(NO_3)_2$ instead of $RbNO_3$ IV which also has a band of the same frequency, because of the absence of the other band of $RbNO_3$ IV at 708 cm^{-1} (Fig. 7.10 (b)). The 1:2 sample contains extra $RbNO_3$ IV and the 710 cm^{-1} band due to $RbNO_3$ IV appeared. Both $RbLi(NO_3)_2$ and $RbNO_3$ contributed to the band at 724 cm^{-1} which was stronger than the bands at 710 and 739 cm^{-1} (Fig. 7.10 (c)). The band at 739 cm^{-1} was not due to $LiNO_3$ because the frequency was a bit higher and the intensity was much less than it should be if it were the band of $LiNO_3$ at 737 cm^{-1}. The 2:1 sample had extra lithium nitrate which made the 738 cm^{-1} band appear much stronger than the band at 712 cm^{-1} (Fig. 7.10 (a)).

In the ν_1 region, the two bands of $RbLi(NO_3)_2$ at 1047 and 1069 cm^{-1} are both due to the new compound and cannot be attributed to the ν_1 vibration of NO_3^- in $LiNO_3$ and $RbNO_3$ IV because they are distinctly lower than the corresponding bands in the two pure nitrates. These two bands coexist with the ν_1 band of the extra nitrate in the Raman spectra of the non-equimolar mixtures. The 1059 cm^{-1} band in the Raman spectrum of the 1:2 sample was

assigned to $RbNO_3$ IV (Fig. 7.10 (c)). The ν_1 band of $LiNO_3$ in the 2:1 sample combined with the 1069 cm^{-1} band of $RbLi(NO_3)_2$, to make it much stronger than the other band of $RbLi(NO_3)_2$ at 1047 cm^{-1} (Fig. 7.10 (a)).

In the ν_3 region the separation of the two bands in the spectrum of $RbLi(NO_3)_2$ was as large as 139 cm^{-1}, while the largest separation among the alkali metal nitrates was less than 100 cm^{-1} observed in the Raman spectra of $RbNO_3$ IV, $CsNO_3$ II or KNO_3 III. The 1:2 sample contains $RbLi(NO_3)_2$ and $RbNO_3$ IV, and the two bands due to the former were much stronger and sharper than those due to the latter (Fig. 7.10 (c)). In the Raman spectrum of the 2:1 sample the two bands due to $RbLi(NO_3)_2$ had an intensity comparable to that of the band at 1386 cm^{-1} due to $LiNO_3$ (Fig. 7.10 (a)).

In summary, the congruently melting compound $RbLi(NO_3)_2$ has Raman bands quite different from those of $LiNO_3$ and $RbNO_3$ IV. These Raman bands coexist with bands due to $LiNO_3$ or $RbNO_3$ IV in the spectra of the non-equimolar samples, indicating eutectic mixtures of $RbLi(NO_3)_2$ and $LiNO_3$ or $RbNO_3$ IV.

The important Raman features of $LiNO_3$-$CsNO_3$ at different ratios are summarized in Table 7.4. Cesium nitrate and rubidium nitrate have the same crystal structure at room temperature and they have very similar Raman spectra. The mixed crystals of $LiNO_3$- $CsNO_3$ and $LiNO_3$-$RbNO_3$ with the same ratios also have very similar Raman spectra.

The equimolar sample of $LiNO_3$-$CsNO_3$ has the Raman bands due to the congruently melting compound $CsLi(NO_3)_2$ alone. There was a band at 108 cm^{-1} and a shoulder at about 66 cm^{-1} in the external vibrational region located on a strong Rayleigh wing extending to 200 cm^{-1}. Doublet bands with comparable intensities appeared in the four internal vibrational

regions of the nitrate ion: 718 and 738 cm^{-1} for ν_4, 1047 and 1068 cm^{-1} for ν_1, 1324 and 1454 cm^{-1} between which was a weak and broad feature around 1420 cm^{-1} for ν_3, 1644 and 1657 cm^{-1} for $2\nu_2$. The band with higher frequency in the ν_4 region had a flat top and a small peak at 727 cm^{-1}.

The Raman bands due to $CsLi(NO_3)_2$ coexisted with bands due to $LiNO_3$ or $CsNO_3$ II in the Raman spectra of the non-equimolar samples, just as in the case of $LiNO_3$-$RbNO_3$. This is in agreement with the phase diagram [43] that $LiNO_3$-$CsNO_3$ has a congruently melting compound $CsLi(NO_3)_2$ which forms eutectic mixtures with the end members.

7.3 Raman Spectroscopic Studies of the Structure of the Congruently Melting Compounds $MLi(NO_3)_2$ (M = K, Rb, Cs).

Although no crystallographic data are available and there is no information about the coordination state of the nitrate ion in these compounds, some of the structural features may be deduced from their Raman spectra. The main Raman features of the congruently melting compounds $KLi(NO_3)_2$, $RbLi(NO_3)_2$ and $CsLi(NO_3)_2$ are summarized in Table 7.5. The three compounds have strikingly similar Raman spectra in the external and internal vibrational regions. In the external vibrational region the most distinct features are a band at about 108 cm^{-1} and a shoulder at about 63 cm^{-1} which are on a strong Rayleigh wing extending to 200 cm^{-1} (Fig. 7.11).

The spectral patterns in the internal vibrational region for the three compounds are similar and manifest regular changes (Fig. 7.12). The two ν_1 bands have practically the same

frequencies, at 1047 and 1068 cm^{-1}, and their relative intensity changes a little from $KLi(NO_3)_2$ to $CsLi(NO_3)_2$. The profile in the ν_3 region is unique among nitrate salts. There are two relatively strong bands at both ends between which are weak and diffuse features. The band at 1324 cm^{-1} remains unchanged and the band at about 1460 cm^{-1} shifts to lower frequency as the large cation changes from potassium to cesium. The band at about 1425 cm^{-1} is much stronger in $KLi(NO_3)_2$ and becomes barely detectable in $CsLi(NO_3)_2$. The bands in the ν_4 region seem also to shift to lower frequencies while the bands in the $2\nu_2$ region shift to higher frequencies.

Another notable feature about the Raman spectra of the compounds is the broadness of the bands. Although the two ν_1 bands are separated more in the compound $KLi(NO_3)_2$ (22 cm^{-1}) than the two bands in the eutectic mixture of $LiNO_3$ and KNO_3 (17 cm^{-1}), the former overlaps more than the latter (Fig. 7.6). The ν_1 vibration of the naturally abundant $N^{18}O^{16}O_2^-$ stands distinctly about 20 cm^{-1} lower than the $N^{16}O_3^-$ counterpart in the eutectic mixture while it cannot be distinguished in the compound. In the ν_4 region the two bands of the compound also appear broader than the two bands in the eutectic mixture (Fig. 7.6).

The similar Raman spectra suggest a similar environment for the nitrate ions in the compounds $KLi(NO_3)_2$, $RbLi(NO_3)_2$ and $CsLi(NO_3)_2$. The frequency of the ν_1 vibration is most sensitive to the disturbance of the external field. The doublet nature of ν_1 band with practically same frequencies implies the practically same disturbance in the compounds containing potassium, rubidium or cesium ions. The band profile in the ν_3 region is another sensitive indicator for the structural changes in nitrates. The similar pattern in the ν_3 region indicates that the changes around the nitrate ions due to the existence of potassium, rubidium

or cesium ions are minor. The external modes are directly related to the lattice of the crystal. The identical band profile in the external vibrational region suggests the same crystal structure. Thus, Raman studies indicate that the three congruently melting compounds $KLi(NO_3)_2$, $RbLi(NO_3)_2$ and $CsLi(NO_3)_2$ have the same crystal structure and the nitrate ions have the same environment. The environment about the nitrate ion seems most sensitive to lithium ions alone since the other cations have little effect. There could be a complex of lithium and nitrate ions while the other cations primarily act as counterions to make the compounds electrically neutral. The counterions cause the internal vibrations of the nitrate ion in the complexes to change gradually. The Raman spectrum of $KLi(NO_3)_2$ appears a bit different form those of $RbLi(NO_3)_2$ and $CsLi(NO_3)_2$ partly because it is metastable.

A detailed analysis of the Raman spectra should reveal some important features about the structure of the postulated complex between lithium and nitrate ions. In the ν_1 region there are two strong bands about 22 cm^{-1} apart and with comparable intensities. Two mechanisms may account for the multi-band feature of the non-degenerate symmetrical stretching vibration of the nitrate ion: correlation splitting and multi-site splitting. It is not likely that the former can account for the two peaks because the correlation splitting for the ν_1 vibration of alkali metal nitrates is usually small (less than 7 cm^{-1}) and the intensities of the correlation field components differ greatly [135]. The two peaks must correspond to the nitrate ions on two distinct lattice sites with different potential energy environments perhaps as for a complex of lithium and nitrate ions.

There is a theory [136] which attributes the variation in energy of the symmetrical stretching of the nitrate ion to environmental perturbation on the ion. Symmetric perturbation

will cause the vibration to shift to higher energy, while an asymmetrical one will cause a shift to lower energy. In the crystal of $LiNO_3$, the nitrate ions are in an average potential field of the lithium ions compared to that in the compounds. The ν_1 band in pure $LiNO_3$ (1072 cm^{-1}) shifts to lower frequency in the compounds $MLi(NO_3)_2$ (1047 and 1068 cm^{-1}) because coordination of $Li\text{-}ONO_2$ in the complexes causes the nitrate ions to be under a less symmetrical field. The nitrate group may act as unidentate or bidentate ligands in the complex. The unidentate nitrate ion usually experiences a more directional polarization than the bidentate ion does. The band at 1047 cm^{-1} may be due to the nitrate ions at unidentate position and the 1068 cm^{-1} band may be due to bidentate nitrate ions.

The suggestion of unidentate and bidentate nitrate ions is supported by work on magnesium nitrate [133]. A 21 cm^{-1} difference has been noted between the ν_1 vibrations of the nitrate ion in $Mg(NO_3)_2 \cdot 4H_2O$ which contained unidentate coordinated nitrate ions and $Mg(NO_3)_2 \cdot 2H_2O$ which contained bidentate coordinated nitrate ions. The Raman spectrum of $Mg(NO_3)_2 \cdot 2.9H_2O$ in which there would be nearly equimolar unidentate and bidentate nitrate ions has a doublet structure very similar to $MLi(NO_3)_2$ in the ν_1 region: there were two well separated bands of comparable intensities and the band due to the unidentate nitrate ion was 21 cm^{-1} lower than the band due to the bidentate nitrate ion. In the ν_3 region the Raman spectral profile in the congruently melting compounds is also similar to the profile in $Mg(NO_3)_2 \cdot 2.9H_2O$ in which there were multiple Raman features around both ends of a broad profile which was 130 cm^{-1} apart. The observed peaks at 1324, 1425 and 1463 cm^{-1} for $MLi(NO_3)_2$ have their counterparts in the magnesium compound at 1330, 1352, 1453 and 1466 cm^{-1}. The similar chemistry of lithium and magnesium ions follows from the diagonal

rule. The smaller but less charged lithium ion and the larger but more charged magnesium ion would produce a similar cation field for unidentate or bidentate nitrate ion. It is expected that similar Raman features in the internal vibrational region might be observed for a mixture of unidentate and bidentate nitrate ions which are coordinated to a lithium ion or magnesium ion.

The suggestion of unidentate and bidentate nitrate ions in the congruently melting compounds $MLi(NO_3)_2$ is also supported by striking similarity of the Raman spectra of the compound to the spectrum of molten $LiNO_3$ (Table 7.5) with allowance for differences in state and temperature. In the melt, the ν_3 vibration of the nitrate ion split into two peaks because of the strong interaction between lithium and nitrate ions. Analysis of the band contour [137] revealed four bands at 1355, 1380, 1445 and 1480 cm^{-1} respectively. This was the same band profile in the ν_3 region as in the congruently melting compounds. The ν_1 band at 1064 cm^{-1} in the molten $LiNO_3$, which was slightly asymmetric on the low frequency side, was equivalent to the two bands at 1047 and 1068 cm^{-1} in the solid compounds. The 1641 cm^{-1} band in the melt, which was asymmetric on the high frequency side, was similar to the two bands of the compounds at 1644 and 1659 cm^{-1} in the $2\nu_2$ region. In the ν_4 region, two bands of approximately the same frequencies were observed in the Raman spectra of both the crystalline $MLi(NO_3)_2$ and the liquid $LiNO_3$ (Table 7.5). Obviously the nitrate ions had two non-equivalent environments in molten $LiNO_3$ and such a coordinated state remained in the congruently melting compounds stabilized by M^+ cations.

The two non-equivalent environments might be involved with unidentate and bidentate nitrate ions. A vibrational analysis of monovalent metal nitrates [31] has been made, which was based on a contact ion-pair model in which the cations interacted with the oxygen of the

nitrate ion at unidentate site. The calculated force constants of M-ONO_2 interaction were found to be extraordinarily small in the case of lithium nitrate. This was attributed to a bidentate coordination site due to small and highly polarizing lithium ion. Neutron diffraction studies of molten $LiNO_3$ [34,36] suggested that there were strong interactions between lithium ion and oxygen atom of the nitrate ion. Lithium ion was tetrahedrally surrounded by four nearest nitrate ions, each providing one oxygen atom. Since the ratio of Li^+ to NO_3^- is 1:1 in molten $LiNO_3$, each nitrate ion must coordinate to more than one lithium ion. The nitrate ions may act as unidentate or bidentate ligands, when they bridge lithium ions.

In the melts of the congruently melting compounds $MLi(NO_3)_2$, the lithium ions may be also tetrahedrally surrounded by four nearest neighbouring nitrate ions which have two non-equivalent environments. Neutron diffraction studies [34] indicated that the structure of the nitrate ion and the lithium-nitrate ion interaction were the same in an equimolar melt of $LiNO_3$-$RbNO_3$ as in molten $LiNO_3$. The preparation of $KLi(NO_3)_2$ by quenching indicated that the coordination state of the melt could be frozen in the solid. The function of lager K^+, Rb^+ or Cs^+ appears to make it possible for the coordination between lithium and nitrate ions in the melt to be retained in the crystal when the temperature decreased and the congruently melting compound formed. As was noted previously, the compounds $MLi(NO_3)_2$ had broad bands over the whole spectrum and a strong Rayleigh wing. This is typical for a polymeric structure. It seems likely that the nitrate ions remained bridging the lithium ions in the congruently melting compounds.

According to the Raman studies, the congruently melting compounds $MLi(NO_3)_2$ (M = K, Rb, Cs) have the following structural features. In the compounds, lithium and nitrate

ions form complexes and the other cations act as counterions. In the lithium-nitrate complexes, the lithium ions are tetrahedrally surrounded by four nitrate ions which may act as unidentate or bidentate ligands. The nitrate ions bridge the lithium ions to form a polymeric structure. Similar structural features have been determined by single crystal XRD [26] in the crystals $KAg(NO_3)_2$ and $RbAg(NO_3)_2$. The silver and nitrate ions formed a polymeric complex $[Ag_2(NO_3)_4]_n^{2n-}$ (Fig. 1.1) and K^+ or Rb^+ acted as counterions. The compounds $M(Li(NO_3)_2$ (M = K, Rb, Cs) appear to have a structure similar to that of $KAg(NO_3)_2$ and $RbAg(NO_3)_2$. Silver ions in molten $AgNO_3$ were also found [34,36] to have the same tetrahedral coordination structure with the nitrate ions as lithium ions in molten $LiNO_3$. The Raman studies of $KAg(NO_3)_2$ and $RbAg(NO_3)_2$ support the suggestion that $MLi(NO_3)_2$ have a structure similar to the silver compounds (Chapter 8).

7.4 Conclusions

Raman studies suggested that a congruently melting compound $KLi(NO_3)_2$ was formed in the system $LiNO_3$-KNO_3 formerly regarded as a eutectic system. The new compound could only exist in a narrow composition range near the equimolar point and in a short temperature range just below the solidus (Fig. 7.13). Standing at room temperature, $KLi(NO_3)_2$ decomposed gradually into $LiNO_3$ and KNO_3.

Raman studies confirmed the phase diagrams obtained by thermal analysis for $LiNO_3$-$RbNO_3$ and $LiNO_3$-$CsNO_3$. There were congruently melting compounds $RbLi(NO_3)_2$ and $CsLi(NO_3)_2$ which formed eutectic mixtures with the end members.

The congruently melting compounds $KLi(NO_3)_2$, $RbLi(NO_3)_2$ and $CsLi(NO_3)_2$ had very similar Raman spectra in both external and internal vibrational regions, indicating the same crystal structure of the crystals and the same coordination and environment of the nitrate ions. A detailed analysis of the Raman spectra revealed that there were two crystallographically different sites in the crystals. The lithium ions were tetrahedrally coordinated to the nitrate ions to form polymeric complexes in which the nitrate ions acted as unidentate or bidentate ligands.

Table 7.1 Observed wavenumbers for Raman bands of $LiNO_3$-KNO_3 at different mole ratios measured at 298 K.

Li:K	external	ν_4	ν_1	ν_3	$2\nu_2$
A					
2:1	125,238	719,737	1055,1072	1351,1386,1433,1442	1666,1677
1:1	125,238	718,736	1054,1071	1351,1385,1431,1442	1664,1676
1:2	125,238	719,737	1055,1072	1352,1386,1431,1442	1665,1676
B					
2:1	52,85,125,238	717,736	1052,1071	1346,1361,1385	1676
1:1	52,85,125,237	716,736	1052,1071	1346,1360,1385	1676
1:2	52,85,125,238	717,736	1052,1071	1336,1361,1385	1676

A. The samples were cooled naturally in the oven.

B. The A samples were annealed at 333 K for 24 hours.

Table 7.2 Observed wavenumbers for Raman bands of quenched equimolar $LiNO_3$-KNO_3 measured at 298 K.

sample	external	ν_4	ν_1	ν_3	$2\nu_2$
A					
(a)	63,106	724,739	1046,1068	1323,1424,1467	1642,1660
B					
(a)	63,106	724,738 [c]	1047,1069 [c]	1324,1426,1467	1645,1661
(b)	52,85,237	716,738 [c]	1052,1069 [c]	1346,1361,1385	1676
C					
(a)	102			1323,1426,1466	
(b)	52,84,237	716,738	1052,1071	1346,1360,1385	1676

A. The freshly prepared sample.

B. Sample A was allowed to stand at room temperature for a month.

C. Sample A was annealed at 333 K for 24 hours.

a. Raman bands due to the new compound $KLi(NO_3)_2$.

b. Raman bands due the mechanical mixture of $LiNO_3$ and KNO_3 II.

c. Raman bands due to both $LiNO_3$ and the new compound.

Table 7.3 Observed wavenumbers for Raman bands of $LiNO_3$-$RbNO_3$ at different mole ratios measured at 298 K.

Li:Rb		external	ν_4	ν_1	ν_3	$2\nu_2$
0:1	a)	62,111	708,722	1058	1349, ~1400,1437	1675
1:2	a)	111 [d]	710,724 [d]	1059	1348	1677
	b)	111 [d]	724 [d],738	1048,1069	1325,1421,1465	1643,1660
1:1	b)	63,110	722,739	1047,1069	1324,1425,1463	1644,1659
2:1	b)	63,110	721,738 [e]	1048,1072 [e]	1324,1463	1644,1659
	c)	120,239	738 [e]	1072 [e]	1386	1677
1:0	c)	124,239	737	1072	1383	1677

a. Raman bands due to pure $RbNO_3$.

b. Raman bands due to the congruently melting compound $RbLi(NO_3)_2$.

c. Raman bands due to pure $LiNO_3$.

d. Raman bands due to both $RbNO_3$ and $RbLi(NO_3)_2$.

e. Raman bands due to both $LiNO_3$ and $RbLi(NO_3)_2$.

Table 7.4 Observed wavenumbers for Raman bands of $LiNO_3$-$CsNO_3$ at different mole ratios measured at 298 K.

Li:Cs	external	ν_4	ν_1	ν_3	$2\nu_2$
0:1 a)	117	707,718	1053	1348,1398	1669
1:2 a)	117 [d]	708,718 [d]	1053	1343,1399	1670
b)	117 [d]	718 [d],739	1047,1068	1324,1421,1454	1645,1656
1:1 b)	66,108	718,727,738	1047,1068	1324,1429,1456	1646,1657
2:1 b)	66,107	718,727,737 [e]	1047,1072 [e]	1324,1454	1644,1657
c)	120,238	737 [e]	1072 [e]	1386	1677
1:0 c)	124,239	737	1072	1386	1677

a. Raman bands due to pure $CsNO_3$ II.

b. Raman bands due to the congruently melting compound $CsLi(NO_3)_2$.

c. Raman bands due to pure $LiNO_3$.

d. Raman bands due to both $CsNO_3$ II and $CsLi(NO_3)_2$.

e. Raman bands due to both $LiNO_3$ and $CsLi(NO_3)_2$.

Table 7.5 Observed wavenumbers for Raman bands of the congruently melting compounds $MLi(NO_3)_2$ (M = K, Rb, Cs) measured at 298 K and those of molten $LiNO_3$ for comparison.

samples	external	ν_4	ν_1	ν_3	$2\nu_2$
$KLi(NO_3)_2$	63,106	724,739	1046,1068	1323,1424,1467	1642,1660
$RbLi(NO_3)_2$	63,110	722,739	1047,1069	1324,1425,1463	1644,1659
$CsLi(NO_3)_2$	66,108	718,727,738	1047,1068	1324,1429,1456	1646,1657
$LiNO_3$ [a]	145	718,746	1064 [b]	1360,1465 [c]	1641 [d]

a. Data for the melt at 531 K [137].

b. Slightly asymmetric on the low frequency side.

c. Analysis of the band contour revealed four bands: 1355, 1380, 1445 and 1480 cm^{-1}.

d. Slightly asymmetric on the high frequency side.

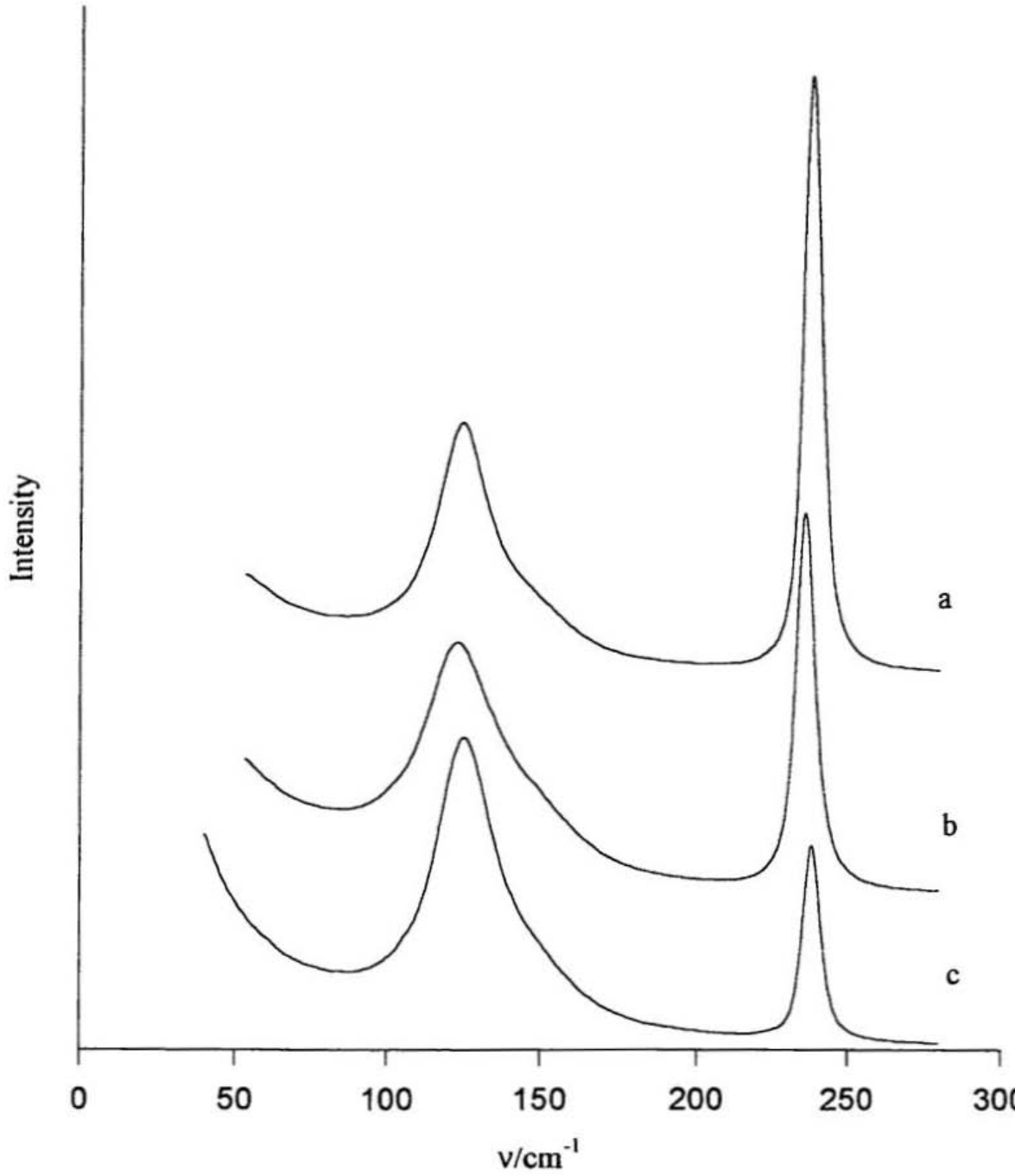

Fig. 7.1 Raman spectra in the external vibrational region of the naturally cooled $LiNO_3$-KNO_3 at 298 K. The mole ratio of $LiNO_3$ to KNO_3 is: (a) 2:1, (b) 1:1, (c) 1:2.

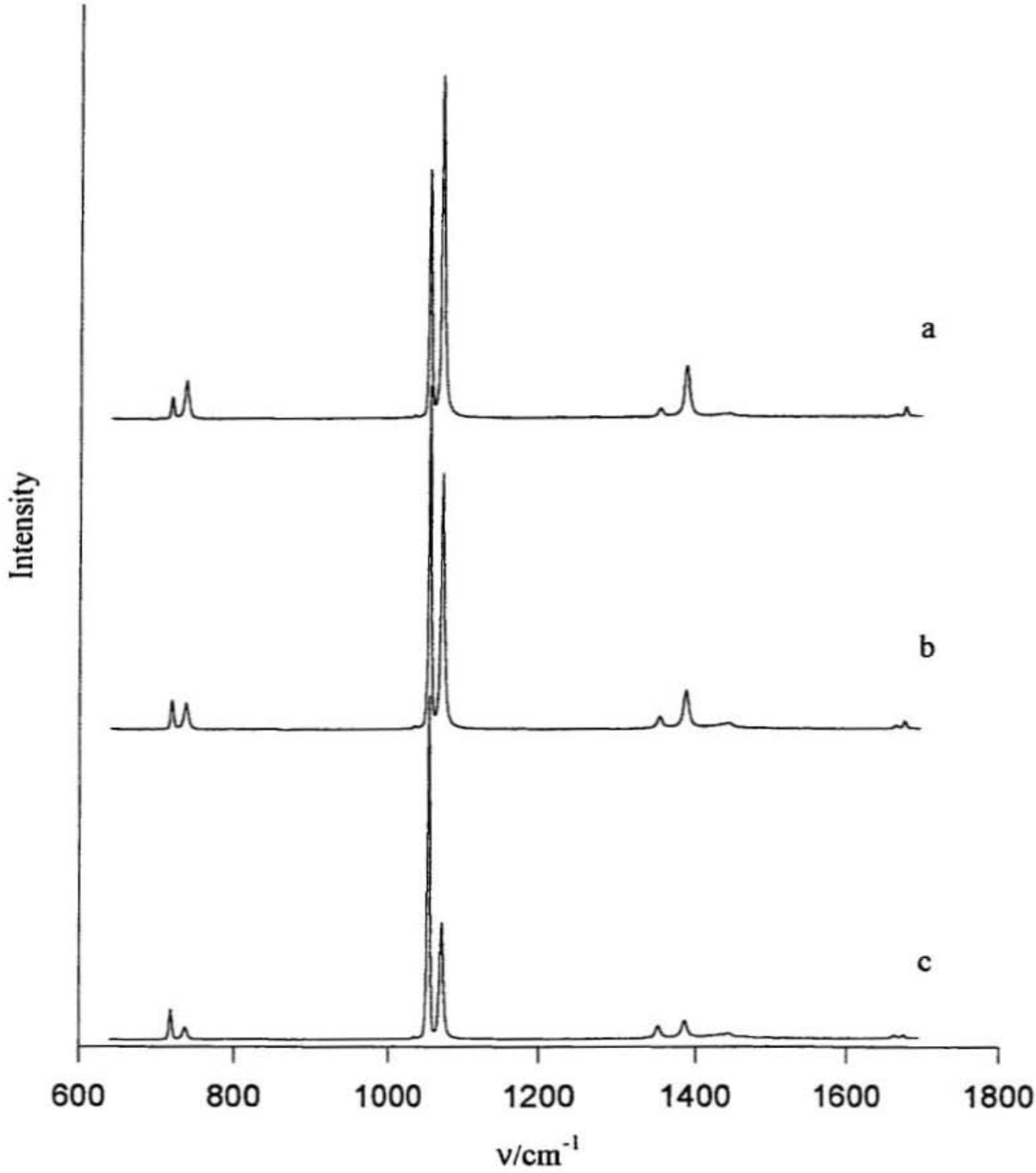

Fig. 7.2 Raman spectra in the internal vibrational region of the naturally cooled $LiNO_3$-KNO_3 at 298 K. The mole ratio of $LiNO_3$ to KNO_3 is: (a) 2:1, (b) 1:1, (c) 1:2.

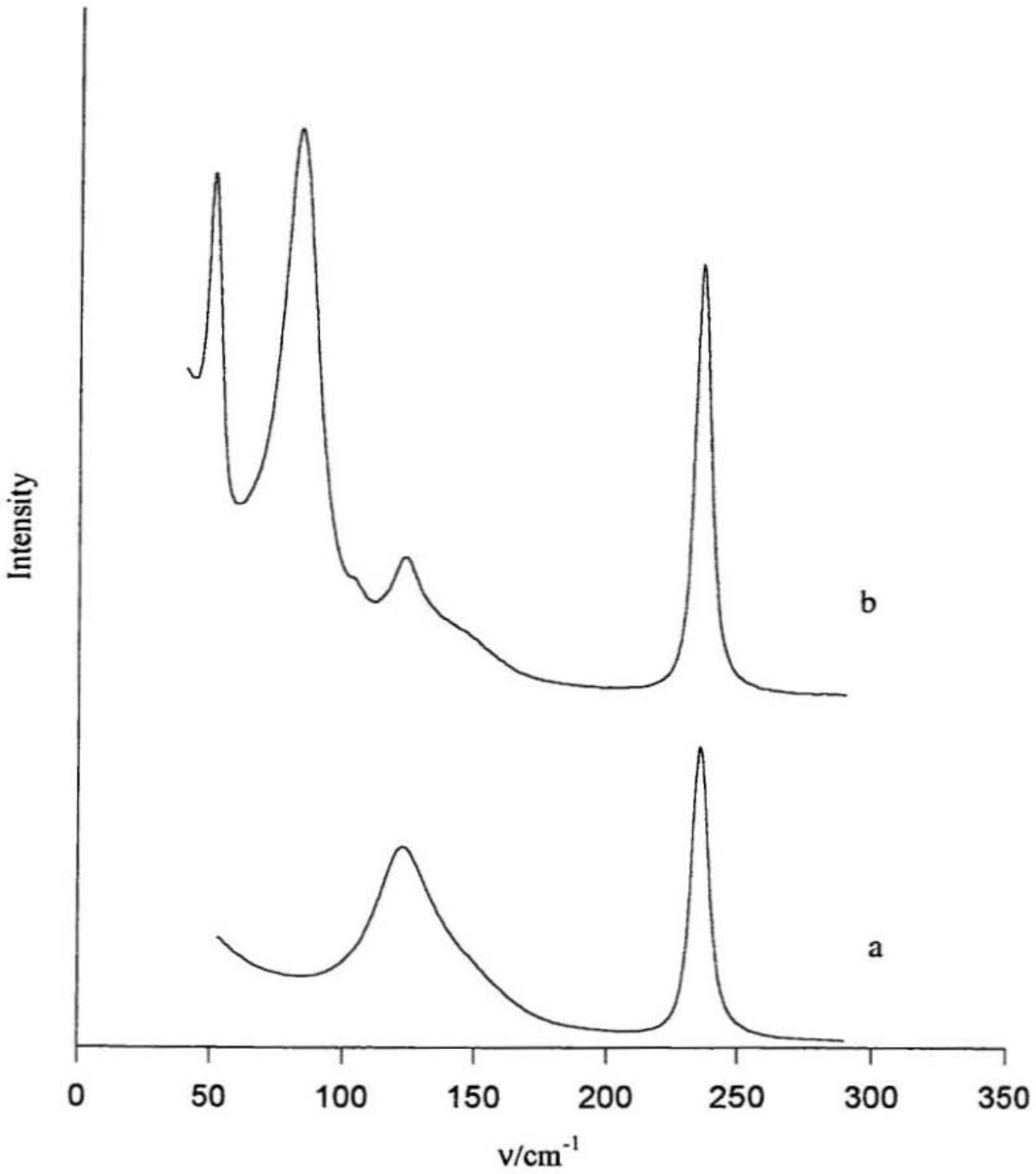

Fig. 7.3 Raman spectra in the external vibrational region of equimolar $LiNO_3$-KNO_3 at 298 K: (a) the naturally cooled sample; (b) the same sample annealed at 333 K for 24 hours.

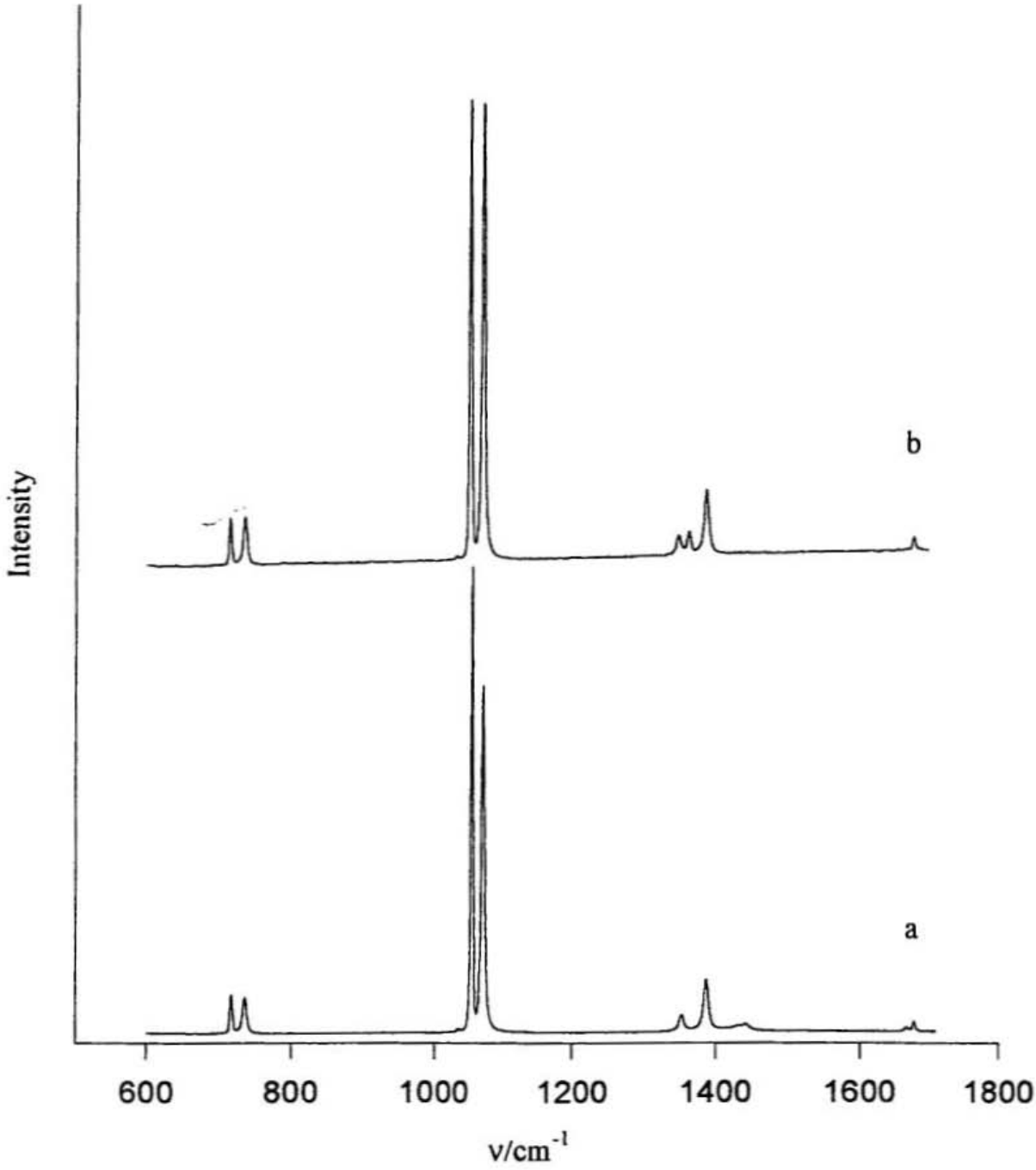

Fig. 7.4 Raman spectra in the internal vibrational region of equimolar $LiNO_3$-KNO_3 at 298 K: (a) the naturally cooled sample; (b) the same sample annealed at 333 K for 24 hours.

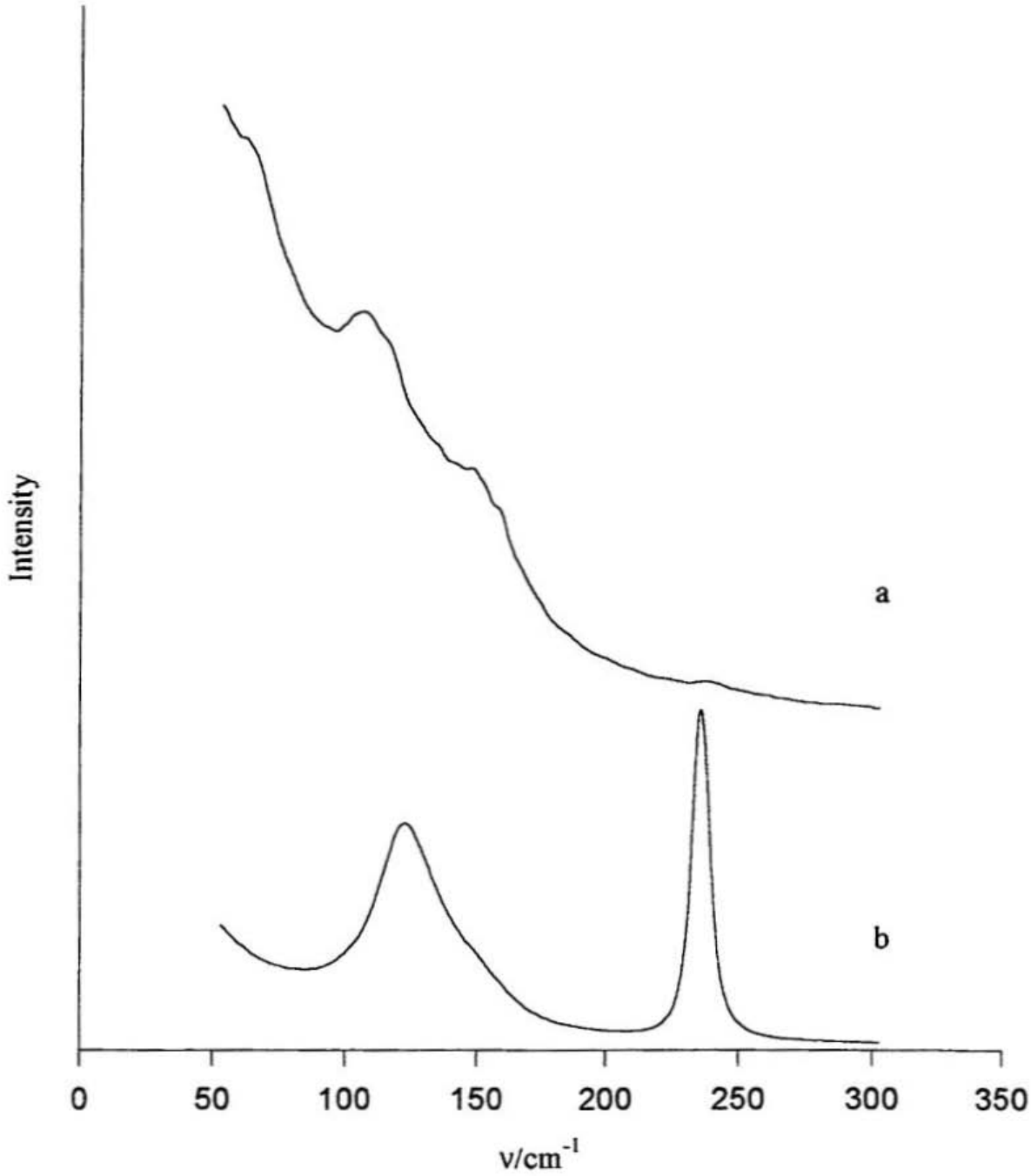

Fig. 7.5 Raman spectra in the external vibrational region of equimolar $LiNO_3$-KNO_3 at 298 K: (a) the quenched sample; (b) the naturally cooled sample.

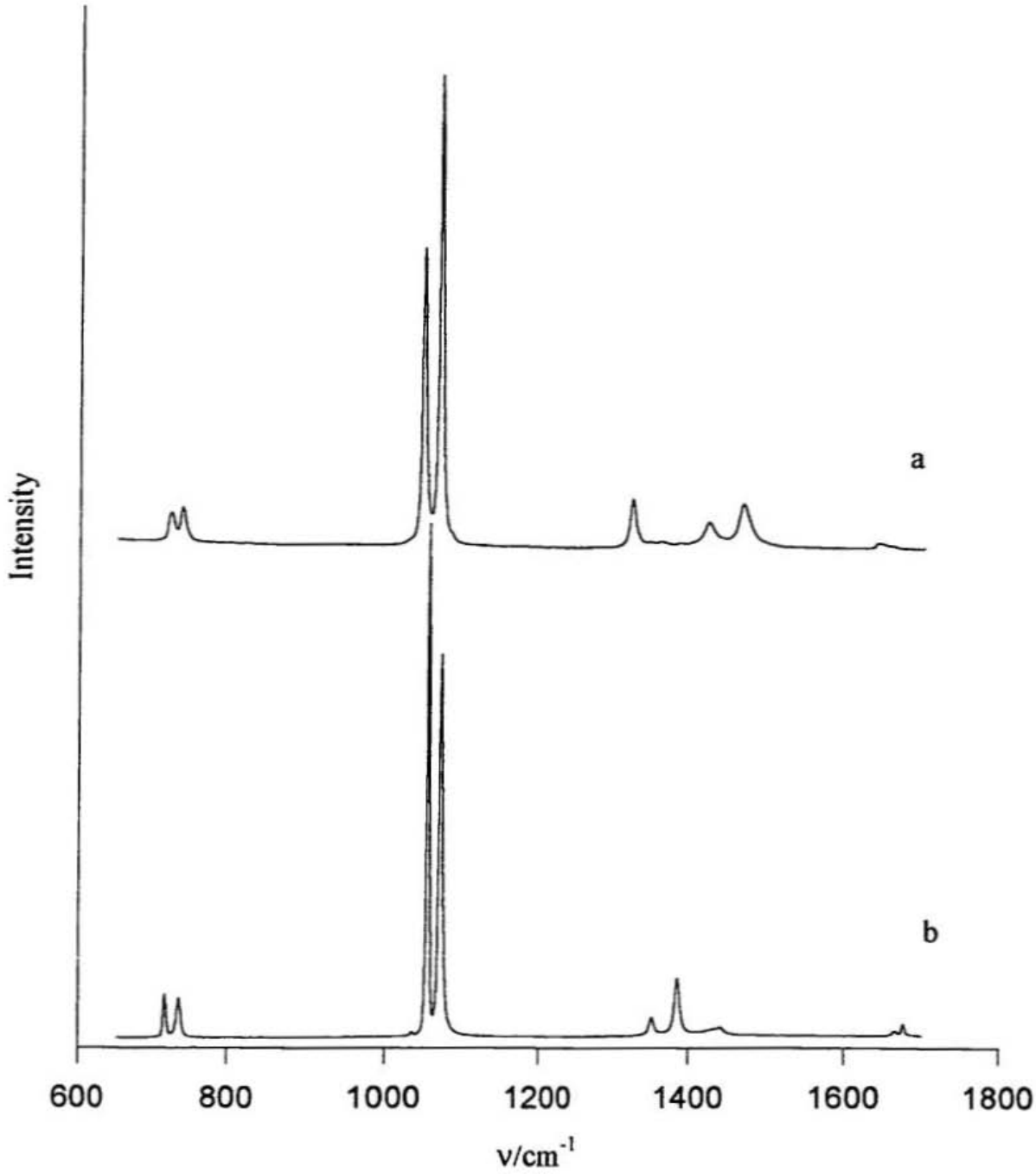

Fig. 7.6 Raman spectra in the internal vibrational region of equimolar $LiNO_3$-KNO_3 at 298 K: (a) the quenched sample, (b) the naturally cooled sample.

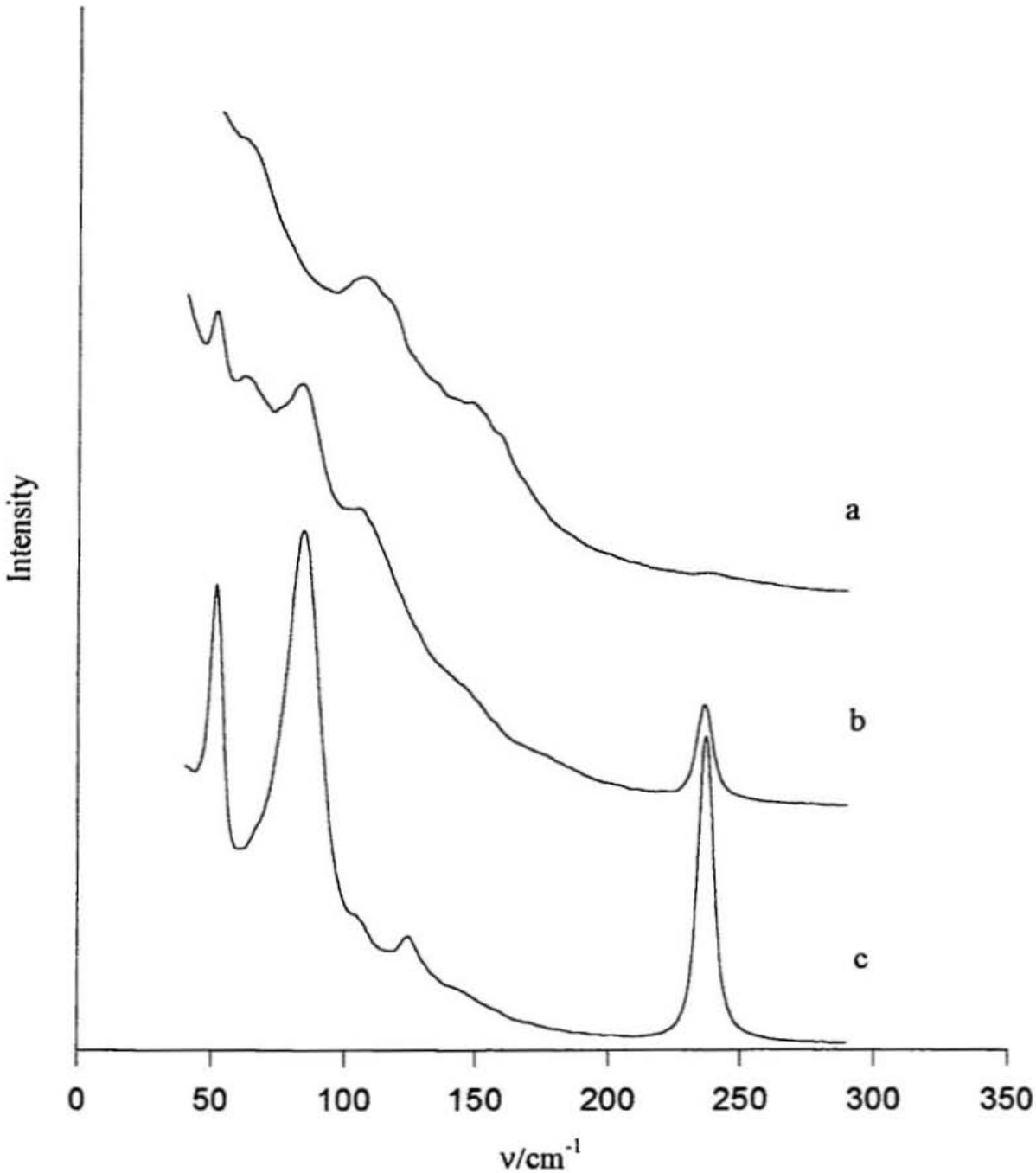

Fig. 7.7 Raman spectra in the external vibrational region of the new compound $KLi(NO_3)_2$ at 298 K: (a) freshly prepared, (b) one month later, (c) annealed at 333 K for 24 hours.

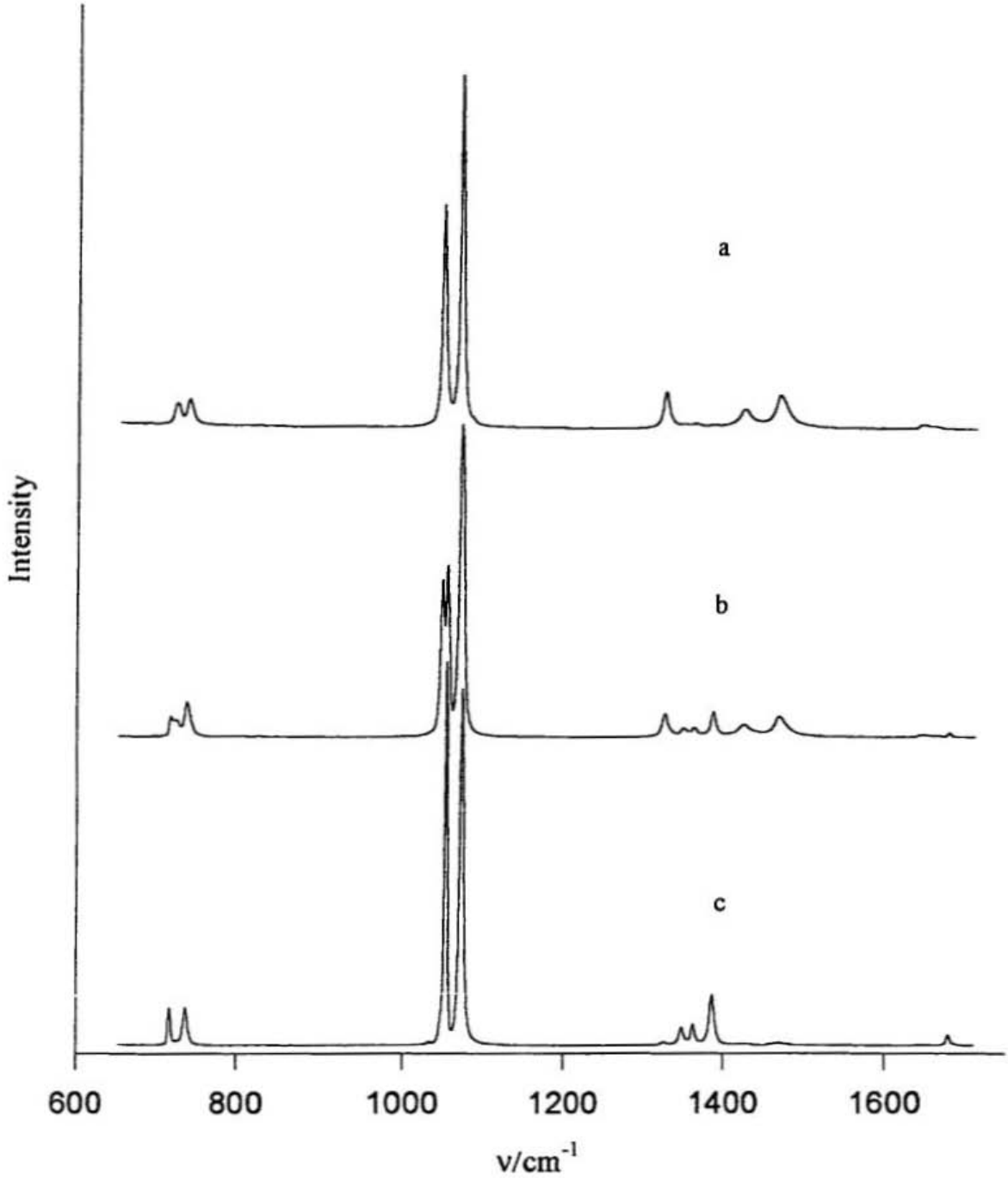

Fig. 7.8 Raman spectra in the internal vibrational region of the new compound $KLi(NO_3)_2$ at 298 K: (a) freshly prepared; (b) one month later; (c) annealed at 333 K for 24 hours.

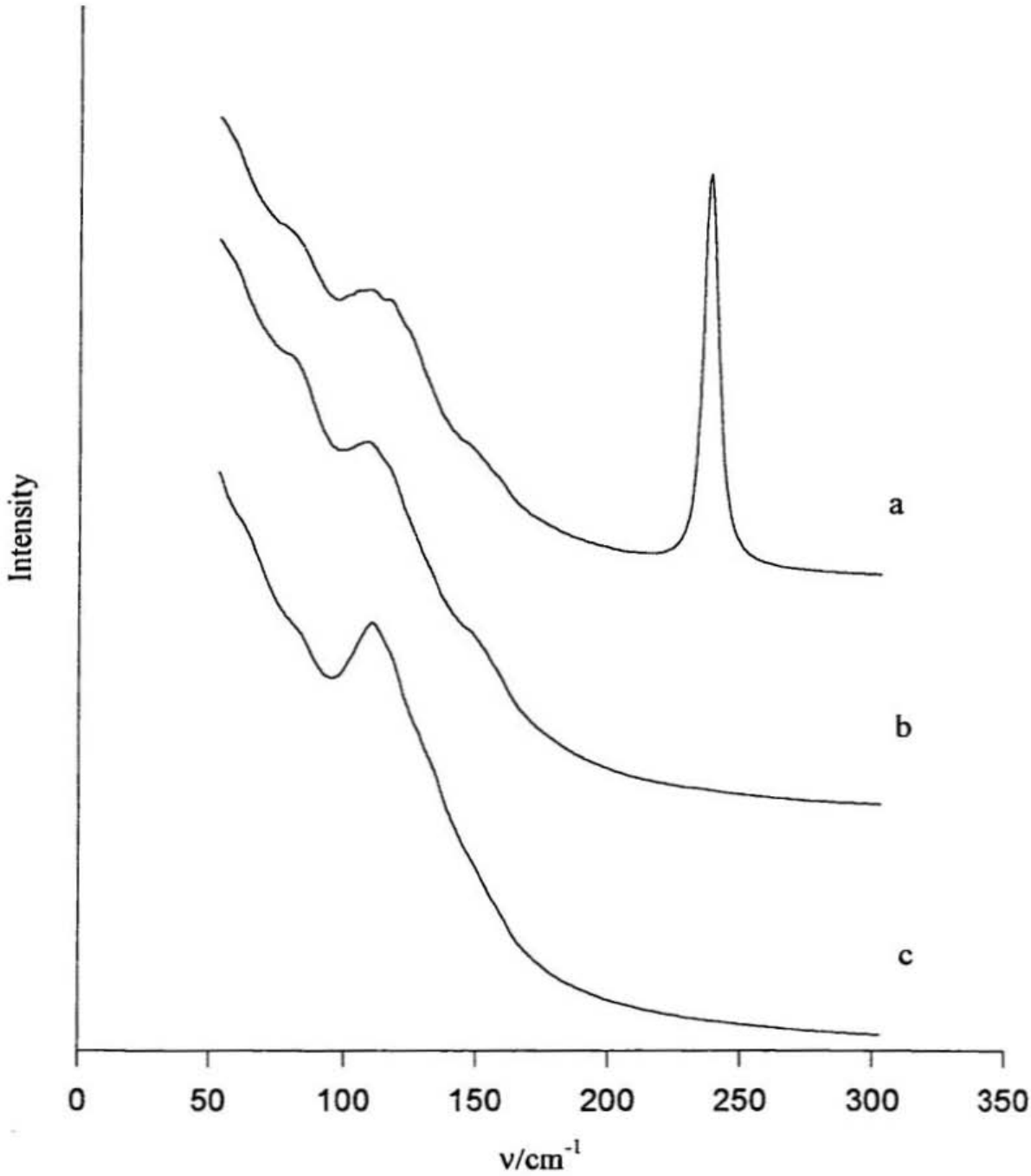

Fig. 7.9 Raman spectra in the external vibrational region of $LiNO_3$-$RbNO_3$ at 298 K. The mole ratio of $LiNO_3$ to $RbNO_3$ is: (a) 2:1, (b) 1:1, (c) 1:2.

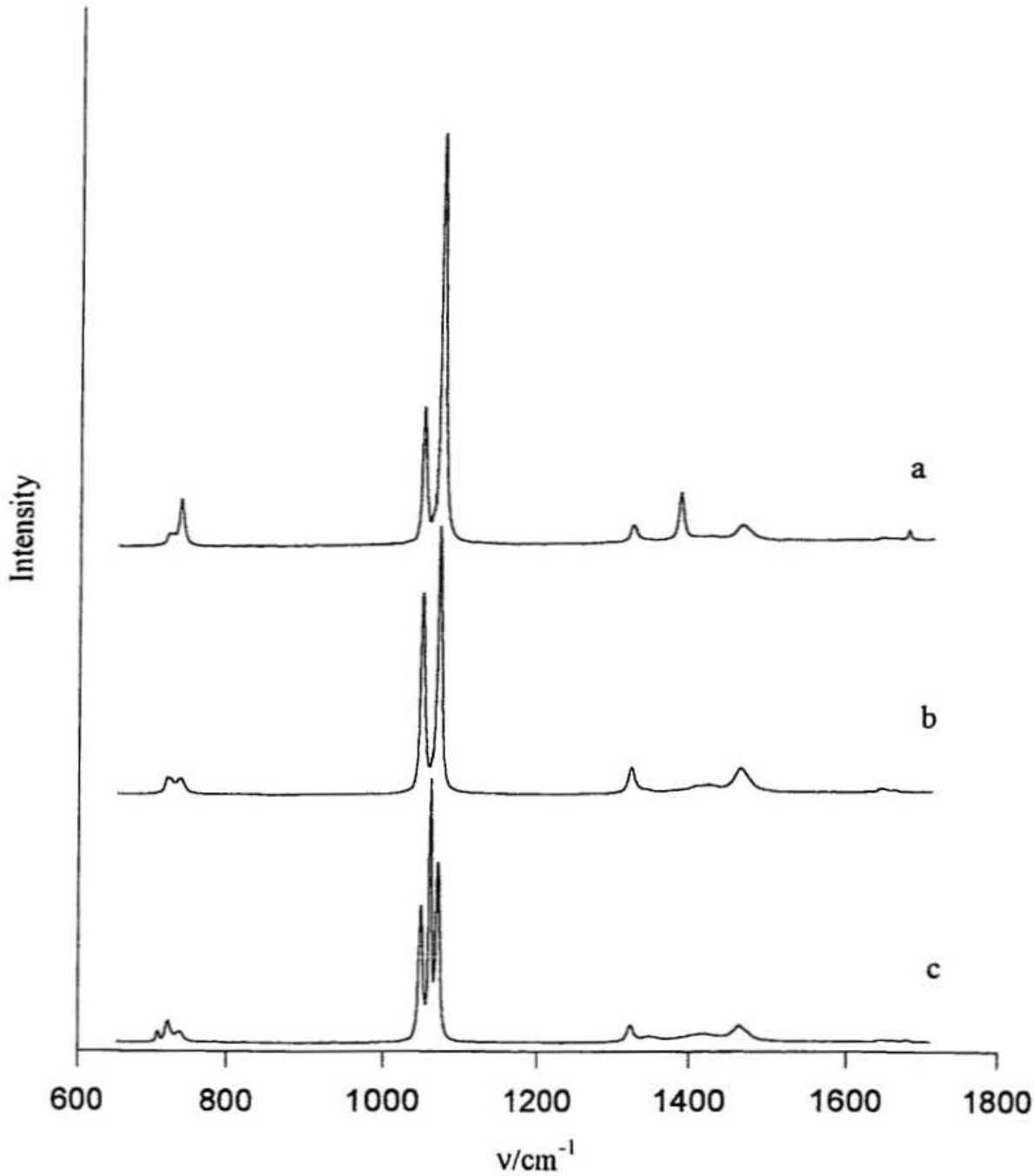

Fig. 7.10 Raman spectra in the internal vibrational region of $LiNO_3$-$RbNO_3$ at 298 K. The mole ratio of $LiNO_3$ to $RbNO_3$ is: (a) 2:1, (b) 1:1, (c) 1:2.

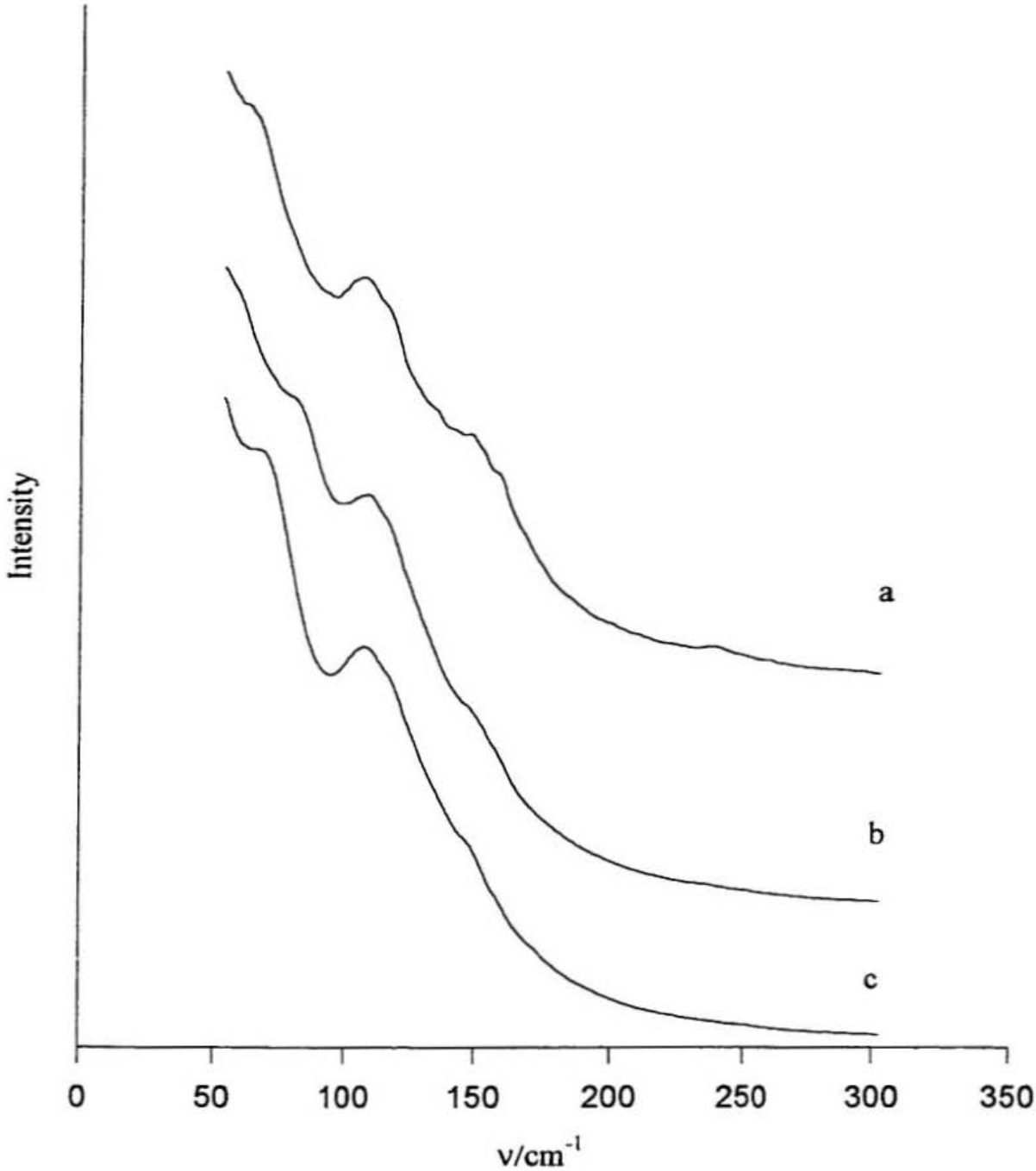

Fig. 7.11 Raman spectra in the external vibrational region of the three compounds at 298 K: (a) $KLi(NO_3)_2$, (b) $RbLi(NO_3)_2$, (c) $CsLi(NO_3)_2$.

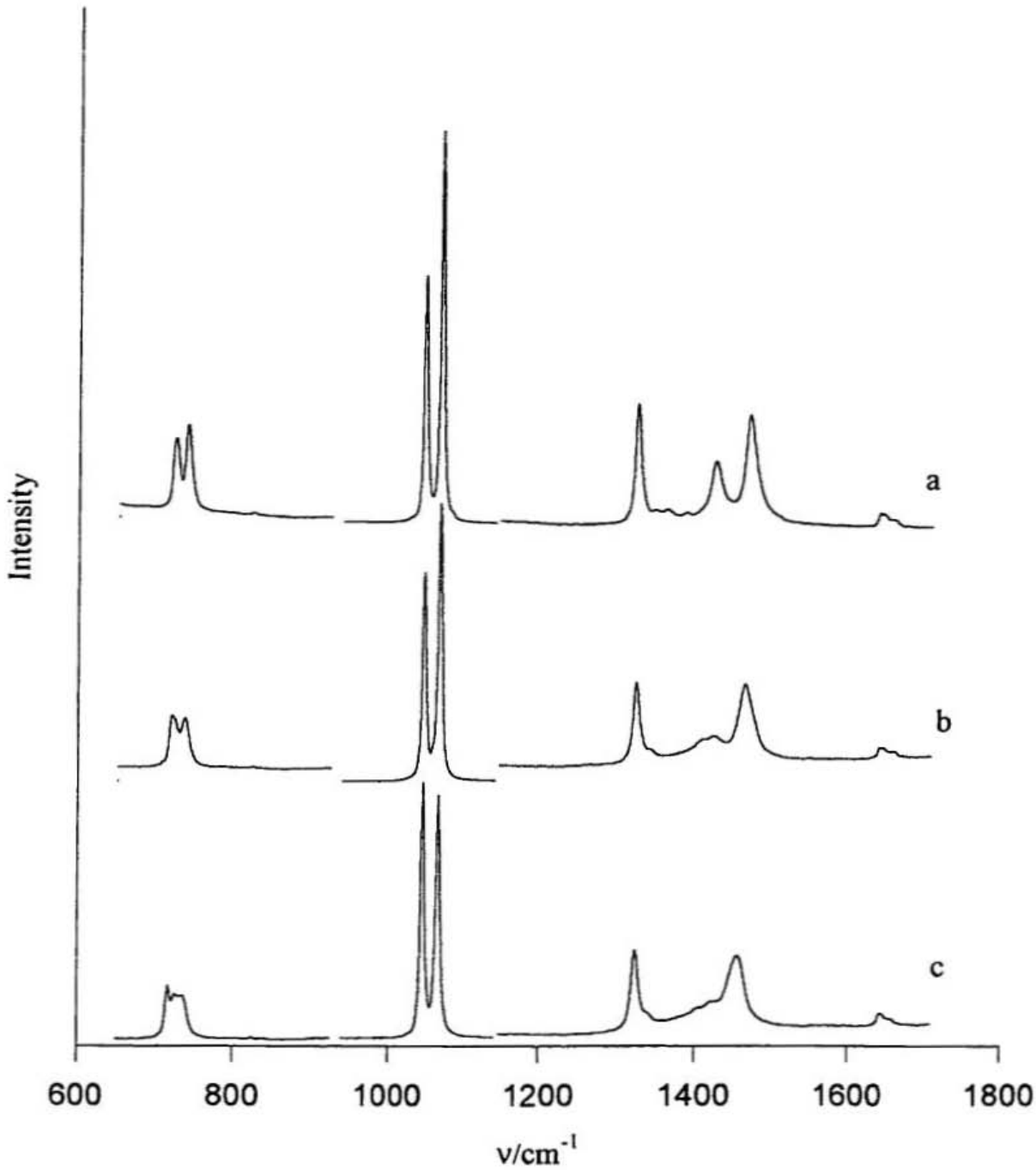

Fig. 7.12 Raman spectra in the internal vibrational region of the three compounds at 298 K: (a) $KLi(NO_3)_2$, (b) $RbLi(NO_3)_2$, (c) $CsLi(NO_3)_2$.

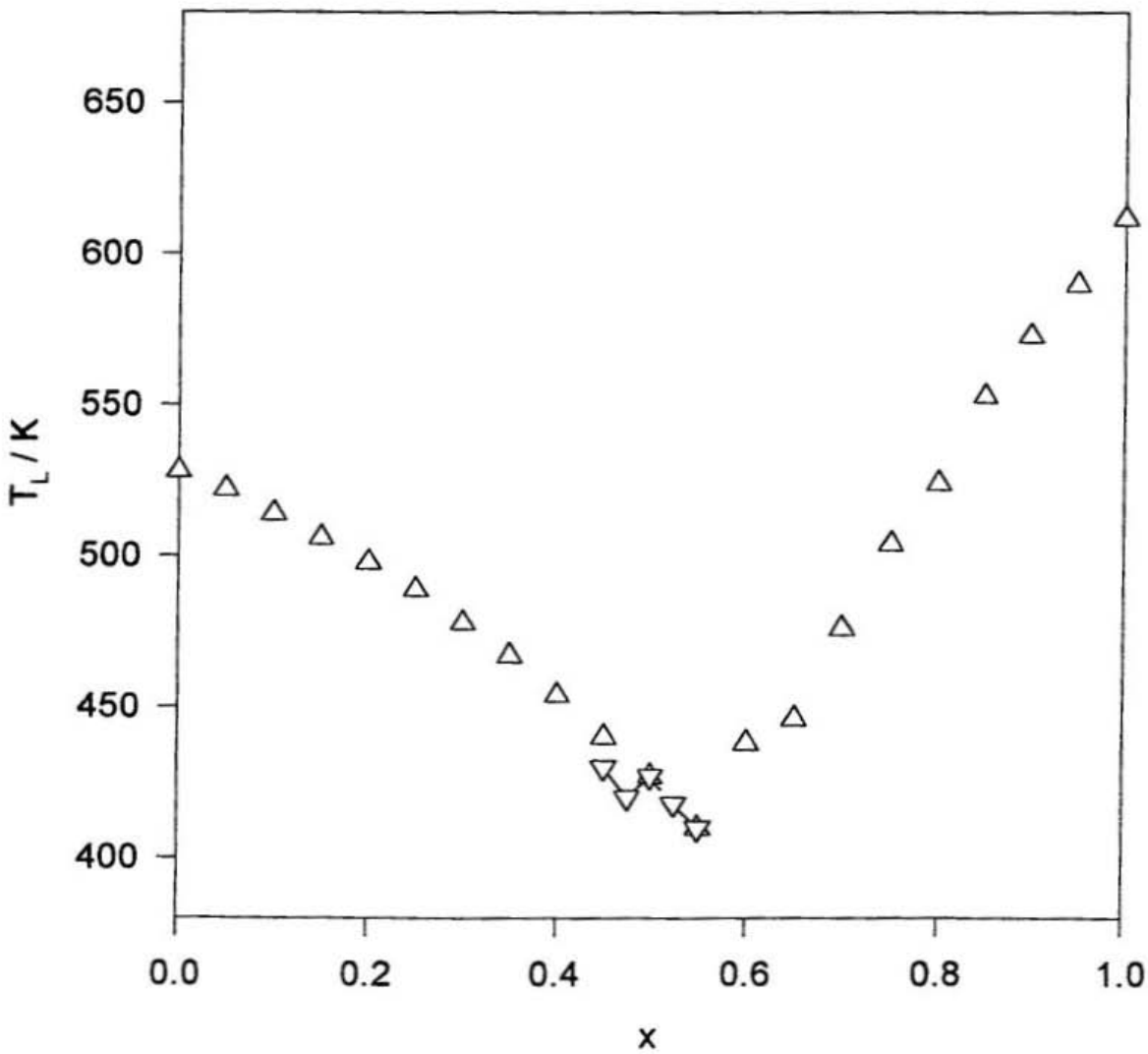

Fig. 7.13 DSC data (△) [1] for liquidus indicate a eutectic system for the $LiNO_3$-KNO_3 system. The Raman studies suggest a simple syntectic system with congruently melting compound $KLi(NO_3)_2$ (▽). X is the mole fraction of KNO_3.

CHAPTER 8

RAMAN SPECTROSCOPIC STUDIES OF THE CRYSTALS FORMED FROM AQUEOUS SOLUTIONS OF $AgNO_3$-MNO_3 (M = K, Rb, Cs)

8.1 Introduction

Silver nitrate and potassium nitrate or silver nitrate and rubidium nitrate form congruently melting compounds $KAg(NO_3)_2$ or $RbAg(NO_3)_2$ [47,49]. These compounds can also crystallize from the aqueous solutions [26,138]. An X-ray diffraction study [26] on the single crystals revealed that both $KAg(NO_3)_2$ and $RbAg(NO_3)_2$ belonged to space group $P2_1/a$. In the crystal the silver ions and nitrate ions formed infinite chains $[Ag_2(NO_3)_4]_n^{2n-}$ (Fig. 1.1) which were linked by K^+ or Rb^+. The silver ions were tetrahedrally coordinated by four nearest oxygen atoms from four different nitrate ions. Half of the nitrate ions acted as unidentate ligands and the other half acted as bidentate ligands.

Phase diagram studies [50,139] of the $AgNO_3$-$CsNO_3$ system by thermal methods indicated that there is an incongruently melting compound $CsAg(NO_3)_2$ and a congruently melting compound $CsAg_3(NO_3)_4$. It is interesting that a study of the system $AgNO_3$-$CsNO_3$-H_2O found [140] that the incongruently melting compound $CsAg(NO_3)_2$ crystallized readily from the aqueous solutions over a wide concentration range, while the congruently melting compound

$CsAg_3(NO_3)_4$ did not crystallize from the aqueous solutions. Chemical analysis, thermal analysis and X-ray diffraction were applied to confirm the compound $CsAg(NO_3)_2$ from the aqueous solutions.

Raman and IR are important techniques for structural determination of binary nitrate solids. Vibrational spectroscopy has been employed to distinguish between the various types of coordinated nitrate groups [141,142]. The symmetry of the free nitrate ion is D_{3h}. There are three IR active fundamental modes at about 1390, 830 and 720 cm^{-1} and three Raman active fundamentals at about 1390, 1050 and 720 cm^{-1}. Coordination lowers the symmetry of the nitrate ion to C_{2v} or C_s and there should be six fundamentals which are active in both IR and Raman. Coordination to cations will result in a more directional perturbing field on the nitrate ion and may lower the vibrational energy of ν_1 [136]. The splitting of the doubly degenerate ν_3 mode of the free nitrate ion is most informative. It was found [141-144] that the separation of the split bands was larger for bidentate than for unidentate coordination and the intensity of the Raman band with lower frequency was stronger in unidentate coordination and weaker in bidentate coordination.

The structural details of the compound formed in a binary system are helpful for a better understanding of the phase diagram. Raman spectra of the congruently melting compounds $KLi(NO_3)_2$, $RbLi(NO_3)_2$ and $CsLi(NO_3)_2$ have been measured and a structure similar to $KAg(NO_3)_2$ has been deduced. The structural studies also confirmed the existence of the new compound $KLi(NO_3)_2$ which melted congruently (Chapter 7). In this work Raman spectra of the compounds $KAg(NO_3)_2$, $RbAg(NO_3)_2$ and $CsAg(NO_3)_2$ have been measured, correlation between the structural and Raman features has been suggested, and a comparison

of these features to those of the lithium compounds has been made.

8.2 Raman Spectra of the Compounds $MAg(NO_3)_2$ (M = K, Rb, Cs)

The Raman spectra of $KAg(NO_3)_2$ and $RbAg(NO_3)_2$ were similar in both external and internal vibrational regions (Table 8.1). This is in agreement with the fact that both compounds have the same crystallographic structure ($P2_1/a$) and only silver ions coordinate directly to the nitrate ions in the crystals. The factor group analysis of the crystals predicts 24 Raman active internal modes (A_g and B_g symmetries). We cannot do a full assignment without single crystals.

In the external vibrational region four distinct bands are observed at 153, 121, 88 and 46 cm^{-1} for $KAg(NO_3)_2$ and five distinct bands at 157, 131, 99, 74 and 39 cm^{-1} for $RbAg(NO_3)_2$. The strong Raman bands at 52 and 82 cm^{-1} of KNO_3 II or the Raman features at 108 and 53 cm^{-1} of $RbNO_3$ IV were not detected because of the formation of the compounds. The whole spectral profile was similar to that of $AgNO_3$ II (Fig. 8.1): a band at about 40 cm^{-1} and multi band features between 60 and 200 cm^{-1}.

The similarity of the Raman spectra of the two compounds was more evident in the internal vibrational region. Raman bands in each of the ν_1, ν_2, ν_3 and ν_4 regions have practically the same frequencies with the same intensity patterns (Table 8.1 and Fig. 8.2). The Raman features of $AgNO_3$ II and KNO_3 II or $RbNO_3$ IV do not appear. The observed Raman bands are due to the complex $[Ag_2(NO_3)_4]_n^{2n-}$ in the crystals.

In the ν_1 region there is only one band at 1042 cm^{-1}. Judged by the two differently

coordinated types of the nitrate ion in the compounds $KAg(NO_3)_2$ and $RbAg(NO_3)_2$ there should be two bands. We failed in our attempt to resolve this band by measuring the spectrum at liquid nitrogen temperature and under the conditions of 0.25 cm^{-1} slits and eight data points per wavenumber. Still only one band appeared (Fig. 8.3). The ν_1 vibration of the nitrate ion in the silver compounds is not so sensitive to the change of the force field experienced by the nitrate ion, as is illustrated by the small difference (2 cm^{-1}) between the ν_1 bands of pure $AgNO_3$ and the compounds. It seems likely that the ν_1 mode of the nitrate ion in the compounds $KAg(NO_3)_2$ and $RbAg(NO_3)_2$ has very similar energy in both unidentate and bidentate coordination environments, resulting in the coincidence of the two bands.

The ν_2 vibration of the nitrate ion is also non-degenerate. It was at 820 cm^{-1} in the room temperature Raman spectra and the band looks flat at the top. At 77 K this band was resolved into two peaks (Fig. 8.4): 824 and 818 cm^{-1} for $KAg(NO_3)_2$ and 821 and 817 cm^{-1} for $RbAg(NO_3)_2$. There were also two bands at 1632 and 1642 cm^{-1} in the $2\nu_2$ region. The multi-band feature of the non-degenerate mode may indicate the symmetrically nonequivalent sites of the nitrate ions in the compounds. The ν_2 mode of the nitrate ion in the silver compounds appears to be more sensitive to the environment of the nitrate ion than the ν_1 mode because relative large difference was observed between the ν_2 bands in the Raman spectra of pure $AgNO_3$ (806 cm^{-1}) and the compounds (820 cm^{-1}). It is interesting to note that the ν_2 band shifts to higher wavenumber in the compounds while the ν_1 band shifts to lower wavenumber. Another possible explanation for the two bands in the ν_2 region is correlation field splitting.

At least four bands could be distinguished in the ν_3 region. They were bands at 1282, 1306, 1402 and 1432 cm^{-1} for $KAg(NO_3)_2$ and 1281, 1303, 1408 and 1435 cm^{-1} for $RbAg(NO_3)_2$. The spectral profile of the silver compounds in this region was similar to that of the lithium compounds $MLi(NO_3)_2$ (M = K, Rb, Cs): Raman features appear over a wide frequency range (160 cm^{-1}) and relative strong bands at both ends. There were three bands in the ν_4 region: 701, 714 and 724 cm^{-1} for $KAg(NO_3)_2$ and 702, 715 and 724 cm^{-1} for $RbAg(NO_3)_2$. The band with the highest frequency was the strongest of the three while the other two bands appeared to have the same intensity (Fig. 8.4).

The Raman spectrum of the crystal obtained from the aqueous solution of equimolar $AgNO_3$-$CsNO_3$ was different from the spectrum of either component (Table 8.1), indicating the formation of a compound from the solution. The spectrum was different from the Raman spectra of $KAg(NO_3)_2$ and $RbAg(NO_3)_2$ (Figs. 8.1 and 8.5). The crystal was the compound $CsAg(NO_3)_2$ which has a different structure from $KAg(NO_3)_2$ and $RbAg(NO_3)_2$.

Four distinct peaks appeared in the external vibrational region at 48, 112, 132 and 224 cm^{-1}. The most distinct feature was the band at 224 cm^{-1} (Fig. 8.1). It had no equivalent in the Raman spectra of pure $AgNO_3$ and $KAg(NO_3)_2$ or $RbAg(NO_3)_2$. The band was well separated from the other external modes of the compound and the frequency was higher than any of the external modes in other silver compounds (Fig 8.1). The two bands at 112 and 132 cm^{-1} appeared sharper and Rayleigh wing was less intense than for the external bands of $KAg(NO_3)_2$ and $RbAg(NO_3)_2$.

In the ν_1 region there was a band at 1043 cm^{-1} which was resolved into two bands at 1042.9 and 1044.9 cm^{-1} at liquid nitrogen temperature (Fig. 8.3). There were two bands at

811 and 822 cm^{-1} in the ν_2 region. The 11 cm^{-1} separation of the two bands was much greater than the separation of the two ν_2 bands in $KAg(NO_3)_2$ (4 cm^{-1}) (Fig. 8.4).

Unlike $KAg(NO_3)_2$ and $RbAg(NO_3)_2$, $CsAg(NO_3)_2$ had a three-peak profile in the ν_3 region. Besides the two bands at 1293 and 1425 cm^{-1} at both ends, there was a band at 1350 cm^{-1} with comparable intensity in the middle. At 77 K the middle band was resolved into two bands with intensities stronger than those at both ends (Fig. 8.6). In the ν_4 region only two bands were observed at 713 and 722 cm^{-1} instead of three.

Raman studies suggest that $KAg(NO_3)_2$ and $RbAg(NO_3)_2$ have the same structure while $CsAg(NO_3)_2$ has a different structure.

8.3 Discussion

One of the most notable structural features of the compounds $KAg(NO_3)_2$ and $RbAg(NO_3)_2$ revealed by XRD studies [26] is the two crystallographically different sites for the nitrate ions (Fig. 1.1). The nitrate group may act as either a unidentate or bidentate ligand. As a result, the non-degenerate modes ν_1 and ν_2 of the free nitrate ion may present multi-band features and the degenerate modes ν_3 and ν_4 may split in different ways. The Raman spectroscopic studies are consistent with the structural analysis. The fact that the ν_1 vibration cannot be resolved into two bands is probably due to accidental coincidence. However, the ν_2 vibration and the $2\nu_2$ region did exhibit a doublet structure. The band profiles in the ν_3 and ν_4 regions are in good agreement with the rule of thumb [145] which identifies unidentate and bidentate nitrate ions.

Among the normal modes of the free nitrate ion, ν_3 is the most sensitive to coordination. It was noted [143,146] that the splitting of the ν_3 vibration was distinctly less for unidentate nitrate ions than for bidentate nitrate ions in the complexes of similar structures. On this basis, $Ni(dien)_2(NO_3)_2$ (dien = diethylenetriamine) was believed to consist of both unidentate and bidentate nitrate ions. The observed IR bands [143] at 1315 and 1440 cm^{-1} or 1300 and 1480 cm^{-1} fitted well to the splittings of unidentate or bidentate nitrate ions in the same series of Ni(II) complexes. The splittings of ν_3 were also observed [31,147] in the IR and Raman spectra of $AgNO_3$ solutions or melt due to coordination of silver ions to nitrate ions. The typical frequencies were 1280 and 1400 cm^{-1}. In the Raman spectra of $KAg(NO_3)_2$ and $RbAg(NO_3)_2$, two bands of comparable intensities can be distinguished in each of the two locations: 1282, 1306 and 1402, 1432 cm^{-1} for the former; 1281, 1303 and 1408, 1435 cm^{-1} for the latter. By analogy to the Ni(II) complexes, the bands at 1306 and 1402 cm^{-1} (or 1303 and 1408 cm^{-1}) may be attributed to unidentate nitrate ions and the bands at 1282 and 1432 cm^{-1} (or 1281 and 1435 cm^{-1}) may be attributed to bidentate nitrate ions. The splittings are larger in $RbAg(NO_3)_2$ than in $KAg(NO_3)_2$ probably because the larger counterion Rb^+ has less effect on the coordination in the $Ag\text{-}ONO_2$ complex than the smaller K^+.

The three bands in the ν_4 region may also be attributed to splitting of this doubly degenerate mode due to unidentate or bidentate coordination of the nitrate ion, assuming that the much stronger band at 724 cm^{-1} is a combination of two bands of similar energy.

Another structural particular about $KAg(NO_3)_2$ and $RbAg(NO_3)_2$ is the polymeric complex $[Ag_2(NO_3)_4]_n^{2n-}$. It may account for the stronger Rayleigh wing in these compounds than in $CsAg(NO_3)_2$ or pure $AgNO_3$ (Fig. 8.1) and the unique frequency shift in the external

vibrational region. Usually larger ions expand the lattice so that the external vibrations shift to lower frequencies. However, the bands at 88, 121 and 153 cm^{-1} in $KAg(NO_3)_2$ shift to higher frequencies in $RbAg(NO_3)_2$ which are at 99, 131 and 157 cm^{-1}. These three bands are primarily due to the vibrations within the frame of the complex $[Ag_2(NO_3)_4]_n^{2n-}$ because they have the highest energies in this region and because the band profiles are both similar to the band profile of the three highest frequencies of $AgNO_3$ in the same region (Fig. 8.1). The alkali metal ions, being outside the complexes, compete with the silver ion for the nitrate ions. The larger rubidium ion is a weaker competitor and the lattice vibrations of $[Ag_2(NO_3)_4]_n^{2n-}$ in $RbAg(NO_3)_2$ shift to higher frequencies.

As the size of the alkali metal ion increases to that of cesium, the influence of the counterion on the complex becomes even less and the polymeric chain may break down to form a smaller one. The Raman spectrum of the compound $CsAg(NO_3)_2$ in the external vibrational region is quite different from those of $KAg(NO_3)_2$ and $RbAg(NO_3)_2$. The Rayleigh wing background is not so strong. The three highest energy bands in the external vibrational region become much sharper and shift to higher frequencies (Fig. 8.1). All these are consistent with the indications that polymeric complexes reduce to simpler ones [148,149]. The highest frequency band shifts the greatest and becomes an isolated band at 224 cm^{-1}. The frequency is within the range of 350 to 200 cm^{-1} for metal-oxygen stretching vibrations in nitrato complexes [150,151]. Judged by its frequency and intensity, this well separated band at 224 cm^{-1} may be due to the stretching vibration of Ag-ONO_2 in the smaller entity. This is similar to the case of $KMgCl_4$ and $CsMgCl_4$ [71]. Larger Cs^+ was able to support a discrete tetrahedral $MgCl_4^{2-}$ while smaller K^+ could not. In $KMgCl_4$ there was polymeric $MgCl_6^{4-}$

with bridging Cl^-.

The Raman bands in the internal vibrational region support the idea that the nitrate ions are in a unique coordination mode in $CsAg(NO_3)_2$. The doublet feature in the ν_1 region may suggest that there are crystallographically different sites for the nitrate ions in the compound. Unlike $KAg(NO_3)_2$ and $RbAg(NO_3)_2$, the differently coordinated nitrate ions are not simply half unidentate and half bidentate. The splitting of ν_3 does not fit in the pattern of relatively strong bands on both ends. Only one band is distinguished at 1280 or 1420 cm^{-1} while two relatively strong bands are observed in the middle.

It is interesting to make a brief comparison of the compounds $MAg(NO_3)_2$ and $MLi(NO_3)_2$ (M = K, Rb, Cs). The compounds consist of complexes of the nitrate ion with silver ion or lithium ion. Potassium, rubidium or cesium ions act as counterions. The lithium complexes are similar to the silver complexes in $KAg(NO_3)_2$ and $RbAg(NO_3)_2$ because they have similar Raman features: multi bands in the non-degenerate ν_1 or ν_2 region of the free nitrate ion, relatively strong bands on both ends of the envelope in the ν_3 region, broadened Raman bands and a strong Rayleigh wing. $CsAg(NO_3)_2$ belongs to another structure. Lithium nitrate and silver nitrate form congruently melting compounds with heavier alkali metal nitrates because of the much greater coordination capability of the lithium ion or silver ion than the other cations. It seems that the silver ion is more capable than the lithium ion to coordinate with a nitrate ion. Lithium nitrate can hardly form compounds with potassium nitrate while silver nitrate can with ease. The compound $CsLi(NO_3)_2$ has the same structure as the other two lithium compounds while $CsAg(NO_3)_2$ has a different structure from the other two silver compounds, probably due to formation of discrete complexes.

The nature of the bonding in the lithium complexes is quite different from that in the silver complexes. In the former the bonding is primarily ionic while in the latter there is covalent character. The covalent nature of the Ag-ONO_2 bond accounts for the formation of the congruently melting compound $KAg(NO_3)_2$. The size difference between silver (126 pm) and potassium (133 pm) ions is much smaller than the size difference between sodium (97 pm) and potassium ions. Sodium and potassium nitrates can form solid solutions [4]. If not for the covalent character, silver and potassium nitrates would have formed a continuous series of solid solutions. It is likely that the ionic character of lithium complexes explains some detailed Raman features which are different from the silver complexes. In the Raman spectra of the lithium complexes, the Rayleigh wing is much stronger and the external bands are fewer and more diffuse. The Raman bands in the internal vibrational region are broader in the lithium complexes than in the silver complexes. These differences are not likely caused by different preparations. We have melted the silver compounds and then let them recrystallize. No changes were detected in the Raman spectra of the compounds before and after melting.

Bonding differences between Ag-ONO_2 and Li-ONO_2 were also observed in melts and aqueous solutions of the nitrates. The covalent character in $AgNO_3$ caused the ν_1 vibration of the nitrate ion in the aqueous solutions to shift to lower frequency while the ionic character in $LiNO_3$ caused it to shift to higher frequency [152]. Long range orientations of Ag-ONO_2 interactions in the melt were detected [34]. In the same work, no specific orientation of the lithium ion to the nitrate ion was observed. Finally, the Raman forbidden ν_2 mode appears in molten and crystalline $AgNO_3$ while it does not appear in the lithium counterparts.

The strong interaction between silver and nitrate ions accounts for the nonequivalent

sets of nitrate group in molten $AgNO_3$, such as ion pair and multiple ion aggregate which were suggested by Raman studies [57,152]. According to the neutron diffraction study [34], about four oxygen atoms from four nitrate groups coordinated to a silver atom in molten $AgNO_3$. Therefore, the nitrate ions must be shared by the cations and thus may act as bidentate and unidentate ligands. Such a coordination state may also be present in the melts of the congruently melting compounds $KAg(NO_3)_2$ and $RbAg(NO_3)_2$. When the melts crystallize, the complex structure of $Ag\text{-}ONO_2$ remains and is stabilized by the counterion K^+ or Rb^+. This suggestion is supported by the similarity of the Raman spectrum of the congruently melting compounds of $KAg(NO_3)_2$ to the Raman spectra of the melt and the acetonitrile solution of $AgNO_3$. Considering the differences in state and temperature, the similarity is striking (Table 8.2).

There are discrepancies in the phase diagrams of $AgNO_3$-KNO_3 and $AgNO_3$-$CsNO_3$. The three most recent reports about $AgNO_3$-KNO_3 presented three different pictures of phase diagrams: congruently melting compound $KAg(NO_3)_2$ [47]; incongruently melting compound $KAg(NO_3)_2$ [48]; and eutectic [153]. $CsAg(NO_3)_2$ was generally regarded as an incongruent melting compound [139]. An early report [51] suggested that it was a congruently melting compound. The phase diagrams looked very much alike. The sole difference was that the discontinuity at $x(Ag^+) = 0.52$ for incongruently melting compound $CsAg(NO_3)_2$ [139] shifted a little to $x(Ag^+) = 0.50$, indicating a congruently melting compound [51]. The discrepancies were caused chiefly by the non-equilibrium conditions which were noted by most of the authors [48,153,154] when they applied thermal methods to investigate the binary nitrate systems. The Raman spectroscopic studies in this work appear to favour the suggestion that

$KAg(NO_3)_2$ and $CsAg(NO_3)_2$ are congruently melting compounds. They readily crystallize from aqueous solutions, especially $CsAg(NO_3)_2$. Melting did not seem to change the structures of the compounds since the Raman spectra of the compounds before and after melting were practically the same. The Raman spectrum of $KAg(NO_3)_2$ is similar to molten $AgNO_3$, just as in the case of the congruently melting compound $MLi(NO_3)_2$ (M = K, Rb, Cs) (Section 7.3).

8.4 Conclusions

Raman spectroscopic studies of $KAg(NO_3)_2$ and $RbAg(NO_3)_2$ are consistent with the crystal structure revealed by XRD determination. There exist polymeric complexes of silver and nitrate ions in the compounds. The nitrate ions act as both unidentate and bidentate ligands.

The compound $CsAg(NO_3)_2$ can crystallize from the aqueous solutions but it has a different structure from $KAg(NO_3)_2$. The polymeric complex of silver and nitrate ions may have broken down to form smaller ones.

$KAg(NO_3)_2$, $RbAg(NO_3)_2$, $KLi(NO_3)_2$, $RbLi(NO_3)_2$ and $CsLi(NO_3)_2$ appear to be isostructural although the bonding in the lithium complex is primarily ionic while the bonding in the silver complex is more covalent.

Table 8.1 Observed wavenumbers for Raman bands of the compounds $MAg(NO_3)_2$ (M = K, Rb, Cs) measured at 298 K.

$MAg(NO_3)_2$	external	ν_4	ν_2	ν_1	ν_3	$2\nu_2$
$KAg(NO_3)_2$	46,88, 121,153	701,714, 724	816,821	1042	1282,1306, 1402,1432	1632,1642
$RbAg(NO_3)_2$	39,74,99, 131,157	702,715, 724	820 [a]	1042	1281,1303, 1408,1435	1631,1642
$CsAg(NO_3)_2$	48,112, 132,224	713,722	811,822	1043	1293,1425, 1350 [b]	1622,1644

a. The band is flat at the top which can be resolved to two bands at 817 and 821 cm^{-1} at 77 K.

b. The band is resolved to two bands of similar intensity at 77 K.

Table 8.2 Wavenumbers of Raman bands for $KAg(NO_3)_2$ (A), molten $AgNO_3$ (B) [57] and the acetonitrile solution of $AgNO_3$ (C) [152] in the internal vibrational region.

sample	ν_4	ν_2	ν_1	ν_3	$2\nu_2$
A	701,714,724	816,821	1042	1282,1306,1402,1432	1632,1642
B	706,727	799,813	1014,1034	1275, *, *, 1423	1605
C	709,719-723	818-820	1031,1038, 1042	1290,1304, --	1636,1648, 1664

* Weak components may contribute intensity at 1350 and 1400 cm^{-1}.

-- A dash indicates that the 1400-1450 cm^{-1} region is masked by solvent bands.

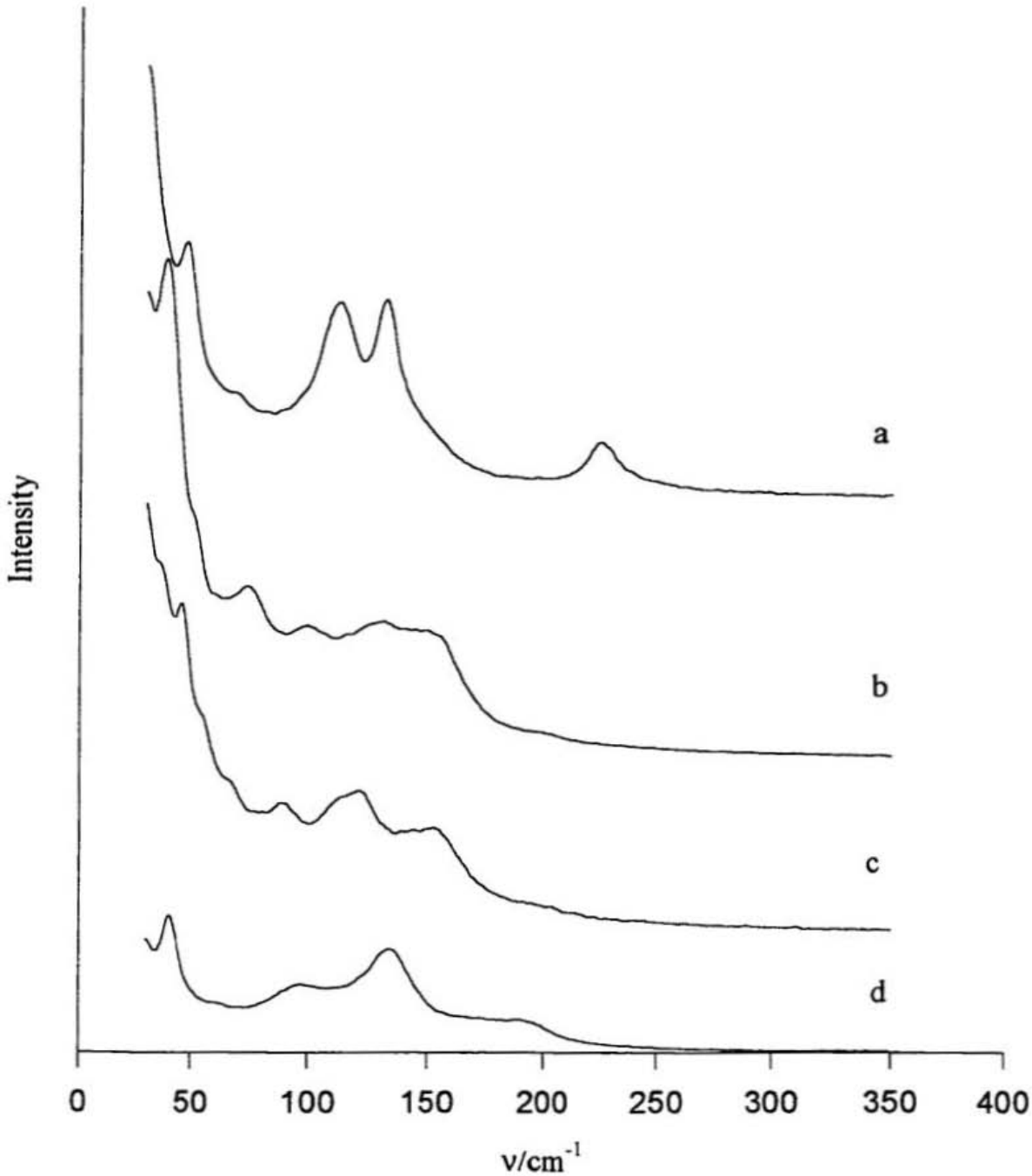

Fig. 8.1 Raman spectra in the external vibrational region of (a) $CsAg(NO_3)_2$, (b) $RbAg(NO_3)_2$, (c) $KAg(NO_3)_2$ (d) and $AgNO_3$ at 298 K.

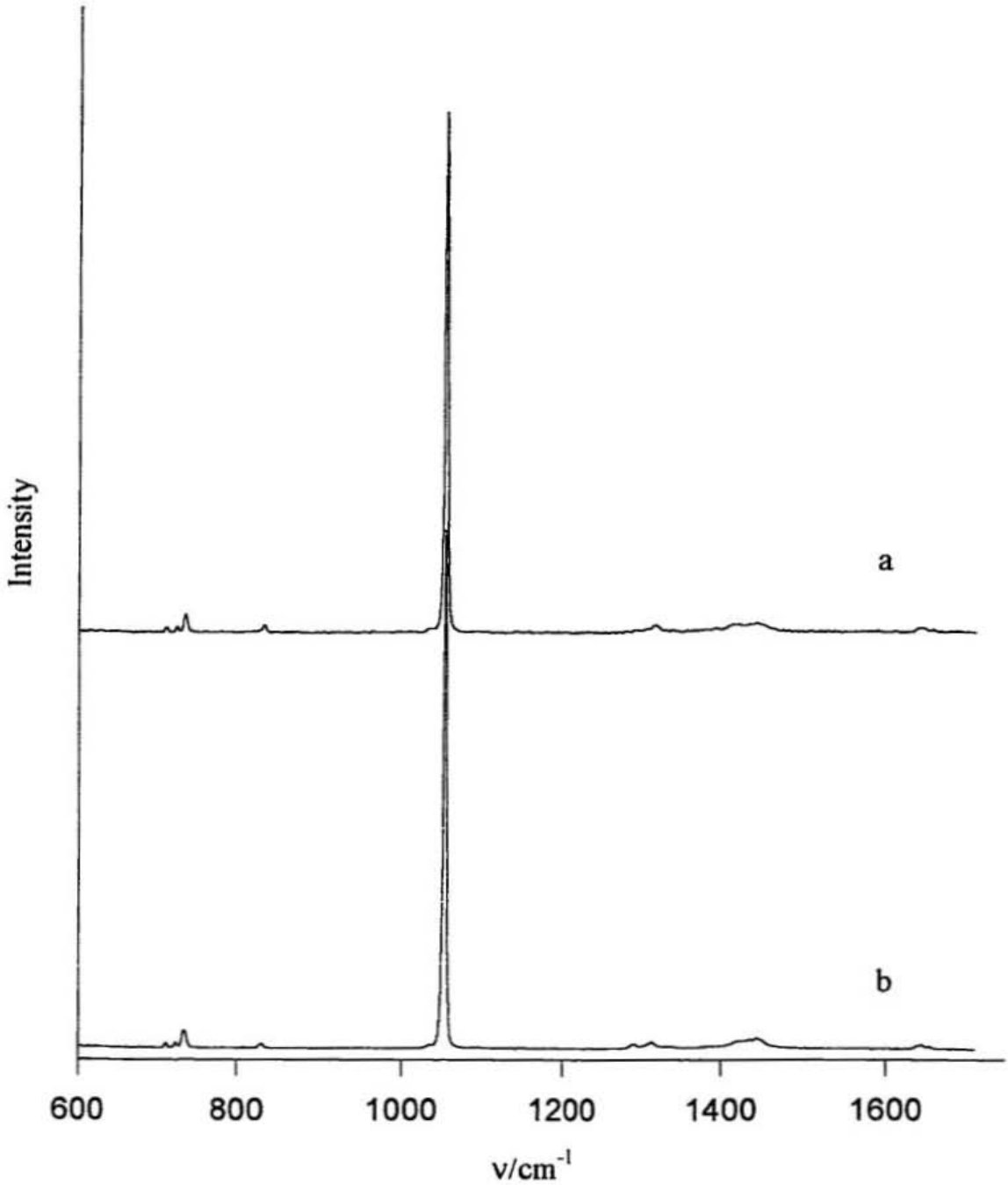

Fig. 8.2 Raman spectra in the internal vibrational region of (a) $KAg(NO_3)_2$ and (b) $RbAg(NO_3)_2$ at 298 K.

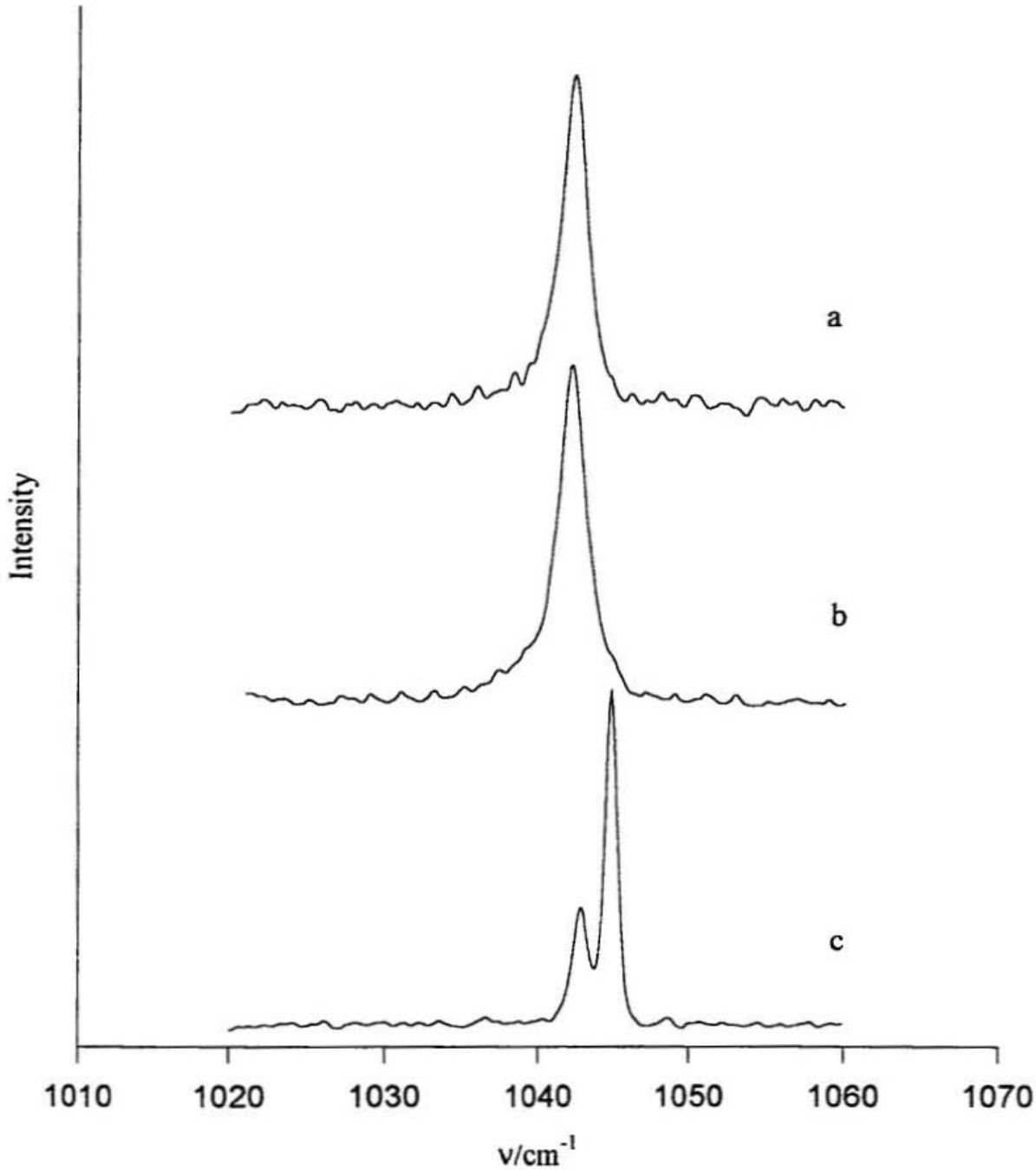

Fig. 8.3 Raman spectra in the ν_1 region of (a) $KAg(NO_3)_2$, (b) $RbAg(NO_3)_2$, and (c) $CsAg(NO_3)_2$ at 77 K.

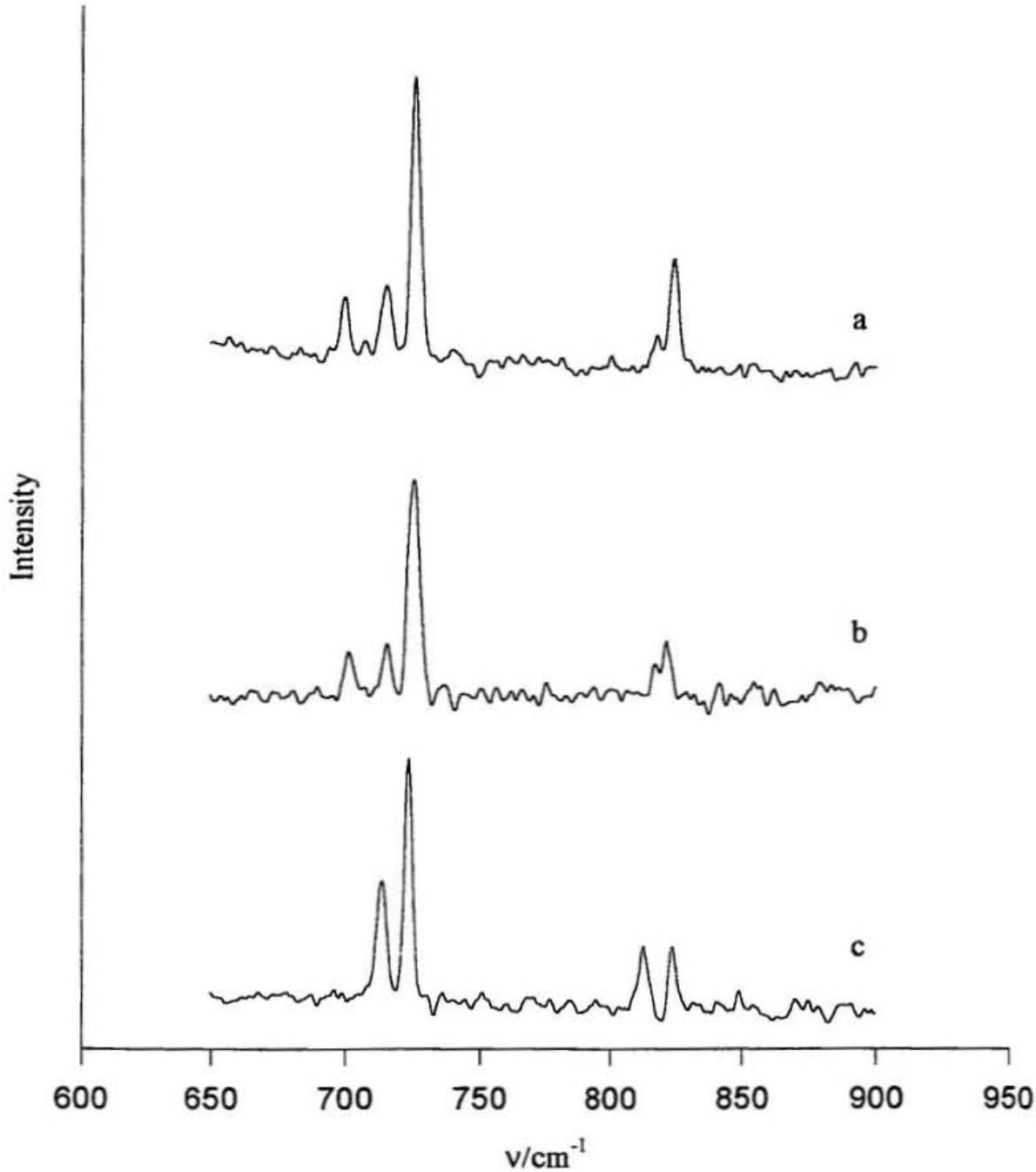

Fig. 8.4 Raman spectra in the ν_2 and ν_4 regions of (a) $KAg(NO_3)_2$, (b) $RbAg(NO_3)_2$, and (c) $CsAg(NO_3)_2$ at 77 K.

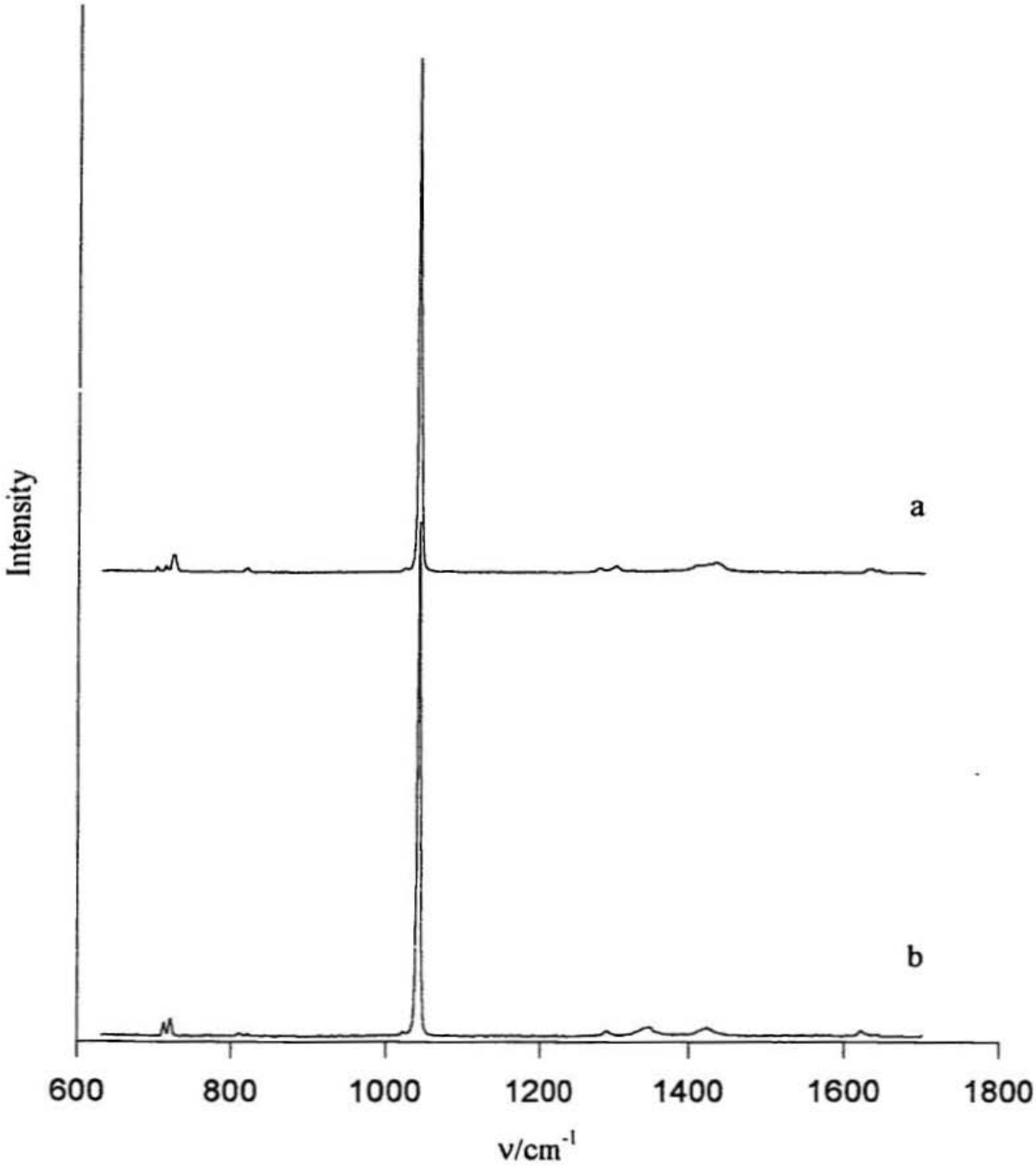

Fig. 8.5 Raman spectra in the internal vibrational region of (a) $RbAg(NO_3)_2$ and (b) $CsAg(NO_3)_2$ at 298 K.

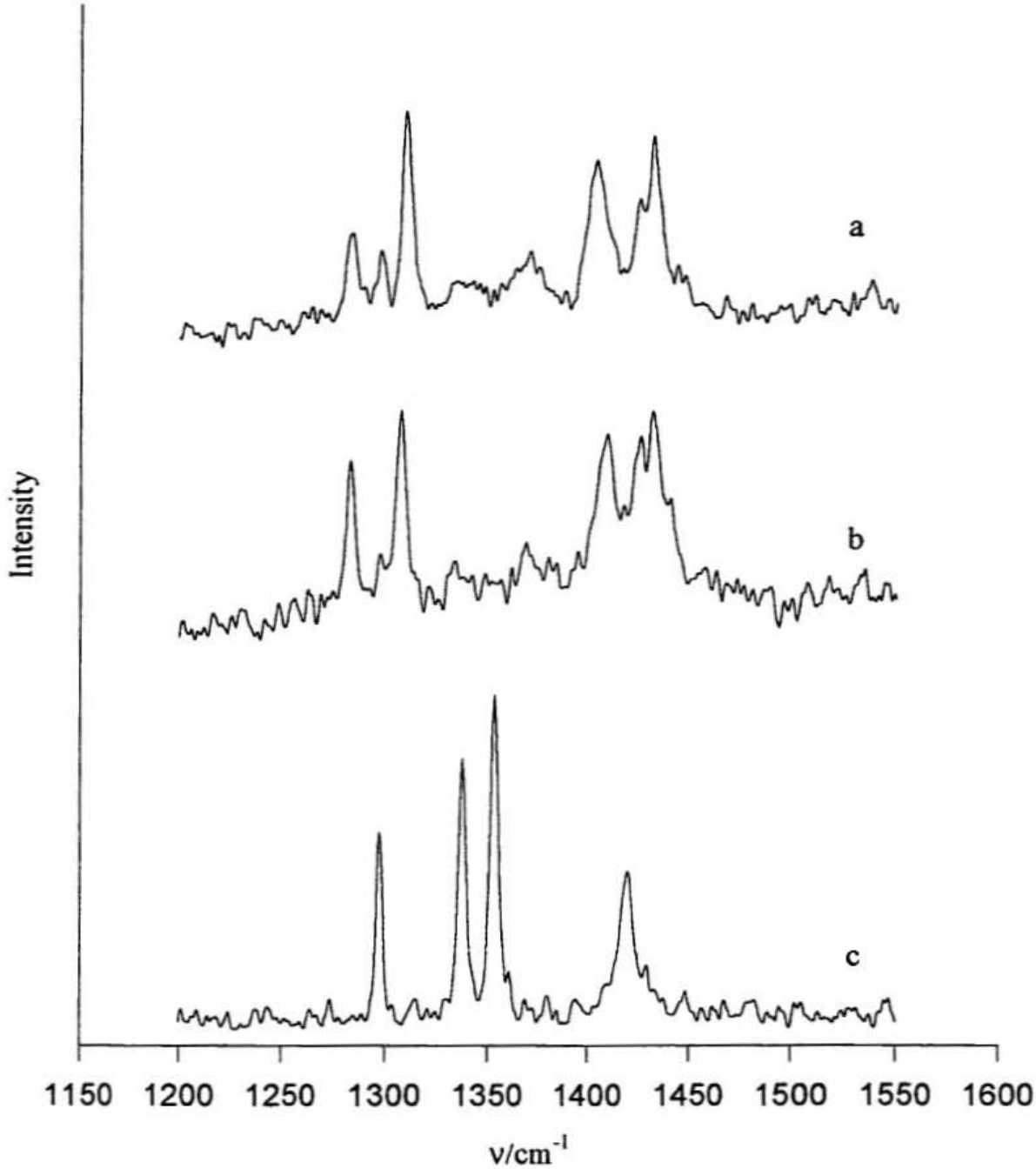

Fig 8.6 Raman spectra in the ν_3 region of (a) $KAg(NO_3)_2$, (b) $RbAg(NO_3)_2$ and (c) $CsAg(NO_3)_2$ at 77 K.

General Conclusions

Raman spectroscopy has proven to be an effective tool in phase equilibrium studies of new materials. In the present work Raman spectroscopy has been successfully applied:

1. to determine the solubility of solid solutions (KNO_3-$RbNO_3$ and $NaNO_3$-KNO_3).
2. to interpret phase diagrams on atomic terms (KNO_3-$RbNO_3$ and $NaNO_3$-KNO_3).
3. to establish the structure of new compounds [(K/Rb/Cs)Li$(NO_3)_2$].
4. to connect the structure of complexes in the crystal to Raman patterns [(K/Rb/Cs)Ag$(NO_3)_2$].

The Raman studies of the binary monovalent metal nitrate solids have resulted in the following important new information about the phase diagrams investigated in this program.

1. Continuous solid solutions are formed between KNO_3 I and $RbNO_3$ II. Two transitions of $RbNO_3$ (phase IV to III and phase II to I) were not detected for the solid solutions with the $RbNO_3$ structure.
2. The sodium and potassium nitrate system was found to be a system of limited solid solutions instead of a continuous series of solid solutions as previously reported.
3. Lithium and potassium nitrate is a syntectic system with congruently melting compound K$Li(NO_3)_2$ instead of a simple eutectic system as previously reported.
4. The evidence indicated that K$Ag(NO_3)_2$ and Cs$Ag(NO_3)_2$ were congruently melting compounds rather than incongruently melting compounds as previously reported.

Our Raman studies of $K_{1-x}Rb_xNO_3$ (KII) indicated that chemical substitution, like isotopic substitution, is a powerful technique for interpretation of vibrational spectra.

REFERENCES

1. M.J. Maeso and J. Largo, *Thermochim. Acta*, **223**, 145(1993).
2. J. Wong and C.A. Angell, *GLASS, Structure by Spectroscopy*, p.20, MACEL DEKKER, INC., New York(1976).
3. (a) K.W. Fung and G. Mamantov, in *Adv. Molten Salt Chem.* Vol.2, p.230, J. Braunstein, G. Mamantov and G.P. Smith, Eds., Plenum, New York, 1971.

   (b) A. Piracha, *Report* **1988**, Order No. PB89-225718.
4. C.M. Cramer and C.J. Wilson, *Thermochim. Acta*, **42**, 253(1980).
5. J.F. Scott, et al, *Phys. Rev.*, **B35**, 4044(1987).
6. N. Smyrl and J.P. Devlin, *J. Phys. Chem.*, **76**, 3093(1972).
7. (a) W.H. Leong, D.W. James and M.T. Carrick, *J. Raman Spectro.*, **14**, 11(1983).

   (b) T. Furukawa, S.A. Brawer and W.B. White, *J. Chem. Phys.*, **69**, 2639(1978).
8. O. Abe, T. Utsunomiya and Y. Hoshino, *Thermochim. Acta*, **78**, 251(1984).
9. W.B. White, in *The Infrared Spectra of Minerals*, p. 87, V.C. Farmer Ed. Mineralogical Society, London(1974).
10. C.C. Addison, G.S. Brownlee and N. Logan, *J. Chem. Soc. Dalton*, 1440(1972).
11. R.J. Fereday and D. Sutton, *Chem. Commun.*, **15**, 510(1966).
12. E. Rapoport, *J. Phys. Chem. Solids*, **27**, 1349(1966).
13. P. Cherin, W.C. Hamilton and B. Post, *Acta Cryst.* **23**, 455(1967).
14. K.O. Stromme, *Acta Chem. Scand.*, **23**, 1616(1969).

15. J.K. Nimmo and B.W. Lucas, *J. Phys. C: Solid State Phys.*, **6**, 201(1973).

16. Y. Shinnaka, *J. Phys. Soc. Jpn.*, **17**, 820(1962).

17. J.K. Nimmo and B.W. Lucas, *Acta Cryst.*, **B32**, 1968(1976).

18. M. Shamsuzzoha and B.W. Lucas, *Acta Cryst.*, **B38**, 2353(1982).

19. B.W. Lucas, *Acta Cryst.*, **C39**, 1591(1983).

20. S. F.A.Kettle, E.H.J. Lugwisha and L.J. Norrby, *Canad. J. Appl. Spectrosc.*, **35**, 91(1990).

21. R.W.G. Wyckoff, *Crystal Structures*, Vol.2, p.374, Interscience-John Willey & Sons, New York, 1967.

22. B.W. Lucas, *Material Science Forum*, **27/28**, 95(1989).

23. M. Ahtee and A.W. Hewat, *Phys. Stat. Sol.*, **a58**, 525(1980).

24. C.S. Gibbons and J. Trotter, *J. Chem. Soc. (A)*, 2058(1971).

25. F. Taylor, *Acta Cryst.* **B33**, 311(1977).

26. E. Zobetz, *Mona. Chem.*, **111**, 1252(1980).

27. K. Suzuki and Y. Fukushima, *Z. Naturforsch.*, **32A**, 1433(1977).

28. H. Ohno and K. Furukawa, *J. Chem. Soc. Faraday Trans.* I, **74**, 297(1978).

29. G.J. Janz and D.W. James, *J. Chem. Phys.*, **35**, 739(1961).

30. D. W. James and W.H. Leong, *J. Chem. Phys.*, **51**, 640(1969).

31. S.C. Wait, Jr., A.T. Ward and G.J. Janz, *J. Chem. Phys.*, **45**, 133(1966).

32. J.H.R. Clarke, *Chem. Phys. Lett.*, **4**, 39(1969).

33. B. Holmberg and G. Johansson, *Acta Chem. Scand.*, **A37**, 367(1983).

34. T. Yamaguchi, Y. Tamura, I. Okada, H. Ohtaki, M. Misawa and N. Wadanabe, *Z.*

Naturforsch., **40A**, 490(1985).

35. P. Meyyer, A. Rimsky and R. Chevalier, *Acta Cryst.*, **B32**, 1143(1976).
36. Y. Kameda, S. Kotani and K. Ichikawa, *Mol. Phys.*, **75**, 1(1992).
37. H.F. Fischmeister, *J. Inorg. Nucl. Chem.*, **3**, 182(1957).
38. D.E. Irish and A.R. Davis, *Canad. J. Chem.*, **46**, 943(1968).
39. D.E. Irish, D.L. Nelson and M.H. Brooker, *J. Chem. Phys.*, **54**, 654(1971).
40. S.P. Petrun'kin, V.N. Trostin and G.A. Krestov, *Khim. Khim. Tekhnol.*, **29**, 15(1986).
41. T. Yamaguchi, G. Johansson, B. Holmberg, M. Maeda and H. Ohtaki, *Acta Chem. Scand.*, **A38**, 437(1984).
42. T. Yamaguchi, O. Lindqvist, J.B. Boyce and T. Claeson, *Acta Chem. Scand.*, **A38** 423(1984).
43. K.A. Bol'shakov, B.I. Pokrovskii and V.E. Plyushchev, *Russ. J. Inorg. Chem.*, **6**, 1083(1961).
44. I.I. Il'yasov, T.I. Dunaeva, Yu.G. Litvinov and V.V. Vochanskaya, *Russ. J. Inorg. Chem.*, **21**, 1266(1976).
45. Yu.G. Litvinov, I.I. Il'yasov and V.I. Savva, *Russ. J. Inorg. Chem.*, **20**, 1418(1975).
46. H. Zamaly and M. Jemal, *Colorimetrie et Analyse Thermique* (Paris), **16**, 298(1985).
47. Ye.E. Bakhtinov, S.E. Darienko and Yu.F. Chervinskii, *Russ. J. Inorg. Chem.*, **36**, 1638(1991).
48. K. Meszaros Szecsenyi, K. Tomor and G. Pokol, *J. Thermal Anal.*, **41**, 125(1994).
49. N.P. Luzhnaya, N.N. Evseeva and I.P. Vereshchetina, *Zh. Neorg. Khim.* **1**, 1490(1956).
50. A.P. Palkin, J. *Russ. Phys. Chem. Soc.*, **60**, 317(1928).

51. G. Flor and C. Sinistri, *Ric. Sci.*, **38**, 227(1968).

52. O.J. Kleppa and L.S. Hersh, *J. Chem. Phys.*, **34**, 351(1961).

53. A.V. Tobolsky, *J. Chem. Phys.*, **10**, 187(1942).

54. O.J. Kleppa, R.B. Clarke and L.S. Hersh, *J. Chem. Phys.*, **35**, 175(1961).

55. M.H. Brooker, *J. Phys. Chem. Solids*, **39**, 657(1978).

56. M.H. Brooker and D.E. Irish, *Canad. J. Chem.*, **48**, 1198(1970).

57. C.H. Huang and M.H. Brooker, *Spectrochim. Acta*, **32A**, 1715(1976).

58. M.H. Brooker, *J. Chem. Phys.*, **59**, 5828(1973).

59. M.H. Brooker, *J. Chem. Phys.*, **68**, 67(1978).

60. S.V. Karpov and A.A. Shultin, *Sov. Phys. Solid State*, **17**, 1915(1976).

61. F.J. Owen, *Chem. Phys. Lett.*, **64**, 116(1979).

62. F.El-Kabbany, S. Taha and M. Tosson, *Ann. Phys.* (Leipzig), **46**, 429(1989).

63. K. Akiyama, Y. Morioka and I. Nakagawa, *Bull. Chem. Soc. Jpn.*, **54**, 1667(1981).

64. W. Gerlach, *Two phenomena observed with the aid of the Raman effect*, **CA 26**:4537(1932).

65. M.K. Raju, *Proc. Indian Acad. Sci.*, **22A**, 150(1945).

66. O. Greis, K.M. Bahamdan and B.M. Uwais, *Thermochim. Acta*, **86**, 343(1985).

67. P.I. Protsenko, L.S. Grin'ko, L.N. Venerovskaya and V.A.Lyutsedarskii, *J. Appl. Chem. USSR*, **46**, 2568(1973).

68. F.A. Cotton, *Chemical Applications of Group Theory*, Wiley-Interscience, New York(1963).

69. D.A. Long, *Raman Spectroscopy*, McGraw Hill, New York(1977).

70. M.H. Brooker, in *The Chemical Physics of Solvation*, Part B, p.119, R.R. Dogonadze, E. Kalman, A.A. Kornyshev and J. Ulstrup Eds, Elsevier, Amsterdam(1986).

71. M.H. Brooker and G.N. Papatheodorou, in *Advances in Molten Salt Chemistry*, Vol. 5, p.26, G. Mamanton Ed., Elsevier, Amsterdam(1983).

72. M.H. Brooker, O.F. Nielson and E. Praestgaard, *J. Raman Spectrosc.*, **19**, 71(1988).

73. W.F. Murphy, M.H. Brooker, O.F. Nielson, E. Praestgaard and J.E. Bertie, *J. Raman Spectrosc.*, **20**, 695(1989).

74. J.C. Decius and R.M. Hexter, *Molecular Vibrations in Crystals*, Mcgraw-Hill, New York (1972).

75. D. L. Rousseau, R.P. Bauman and S.P.S. Porto, *J. Raman Spectrosc.*, **10**, 253(1981).

76. W.G. Feteley, F.R. Dollish, N.T. McDevitt and F.F. Bentley, *Infrared and Raman Selection Rules for Molecular and Lattice Vibrations: the Correlation Method*, Wiley-Interscience, New York(1972).

77. *International Tables for X-ray Crystallography*, Vol. I, N.F.M. Henry and K. Lonsdale Eds., Kynoch Press, Birmingham(1952).

78. *Solid State Chemistry*: *Techniques*, A.K. Cheetham and P. Day Eds, Clarendon Press., Oxford(1987).

79. G.L. Paul and A.W. Pryor, *Acta Cryst.*, **B28,** 2700(1972).

80. U. Kawabe, T. Yanagi and S. Sawada, *J. Phys. Soc. Jpn.*, **20**, 2059(1965).

81. V.E. Plyushchev and R.G. Samuseva, *Russ. J. Inorg. Chem.*, **11**, 636(1966).

82. R.G. Samuseva and V.E. Plyushchev, *Russ. J. Inorg. Chem.*, **12**, 111(1967).

83. P.K. Davies and A. Navrotsky, *J. Solid State Chem.*, **46**, 1(1982).

84. V.S. Urusov, in *Thermodynamic Data*, p.162, S.K. Saxena Ed., Springer-Verlag, New York(1992).

85. V.S. Urusov, *Russ. J. Phys. Chem.*, **43**, 1705(1969).

86. A.I. Kitaigorodsky, *Mixed Crystals*, Spriger-Verlag, Berlin(1984).

87. A.C. Mclaren, *Rev. Pur. Appl. Chem.*, **12**, 54(1962).

88. H.M. Lu and J.R. Hardy, *Phys. Rev.*, **B44**, 7215(1991).

89. H.D. Megaw, *Crystal Structure: A Working Approach*, Chapter 15, W.B. Saunders Co., Philadelphia(1973).

90. K.O. Stromme, *Acta Chem. Scand.*, **25**, 211(1971).

91. P.P. Salhotra, E.C. Subbarao and P. Venkateswarlu, *Phys. Stat. Sol.*, **29**, 859(1968).

92. A.R. Ubbelohde, *The molten State of Matter*, John Wiley & Sons, Bristol(1978).

93. *Lange's Handbook of Chemistry*, 14th edn., J. A. Dean Ed., Mcgraw-Hill, New York(1992).

94. *CRC Handbook of Chemistry and Physics*, 75th edn., D.R. Lide Ed., CRC Press, Boca Raton , Florida(1994).

95. A.N. Kirqintsev and N.Ya. Yacobi, *Russ. J. Inorg. Chem.*, **16**, 1681(1971).

96. B.D. Stepin, Z.A. Stanikova, A.N. Knyazeva, G.A. Lovetskaya and V.K. Trunov, *Russ. J. Inorg. Chem.*, **23**, 126(1978).

97. P.P. Salhotra, E.C. Subbarao and P. Venkateswarlu, *J. Phys. Soc. Jpn.*, **27**, 621(1969).

98. N.A. Puschin and M. Radoicic, *Z. Anorg. Alig. Chem.*, **233**, 41(1937).

99. M.H. Brooker, *Canad. J. Chem.*, **55**, 1242(1977).

100. K. Akiyama, Y. Morioka and I. Nakagawa, *J. Phys. Soc. Jpn.*, **48**, 898(1980).

101. D. Liu, F.G. Ullman and J.R. Hardy, *Phys. Rev.*, **B45**, 2142(1992).

102. J.P. Devlin and R. Frech, *J. Chem. Phys.*, **63**, 1663(1975).

103. F. Brehat and B. Wyncke, *J. Phys.*, **C21**, 689(1988).

104. J.P. Devlin and D.W. James, *J. Chem. Phys.*, **53**, 4394(1970).

105. M.J. Harris, *Solid State Commun.*, **84**, 557(1992).

106. Y. Shinnaka, *J. Phys Soc. Jpn.*, **17**, 820(1962).

107. Midorikawa, et al, *J. Phys. Soc. Jpn.*, **30**, 449(1971).

108. P. Nolta, N.N. Schrubring and R.A. Dork, in *Ferroelectricity*, p.267, E.F. Weller Ed., Elsevier, Amsterdam(1967).

109. *Handbook of Solid-liquid Equilibra in Systems of Anhydrous Inorganic Salts*, N.K. Voskresenskaya Ed., Ket Press, Jerusalem(1970).

110. H. Zamali, T. Jriri, J. Rogez, M. Jemal and J.C. Mathieu, *Thermochim. Acta*, **233**,1(1994).

111. D.J. Rogers and G.J. Janz, *J. Chem. Eng. Data*, **27**, 424(1982).

112. D.J. Hussink, *Z. Phys. Chem.*, **32**, 536(1900).

113. A. Kofler, *Mona. Chem.*, **86**, 643(1955).

114. M. Kamimoto, *Thermochim. Acta*, **49**, 319(1981).

115. R. Kern, *Pur. Appl. Chem.*, **56**, 1697(1984).

116. C. Suryanarayana, in *Materials Science and Technology*, Vol. 15, p.57, R.W. Cahn Ed, VCH, Weinheim, Germany(1991).

117. C.N.R. Rao, B. Prakash and M. Natarajan, *Natl. Stand. Ref. Data Ser. 53*, May, 1975.

118. H.V. Briscoe and W.H. Madgin, *J. Chem. Soc.*, **123**, 1608,2914(1923).

119. P.I. Protsenko and A.G. Bergman, *J. Gen. Chem. USSR*, **20**, 1421(1950).

120. M.H. Brooker and D.E. Irish, *Canad. J Chem.*, **48**, 1198(1970).

121. E.V. Chisler, *Sov. Phys. Solid State*, **11**, 1032(1969).

122. T.Y. Shen, S.S. Mitra, H. Prask and S.F. Trevino, *Phys. Rev.*, **B12**, 4530(1976).

123. W. Klement, *J. Inorg. Nucl. Chem.*, **36**, 1916(1974).

124. M.J. Harris, E. Salje and B. Guttler, *J. Phys. Condens. Matter*, **2**, 5517(1990).

125. R.M. Lynden-Bell, M. Ferrario, I.R. McDonnald and E. Salje, *J. Phys. Condens. Matter*, **1**, 6523(1989).

126. W.W. Schmahl and E. Salje, *Phys. Chem. Minerals*, **16**, 790(1989).

127. R.J. Reeder, S.A.T. Redfern and E. Salje, *Phys. Chem. Minerals*, **15**, 605(1988).

128. F. Brehat and B. Wyncke, *Phys. C: Solid State Phys.*, **18**, 4247(1985).

129. C. Vallet, *J. Chem. Thermodynamics*, **4**, 105(1972).

130. C. Sinistri and P. Franzosini, *Ric. Sci. Parte 2, Sez. A*, **4**, 419(1963).

131. M.H. Miles and A.N. Fletcher, *J. Electroanal. Chem.*, **221**, 115(1987).

132. N. Smyrl and J.P. Devlin, *J. Phys. Chem.*, **77**, 3067(1973).

133. T.G. Chang and D.E. Irish, *Canad. J. Chem.*, **51**, 118(1973).

134. I.V.P. Oshida and Y. Hase, *Appl. Spectrosc.*, **32**, 590(1978).

135. M.H. Brooker, *J. Chem. Phys.*, **53**, 2670(1970).

136. D.W. James and M.T. Carrick, *Aust. J. Chem.*, **39**, 325(1986).

137. M.H. Brooker, A.S. Quist and G.E. Boyd, *Chem. Phys. Lett.*, **9**, 242(1971).

138. P. Friedlander, *Z. Krist.*, **3**, 215(1879).

139. D. Leonesi, M. Brehetti and A. Cingolani, *Ann. Chim.* (Rome), **66**, 489(1976).

140. F.M. Khutsistova, V.A. Berdyukova, T.B. Popova, V.N. Trufanov and L.G. Kolomin, *Russ. J. Inorg. Chem.*, **33**, 579(1988).

141. C.C. Addison, N. Logan, S.C. Wallwork and C.D. Garner, *Quart. Rev.*, **25**, 289(1971).

142. R.M. Gatehouse, S.E. Livingstone and R.S. Nyholm, *J. Chem. Soc.*, 4222(1957).

143. N.F. Curtis and Y.M. Curtis, *Inorg. Chem.*, **4**, 804(1965).

144. K.B. Yatsimirskii, *Pur. Appl. Chem.*, **49**, 115(1977).

145. K. Nakamoto, *Infrared and Raman Spectra of Inorganic and Coordination Compounds*, 4th edn., p.254, Wiley-Interscience, New York(1986).

146. C.C. Addison, D.W. Amos and D. Sutton, *J. Chem. Soc. (A)*, 808(1967).

147. D.W. James and W.H. Leong, *J. Chem. Phys.*, **51**, 640(1969).

148. R.J.H. Clark and C.S. Williams, *Inorg. Chem.*, **4**, 350(1965).

149. C. Postmus, J.R. Ferraro, A. Quattrochi and K.N. Nakamoto, *Inorg. Chem.*, **8**, 1851(1969).

150. J.R. Ferraro, *Low-Frequency Vibrations of Inorganic and Coordination Compounds*, Plenum Press, New York(1971).

151. L.A. Bengtsson and M.H. Brooker, *J. Raman Spectrosc.*, **24**, 815(1993).

152. T.G. Chang and D.E. Irish, *J. Solution Chem.*, **3**, 161(1974).

153. H. Zamali and Jemal, *J. Phase Equilibria*, **16**, 235(1995).

TEST TARGET (QA–3)

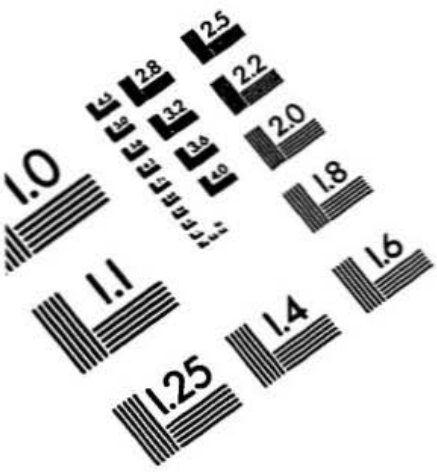

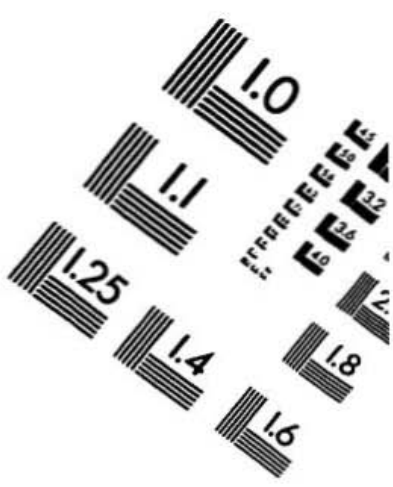

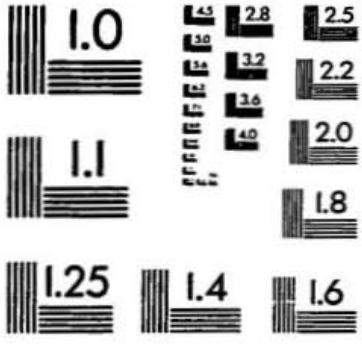

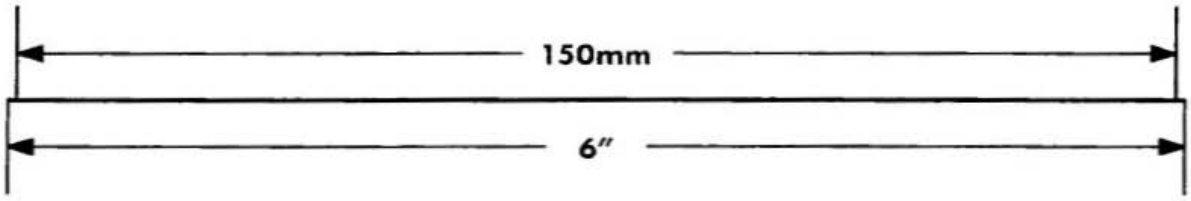

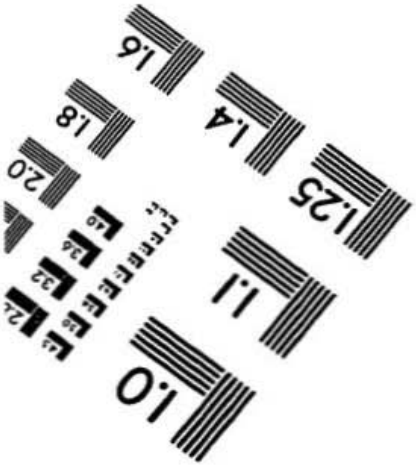

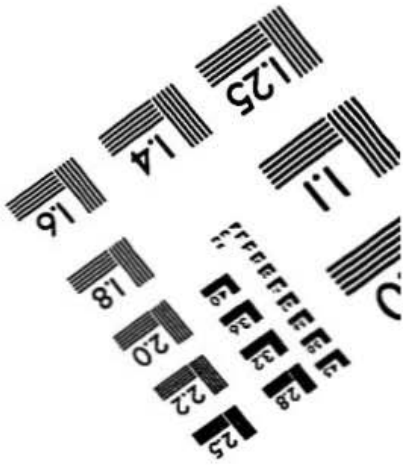

APPLIED IMAGE, Inc
1653 East Main Street
Rochester, NY 14609 USA
Phone: 716/482-0300
Fax: 716/288-5989